Chemical Nature and Sources of Particulate Matter in Urban Areas

A thesis presented to

National University of Ireland Galway

For the Degree of Doctor of Philosophy

By

Chunshui Lin

Supervisor: Professor **Colin O'Dowd**

Co-supervisor: Dr. **Jurgita Ovadnevaite** (Internal)

and Dr. **Ru-Jin Huang** (External)

School of Physics

National University of Ireland Galway

May 2019

Table of Contents

Table of Contents

Declaration

This dissertation is the result of my own work. It has not been previously submitted, in part or whole, to any university or institution for any degree, diploma, or other qualification.

Chunshui Lin, May 2019

Abstract

Particulate matter (PM) air pollution adversely affects human health and can lead to premature deaths. The sources of air pollution, however, remain poorly understood especially in urban areas with intense human activities. This thesis presents source apportionment studies of PM air pollution to improve our knowledge of the most important sources in urban cities regarded as typical of those found in moderately populated developed-world countries (e.g. Ireland) and heavily-polluted megacities in developing-world countries (e.g. China).

An advanced nation-wide air quality (AQ) pilot monitoring network was established in Ireland using high-time resolution aerosol chemical speciation monitors. The AQ network is capable of providing real-time information about PM mass concentration and chemical composition. Using the sophisticated fingerprinting techniques associated with the mass spectrometry technology, we can better inform emissions reduction policies and help to ensure the most appropriate air pollution sources are targeted. Dublin experienced frequent particulate air pollution events during winter 2016, with episodic PM_1 concentrations exceeding 300 $\mu g\ m^{-3}$. Solid fuel, such as peat and wood, though consumed by <13% of the households, contributed up to 70% of the pollution during these exceedance episodes. Pollution events due to solid fuel burning were also observed in Galway. Thus, emission control of solid fuel burning, especially peat burning, should be targeted to improve the air quality across Ireland in winter. In contrast, in summer, the PM was dominated by secondary organic and inorganic aerosol which was found to originate from the long-range transport.

In urban cities in North China, traffic, biomass burning, cooking, and coal combustion were the major pollution sources. In addition, secondary aerosol was found to contribute substantially (up to 55%) to PM in episodic events. In Beijing, traffic-related emissions were dominant during low pollution periods, contributing ~65% of total trace element mass. However, coal combustion-related particulate trace elements dominate (58%) during pollution periods. Therefore, reducing the primary emission and controlling the emission of secondary precursor gases are important to improve the air quality in China.

Acknowledgments

First and foremost, I would like to express my gratitude to my supervisor Professor Colin O'Dowd for his patience, motivation, and immense knowledge. And to my co-supervisors, Jurgita Ovadnevaite and Ru-Jin Huang, for their time, support and encouragement throughout my Ph.D. studies. Without their support, I would not be able to finish my Ph.D. research.

I am also grateful to the members of my GRC committee for their patience and support in overcoming numerous obstacles I have been facing through my research.

I would like to thank my fellow doctoral students for their feedback, cooperation and of course friendship. In addition, I would like to express my gratitude to the staff of the Centre of Climate and Air Pollution Studies (C-CAPs) for the support and encouragement, in particular, Darius Ceburnis, for the extensive support received in the field studies.

I would also like to thank my friends for their company and good food during my feeling lonely times abroad. Last but not least, I would like to thank my family for supporting me throughout my study.

Publications

This thesis consists of 7 publications; 3 publications as lead author, 2 with major roles, and 2 with a moderate contribution.

1) **Lin, C.;** Huang, R.-J.; Ceburnis, D.; Buckley, P.; Preissler, J.; Wenger, J.; Rinaldi, M.; Facchini, M.C.; O'Dowd, C.; Ovadnevaite, J. Extreme air pollution from residential solid fuel burning. Nature Sustainability 2018, 10.1038/s41893-018-0125-x.
2) **Lin, C.;** Ceburnis, D.; Hellebust, S.; Buckley, P.; Wenger, J.; Canonaco, F.; Prévôt, A.S.H.; Huang, R.-J.; O'Dowd, C.; Ovadnevaite, J. Characterization of primary organic aerosol from domestic wood, peat, and coal burning in Ireland. Environmental Science and Technology 2017, 51, 10624-10632.
3) **Lin, C.;** Ceburnis, D.; Huang, R.-J.; Canonaco, F.; Prévôt, A.S.H.; O'Dowd, C.; Ovadnevaite, J. Summer time aerosol over the west of Ireland dominated by secondary aerosol during long-range transport. Atmosphere 2019, 10, 59
4) Huang, R. J.; Wang, Y.; Cao, J.; **Lin, C.;** Duan, J.; Chen, Q.; Li, Y.; Gu, Y.; Yan, J.; Xu, W.; Fröhlich, R.; Canonaco, F.; Bozzetti, C.; Ovadnevaite, J.; Ceburnis, D.; Canagaratna, M. R.; Jayne, J.; Worsnop, D. R.; El-Haddad, I.; Prévôt, A. S. H.; O'dowd, C. D. Primary emissions versus secondary formation of fine particulate matter in the most polluted city (Shijiazhuang) in North China. Atmospheric Chemistry and Physics 2019, 19, 2283-2298.
5) Huang, R.J.; Cheng, R.; Jing, M.; Yang, L.; Li, Y.; Chen, Q.; Chen, Y.; Yan, J.; **Lin, C.;** Wu, Y.; Zhang, R.; El Haddad, I.; Prevot, A. S. H.; O'dowd, C. D.; Cao, J. Source-Specific Health Risk Analysis on Particulate Trace Elements: Coal Combustion and Traffic Emission As Major Contributors in Wintertime Beijing. Environmental Science and Technology 2018, 52, 10967-10974.
6) Huang, R.J.; Cao, J.; Chen, Y.; Yang, L.; Shen, J.; You, Q.; Wang, K.; **Lin, C.;** Xu, W.; Gao, B.; Li, Y.; Chen, Q.; Hoffmann, T.; O'Dowd, C. D.; Bilde, M.; Glasius, M. Organosulfates in atmospheric aerosol: Synthesis and quantitative analysis of PM2.5 from Xi'an, northwestern China. Atmospheric Measurement Techniques 2018, 11, 3447-3456.
7) Huang, R.J.; Yang, L.; Cao, J.; Chen, Y.; Chen, Q.; Li, Y.; Duan, J.; Zhu, C.; Dai, W.; Wang, K., **Lin, C.;** Ni, H.; Corbin, J..; Wu, Y.; Zhang, R.; Tie, X.; Hoffmann, T.; O'Dowd, C.; Dusek, U. Brown Carbon Aerosol in Urban Xi'an, Northwest China: The Composition and Light Absorption Properties. Environmental Science and Technology 2018, 52, 6825-6833.

1. Introduction

1.1 Motivation and Objectives of this Study

Atmospheric particulate matter (PM) or aerosol particles are condensed (solid or liquid) material suspended in the atmosphere. They influence the Earth's radiative budget, and ultimately climate, by scattering and absorbing radiation (Twomey, 1974; Albrecht, 1989). They also play an important role in the formation of cloud and precipitation by serving as cloud condensation (CCN) and ice nuclei (IN) (Fuzzi et al., 2015). In addition, aerosol particles influence air quality both locally and regionally, and adversely affects human health, causing morbidity and even premature mortality. A recent World Health Organization (WHO) report highlights that approximately 7 million premature deaths every year are associated with particulate air pollution and demonstrates that the pollution risks are far greater than previously thought (WHO, 2018). However, there remain significant uncertainties in the true impact of atmospheric aerosols on climate and health, due in large part to the lack of detailed knowledge on their sources, composition, chemical and physical properties, and the mechanisms of formation (Hallquist et al., 2009). A quantitative understanding of atmospheric aerosol particles has proven extremely challenging because of spatial and temporal variability in the sources of aerosols and their precursor gases, the complexity of particle composition, and the uncertainties associated with the nature and timescales of atmospheric aging processes of existing particles.

Today, over half the world's population resides in urban areas, and this proportion is expected to grow to 66% by 2050 (UN, 2014). Urban areas are usually more polluted than rural areas due to proximity to emission sources such as motor vehicles, residential heating, cooking, and some industry activities. It has been reported that over 80% of the people living in urban areas are exposed to PM air pollution (WHO, 2016). One of the key trends is that the global urban PM air pollution levels increased by 8% from 2008 to 2013, despite some improvements in some regions (WHO, 2016). As the air quality declines, the risk of respiratory diseases, stroke, heart disease, lung cancer, and other long-term health problems increases for the people living in urban areas. In general, the population in low- and mid-income countries are most at risk as 98% of cities with more than 1 million

inhabitants do not meet the WHO air quality guidelines, according to the WHO report in 2016. By way of comparison, in high-income countries, that percentage is 56% (WHO, 2016). WHO urges countries with areas not meeting the air quality guideline values to undertake immediate action to improve air quality. It is worth noting that reducing air pollution is also an important part of countries' commitment to the Paris Agreement on climate change.

This project aims to elucidate the chemical nature and sources of aerosol particles in urban areas in Ireland, a moderately populated developed-world country, and in China, a heavily-polluted developing-world country. The aims are achieved *via* the analysis of data collected from the deployment of high-time resolution aerosol chemical speciation monitor (ACSM) and a suit of other *in-situ* instrument measuring the chemical and physical properties of aerosol particles in the cities in both Ireland and China in combination with source apportionment model of Positive Matrix Factorization (PMF) and Multilinear Engine (ME-2).

The objectives of this research are:

1. To identify the major sources of PM and assess their impact on air quality in Dublin city (Paper 1) and Galway city (Paper 2) in Ireland during winter;

2. To quantify the impact of long-range aerosol transport on air quality in Galway during summer (Paper 3);

3. To identify and quantify the primary and secondary sources of PM and to assess their impact on air quality in wintertime Shijiazhuang, China (Paper 4);

4. To quantify the contribution of traffic and coal burning to trace elements and to assess their impact on health risks in wintertime Beijing, China (Paper 5);

5. To identify the sources of organosulfates in ambient aerosols (Paper 6) and to assess the link between the chemical composition and optical properties of brown carbon (Paper 7) in Xi'an, China.

1.2 Review of the Current State of Knowledge

1.2.1 Sources and Compositions of Particulate Matter

Atmospheric aerosol particles consist of liquid or solid particles suspended in the air. The sources of PM can be natural and anthropogenic. As shown in Figure 1, natural processes such as volcanic activity, forest fires, marine activity generate aerosol particles such as volcano ash, dust, soot, and sea salt. Natural biological emissions include spores, pollen, and other microscopic particles. Human activities, such as the combustion of fossil fuel in engines, power plants, and various industrial processes, also generates a significant amount of PM in the atmosphere. Generally, airborne aerosols are divided into two types, primary and secondary (Hallquist et al., 2009; Fuzzi et al., 2015). Primary aerosols are directly emitted or injected into the atmosphere while secondary aerosols are formed by the nucleation/oxidation/condensation of its precursor gases. Human activities such as traffic, cooking, and coal burning emit both primary aerosol (e.g., black carbon and organic matter) and secondary aerosol precursor gases such as sulfur dioxide, nitrogen oxides, and volatile organic compounds (VOCs) which are converted into their corresponding particulate phase upon oxidation/nucleation/condensation (Hallquist et al., 2009). Note that both primary and secondary aerosols undergo a dynamic change in both composition and properties resulting from oxidation, gas-to-particle partitioning, fragmentation and cloud processing (Kroll and Seinfeld, 2008; Gentner et al., 2017).

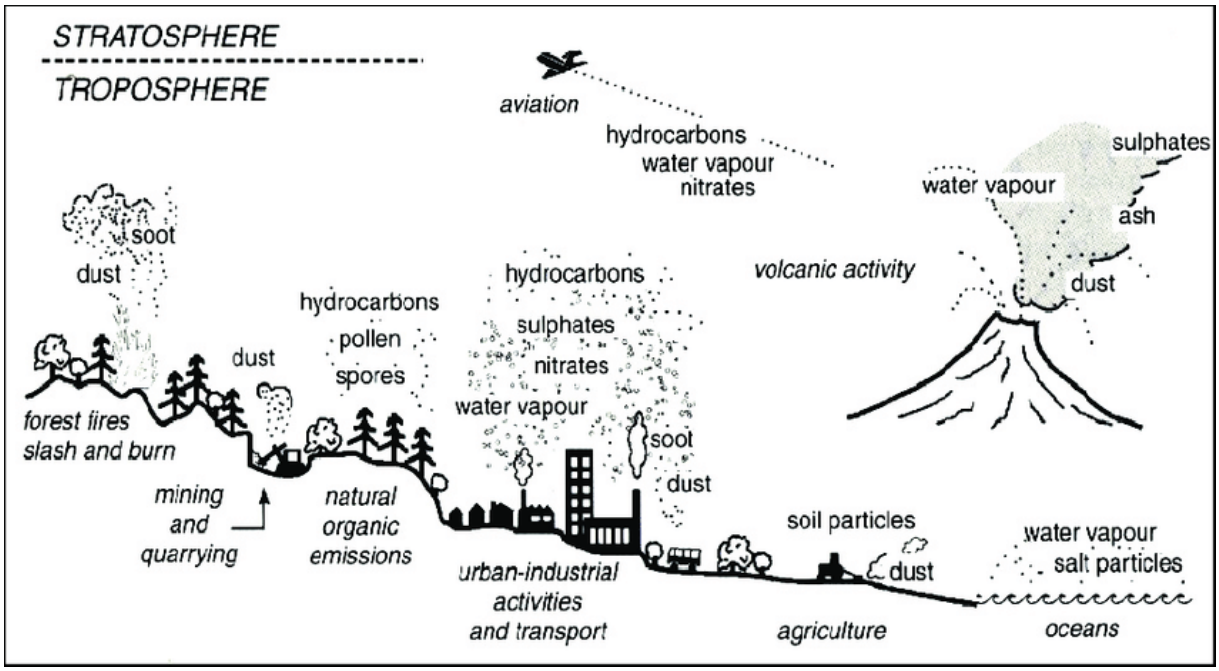

Figure 1. Sources of particulate matter in the environment, reproduced from Kemp et al. (2004). Volcanic activity, forest fires, natural organic emission, and marine activity are the natural sources of aerosol particles while mining and quarrying, urban-industrial activities, transport, agriculture are the man-made sources.

Airborne aerosol particles have very complex and variable chemical composition ranging from inorganic compounds (e.g., sulfate, nitrate, sea salt, and elemental carbon) to organic matter (e.g., *n*-alkanes, fatty acids, sugars, hopanes, fatty alcohols, phthalates, polyols/polyacids, sterols, lignin, and resin products). Due to the various sources and transformations, the chemical composition of aerosols can vary a lot depending on the location, time, season or weather conditions (Figure 2).

Inorganic compounds are found in both marine and continental aerosols. For example, primary sea salt particles including ions like Na^+, Cl^-, Mg^{2+}, K^+, and Ca^{2+} are generated through bubble bursting and wave breaking at the sea surface (O'Dowd and de Leeuw, 2007). Therefore, sea salt generation is strongly correlated with wind speed. Sulfate (SO_4^{2-}) is secondary and formed from the gas-to-particle conversion of sulfur dioxide (SO_2) which is emitted from anthropogenic sources (e.g., coal burning (Zhang et al., 2012)) and volcanoes. In the marine environment, dimethyl sulfide (DMS) from biogenic sources, especially from marine planktons is also an important sulfur dioxide source which is then converted into sulfate upon oxidation (O'Dowd et al., 1997; Ovadnevaite et al., 2014).

Nitrate (NO_3^-) is common in continental aerosols and is formed mainly from the oxidation of atmospheric nitrogen dioxide (NO_2) which is mainly emitted from anthropogenic sources e.g., traffic emissions (Geng et al., 2008). In contrast, seawater contains negligible amounts of nitrate (Ovadnevaite et al., 2014).

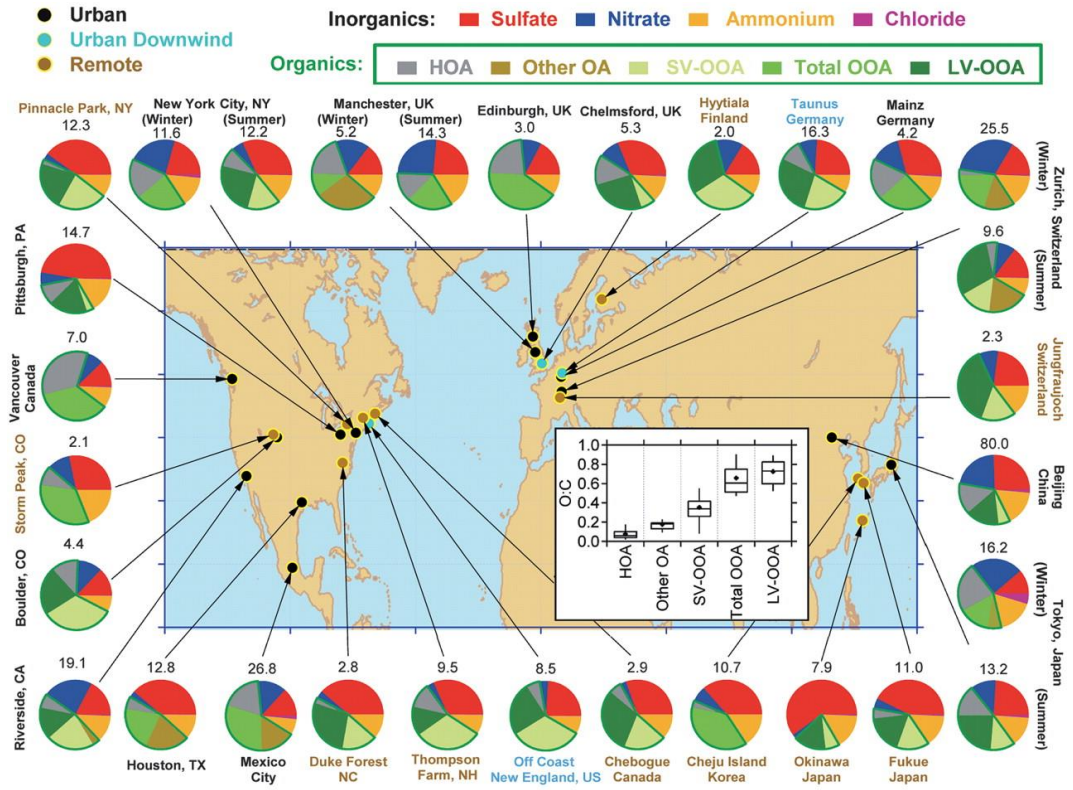

Figure 2. Average mass concentration (in μg m^{-3}) and fractions of nonrefractory inorganic species (sulfate, nitrate, ammonium, and chloride) and organic components in PM_1 aerosols measured with the Aerosol Mass Spectrometer at multiple surface locations, reproduced from Jimenez et al. (2009).

Ammonium salts (NH_4^+) are formed when gas ammonia (NH_3) reacts with various acids, such as sulfuric (H_2SO_4) and nitric acid (HNO_3). With sufficient amount of ammonia in the atmosphere, the sulfuric acid is fully neutralized and forms ammonium sulfate, $(NH_4)_2SO_4$, with the molar ratio of NH_4^+ to SO_4^{2-} equal to 2 (Wang et al., 2013). However, in the marine environment, due to the lack of ammonia source, the aerosol phase sulfuric acid is not always fully neutralized and has molar ratios <2 and even <1. Therefore, sulfate is mainly in the form of NH_4HSO_4 or H_2SO_4 in marine aerosol (Ovadnevaite et al., 2014).

Elemental carbon is the sooty black materials emitted during the combustion of fossil fuel or biomass burning, often with other chemicals attached to its surface. BC is a strong absorber of solar radiation and its emissions are the second largest contribution to current global warming after carbon dioxide (Ramanathan and Carmichael, 2008).

Organic aerosol (OA) comprises numerous individual organic compounds (Bi et al., 2003). In comparison to inorganic aerosol, organic aerosol remains poorly understood due to the various sources and transformation (Jimenez et al., 2009). Primary OA (POA) are directly emitted by biogenic (e.g., marine (O'Dowd et al., 2004)) or anthropogenic sources (e.g., traffic) (Hallquist et al., 2009). Secondary OA (SOA) are formed from the oxidation of biogenic or anthropogenic volatile organic compounds (VOC) (Kroll and Seinfeld, 2008). As a result of strict regulations for sulfur-containing compounds, the atmospheric concentrations of SO_2 and sulfate reduced significantly (~ 80% over 35 year period), resulting in an aerosol composition dominated by organic matter (Grigas et al., 2017). As observed at the Mace Head research station on the Irish coast, organic aerosol prevails over inorganic compounds under polluted conditions, contributing 50% or more of the submicron PM (PM_1) mass and exhibiting a trend whereby its contribution increases with increasing pollution levels (Grigas et al., 2017).

1.2.2 Health Effects

The size of the particle is an important parameter to evaluate where in the respiratory tract the particle will come to rest when inhaled. Larger particles tend to be filtered in the nose, throat or mouth, but particulate matter smaller than 10 μm (i.e., PM_{10}) can settle in the lungs, causing health problems. Similarly, $PM_{2.5}$ is PM smaller than 2.5 μm. $PM_{2.5}$ is generally described as fine particulate matter and it tends to penetrate deeper into the lungs, reaching the gas-exchange regions of the lungs (alveolus). As a comparison, a human hair is about 100 μm, so roughly 40 times the size of $PM_{2.5}$. Ultrafine particulate matter ($PM_{0.1}$) may be more damaging to humans as it tends to pass through cell membranes of the lungs and affect other organs. The particles emitted from the modern diesel engine are typically in the same size ranges as $PM_{0.1}$ (Neer and Koylu, 2006), and therefore, potentially cause more health problems than coarse and fine particulate matter. However, penetration of particles is not wholly dependent on their size because the particle shape and its chemical composition also play a part. Despite this, most regulatory agencies including the European Environmental Agency

(2008/50/EC) and the World Health Organization have used the particulate mass concentration as a guideline value to regulate the air quality.

The inhalation of atmospheric particulate matter increases the risk of lung cancer, respiratory diseases, cardiovascular disease, premature delivery, birth defects, low birth weight, and premature death (Sandström et al., 2005). Globally, millions of premature deaths per year have been estimated to be associated with outdoor air pollution caused by fine particulate matter (Lelieveld et al., 2015). As shown in Figure 3, China, India, and many of the large urban centers are the hotspot locations with higher premature mortality rates (Lelieveld et al., 2015). Most of the premature deaths are caused by cerebrovascular disease and ischaemic heart disease (Lelieveld et al., 2015). Moreover, Lelieveld et al. (2015) predicted that the contribution of outdoor pollution to premature death could double by 2050 if the current trend of energy usages continued.

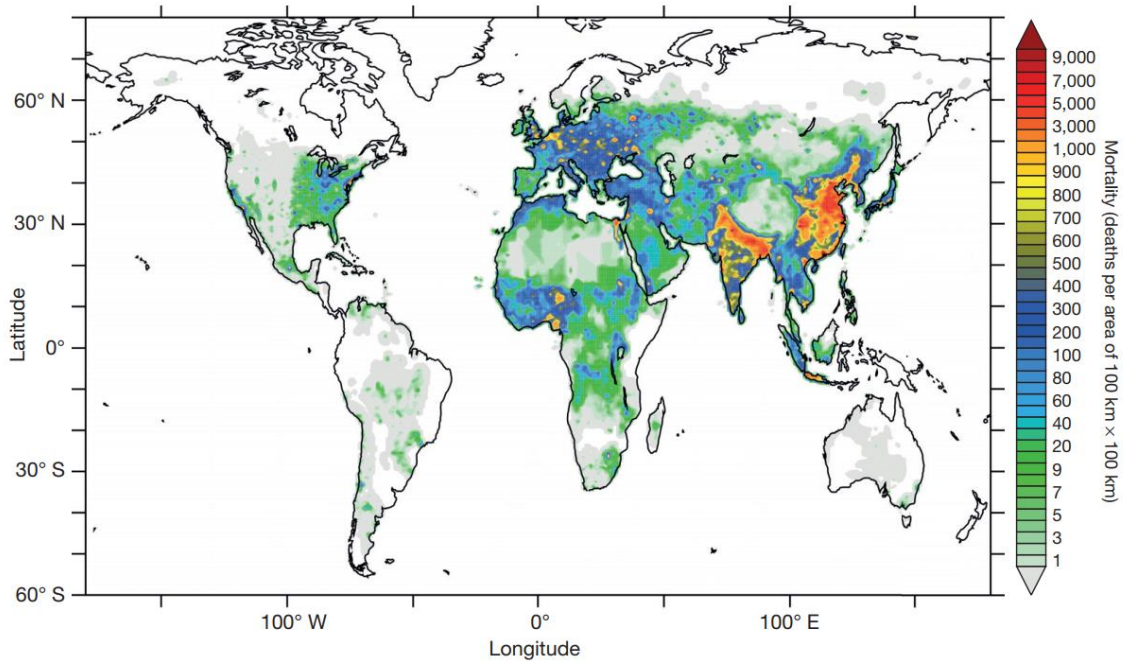

Figure 3. Mortality linked to outdoor air pollution in 2010, reproduced from Lelieveld et al. (2015).

The health effects of long-term exposure to atmospheric aerosol particles are stronger than short-term exposure (Liang et al., 2018). However, even short-term exposure to outdoor $PM_{2.5}$ pollution is associated with an increased risk of mortality, morbidity, and increased emergence admission to the hospital (Atkinson et al., 2014). World Health Organization (WHO) recommends a 24 h average

concentration of 25 μg m^{-3} as the short-term guideline value for $PM_{2.5}$ and urges countries with areas not meeting the 24 h guideline values to undertake immediate action to achieve these levels in the shortest possible time. As for the long-term guideline for $PM_{2.5}$, an annual average of 10 μg m^{-3} was recommended.

Particulate mass concentration is not a proper measure of the health effects because not every PM component is equally important in causing adverse health effects. Certain aerosol chemical components (e.g., PAHs) and sources such as traffic and biomass burning have been reported to have a higher association with mortality or adverse health effects (Sbihi et al., 2013; Kamal et al., 2015). Therefore, elucidating the link between the pollution source and their corresponding adverse health effects is important to get the maximized health effects from air quality controls by targeting the sources most closely related to adverse health effects.

The oxidative potential of atmospheric PM is a measure of its capacity of generating reactive oxygen species (ROS) in vivo that induces oxidative stress, damaging the living cells (Künzli et al., 2006). This is recognized as one of the major mechanisms responsible for the negative effects of PM on human health. Generally, there are two types of methods for the measurement of the oxidative potential of PM, i.e., cellular and acellular (or cell-free) methods (Valavanidis et al., 2008). Xia et al., (2006) tested the cellular effects of ambient ultrafine particles in a phagocytic cell line that is representative of a lung target for ultrafine particles. It was found that the particles induced toxicity involves mitochondrial injury through increased calcium uptake and structural organellar damage (Xia et al., 2006). In addition, they have demonstrated that ROS generation and oxidative stress are a valid test paradigm to compare cellular toxicity caused by the ambient particles and various manufactured particles including titanium dioxide (TiO_2), carbon black, fullerol, and polystyrene (PS) nanoparticles. However, the direct measurements of the cellular effects of PM require a highly-controlled environment and are labor intensive. In contrast, cell-free methods are relatively simple and provide faster readouts of PM oxidative potential. DTT (Dithiothreitol, $HSCH_2(CH(OH))_2CH_2SH$) essay is one of the most widely used cell-free methods to measure the oxidative potential of PM (Charrier and Anastasio, 2012; Delfino et al., 2013). The in vivo production of ROS involves the reduction of molecular oxygen (O_2) to superoxide anion (O_2^-) by accepting electrons from cellular reductants in mitochondria and endoplasmic reticulum. The DTT assay simulates this electron-transfer mechanism by transferring electrons from DTT to oxygen, and the DDT consumption rate is proportional to the concentration of redox-active species in PM extracts.

Thus, DDT assay is considered as a surrogate measure of the in vivo oxidative potential of PM. Various chemical components have been found to induce oxidative stress initiated by ROS, including PAHs (Totlandsdal et al., 2015), quinones (Charrier and Anastasio, 2012), transition metals (Charrier and Anastasio, 2012), water-soluble organic carbon (WSOC) (Verma et al., 2009), and HUmic-LIke Substances (HULIS) (Verma et al., 2015).

1.2.3 Climate Effects

Atmospheric aerosol particles affect the Earth's radiation budget, causing changes to the Earth's climate system (Myhre et al., 2013). Through several distinct mechanisms such as direct and indirect aerosol effects, aerosol alters the Earth's radiative equilibrium, forcing the temperature to rise or fall. Positive forcing means a net gain of energy which causes warming; negative forcing means a net loss of energy which causes cooling. As shown in Figure 4, aerosol generally causes a negative forcing which could counter the warming effect of greenhouse gases (Myhre et al., 2013). However, the Intergovernmental Panel on Climate Change (IPCC) highlighted that uncertainty related to aerosol radiative forcing remain large, limiting the capability of future climate prediction models. The uncertainty arises mainly from a poor understanding of the aerosol sources, composition, and properties, as well as their interaction with climate (Fuzzi et al., 2015).

Direct interaction between the atmospheric aerosols and radiation include scattering and absorption of both the incoming shortwave radiation and outgoing longwave radiation, producing a net negative radiative forcing (Ramaswamy et al., 2001). Typically, the direct aerosol effects change the albedo of the atmosphere which affects the net amount of radiation scattered or absorbed. Highly scattering atmospheric aerosol, such as sea salt and sulfate, increases the albedo of the atmosphere, indicating a larger amount of solar energy is reflected back into space than being absorbed. Conversely, some absorbing aerosol such as black carbon (BC) decreases the albedo of atmosphere, absorbing more solar radiation than scattering. BC has been reported to be the second largest contribution to current global warming after carbon dioxide (Ramanathan and Carmichael, 2008). Therefore, the cooling effect of some natural aerosols, such as sea salt from marine and sulfate from volcanic eruptions, may be compensated by some anthropogenic aerosols primarily by BC from fossil fuel and biomass burning. For example, the radiative forcing for sulfate is in the range of -0.2 to -0.8 watts per square meter ($W\ m^{-2}$) while it is +0.1 to + 0.4 $W\ m^{-2}$ for BC (IPCC).

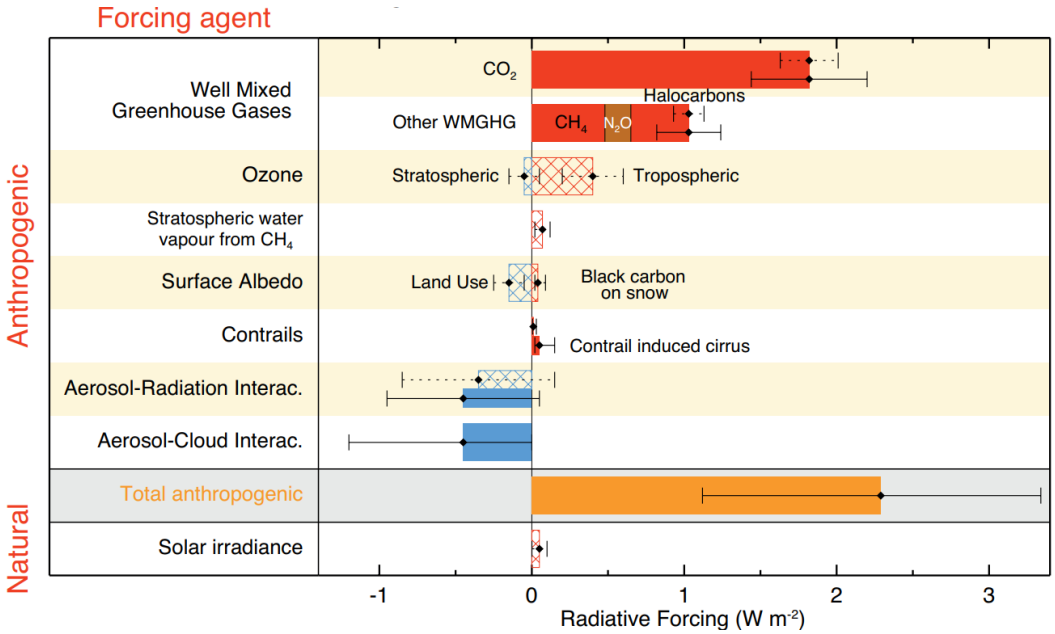

Figure 4. Radiative forcing for various anthropogenic and natural sources including greenhouse gases, ozone, and aerosol, reproduced from Myhre et al. (2013).

Aerosol also affects the climate indirectly as it involves the formation of clouds (Lohmann and Feichter, 2005). Cloud droplets are formed onto pre-existing aerosol particles through the condensation of water vapor in the atmosphere. These aerosol particles are known as cloud condensation nuclei (CCN) or ice nuclei (IN) (Pöschl, 2005). Therefore, the properties and the number of aerosol particles can affect the properties of clouds, changing the climate. Generally, an increase in the number of CCN leads to an increase in the cloud droplet number (Radke et al., 1989). As a result, it reduces the sizes of the cloud droplet as the same amount of water is divided by a larger number of cloud droplets. The more numerous smaller cloud droplets lead to more scattering and therefore increase the cloud albedo, reflecting more solar radiation. Moreover, smaller cloud droplets decrease precipitation efficiency, thereby increasing the cloud lifetime (Ferek et al., 2000). However, the absorbing atmospheric aerosol such as black carbon may heat the surrounding air which may cause evaporation of cloud particles, resulting in fewer cloud droplets. Although large uncertainty remains, the net indirect effect of aerosols was estimated to cause a negative radiative forcing in the range of –0.3 to –1.8 W m^{-2} (Figure 4).

1.2.4 Historical Measurements of Particulate Air Pollution: Black Smoke

Black smoke (BS) measurements were the earliest systematic measurements of particulate air pollution in Ireland (Kelly and Clancy, 1984). BS has been reported to be a useful metric for health studies, showing a strong correlation with morbidity and mortality in epidemiological studies (Clancy et al., 2002; Kelly and Clancy, 1984).

Ireland experienced severe air pollution in the 1980s due to the use of solid fuel (e.g., coal and peat) for space heating (Figure 5). In 1982, one serious pollution episode featured a city-wide BS concentration of over 750 μg m^{-3} in Dublin City and was associated with a doubling in fatality rates at a central Dublin hospital (Kelly and Clancy, 1984). After the introduction of the ban on marketing, sale, and distribution of coal in 1990, a significant reduction in BS (up to 70 %) has been observed in Dublin (Figure 5). Later, the coal ban was extended to other areas with over 15,000 population including Cork and Galway (Goodman et al., 2009).

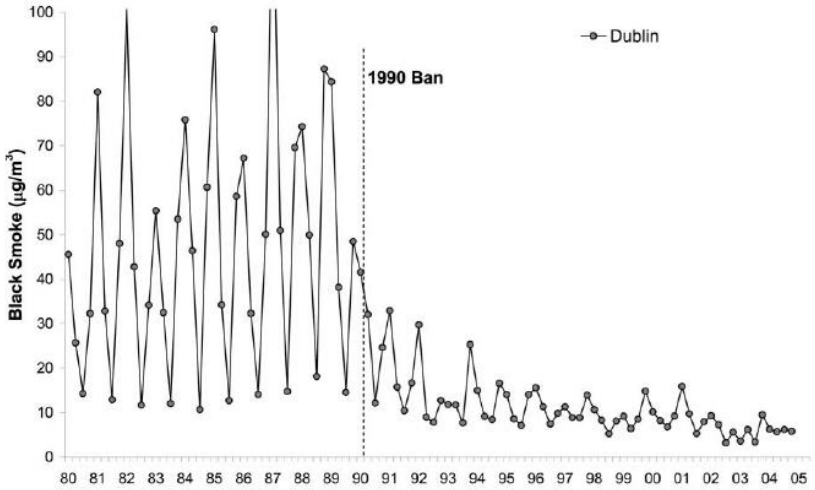

Figure 5. Season-specific black smoke concentrations before and after the 1990 ban on coal in Dublin, reproduced from Goodman et al. (2009).

Measurement of BS is based on the optical reflectance of the PM sample collected on a filter by pumping a known volume of air through a known area of the filter. The reflectance, volume, and filter area are converted to a BS Index, given in units of μg m^{-3}. BS measurement is based on the optical darkness of total PM which is, however, dominated by sub-micron (PM_1) elementary carbon particles

(Heal et al., 2005). Black smoke is a good surrogate of primary combustion emissions but it is insensitive to secondary inorganic aerosols such as sulfate and nitrate. Therefore, black smoke cannot represent the total mass concentration of PM when the composition of the PM has changed greatly, notably as coal burning in cities has declined. For example, Heal et al., (2005) reported that the daily BS: PM10 ratios at an urban background site in Edinburgh were significantly lower in summer than in winter because secondary particles dominate the PM mass in summer which failed to be represented by BS measurement.

Interpretation of historical Black Smoke data is important for human health and climate change studies. Measurement of black carbon (BC) has been made available only recently with real time measurement. It is to measure the mass concentration of the elementary carbon by the absorption of light passing through PM collected on a filter (Drinovec et al., 2015). BC measurement is based on different instrumentation and data processing than the black smoke method (Quincey, 2007). However, a simple quadratic relationship between BS and BC has been reported by Quincey et al., (2007), which could be useful in the interpretation of historical BS data.

1.2.5 Aerosol Mass Spectrometer

The development of high time resolution Aerosol Mass Spectrometer (AMS) has greatly improved our understanding about the chemical composition and sources of ambient aerosol (Jayne et al., 2000; Jimenez et al., 2009; Lanz et al., 2010). AMS determines the mass spectra of the major non-refractory (organic and inorganic) components of the ambient aerosol in near real-time (Canagaratna et al., 2007). Through the typical mass spectral fragmentation patterns, the measured mass spectra are assigned to several inorganic components (i.e., sulfate, nitrate, ammonium, and chloride) and to the organic fraction (Jayne et al., 2000; Allan et al., 2004; Drewnick et al., 2005; DeCarlo et al., 2006; Canagaratna et al., 2007; Ng et al., 2011; Fröhlich et al., 2013).

Figure 6 shows the basic schematic of the AMS. The particle inlet with a critical orifice controls the flow into the instrument and a skimmer cone subsequently removes most of the gas from the sample flow before the aerosol beam enters the second chamber (the time of flight (ToF) region). The PM_1 inlet is the most commonly used inlet (Canagaratna et al., 2007). The PM_1 inlet allows particles between diameters of 30 nm and 600 nm to be focused with near 100% efficiency, which quantifies

the majority of accumulation mode aerosol particles (Canagaratna et al., 2007). Particles not in this size range are either too small to be aerodynamically focused or have a low transmission efficiency (DeCarlo et al., 2006). $PM_{2.5}$ inlet allows particles sizes between 80 nm and at least 3 μm to be efficiently transmitted (Williams et al., 2013; Elser et al., 2016).

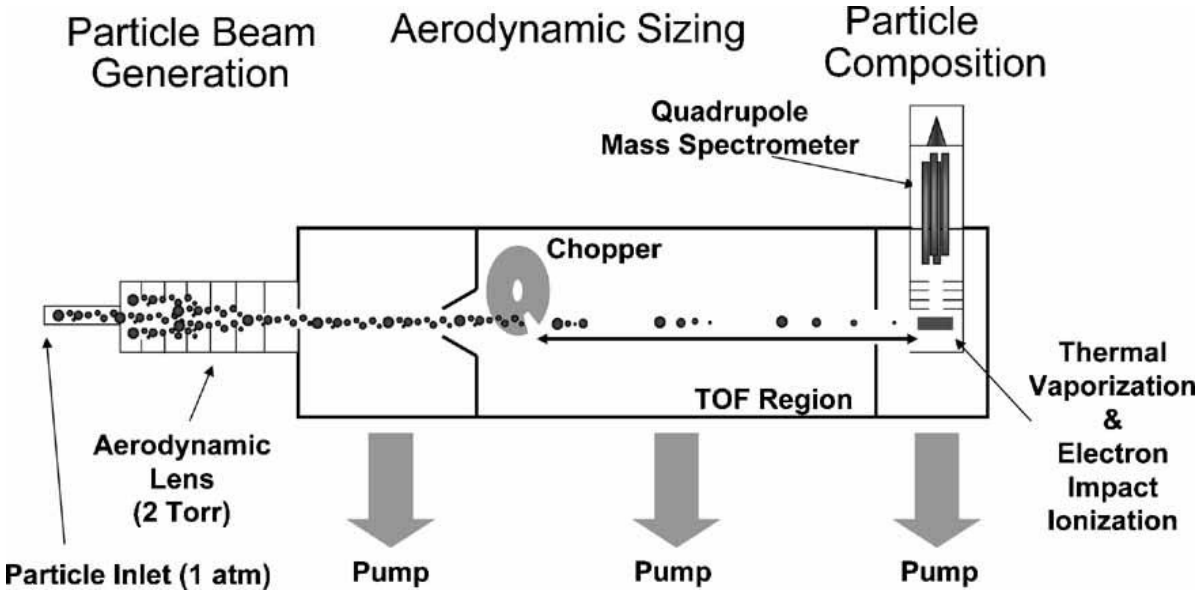

Figure 6. Schematic of the Aerodyne Aerosol Mass Spectrometer, reproduced from Canagaratna et al. (2007). Submicron particles that enter the aerodynamic lens are focused into a narrow beam that impacts a hot vaporizer. The resulting vapor is ionized with electron impact and chemically characterized with a quadrupole mass spectrometer.

In the ToF region, a chopper wheel controls the passage of the beam; it can either let the beam pass freely or completely block it (Figure 6). Because the particle velocity is associated with the particle size, the time taken to reach the detection region after passing the chopper is used to calculate the particle velocity and the corresponding particle size. The third chamber is equipped with a vaporizer (usually 600 ^{o}C) and an ionizer. Non-refractory particles are flash-vaporized as they hit a hot surface of the vaporizer. The resulting vapor plume is ionized by electron impact and then the positive ions are introduced into the mass spectrometer to be identified and quantified. Note that the pump for each chamber ensures a vacuum condition to reduce interference of vapor component in the measured particulate mass spectrum. Research grade High-Resolution Time of Flight Aerosol Mass Spectrometer (HR-ToF-AMS) has better resolution than Quadrupole-AMS. HR-ToF-AMS allows the quantification of several types of organic fragments (C_xH_y, $C_xH_yO_z$, $C_xH_yN_p$, and $C_xH_yO_zN_p$) and the

direct identification of some organic nitrogen and organosulfur content (DeCarlo et al., 2006), providing valuable information on the chemical composition of the measured aerosol. Decarlo et al., (2016) provided detailed information on the operation of HR-ToF-AMS and deployed this instrument in Riverside, CA, for ambient aerosol measurement, in which the spectra of organic species are dominated by C_xH_y and $C_xH_yO_z$ fragments.

While the research grade AMS provides valuable information about the aerosol, it is not well suited for routine air quality monitoring applications due to the high cost and complexity of maintenance (Ng et al., 2011). Aerodyne Aerosol Chemical Speciation Monitor (ACSM), a simplified version of AMS, is specially designed for long-term monitoring applications (Parworth et al., 2015; Petit et al., 2015; Ripoll et al., 2015; Sun et al., 2015; Sun et al., 2018). ACSM has a smaller size, weight, cost and power requirements than the AMS (Ng et al., 2011). As shown in Figure 7, ACSM is not equipped with a particle beam chopper system for measuring particle time-of-flight to obtain particle size information. In addition, it uses a lower performance residual gas analyzer (RGA) type quadrupole mass spectrometer instead of the high-performance quadrupole and time-of-flight spectrometers used on AMS systems. However, the sensitivity and time resolution of ACSM has proved to be sufficient to identify and quantify the major types of aerosols in the urban environment (Parworth et al., 2015; Petit et al., 2015; Ripoll et al., 2015; Sun et al., 2015; Sun et al., 2018). Moreover, ACSM has been deployed for periods of up to two years (Petit et al., 2015; Sun et al., 2018), showing that such systems can be used in a routine manner.

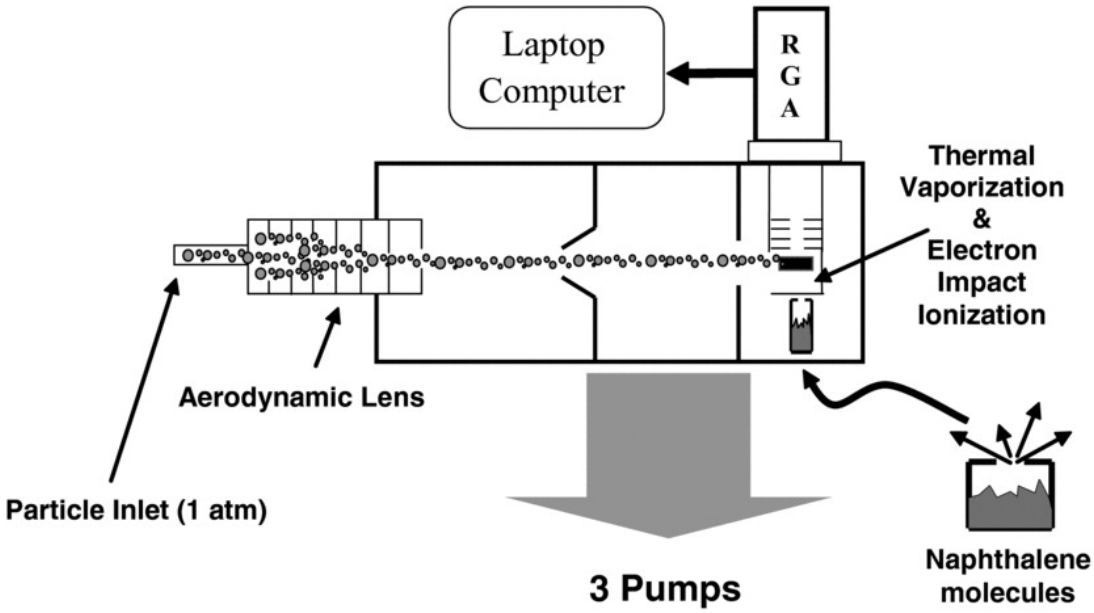

Figure 7. Schematic of the ACSM, reproduced from Ng et al. (2011). Submicron particles are focused into a narrow beam which are vaporized and ionized in the ACSM chamber. The resulting ions are chemically characterized with an RGA quadrupole mass spectrometer. Naphthalene is used for calibration and routine monitoring of instrument performance (Ng et al., 2011).

1.2.6 Source Apportionment

Source apportionment identifies the specific types of aerosol particles that make up the particulate air pollution and identifies the contributing sources. Source apportionment improves our quantitative understanding of each source's contribution to particulate air pollution.

Receptor-based models are the most widely used source apportionment technique (Lee et al., 2008). Typically, receptor models attribute the observed concentrations to specific sources using the chemical composition or mass spectra in those samples as tracers for the particular source type. The outcome of such an analysis is the identification of the pollution source types and their corresponding contributions to the observed concentrations. Receptor models are based on the mass balance of the measured species which can be written in the form:

$$X_{ij} = \sum_{k=1}^{N} G_{ik} F_{kj} + E_{ij} \quad i=1, \ldots, m; j=1, \ldots, n; k=1, \ldots, N \quad (1)$$

where X_{ij} represents the ambient concentration of species j in sample i, F_{kj} represents the profile (or mass spectra) of species j in Factor k, G_{ik} represents the source contribution of Factor k, and E_{ij} represents the residue not represented by the model.

Chemical mass balance (CMB) and positive matrix factorization (PMF) are the two types of the receptor-based bilinear algorithms that represent the time series of ambient measurement as a linear combination of static factor profiles and their respective time series (Lee et al., 2008; Canonaco et al., 2013). CMB requires a priori knowledge of major sources (e.g., chemical composition or mass spectra), while PMF does not require any priori assumptions for either source or time profiles. However, PMF requires non-negative entries for G and F to be physically meaningful. PMF uses a least squares algorithm that iteratively minimizes the objective function Q, defined as

$$Q^m = \sum_{i=1}^{m} \sum_{j=1}^{n} \left(\frac{e_{ij}}{\sigma_{ij}}\right) \quad (2)$$

where σ_{ij} represents measurement uncertainty.

Both CMB (i.e., known sources) and PMF (i.e., unknown sources) have their own advantages and disadvantages. CMB source apportionment relies on the source-specific chemical composition or mass spectra as the input to the bilinear algorithm model to assess the contribution of certain emission source to the air pollution. However, CMB is unable to directly apportion secondary sources. Instead, the fraction that is not attributed to the primary sources in the CMB model is regarded as the upper limit of the secondary sources. Although PMF does not require any priori source information, the model solution often suffers from high rotational ambiguity resulting in non-meaningful or mixed factors especially when all the measured species exhibit temporal co-variation, e.g., due to boundary layer evolution or certain meteorological conditions such as rainfall. As a solver of PMF, the multilinear engine (ME-2) is capable of directing the PMF model towards an optimal solution by utilizing a priori information in the form of the factor profiles and/or time series. The ME-2 can be defined as:

$$F_{kj,\,solution} = F_{kj,\,reference} \pm a \times F_{kj,\,reference} \quad (3)$$

$$G_{ik,\,solution} = G_{ik,\,reference} \pm a \times G_{ik,\,reference} \quad (4)$$

where the scalar *a* value determines the extent to which the output solution of $F_{kj,\,solution}/G_{ik,\,solution}$ is allowed to vary from the reference $F_{kj,\,reference}/G_{ik,\,reference}$. For example, an *a* value of 0.05 represents

5% variation.

ME-2 has been utilized in several source apportionment studies to find acceptable solutions in which PMF did not properly represent the measured data (Lanz et al., 2008; Canonaco et al., 2013; Reyes-Villegas et al., 2016). Typically, the ME-2 engine is constructed in a way to solve (1) free PMF, if no factor profiles are constrained or an *a* value set at 1 as 100% variation; (2) ME-2, if some factors are constrained; and (3) CMB, if all factors are constrained i.e., an *a* value of 0. In addition, different variabilities of the reference profiles can be chosen for the factors in ME-2 analysis (Paatero et al., 2002; Canonaco et al., 2013).

The application of source apportionment techniques on high time resolution data (seconds to minutes) enables the identification and quantification of the pollution sources on a near real-time basis. This is very important to understand the sources of particularly intense and time-limited (a few hours) pollution events which would otherwise be missed by the poor time resolution (days to weeks) measurement e.g., filter-based sampling.

1.2.7 Source Apportionment of Organic Aerosol

Organic aerosol has been found to make up a large fraction (20 - 90%) of the submicron particulate mass and has, thus, attracted much attention to infer its sources (Jimenez et al., 2009). However, the source apportionment of organic aerosol is still challenging because of very large chemical space with respect to molecular weight, functional groups, and polarity (Jimenez et al., 2009; Huang et al., 2014). Over the past decade, numerous studies have successfully exploited the resolving power of PMF to apportion the AMS measured organic mass spectra to different sources based on the source/process-specific factor profiles or time series (Zhang et al., 2011; Li et al., 2017). Typically, PMF interprets the time series of measured organic mass spectra as a linear combination of static factor profiles (i.e. mass spectra) and their respective time series (Paatero and Tapper, 1994; Canonaco et al., 2013).

AMS-PMF studies have been carried out at a variety of sites including urban, rural, and remote stations across the world (Jimenez et al., 2009; Lanz et al., 2010; Crippa et al., 2014; Li et al., 2017). Depending on sites, different sets of organic factors, including various POA and SOA factors corresponding to different sources/processes, have been identified (Jimenez et al., 2009; Li et al.,

2017). For example, hydrocarbon-like OA (HOA) is a POA factor and is associated with vehicular emission which is common in urban areas (Canagaratna et al., 2004; DeWitt et al., 2015). Cooking-like OA (COA) represents POA from cooking activities and its diurnal cycle usually exhibits mealtime peaks (e.g., lunch or dinner; Mohr et al., 2012). Biomass burning OA (BBOA) is associated with emissions from wood burning, as well as crop residue burning which is popular in rural China after harvesting (Zhang et al., 2015). Coal combustion OA (CCOA) is associated with the emission from coal combustion which has been identified in Beijing for its widespread use for domestic heating (Sun et al., 2013). Oxygenated OA (OOA) is characterized by high oxygen content with a high atomic O:C ration (0.25 - ~1; Jimenez et al., 2009). Most OOA is secondary and the increase in OOA mass is usually associated with strong photochemical activities and other secondary species e.g., sulfate. Based on the volatility, OOA can be divided into semi-volatile OOA (SV-OOA) and low-volatile oxygenated OA (LV-OOA), representing newly formed and aged OOA, accordingly (Zhang et al., 2011; Canonaco et al., 2015). The formation of SV-OOA depends on the emission of its precursor gases (e.g., VOC) and subsequent photo-oxidation process (Jimenez et al., 2009). The concentration of SV-OOA is usually more elevated in the afternoon due to the stronger solar radiation. Further oxidation of SV-OOA forms LV-OOA which is more oxidized than SV-OOA.

As shown in Figure 8, AMS-PMF studies conducted across Europe show that for most sites four organic factors were retrieved including two POA factors (i.e., HOA and BBOA) and two SOA factors (SV-OOA and LV-OOA) (Crippa et al., 2014). Cooking-related COA was only resolved at urban locations while MSA (marine related sources) was only separated in the marine environment. The traffic-related HOA was season independent and represented 11 ± 6% of total OA across Europe. In contrast, domestic heating-related BBOA was more intense during winter and represented 12 ± 5% of the total OA mass. However, SOA (the sum of SV-OOA and LV-OOA) was the dominant fraction of OA (>70%). Therefore, in general, it is an urgent need to control the sources of SOA precursors while governing the POA emissions at the same time over Europe.

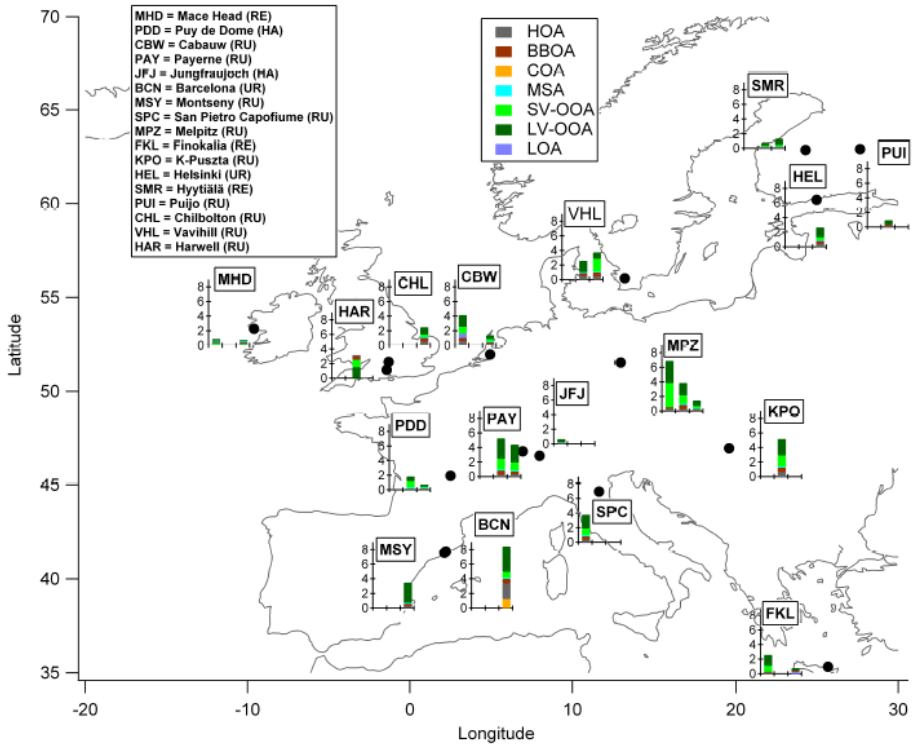

Figure 8. 17 measurement sites across Europe and average organic aerosol factor contributions resulting from PMF conducted on AMS organic spectra with ME-2 (Crippa et al., 2014).

As part of the Aerosol, Clouds, Trace gas Research InfraStructure network (ACTRIS) program aiming at pooling high-quality data from the state-of-the-art instrument, ACSM was widely used throughout Europe (Fröhlich et al., 2015; Minguillón et al., 2015; Crenn et al., 2015). The 1-year campaign in Cabauw, Netherlands using an ACSM in combination with PMF found OOA dominated the OA throughout the campaign (61-84%) (Schlag et al., 2016). Due to the large secondary fraction (ammonium nitrate, sulfate, and OOA), the reduction of particulate air pollution is challenging on a local scale but requires a regional effort (Schlag et al., 2016). The 1-year deployment of ACSM at Montseny regional background site in the western Mediterranean, Spain, found OA was the major component of PM_1 mass (53%) (Ripoll et al., 2015). Source apportionment revealed that OOA dominated the OA, with a higher contribution in summer (85% of OA) than winter (60%). Two POA factors (BBOA and HOA) were found in winter while only one POA (i.e., traffic-related HOA) was resolved in summer (Ripoll et al., 2015). Petit et al. (2015) launched a two-year campaign in the region of Paris using an ACSM and other collocated instruments (e.g., Aethalometer). PMF analysis found OOA was a major component of OA during spring and summer while POA was more

pronounced during wintertime (Petit et al., 2015).

As mentioned above, Ireland experienced severe air pollution in the 1980s due to the solid fuel burning especially from coal burning (Kelly and Clancy, 1984). After the introduction of the ban on the marketing, sale, and distribution of coal in 1990, the air quality has improved significantly (Goodman et al., 2009). However, a recent study in Cork (Kourtchev et al., 2011) found that domestic solid fuel is still the major source of organic carbon during autumn (66.4%) and winter (74.9%), despite the ban on bituminous coal. Later, the AMS-PMF study in winter Cork (Dall'Osto et al., 2013) found 4 types of POA (HOA, BBOA, COA, and peat/coal burning (PCOA)) and one type of OOA (LV-OOA). The sum of POA accounted for 82% of OA, indicating an important role of local emission especially from wood, peat, and coal burning. These studies suggest that the ban on bituminous coal alone is not sufficient to improve air quality since peat and wood emit similar or higher amounts of PM when burned.

The two studies mentioned above were conducted in Cork city, located in the southern part of Ireland (Kourtchev et al., 2011; Dall'Osto et al., 2013). However, sources contributing to air quality in other locations, such as Dublin or west coast of Ireland, remain poorly understood. Therefore, more source apportionment studies are still needed in order to investigate the spatial distribution of aerosol and to evaluate local and regional aerosol sources. What's more, the information on sources retrieved from the source apportionment is important to study the particle related health effects.

1.2.8 AQ Network

AQ (air quality) monitoring network provides real-time, publicly accessible data from a number of monitoring stations in a specific region or country. AQ networks allow the public and authorities to gauge the air quality in relation to international standards and to report air pollution to encourage individual participation in improving the air quality. However, regulatory AQ networks mainly focus on PM mass monitoring and have no requirement to routinely measure chemical composition, let alone source apportionment. However, without the capabilities of source-apportionment, and the ability to unravel which sources contribute most to air pollution, effective emissions reduction strategies can perhaps only be a shot-in-the-dark. Sophisticated emissions reductions strategies are clearly required and these strategies need to be accurately informed by a next-generation observation

AQ network.

During historic air pollution events, Sulphur (Sulphur dioxide and sulfate) and black smoke often dominated the pollution levels, and were relatively straight forward to analytically quantify; however, as sulfate emissions have more or less been reduced by an order of magnitude since the acid rain days (Grigas et al., 2017), OA has typically replaced Sulphur as the main contributor to PM_1 pollution and its relative contribution, at least in developed regions like Europe and the USA, contributing 50% or more during the most severe pollution events (Grigas et al., 2017). The problem with OA dominating PM levels lies in the diversity of sources, both natural and anthropogenic, and the chemical complexity of the organic matter further compounded by the analytical challenges to source apportion organic species many of which have not yet even been identified. Without even broaching the aforementioned problems, the biggest problem is that OA is not chemically quantified in any AQ network, to begin with, let alone speciated. Therefore, sophisticated fingerprinting strategies in a next-generation air pollution observation network are critically required to better inform the development of effective mitigation policies and to ensure the most appropriate air pollution sources are targeted.

1.2.9 References

Albrecht, B. A.: Aerosols, cloud microphysics, and fractional cloudiness, Science (Washington, DC, United States), 245, 1227-1231, 1989.
Allan, J. D., Jimenez, J. L., Williams, P. I., Alfarra, M. R., Bower, K. N., Jayne, J. T., Coe, H., and Worsnop, D. R.: Quantitative sampling using an Aerodyne aerosol mass spectrometer 1. Techniques of data interpretation and error analysis, Journal of Geophysical Research: Atmospheres (1984–2012), 108, 2003.
Allan, J. D., Delia, A. E., Coe, H., Bower, K. N., Alfarra, M. R., Jimenez, J. L., Middlebrook, A. M., Drewnick, F., Onasch, T. B., Canagaratna, M. R., Jayne, J. T., and Worsnop, D. R.: A generalised method for the extraction of chemically resolved mass spectra from Aerodyne aerosol mass spectrometer data, J. Aerosol Sci., 35, 909-922, 2004.
Atkinson, R. W., Kang, S., Anderson, H. R., Mills, I. C., and Walton, H. A.: Epidemiological time series studies of PM_{2.5} and daily mortality and hospital admissions: a systematic review and meta-analysis, Thorax, 69, 660-665, 2014.
Bi, X., Sheng, G., Peng, P. a., Chen, Y., Zhang, Z., and Fu, J.: Distribution of particulate- and vapor-phase n-alkanes and polycyclic aromatic hydrocarbons in urban atmosphere of Guangzhou, China, Atmospheric Environment, 37, 289-298, 2003.
Canagaratna, M. R., Jayne, J. T., Ghertner, D. A., Herndon, S., Shi, Q., Jimenez, J. L., Silva, P. J., Williams, P., Lanni, T., Drewnick, F., Demerjian, K. L., Kolb, C. E., and Worsnop, D. R.: Chase Studies of Particulate Emissions from in-use New York City Vehicles, Aerosol Sci. Tech., 38, 555-573, 2004.
Canagaratna, M. R., Jayne, J. T., Jimenez, J. L., Allan, J. D., Alfarra, M. R., Zhang, Q., Onasch, T. B., Drewnick, F., Coe, H., Middlebrook, A., Delia, A., Williams, L. R., Trimborn, A. M., Northway, M. J., DeCarlo, P. F., Kolb, C. E., Davidovits, P., and Worsnop, D. R.: Chemical and microphysical characterization of ambient aerosols with the Aerodyne aerosol mass spectrometer, Mass Spectrom. Rev., 26, 185-222, 2007.
Canonaco, F., Crippa, M., Slowik, J. G., Baltensperger, U., and Prévôt, A. S. H.: SoFi, an IGOR-based interface for the efficient use of the generalized multilinear engine (ME-2) for the source apportionment: ME-2 application to aerosol mass spectrometer data, Atmos. Meas. Tech., 6, 3649-3661, 2013.
Canonaco, F., Slowik, J. G., Baltensperger, U., and Prévôt, A. S. H.: Seasonal differences in oxygenated organic aerosol composition: Implications for emissions sources and factor analysis, Atmospheric Chemistry and Physics, 15, 6993-7002, 2015.
Charrier, J. G., and Anastasio, C.: On dithiothreitol (DTT) as a measure of oxidative potential for ambient particles: evidence for the importance of soluble transition metals, Atmospheric Chemistry and Physics, 12, 9321-9333, 2012.
Clancy, L., Goodman, P., Sinclair, H., and Dockery, D. W.: Effect of air-pollution control on death rates in Dublin, Ireland: an intervention study, The Lancet, 360, 1210-1214, 2002.
Crenn, V., Sciare, J., Croteau, P. L., Verlhac, S., Fröhlich, R., Belis, C. A., Aas, W., Äijälä, M., Alastuey, A., Artiñano, B., Baisnée, D., Bonnaire, N., Bressi, M., Canagaratna, M., Canonaco, F., Carbone, C., Cavalli, F., Coz, E., Cubison, M. J., Esser-Gietl, J. K., Green, D. C., Gros, V., Heikkinen, L., Herrmann, H., Lunder, C., Minguillón, M. C., Močnik, G., O'Dowd, C. D., Ovadnevaite, J., Petit, J. E., Petralia, E., Poulain, L., Priestman, M., Riffault, V., Ripoll, A., Sarda-Estève, R., Slowik, J. G., Setyan, A., Wiedensohler, A., Baltensperger, U., Prévôt, A. S. H., Jayne, J. T., and Favez, O.: ACTRIS ACSM intercomparison – Part I: Reproducibility of concentration and fragment results from

13 individual Quadrupole Aerosol Chemical Speciation Monitors (Q-ACSM) and consistency with Time-of-Flight ACSM (ToF-ACSM), High Resolution ToF Aerosol Mass Spectrometer (HR-ToF-AMS) and other co-located instruments, Atmos. Meas. Tech. Discuss., 8, 7239-7302, 2015.
Crippa, M., Canonaco, F., Lanz, V. A., Äijälä, M., Allan, J. D., Carbone, S., Capes, G., Ceburnis, D., Dall'Osto, M., Day, D. A., DeCarlo, P. F., Ehn, M., Eriksson, A., Freney, E., Hildebrandt Ruiz, L., Hillamo, R., Jimenez, J. L., Junninen, H., Kiendler-Scharr, A., Kortelainen, A. M., Kulmala, M., Laaksonen, A., Mensah, A. A., Mohr, C., Nemitz, E., O'Dowd, C., Ovadnevaite, J., Pandis, S. N., Petäjä, T., Poulain, L., Saarikoski, S., Sellegri, K., Swietlicki, E., Tiitta, P., Worsnop, D. R., Baltensperger, U., and Prévôt, A. S. H.: Organic aerosol components derived from 25 AMS data sets across Europe using a consistent ME-2 based source apportionment approach, Atmospheric Chemistry and Physics, 14, 6159-6176, 2014.
Dall'Osto, M., Ovadnevaite, J., Ceburnis, D., Martin, D., Healy, R. M., O'Connor, I. P., Kourtchev, I., Sodeau, J. R., Wenger, J. C., and O'Dowd, C.: Characterization of urban aerosol in Cork city (Ireland) using aerosol mass spectrometry, Atmospheric Chemistry and Physics, 13, 4997-5015, 2013.
DeCarlo, P. F., Kimmel, J. R., Trimborn, A., Northway, M. J., Jayne, J. T., Aiken, A. C., Gonin, M., Fuhrer, K., Horvath, T., Docherty, K. S., Worsnop, D. R., and Jimenez, J. L.: Field-Deployable, High-Resolution, Time-of-Flight Aerosol Mass Spectrometer, Analytical Chemistry, 78, 8281-8289, 2006.
Delfino, R. J., Staimer, N., Tjoa, T., Gillen, D. L., Schauer, J. J., and Shafer, M. M.: Airway inflammation and oxidative potential of air pollutant particles in a pediatric asthma panel, Journal Of Exposure Science And Environmental Epidemiology, 23, 466, 2013.
DeWitt, H. L., Hellebust, S., Temime-Roussel, B., Ravier, S., Polo, L., Jacob, V., Buisson, C., Charron, A., André, M., Pasquier, A., Besombes, J. L., Jaffrezo, J. L., Wortham, H., and Marchand, N.: Near-highway aerosol and gas-phase measurements in a high-diesel environment, Atmospheric Chemistry and Physics, 15, 4373-4387, 2015.
Drewnick, F., Hings, S. S., DeCarlo, P., Jayne, J. T., Gonin, M., Fuhrer, K., Weimer, S., Jimenez, J. L., Demerjian, K. L., Borrmann, S., and Worsnop, D. R.: A new time-of-flight aerosol mass spectrometer (TOF-AMS) - Instrument description and first field deployment, Aerosol Sci. Techn., 39, 637-658, 2005.
Drinovec, L., Močnik, G., Zotter, P., Prévôt, A. S. H., Ruckstuhl, C., Coz, E., Rupakheti, M., Sciare, J., Müller, T., Wiedensohler, A., and Hansen, A. D. A.: The "dual-spot" Aethalometer: an improved measurement of aerosol black carbon with real-time loading compensation, Atmos. Meas. Tech., 8, 1965-1979, 2015.
Elser, M., Huang, R. J., Wolf, R., Slowik, J. G., Wang, Q., Canonaco, F., Li, G., Bozzetti, C., Daellenbach, K. R., Huang, Y., Zhang, R., Li, Z., Cao, J., Baltensperger, U., El-Haddad, I., and André, P.: New insights into PM2.5 chemical composition and sources in two major cities in China during extreme haze events using aerosol mass spectrometry, Atmospheric Chemistry and Physics, 16, 3207-3225, 2016.
Ferek, R. J., Garrett, T., Hobbs, P. V., Strader, S., Johnson, D., Taylor, J. P., Nielsen, K., Ackerman, A. S., Kogan, Y., and Liu, Q.: Drizzle suppression in ship tracks, Journal of the Atmospheric Sciences, 57, 2707-2728, 2000.
Fröhlich, R., Cubison, M. J., Slowik, J. G., Bukowiecki, N., Prévôt, A. S. H., Baltensperger, U., Schneider, J., Kimmel, J. R., Gonin, M., Rohner, U., Worsnop, D. R., and Jayne, J. T.: The ToF-ACSM: a portable aerosol chemical speciation monitor with TOFMS detection, Atmos. Meas. Tech., 6, 3225-3241, 2013.
Fröhlich, R., Crenn, V., Setyan, A., Belis, C. A., Canonaco, F., Favez, O., Riffault, V., Slowik, J. G., Aas, W., Aijälä, M., Alastuey, A., Artiñano, B., Bonnaire, N., Bozzetti, C., Bressi, M., Carbone, C., Coz, E., Croteau, P. L., Cubison, M. J., Esser-Gietl, J. K., Green, D. C., Gros, V., Heikkinen, L.,

Herrmann, H., Jayne, J. T., Lunder, C. R., Minguillón, M. C., Močnik, G., O'Dowd, C. D., Ovadnevaite, J., Petralia, E., Poulain, L., Priestman, M., Ripoll, A., Sarda-Estève, R., Wiedensohler, A., Baltensperger, U., Sciare, J., and Prévôt, A. S. H.: ACTRIS ACSM intercomparison – Part 2: Intercomparison of ME-2 organic source apportionment results from 15 individual, co-located aerosol mass spectrometers, Atmos. Meas. Tech. Discuss., 8, 1559-1613, 2015.

Fuzzi, S., Baltensperger, U., Carslaw, K., Decesari, S., Denier van der Gon, H., Facchini, M. C., Fowler, D., Koren, I., Langford, B., Lohmann, U., Nemitz, E., Pandis, S., Riipinen, I., Rudich, Y., Schaap, M., Slowik, J. G., Spracklen, D. V., Vignati, E., Wild, M., Williams, M., and Gilardoni, S.: Particulate matter, air quality and climate: lessons learned and future needs, Atmospheric Chemistry and Physics, 15, 8217-8299, 2015.

Geng, F., Tie, X., Xu, J., Zhou, G., Peng, L., Gao, W., Tang, X., and Zhao, C.: Characterizations of ozone, NOx, and VOCs measured in Shanghai, China, Atmospheric Environment, 42, 6873-6883, 2008.

Gentner, D. R., Jathar, S. H., Gordon, T. D., Bahreini, R., Day, D. A., El Haddad, I., Hayes, P. L., Pieber, S. M., Platt, S. M., de Gouw, J., Goldstein, A. H., Harley, R. A., Jimenez, J. L., Prévôt, A. S. H., and Robinson, A. L.: Review of Urban Secondary Organic Aerosol Formation from Gasoline and Diesel Motor Vehicle Emissions, Environmental Science & Technology, 51, 1074-1093, 2017.

Goodman, P. G., Rich, D. Q., Zeka, A., Clancy, L., and Dockery, D. W.: Effect of air pollution controls on black smoke and sulfur dioxide concentrations across Ireland, J. Air Waste Manag. Assoc., 59, 207-213, 2009.

Grigas, T., Ovadnevaite, J., Ceburnis, D., Moran, E., McGovern, F. M., Jennings, S. G., and O'Dowd, C.: Sophisticated clean air strategies required to mitigate against particulate organic pollution, Sci. Rep., 7, 2017.

Hallquist, M., Wenger, J. C., Baltensperger, U., Rudich, Y., Simpson, D., Claeys, M., Dommen, J., Donahue, N. M., George, C., Goldstein, A. H., Hamilton, J. F., Herrmann, H., Hoffmann, T., Iinuma, Y., Jang, M., Jenkin, M. E., Jimenez, J. L., Kiendler-Scharr, A., Maenhaut, W., McFiggans, G., Mentel, T. F., Monod, A., Prévôt, A. S. H., Seinfeld, J. H., Surratt, J. D., Szmigielski, R., and Wildt, J.: The formation, properties and impact of secondary organic aerosol: current and emerging issues, Atmospheric Chemistry and Physics, 9, 5155-5236, 2009.

Heal, M. R., Hibbs, L. R., Agius, R. M., and Beverland, I. J.: Interpretation of variations in fine, coarse and black smoke particulate matter concentrations in a northern European city, Atmospheric Environment, 39, 3711-3718, 2005.

Huang, R.-J., Zhang, Y., Bozzetti, C., Ho, K.-F., Cao, J.-J., Han, Y., Daellenbach, K. R., Slowik, J. G., Platt, S. M., and Canonaco, F.: High secondary aerosol contribution to particulate pollution during haze events in China, Nature, 514, 218, 2014.

Jayne, J. T., Leard, D. C., Zhang, X., Davidovits, P., Smith, K. A., Kolb, C. E., and Worsnop, D. R.: Development of an aerosol mass spectrometer for size and composition analysis of submicron particles, Aerosol Science and Technology, 33, 49-70, 2000.

Jimenez, J. L., Canagaratna, M. R., Donahue, N. M., Prevot, A. S. H., Zhang, Q., Kroll, J. H., DeCarlo, P. F., Allan, J. D., Coe, H., Ng, N. L., Aiken, A. C., Docherty, K. S., Ulbrich, I. M., Grieshop, A. P., Robinson, A. L., Duplissy, J., Smith, J. D., Wilson, K. R., Lanz, V. A., Hueglin, C., Sun, Y. L., Tian, J., Laaksonen, A., Raatikainen, T., Rautiainen, J., Vaattovaara, P., Ehn, M., Kulmala, M., Tomlinson, J. M., Collins, D. R., Cubison, M. J., E., Dunlea, J., Huffman, J. A., Onasch, T. B., Alfarra, M. R., Williams, P. I., Bower, K., Kondo, Y., Schneider, J., Drewnick, F., Borrmann, S., Weimer, S., Demerjian, K., Salcedo, D., Cottrell, L., Griffin, R., Takami, A., Miyoshi, T., Hatakeyama, S., Shimono, A., Sun, J. Y., Zhang, Y. M., Dzepina, K., Kimmel, J. R., Sueper, D., Jayne, J. T., Herndon, S. C., Trimborn, A. M., Williams, L. R., Wood, E. C., Middlebrook, A. M., Kolb, C. E., Baltensperger, U., and Worsnop, D. R.: Evolution of Organic Aerosols in the

Atmosphere, Science (Washington, DC, United States), 326, 1525-1529, 2009.
Kamal, A., Cincinelli, A., Martellini, T., and Malik, R. N.: A review of PAH exposure from the combustion of biomass fuel and their less surveyed effect on the blood parameters, Environmental Science and Pollution Research, 22, 4076-4098, 2015.
Kelly, I., and Clancy, L.: Mortality in a general hospital and urban air pollution, Irish medical journal, 77, 322-324, 1984.
Kemp, D. D.: Exploring environmental issues: An integrated approach, Routledge, 2004.
Kourtchev, I., Hellebust, S., Bell, J. M., O'Connor, I. P., Healy, R. M., Allanic, A., Healy, D., Wenger, J. C., and Sodeau, J. R.: The use of polar organic compounds to estimate the contribution of domestic solid fuel combustion and biogenic sources to ambient levels of organic carbon and PM2.5 in Cork Harbour, Ireland, Science of the Total Environment, 409, 2143-2155, 2011.
Kroll, J. H., and Seinfeld, J. H.: Chemistry of secondary organic aerosol: Formation and evolution of low-volatility organics in the atmosphere, Atmospheric Environment, 42, 3593-3624, 2008.
Künzli, N., Mudway Ian, S., Götschi, T., Shi, T., Kelly Frank, J., Cook, S., Burney, P., Forsberg, B., Gauderman James, W., Hazenkamp Marianne, E., Heinrich, J., Jarvis, D., Norbäck, D., Payo-Losa, F., Poli, A., Sunyer, J., and Borm Paul, J. A.: Comparison of Oxidative Properties, Light Absorbance, and Total and Elemental Mass Concentration of Ambient PM2.5 Collected at 20 European Sites, Environmental Health Perspectives, 114, 684-690, 2006.
Lanz, V. A., Alfarra, M. R., Baltensperger, U., Buchmann, B., Hueglin, C., Szidat, S., Wehrli, M. N., Wacker, L., Weimer, S., Caseiro, A., Puxbaum, H., and Prevot, A. S. H.: Source attribution of submicron organic aerosols during wintertime inversions by advanced factor analysis of aerosol mass spectra, Environ. Sci. Tech., 42, 214-220, 2008.
Lanz, V. A., Prévôt, A. S. H., Alfarra, M. R., Weimer, S., Mohr, C., Decarlo, P. F., Gianini, M. F. D., Hueglin, C., Schneider, J., Favez, O., D'Anna, B., George, C., and Baltensperger, U.: Characterization of aerosol chemical composition with aerosol mass spectrometry in Central Europe: An overview, Atmospheric Chemistry and Physics, 10, 10453-10471, 2010.
Lee, S., Liu, W., Wang, Y., Russell, A. G., and Edgerton, E. S.: Source apportionment of PM2.5: Comparing PMF and CMB results for four ambient monitoring sites in the southeastern United States, Atmospheric Environment, 42, 4126-4137, 2008.
Lelieveld, J., Evans, J. S., Fnais, M., Giannadaki, D., and Pozzer, A.: The contribution of outdoor air pollution sources to premature mortality on a global scale, Nature, 525, 367-371, 2015.
Li, Y. J., Sun, Y., Zhang, Q., Li, X., Li, M., Zhou, Z., and Chan, C. K.: Real-time chemical characterization of atmospheric particulate matter in China: A review, Atmos. Environ., 158, 270-304, 2017.
Liang, F., Xiao, Q., Gu, D., Xu, M., Tian, L., Guo, Q., Wu, Z., Pan, X., and Liu, Y.: Satellite-based short- and long-term exposure to PM2.5 and adult mortality in urban Beijing, China, Environmental Pollution, 242, 492-499, 2018.
Lohmann, U., and Feichter, J.: Global indirect aerosol effects: a review, Atmospheric Chemistry and Physics, 5, 715-737, 2005.
Minguillón, M. C., Ripoll, A., Pérez, N., Prévôt, A. S. H., Canonaco, F., Querol, X., and Alastuey, A.: Chemical characterization of submicron regional background aerosols in the western Mediterranean using an Aerosol Chemical Speciation Monitor, Atmospheric Chemistry and Physics, 15, 6379-6391, 2015.
Mohr, C., DeCarlo, P. F., Heringa, M. F., Chirico, R., Slowik, J. G., Richter, R., Reche, C., Alastuey, A., Querol, X., Seco, R., Peñuelas, J., Jiménez, J. L., Crippa, M., Zimmermann, R., Baltensperger, U., and Prévôt, A. S. H.: Identification and quantification of organic aerosol from cooking and other sources in Barcelona using aerosol mass spectrometer data, Atmospheric Chemistry and Physics, 12, 1649-1665, 2012.

Myhre, G., Shindell, D., Bréon, F.-M., Collins, W., Fuglestvedt, J., Huang, J., Koch, D., Lamarque, J.-F., Lee, D., and Mendoza, B.: Anthropogenic and natural radiative forcing, Climate change, 423, 658-740, 2013.
Neer, A., and Koylu, U. O.: Effect of operating conditions on the size, morphology, and concentration of submicrometer particulates emitted from a diesel engine, Combustion and Flame, 146, 142-154, 2006.
Ng, N. L., Herndon, S. C., Trimborn, A., Canagaratna, M. R., Croteau, P. L., Onasch, T. B., Sueper, D., Worsnop, D. R., Zhang, Q., Sun, Y. L., and Jayne, J. T.: An Aerosol Chemical Speciation Monitor (ACSM) for routine monitoring of the composition and mass concentrations of ambient aerosol, Aerosol Sci. Technol., 45, 780-794, 2011.
O'Dowd, C. D., Smith, M. H., Consterdine, I. E., and Lowe, J. A.: Marine aerosol, sea-salt, and the marine sulphur cycle: A short review, Atmospheric Environment, 31, 73-80, 1997.
O'Dowd, C. D., Facchini, M. C., Cavalli, F., Ceburnis, D., Mircea, M., Decesari, S., Fuzzi, S., Yoon, Y. J., and Putaud, J.-P.: Biogenically driven organic contribution to marine aerosol, Nature, 431, 676-680, 2004.
O'Dowd, C. D., and de Leeuw, G.: Marine aerosol production: a review of the current knowledge, Philosophical Transactions of the Royal Society A: Mathematical, Physical and Engineering Sciences, 365, 1753-1774, 2007.
Ovadnevaite, J., Ceburnis, D., Leinert, S., Dall'Osto, M., Canagaratna, M., O'Doherty, S., Berresheim, H., and O'Dowd, C.: Submicron NE Atlantic marine aerosol chemical composition and abundance: Seasonal trends and air mass categorization, J. Geophys. Res. Atmos., 119, 11,850-811,863, 2014.
Paatero, P., and Tapper, U.: Positive matrix factorization: a non-negative factor model with optimal utilization of error estimates of data values, Environmetrics, 5, 111-126, 1994.
Paatero, P., Hopke, P. K., Song, X. H., and Ramadan, Z.: Understanding and controlling rotations in factor analytic models, Chemometrics and Intelligent Laboratory Systems, 60, 253-264, 2002.
Parworth, C., Fast, J., Mei, F., Shippert, T., Sivaraman, C., Tilp, A., Watson, T., and Zhang, Q.: Long-term measurements of submicrometer aerosol chemistry at the Southern Great Plains (SGP) using an Aerosol Chemical Speciation Monitor (ACSM), Atmospheric Environment, 106, 43-55, 2015.
Petit, J. E., Favez, O., Sciare, J., Crenn, V., Sarda-Estève, R., Bonnaire, N., Močnik, G., Dupont, J. C., Haeffelin, M., and Leoz-Garziandia, E.: Two years of near real-time chemical composition of submicron aerosols in the region of Paris using an Aerosol Chemical Speciation Monitor (ACSM) and a multi-wavelength Aethalometer, Atmospheric Chemistry and Physics, 15, 2985-3005, 2015.
Pöschl, U.: Atmospheric Aerosols: Composition, Transformation, Climate and Health Effects, Angewandte Chemie International Edition, 44, 7520-7540, 2005.
Quincey, P.: A relationship between Black Smoke Index and Black Carbon concentration, Atmospheric Environment, 41, 7964-7968, 2007.
Radke, L. F., Coakley, J. A., and King, M. D.: Direct and remote sensing observations of the effects of ships on clouds, Science (Washington, DC, United States), 246, 1146-1149, 1989.
Ramanathan, V., and Carmichael, G.: Global and regional climate changes due to black carbon, Nature Geoscience, 1, 221, 2008.
Ramaswamy, V., Boucher, O., Haigh, J., Hauglustine, D., Haywood, J., Myhre, G., Nakajima, T., Shi, G., and Solomon, S.: Radiative forcing of climate, Climate change, 349, 2001.
Reyes-Villegas, E., Green, D. C., Priestman, M., Canonaco, F., Coe, H., Prévôt, A. S. H., and Allan, J. D.: Organic aerosol source apportionment in London 2013 with ME-2: exploring the solution space with annual and seasonal analysis, Atmospheric Chemistry and Physics, 16, 15545-15559, 2016.
Ripoll, A., Minguillón, M. C., Pey, J., Jimenez, J. L., Day, D. A., Sosedova, Y., Canonaco, F., Prévôt, A. S. H., Querol, X., and Alastuey, A.: Long-term real-time chemical characterization of submicron aerosols at Montsec (southern Pyrenees, 1570 m a.s.l.), Atmospheric Chemistry and Physics, 15,

2935-2951, 2015.
Sandström, T., Nowak, D., and van Bree, L.: Health effects of coarse particles in ambient air: messages for research and decision-making, European Respiratory Journal, 26, 187-188, 2005.
Sbihi, H., Brook, J. R., Allen, R. W., Curran, J. H., Dell, S., Mandhane, P., Scott, J. A., Sears, M. R., Subbarao, P., Takaro, T. K., Turvey, S. E., Wheeler, A. J., and Brauer, M.: A new exposure metric for traffic-related air pollution? An analysis of determinants of hopanes in settled indoor house dust, Environmental Health, 12, 48, 2013.
Schlag, P., Kiendler-Scharr, A., Johannes Blom, M., Canonaco, F., Sebastiaan Henzing, J., Moerman, M., Prévôt, A. S. H., and Holzinger, R.: Aerosol source apportionment from 1-year measurements at the CESAR tower in Cabauw, the Netherlands, Atmospheric Chemistry and Physics, 16, 8831-8847, 2016.
Sun, Y., Xu, W., Zhang, Q., Jiang, Q., Canonaco, F., Prévôt, A. S. H., Fu, P., Li, J., Jayne, J., Worsnop, D. R., and Wang, Z.: Source apportionment of organic aerosol from two-year highly time-resolved measurements by an aerosol chemical speciation monitor in Beijing, China, Atmos. Chem. Phys. Discuss., 2018, 1-33, 2018.
Sun, Y. L., Wang, Z. F., Fu, P. Q., Yang, T., Jiang, Q., Dong, H. B., Li, J., and Jia, J. J.: Aerosol composition, sources and processes during wintertime in Beijing, China, Atmospheric Chemistry and Physics, 13, 4577-4592, 2013.
Sun, Y. L., Wang, Z. F., Du, W., Zhang, Q., Wang, Q. Q., Fu, P. Q., Pan, X. L., Li, J., Jayne, J., and Worsnop, D. R.: Long-term real-time measurements of aerosol particle composition in Beijing, China: Seasonal variations, meteorological effects, and source analysis, Atmospheric Chemistry and Physics, 15, 10149-10165, 2015.
Totlandsdal, A. I., Låg, M., Lilleaas, E., Cassee, F., and Schwarze, P.: Differential proinflammatory responses induced by diesel exhaust particles with contrasting PAH and metal content, Environmental Toxicology, 30, 188-196, 2015.
Twomey, S.: Pollution and the planetary albedo, Atmospheric Environment (1967), 8, 1251-1256, 1974.
Valavanidis, A., Fiotakis, K., and Vlachogianni, T.: Airborne Particulate Matter and Human Health: Toxicological Assessment and Importance of Size and Composition of Particles for Oxidative Damage and Carcinogenic Mechanisms, Journal of Environmental Science and Health, Part C, 26, 339-362, 2008.
Verma, V., Ning, Z., Cho, A. K., Schauer, J. J., Shafer, M. M., and Sioutas, C.: Redox activity of urban quasi-ultrafine particles from primary and secondary sources, Atmospheric Environment, 43, 6360-6368, 2009.
Verma, V., Wang, Y., El-Afifi, R., Fang, T., Rowland, J., Russell, A. G., and Weber, R. J.: Fractionating ambient humic-like substances (HULIS) for their reactive oxygen species activity – Assessing the importance of quinones and atmospheric aging, Atmospheric Environment, 120, 351-359, 2015.
Wang, Y., Zhang, Q. Q., He, K., Zhang, Q., and Chai, L.: Sulfate-nitrate-ammonium aerosols over China: response to 2000–2015 emission changes of sulfur dioxide, nitrogen oxides, and ammonia, Atmospheric Chemistry and Physics, 13, 2635-2652, 2013.
Williams, L. R., Gonzalez, L. A., Peck, J., Trimborn, D., McInnis, J., Farrar, M. R., Moore, K. D., Jayne, J. T., Robinson, W. A., Lewis, D. K., Onasch, T. B., Canagaratna, M. R., Trimborn, A., Timko, M. T., Magoon, G., Deng, R., Tang, D., de la Rosa Blanco, E., Prévôt, A. S. H., Smith, K. A., and Worsnop, D. R.: Characterization of an aerodynamic lens for transmitting particles greater than 1 micrometer in diameter into the Aerodyne aerosol mass spectrometer, Atmos. Meas. Tech., 6, 3271-3280, 2013.
Xia, T., Kovochich, M., Brant, J., Hotze, M., Sempf, J., Oberley, T., Sioutas, C., Yeh, J. I., Wiesner,

M. R., and Nel, A. E.: Comparison of the Abilities of Ambient and Manufactured Nanoparticles To Induce Cellular Toxicity According to an Oxidative Stress Paradigm, Nano Letters, 6, 1794-1807, 2006.
Zhang, Q., Jimenez, J. L., Canagaratna, M. R., Ulbrich, I. M., Ng, N. L., Worsnop, D. R., and Sun, Y.: Understanding atmospheric organic aerosols via factor analysis of aerosol mass spectrometry: A review, Analytical and Bioanalytical Chemistry, 401, 3045-3067, 2011.
Zhang, X., van Geffen, J., Liao, H., Zhang, P., and Lou, S.: Spatiotemporal variations of tropospheric SO2 over China by SCIAMACHY observations during 2004–2009, Atmospheric Environment, 60, 238-246, 2012.
Zhang, Y. J., Tang, L. L., Wang, Z., Yu, H. X., Sun, Y. L., Liu, D., Qin, W., Canonaco, F., Prévôt, A. S. H., Zhang, H. L., and Zhou, H. C.: Insights into characteristics, sources, and evolution of submicron aerosols during harvest seasons in the Yangtze River Delta region, China, Atmospheric Chemistry and Physics, 15, 1331-1349, 2015.

2. Summary of Research Papers

This thesis consists of 7 peer-reviewed articles; 3 publications as lead author, 2 with major roles, and 2 with a moderate contribution.

Paper 1: lead author

Extreme air pollution from residential solid fuel burning

Lin, C., Huang, R.-J., Ceburnis, D., Buckley, P., Preissler, J., Wenger, J., Rinaldi, M., Facchini, M. C., O'Dowd, C., and Ovadnevaite, J., Nature Sustainability, 2018, 10.1038/s41893-018-0125-x.

This article provides a detailed characterization of the chemical composition and source apportionment of particulate air pollution in Dublin, stemming from the deployment of the national AQ network. Extraordinary levels of air pollution, with submicron aerosol (PM_1) mass concentration surpassing 300 μg m^{-3}, were observed in winter 2016. Carbonaceous aerosol (OA+BC) was the major component of PM_1, accounting for 88-89% of the total PM_1 mass while all inorganic components, sulfate (4%), nitrate (3-4%), ammonium (2%) and chloride (2%), were minor parts of the PM_1. Using the source apportionment technique (ME-2), up to 70% of the pollution were attributed to emissions from residential solid fuel - specifically peat and wood. Furthermore, we find that the consumption of peat and wood in up to 12% and 1% of households, respectively, contributed up to 70% of PM_1. The results from this approach can better inform emissions reduction policies and help to ensure the most appropriate air pollution sources are targeted.

I am credited with the ACSM data collection and quality assurance, as well as the instrument maintenance. I am also responsible for the processing of the ACSM data and writing ~60% of the manuscript.

Paper 2: lead author

Characterization of primary organic aerosol from domestic wood, peat, and coal burning in Ireland

Lin, C., Ceburnis, D., Hellebust, S., Buckley, P., Wenger, J., Canonaco, F., Prévôt, A. S. H., Huang, R.-J., O'Dowd, C., and Ovadnevaite, J., Environmental Science and Technology 2017, 51, 10624-10632.

In this article, an ACSM was deployed to sample the PM emitted from the burning of commercially available solid fuels (peat, coal, and wood). Organic mass spectra (MS) or fingerprints from burning wood, peat, and coal were characterized and intercompared. Their mass spectral profiles were constrained with the multilinear engine (ME-2) to estimate the contribution of solid fuel sources to ambient pollution in Galway, Ireland. The source apportionment results show that local source contribution had a dominant impact and comprised up to 88% of the total organic aerosol mass. Peat was found to be the dominant source, contributing 39% of OA, followed by oil (21%), coal (17%), and wood (11%). The source apportionment results suggest that the use of domestic solid fuels (peat, wood, and coal) for home heating is the major source of evening and night-time particulate pollution events despite their small use.

I am credited with the collection of PM samples emitted by peat, wood, and coal burning using an ACSM. I am also credited with the collection of the ambient PM sample in Galway. I am responsible for the processing of the data, forming the conclusion, and writing ~90% of the manuscript.

Paper 3: lead author

Non-marine summer time aerosol over the west of Ireland dominated by secondary processes during long range transport

Lin, C.; Ceburnis, D.; Huang, R.-J.; Canonaco, F.; Prévôt, A.S.H.; O'Dowd, C.; Ovadnevaite, J. Atmosphere 2019, 10, 59.

This article investigates the chemical composition and sources of non-refractory submicron aerosol (NR-PM_1) in Galway, during summer time in June 2016. Organic aerosol (OA) was found to be the major part of NR-PM_1 (54%). Free PMF and ME-2 factor analysis were conducted on the organic fraction. OOA was found to be the dominant OA factor, on average, accounting for 84% of the total OA. The rest 16% of OA were attributed to the emission from peat burning. Therefore, secondary organic and inorganic aerosol (sulfate (25%), ammonium (11%), and nitrate (10%)) together accounted for 91% of the total NR-PM_1. Concentration-Weighted Trajectory analysis indicates these secondary aerosols were mainly associated with easterly long-range transport from the UK and/or France.

I am credited with the data collection using an ACSM. I am also responsible for processing the data, forming the conclusion, and writing 90% of the manuscript.

Paper 4: Contributing author role – major

Primary emissions versus secondary formation of fine particulate matter in the most polluted city (Shijiazhuang) in North China

Huang, R.J.; Wang, Y.; Cao, J.; **Lin, C.;** Duan, J.; Chen, Q.; Li, Y.; Gu, Y.; Yan, J.; Xu, W.; Fröhlich, R.; Canonaco, F.; Bozzetti, C.; Ovadnevaite, J.; Ceburnis, D.; Canagaratna, M.R.; Jayne, J.; Worsnop, D.R.; El-Haddad, I.; Prévôt, A.S.H.; O'Dowd, C.D. Atmospheric Chemistry and Physics 2019, 19, 2283-2298.

This article studies the chemical composition and sources of PM_1 in urban Shijiazhuang (the capital of Hebei province), China, from 11 January to 18 February in 2014. The average mass concentration (± one standard deviation) of NR-PM_1 was 178 ± 101 μg m^{-3}. OA was the dominant component, accounting for 50% of the total NR-PM_1 mass, followed by sulfate (21%), nitrate (12%), ammonium (11%), and chloride (6%). Five OA sources were identified and quantified with ME-2, including HOA (13%), COA (16%), BBOA (17%), CCOA (27%), and OOA (27%). Secondary aerosol including sulfate, nitrate, ammonium, and OOA was found to contribute substantially (up to 55%) to PM in episodic events. However, the low OOA fraction (27%) in OA and the low sulfur oxidation degree (F_{SO4}) of 0.18 indicated the importance of primary particulate emissions. This study highlights an urgent need to reduce the primary emission while controlling the emission of secondary precursor gases in this highly polluted city in North China.

I am credited with ACSM data processing, ME-2 source apportionment, and interpretation of the results. I contributed to ~30% of the scientific input and writing

Paper 5: Contributing author role – major

Source-Specific Health Risk Analysis on Particulate Trace Elements: Coal Combustion and Traffic Emission as Major Contributors in Wintertime Beijing.

Huang, R.J.; Cheng, R.; Jing, M.; Yang, L.; Li, Y.; Chen, Q.; Chen, Y.; Yan, J.; **Lin, C.;** Wu, Y.; Zhang, R.; El Haddad, I.; Prevot, A.S.H.; O'Dowd, C.D.; Cao, J. Environmental Science and Technology 2018, 52, 10967-10974.

This article presents the link between emission sources of particulate trace elements and health risks in wintertime Beijing. Fe, Zn, and Pb were the most abundant elements over the measurement period and were up to 7.3 times higher during the pollution period. Pb, Mn, Cd, As, Sr, Co, V, Cu, and Ni were found to be present mainly in the bioavailable fraction. Using PMF, four sources were identified including dust, oil combustion, coal combustion, and traffic. Traffic-related emission was dominant during low pollution periods, contributing ~65% of total trace element mass. However, during severe pollution periods, coal combustion increased its contribution to 58%. Through the combination of the source apportionment results and element-specific health risk evaluation, coal combustion-related particulate trace elements were found to dominate the health risks during pollution periods.

I contributed to this paper by providing expertise in PMF analysis of the trace elements source apportionment, as well as interpretation of the results. I contributed to ~20% of the scientific input and writing.

Paper 6: contributing author role – moderate

Organosulfates in atmospheric aerosol: Synthesis and quantitative analysis of $PM_{2.5}$ from Xi'an, Northwestern China

Huang, R.J.; Cao, J.; Chen, Y.; Yang, L.; Shen, J.; You, Q.; Wang, K.; **Lin, C.;** Xu, W.; Gao, B.; Li, Y.; Chen, Q.; Hoffmann, T.; O'Dowd, C.D.; Bilde, M.; Glasius, M. Atmospheric Measurement Techniques 2018, 11, 3447-3456.

This article reports the synthesis of nine authentic organosulfate standards which were used to quantify their ambient concentrations. Ambient $PM_{2.5}$ samples were collected in winter 2013/2014 in urban Xi'an, northwestern China. Glycolic acid sulfate was found to be the most abundant species among the identified organosulfates, with an average concentration of 77.3 ± 49.2 ng m^{-3}. Hydroxyacetone sulfate (1.3 ± 0.5 ng m^{-3}), phenyl sulfate (0.14 ± 0.09 ng m^{-3}), and benzyl sulfate (0.04 ± 0.01 ng m^{-3}) were the minor species. Most of the organosulfates quantified show an increasing trend with an increase in the mass concentrations of organic carbon, indicating their anthropogenic origin. In contrast, Hydroxyacetone sulfate seems to have a biogenic origin in this region.

I contributed to this paper by providing expertise in the interpretation of the ambient organosulfate data. I contributed to ~10% of the scientific input and writing.

Paper 7: contributing author role – moderate

Brown Carbon Aerosol in Urban Xi'an, Northwest China: The Composition and Light Absorption Properties.

Huang, R.J.; Yang, L.; Cao, J.; Chen, Y.; Chen, Q.; Li, Y.; Duan, J.; Zhu, C.; Dai, W.; Wang, K.; **Lin, C.;** Ni, H.; Corbin, J.C.; Wu, Y.; Zhang, R.; Tie, X.; Hoffmann, T.; O'Dowd, C.; Dusek, U. Environmental Science and Technology 2018, 52, 6825-6833.

This article reports the link between BrC optical properties and chemical composition. The spectrophotometric measurements and chemical analyses of BrC samples were collected in Xi'an, Northwest China from July 2008 to June 2009. BrC concentration was 5 times higher in winter than that in summer, due to an increased biomass burning. The light absorption coefficient of methanol-soluble BrC at 365 nm was, on average, twice that of the water-soluble BrC. In addition, it correlated strongly with ($r^2 > 0.61$) that parent-PAHs and carbonyl-OPAHs. The fractional solar absorption by BrC relative to element carbon (EC) in the ultraviolet range (300-400 nm) is 42 ± 18% for water-soluble BrC and 76 ± 29% for methanol-soluble BrC, suggesting the significant role of BrC in affecting the radiative balance and tropospheric photochemistry, therefore, affecting the climate and air quality.

I contributed to this paper by providing expertise in the interpretation of the ambient brown carbon data. I contributed to ~10% of the scientific input and writing

3. Research Papers

ANALYSIS
https://doi.org/10.1038/s41893-018-0125-x
nature sustainability

Extreme air pollution from residential solid fuel burning

Chunshui Lin[1,2,3], Ru-Jin Huang[1,3]*, Darius Ceburnis[1,2], Paul Buckley[4], Jana Preissler[1,2], John Wenger[4], Matteo Rinaldi[5], Maria Christina Facchini[5], Colin O'Dowd[1,2]* and Jurgita Ovadnevaite[1,2]

Atmospheric aerosol particles (also known as particulate matter) are central to the cause of the two greatest threats to human security: air pollution (~5 million premature deaths per year) and climate change (~0.5 million per year). Addressing these threats requires an understanding of particulate matter sources responsible for both extreme air pollution immediately affecting human health and less extreme levels affecting climate over longer timescales. Here, extraordinary levels of air pollution, with submicrometre aerosol (PM_1) mass concentration surpassing 300 $\mu g\,m^{-3}$, were observed in a moderately sized European city and are attributed to emissions from residential solid fuel—specifically peat and wood, often promoted as 'slow-renewable', 'low-carbon' or 'carbon-neutral' biomass. Using sophisticated fingerprinting techniques, we find that consumption of peat and wood in up to 12% and 1% of households, respectively, contributed up to 70% of PM_1. The results from this approach can better inform emissions reduction policies and help to ensure the most appropriate air pollution sources are targeted. Given the far greater abundance of solid fuels and concomitant emissions required to match the calorific benefit of liquid fuels, even modest increases in the consumption of 'green'-marketed solid fuels will disproportionally increase the frequency of extreme pollution events.

Particulate matter (PM) is well known to have adverse effects on human health, both in terms of mortality rates and reduced lifespan[1–3]. The World Health Organization (WHO) recommends a 24 hour average $PM_{2.5}$ (that is, PM mass occurring at sizes less than 2.5 µm diameter) limit value of 25 $\mu g\,m^{-3}$ not to be exceeded[4]. However, WHO also notes that there is no identifiable $PM_{2.5}$ threshold below which no adverse health effects would be anticipated[4]. While the quantification of the health effects of $PM_{2.5}$ is still under intense scientific investigation[5], reduction in $PM_{2.5}$ emissions from power[6], transport[7] and industry[8] sectors has mainly been the focus of policy development. As a result, measures such as the introduction of strict emission standards, fuel regulation (from the Euro 4 to Euro 5 standard) and after treatment, such as an end-of-tailpipe particle filter, have been widely deployed with great success[9–11]. For instance, a French study found that only ~20% of organic PM mass was attributed to traffic emission, even directly adjacent to heavy-traffic roads, with the rest being modern carbon sources (for example, biomass and biogenic sources)[12]. Other studies have also reported high modern carbon fractions, even in cities with high vehicular volume (for example, Mexico City[13] and Barcelona[14]). In contrast, the emissions from private households are relatively less emphasized although they are potentially important sources of air pollution[15].

Solid fuels, such as wood and coal, are widely consumed as primary cooking and heating fuels especially in developing countries[16]. Due to the poor combustion efficiency and lack of emission controls, domestic burning of solid fuels has caused severe air pollution leading to millions of premature deaths[17]. Even in highly developed areas (for example, London and Paris), domestic solid fuel burning was found to affect local air quality significantly[18–22]. For example, 25–34% of organic aerosol (OA) mass was attributed to solid fuel burning in a study conducted in London[22]; however, the implications for policymaking are not clear due to poorly investigated links between solid fuel type, consumption and ultimately their contribution to air pollution.

Regulatory air quality monitoring networks in Europe (for example, www.aqicn.org/map/europe/) mainly focus on PM mass monitoring and have no requirement to routinely measure chemical composition in urban areas. Without information on chemical composition and the ability to unravel which sources contribute most to particulate air pollution, effective emissions reduction strategies can perhaps only be a shot in the dark. Air monitoring networks such as the United State's IMPROVE (Interagency Monitoring of Protected Visual Environments) and CSN (Chemical Speciation Networks)[23] monitor chemically speciated PM in support of regulations; however, sophisticated fingerprinting strategies in a next-generation air pollution observation network are critically required to better inform the development of effective and specifically targeted emission controls[24].

In attempting to meet these challenges, we demonstrate success in identifying dominant contributions from specific sources, despite their consumption not being dominant, stemming from the deployment of the pilot submicrometre aerosol (PM_1) national monitoring network. The pilot network incorporates four nodes that are strategically positioned across Ireland to capture and quantify the import and export of air pollution. In this study, we focus on the source-apportionment results from one node of the network deployed in a low-density residential area of south Dublin due to extremely large PM_1 concentrations registered there.

Details of the methods and measurement sites are available in the Methods. Briefly, an aerosol chemical speciation monitor (ACSM)[25]

[1]School of Physics, Centre for Climate and Air Pollution Studies, Ryan Institute, National University of Ireland Galway, Galway, Ireland. [2]Marine and Renewable Energy Ireland, Ryan Institute, National University Ireland Galway, Galway, Ireland. [3]State Key Laboratory of Loess and Quaternary Geology and Key Laboratory of Aerosol Chemistry and Physics, Institute of Earth Environment, Chinese Academy of Sciences, Xi'an, China. [4]Department of Chemistry and Environmental Research Institute, University College Cork, Cork, Ireland. [5]Instituto di Scienze dell'Atmosfera–CNR, Bologna, Italy.
*e-mail: rujin.huang@ieecas.cn; colin.odowd@nuigalway.ie

NATURE SUSTAINABILITY ANALYSIS

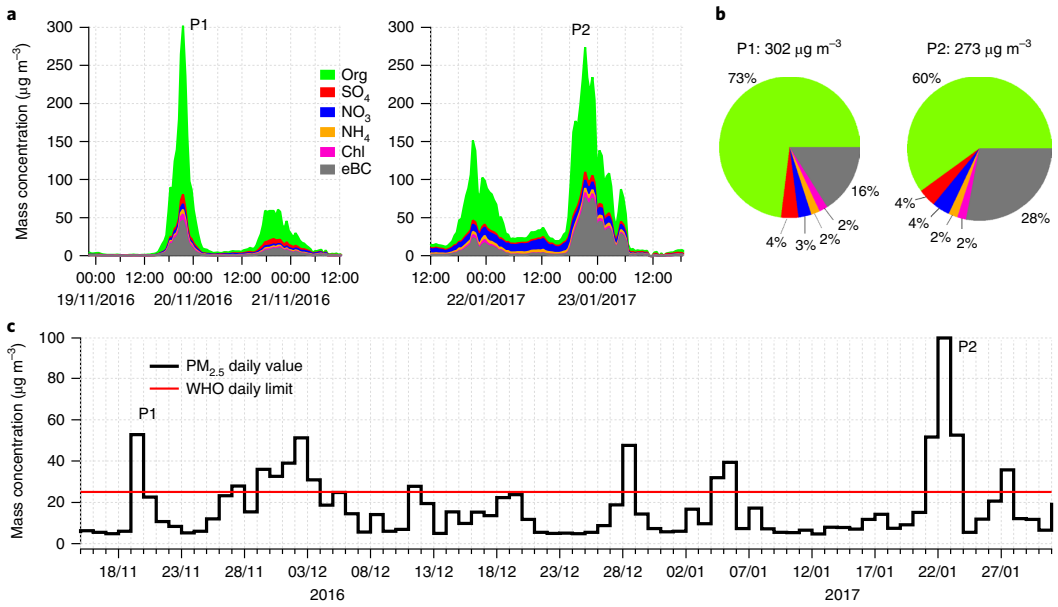

Fig. 1 | Chemical composition of PM_1 during two extreme pollution events. a, Two extreme pollution events on 19 November 2016 (P1) and 22 January 2017 (P2) in Dublin were picked out to be the focus of this study. Organics (Org), sulfate (SO_4), nitrate (NO_3), ammonium (NH_4) and chloride (Chl) were measured at UCD by an Aerodyne ACSM with 30 min resolution. eBC was measured by a collocated aethalometer (AE-33) with 1 min resolution. **b**, Relative contribution of the PM_1 components at the peak concentrations of 302 μg m^{-3} (P1) and 273 μg m^{-3} (P2). **c**, Time series of $PM_{2.5}$ mass concentration measured in Dublin and the WHO[4] daily limit (25 μg m^{-3}). $PM_{2.5}$ was measured with a tapered element oscillating microbalance at Rathmines station, ~3 km away from UCD. Hourly $PM_{2.5}$ data were averaged to 24 h.

and an aethalometer (AE-33)[26] were deployed at University College Dublin (UCD) to measure the PM_1 composition and mass with continuous measurements and have been running since August 2016. Source apportionment of OA was performed on the ACSM data using positive matrix factorization (PMF) with the multilinear engine (ME-2)[27–31]. Equivalent black carbon (eBC) source apportionment was performed with an Ångström exponent model[32].

PM_1 mass concentration and size distribution

Extreme pollution events were observed frequently by the air quality network between 15 November 2016 and 31 January 2017 (Fig. 1). Two events, on 19 November 2016 (P1) and 22 January 2017 (P2), are the focus of this study due to the particularly high concentrations encountered. The PM_1 peak concentrations were 302 μg m^{-3} for P1 and 273 μg m^{-3} for P2.

During winter, the WHO daily limit[4] of $PM_{2.5}$ (25 μg m^{-3}) was frequently exceeded (~20% of the time, or 1 in 5 days; Fig. 1c). $PM_{2.5}$ mass concentration was simultaneously monitored at the Rathmines regulatory air quality station approximately 3 km away from the UCD measurement site. Despite such a distance, an excellent temporal coherence is seen ($R^2 = 0.87$) between PM_1 and $PM_{2.5}$ (Supplementary Fig. 1). The good agreement between the PM concentrations at both locations indicate that these events were not due to a single local source (for example, a car passing by) but were simultaneously influenced by a pollution plume, covering a spatial scale of at least 3 km in radius. Indeed, for a wind speed of 2 m s^{-1}, a 30 min sample time corresponds to a spatial scale of 3.6 km. The slope of the correlation between PM_1 and $PM_{2.5}$ indicates that PM_1 mass, on average, accounted for 74% of $PM_{2.5}$ during the entire measurement period. However, the mass ratios of $PM_1/PM_{2.5}$ were close to 1 during P1 and P2 events, indicating the dominance of smaller particles. For the two events, the observed PM_1 size distribution comprised a monomodal size distribution with modal diameter at 90 nm (Supplementary Fig. 2), present in concentrations 20–25 times higher than those of non-event. Smaller particles can penetrate deeper into lungs and potentially into the bloodstream[5], to cause more acute health problems than larger particles that are mostly removed by the upper respiratory system. However, WHO PM pollution standards are based on mass concentrations of $PM_{2.5}$ and PM_{10} (ref. [4]) and do not account for particle sizes and/or composition.

The observed events demonstrate that the magnitude of PM pollution in Dublin can even rival that in megacities in developing countries. For example, we took a three-week period in Beijing, China, starting on 19 November 2016 (that is, the first of our main events) and found that while Dublin had 8 exceedance days out of 21, Beijing had 18 out of 21 (Supplementary Fig. 3), with the median $PM_{2.5}$ concentration over the exceedance days amounting to 35 μg m^{-3} for Dublin and 95 μg m^{-3} for Beijing. For a city with ~15 times less population and population density[33,34], the number of exceedance days is roughly less than half that of Beijing's, and the median $PM_{2.5}$ concentration is roughly 2.5 times less.

Chemical composition of PM_1

As shown in Fig. 1b, carbonaceous aerosol (OA + eBC) was the major component of PM_1, accounting for 89% of the total PM_1 measured in the P1 pollution peak, and 88% in the P2 pollution peak, while all inorganic components, sulfate (4%), nitrate (3–4%), ammonium (2%) and chloride (2%), were minor parts of the PM_1.

During the P1 event, OA increased from 1.3 μg m^{-3} during the day (from 08:00 to 16:00, local time) to 221.3 μg m^{-3} at ~21:30 while eBC increased from 0.5 μg m^{-3} to 48 μg m^{-3} (Supplementary Table 1). During P2, OA increased from 8.3 μg m^{-3} during the day to 163.6 μg m^{-3} at ~21:30 and eBC increased from 1.9 μg m^{-3} to 76.1 μg m^{-3}. For OA, the peak concentration in the evening was 20–170 times higher than that during the day. Similarly, for eBC, the peak concentration was 40–96 times higher. A shallower planetary boundary layer (PBL) could partially contribute to an increase in the evening

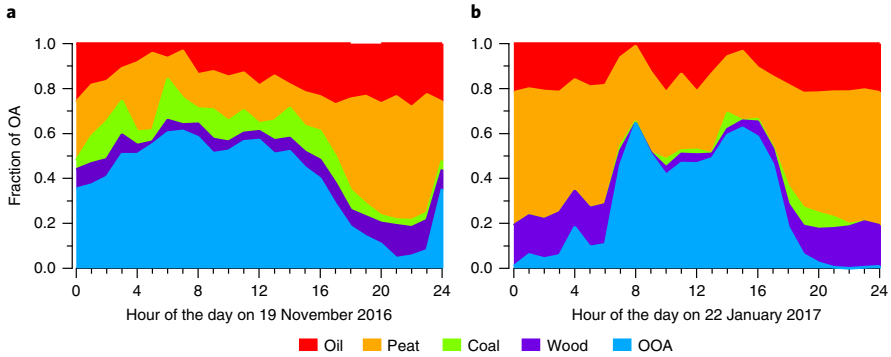

Fig. 2 | The contribution of organic factors, including oil, peat, coal, wood and OOA, to the total OA mass. a, For the P1 event on 19 November 2016. **b**, For the P2 event on 22 January 2017.

concentrations; therefore, the ratio of the daytime (08:00–16:00, local time) PBL to the evening (18:00–23:00) PBL was used to estimate the impact of PBL reduction. Assuming no horizontal losses in a simple box model, we calculate that after accounting for the 1.1–1.8 times PBL reduction (Supplementary Fig. 4), eBC concentration in the evening was still 36–53 times higher than that during the day. eBC is produced exclusively by the combustion processes, such as the combustion of fossil fuel and biomass[35–37]. The coincident increase in both eBC and OA in the evening indicates combustion sources associated with residential heating.

The two selected extreme events (P1 and P2) also have different features due to meteorological conditions and air mass origin. The concentration of the PM_1 components during the day of P2 was higher than P1 (Supplementary Table 1). For example, nitrate was 10.7 μg m^{-3} during the day for P2 and was 0.2 μg m^{-3} for P1 owing to the differences in air masses; for example, an air mass was arriving from Europe for the P2 event while P1 occurred during a westerly marine air mass. The difference was also related to the difference in meteorological conditions (Supplementary Fig. 5). P1 featured a sudden change in wind speed and wind direction in the evening while P2 featured stagnant conditions throughout the day that were favourable for the build-up of pollutants. For P1, wind speed changed from ~6 m s^{-1} during the day to <2 m s^{-1} in the evening and the wind direction changed from the west to north. For P2, the wind was <2 m s^{-1} throughout the day with easterly–northerly wind. The lowest temperature was −1.2 °C for the evening of P1 and was −2.0 °C for P2. Thus, the freezing evening and night-time temperatures during the P1 and P2 events likely resulted in an increase in the burning of extra fuels in houses. However, these burning activities, coupled with low wind speed, could cause recurring PM pollution. It is, therefore, very important to understand what fuels people were burning and how much was consumed.

Sources of PM_1. Natural gas, electricity, oil, coal, peat and wood are mainly used for heating in Dublin[33] (Supplementary Table 2) with natural gas and electricity being the most popular sources. However, they are not expected to emit PM. In contrast, liquid (oil) and solid fuels (peat, coal and wood) are the potential sources of PM_1 due to emission from incomplete combustion. To evaluate their contribution, ME-2 source-apportionment analysis, using the *a*-value approach, was utilized. For this approach, factors are constrained to certain reference profiles allowing them to vary to some degree called the *a* value (for example, an *a* value of 0.1 allows a variability of 10%). Here, the reference profiles of peat, coal and wood were obtained from locally sourced fuels that were burned in a stove typical for Irish households[31] while that for oil was taken from the literature[18]. Based on a correlation with eBC, ME-2 solutions with an *a* value of 0–0.2 were selected as environmentally reasonable ones (Supplementary Fig. 6). All accepted solutions were then averaged to obtain the mean concentration and contribution for each factor (Supplementary Table 3) while the variation between the solutions represented the overall approach uncertainty and ranged from 9% to 28%.

Supplementary Figs. 7 and 8 show the mass spectra and time series of individual OA factors, respectively. The mass spectrum of oil, known as hydrocarbon OA[18,38], is dominated by the signals at mass to charge (*m*/*z*) ratios of 27, 29, 41, 43, 55, 57, 69 and 71, characteristic of aliphatic hydrocarbons. The pyrosis of cellulose or wood produces levoglucosan and the fragmentation of levoglucosan gives rise to a signal at *m*/*z* 60 in ACSM spectra[39]. Peat is the transition state between wood and coal[40]. The incomplete decay of cellulose during peat formation results in a signal at *m*/*z* 60. However, the contribution of *m*/*z* 60 (that is, f60) in the peat profile is less than that in the wood profile. Coal is formed from biomass after millions of years under pressure and heat. In the coal profile, f60 is reduced to nearly 0, because of the complete decay of vegetation during coal formation. The concentrations of oil, peat, coal and wood increase significantly in the evening (Supplementary Fig. 8), which is consistent with the time when people are most likely to stay at home and burn these fuels for heating.

In addition to these fuel factors, an oxygenated organic aerosol (OOA) factor was also resolved. As shown in Supplementary Fig. 7, the mass spectrum of OOA shows a great contribution from *m*/*z* 44, mainly arising from the fragmentation of oxygenated species such as organic acids[41]. OOA can be of several origins, the most likely and common one is related to regional transport of aged/oxidized aerosol[42]. In this study, moderate OOA correlation with sulfate (R^2 = 0.59) indicates a contribution from long-range transport or secondary formation processes during the day; however, its simultaneous increase with primary factors, during the evening (Supplementary Fig. 8), points to a condensation of semi-volatile species as also being an important source of OOA[43], (R^2 = 0.64 with nitrate). The increase in locally formed OOA concentration was also partially due to the decreasing PBL during the evening. In this study, OOA could not be separated into low-volatility and semi-volatility[42] OOA even by increasing the number of factors, probably due to the unit mass resolution of ACSM.

Concentrations and contributions from each factor during the P1 and P2 events are presented in Supplementary Table 3. The peat factor shows the highest concentration of 101.7 μg m^{-3} during P1 and 89.6 μg m^{-3} during P2. The contribution to OA mass was 46% and 55%, respectively. As shown in Fig. 2, peat burning was the most dominant factor in the evening (18:00–23:00; local time) and, in the case of stagnant meteorological conditions for P2

(Fig. 2b), peat dominance was persistent until early morning (06:00). Such a significant contribution from peat burning is rather surprising because, to the best of our knowledge, no other countries have ever reported similar kind of pollution from peat burning so far. Our previous study in Galway, a small city in Ireland, also found a prominent peat factor but with lower concentrations (~10 $\mu g\,m^{-3}$ or 39% of total OA)[31].

The other solid fuel factors, the coal factor (3.4–13.9 $\mu g\,m^{-3}$) and the wood factor (27.2–32.7 $\mu g\,m^{-3}$), contributed 2–6% and 15–17% to the total OA (Supplementary Table 3), respectively. In total, solid fuels (the sum of peat, coal and wood) contributed 67–74% to the total OA in the evening. Peat and wood, two types of biomass, collectively contributed 61–72% to the total OA, which was greater than that from fossil fuels (the sum of oil and coal; 26–35%). During the daytime, however, the concentration (0.5–3.4 $\mu g\,m^{-3}$; Supplementary Fig. 8) and contributions (36–59%; Fig. 2) of solid fuel factors decreased, corresponding to the reduction in domestic heating activities. In contrast, OOA was the dominant OA factor (0.8–4.0 $\mu g\,m^{-3}$; 41–64%) during the day, which is likely related to its secondary production and/or aerosol aging.

eBC source apportionment, using the Ångström exponent (α) model[31], separated eBC into fossil fuel (eBC_{ff}) and biomass burning (eBC_{bb}) sources. However, the model was not capable of separating eBC_{bb} further into peat burning or wood burning eBC or separating eBC_{ff} into oil or coal burning eBC due to the similarities in α values. In this study, α_{ff} was set to 1.0 and α_{bb} was set to 2, the mid-range values of the ones used in previous studies, for example, $\alpha = 0.9–1.1$ for eBC_{ff} and $\alpha = 1.8–2.2$ for eBC_{bb}[32,44–47]. Sensitivity tests were performed here by varying α_{ff} from 0.9 to 1.1 and α_{bb} from 1.8 to 2.2, showing an overall uncertainty of the model ranging from 5% to 28%. Supplementary Table 4 shows the apportionment result for eBC_{bb} and eBC_{ff} during P1 and P2 events. For the P1 and P2 events, 23.2 $\mu g\,m^{-3}$ (or 48%) and 72.1 $\mu g\,m^{-3}$ (or 95%) of eBC was attributed to eBC_{bb}, respectively. This, again, highlights the importance of biomass burning.

The OA factors of peat and wood together with eBC_{bb} were directly associated with biomass burning emission; thus, in total, the biomass burning factor (the sum of peat, wood and eBC_{bb}) contributed 52–70% of PM_1 mass during the pollution events. The fossil fuel factor (the sum of oil, coal and eBC_{ff}) contributed 17–34% of PM_1 mass, about 1.5–4.1 times smaller than the biomass-related contribution. Inorganic aerosol (sulfate, nitrate, ammonium and chloride) and OOA accounted for the remaining 13–14% of PM_1, but we could not apportion them into biomass or fossil fuel exclusively.

Disproportionate impact from solid fuel burning

The emission factors and calorific values for each fuel common in residential use are shown in Supplementary Table 5. The calorific value of oil (43 $MJ\,kg^{-1}$) is approximately three times higher than that of peat (13.1 $MJ\,kg^{-1}$); therefore, approximately three times more peat should be burned to get an equal amount of heat. Moreover, peat has a four times higher $PM_{2.5}$ emission factor (0.79 g $PM_{2.5}\,kg^{-1}$) compared with oil (0.22 g $PM_{2.5}\,kg^{-1}$), further increasing the emissions per unit of heat. Using these numbers (Supplementary Methods), it is estimated that 87–88% of the households had to consume oil, 9–12% peat, 1–2% coal and <1% wood to get the fractional contribution of organic factors for the P1 and P2 events. This estimation is consistent with the latest census data[33] (Supplementary Table 2), which show only a few households use solid fuels as primary heating sources. Note that most households use relatively clean fuels such as natural gas (26,317 households) and electricity (8,800 households), which are not supposed to emit PM directly. Among those households that don't use clean fuels, oil burning (429 households) is the most popular choice followed by wood (81), coal (23) and peat (2). However, 260 unstated households and the households that claim to use clean fuels are likely to turn to solid fuels as a secondary choice.

Dublin, as the capital city of Ireland with a population of ~1.4 million, has historically suffered from severe air pollution mainly arising from coal burning activities with a seasonal mean black smoke concentration of ~100 $\mu g\,m^{-3}$ during the heating season in the 1980s[48]. After the ban on the marketing, sale and distribution of smoky coal was introduced in 1990, a 70% reduction in black smoke was observed[49]. As shown in Supplementary Table 2, more and more households are turning to clean fuel. For example, the households that claim to use coal for heating decreased from 608 in 1980 (before the coal ban) to 23 in 2011 (after the coal ban). However, this study demonstrates how only a few households (<13%) that burn biomass for heating (especially peat) could cause recurring extreme pollution events, influencing the overall air quality in the city.

Implication for policymaking

This study demonstrates how critical it is to augment standard regulatory air quality networks with analytically advanced measurement approaches that can essentially fingerprint the main pollution contributors, which, in turn, can enable and better inform policy measures to develop specifically targeted and sophisticated emission reductions while minimizing the economic impact.

The current advanced ACSM network, comprising four strategically positioned nodes, augments and overlies the national air quality monitoring network. In this study, we estimate that specifically targeting 100% reduction of emissions of wood (<1% households) and peat (9–12% households) would reduce the PM_1 concentrations by 52–70%. Assuming that $PM_{2.5}$ concentration would reduce proportionally, the elimination of wood and peat burning would reduce exceedance of the WHO $PM_{2.5}$ daily limit to 1 in 75 days, compared with the currently observed 1 in 5 days. However, 100% reduction of peat and wood emission is unlikely in real terms. It is further estimated that reducing peat and wood consumption by 50% leads to approximately 1 in 10 days exceedance while increasing by 50% leads to 1 in 3 days exceedance.

Discussion

The Renewable Energy Directive[50] requires all European Union countries to obtain at least 20% of their energy from renewable sources by 2020. The green agenda promotes low-carbon or carbon-neutral usage, which is considered an environmentally friendly solution for the mitigation of global warming from emissions of greenhouse gases[51]. One of the most popular choices of 'green' solid biomass is wood pellets[52], regarded as a low-carbon fuel, where currently Europe accounts for about 60% of the global demand (equivalent to 10 Mt of solid biomass). Biomass-based heating in Europe is set to increase to more than 20 Mt by 2020 and similar growth is expected from other world markets leading to a conservative estimate of a factor of three increase in global consumption from 2010 to 2030 (ref. [53]).

Peat, similarly, is perceived as a 'green' energy source and was added to the list of renewable energy sources by European Parliament in 2000. Peat is widely used for both residential and energy production area[54]. As we have illustrated, in addition to wood, residential peat burning could cause severe PM pollution. The results from this study suggest that rather than promoting low-carbon or carbon-neutral solid fuels, it is especially urgent to introduce new emission controls on residential solid fuel burning.

Methods

Sites and instrumentation. An Aerodyne ACSM (Aerodyne Research), an aethalometer (AE-33, Magee Scientific) and a scanning mobility particle sizer (SMPS, TSI) were deployed at UCD (53.3053° N, 6.2207° W). All three instruments were located in the same laboratory, sampling from one $PM_{2.5}$ inlet on the roof of the School of Physics building (~30 m above the ground). The ACSM was deployed to measure OA, sulfate, nitrate, ammonium and chloride with a time resolution of

30 min. The AE-33 was used to measure eBC with 1 min resolution. The SMPS was deployed to measure the number and size distribution of particles in the range of 10–495 nm with 15 min resolution.

A tapered element oscillating microbalance (ThermoFisher Scientific) was deployed to measure $PM_{2.5}$ with 1 h resolution at the Environmental Protection Agency's Rathmines station, which is ~3 km away from the UCD measurement site.

Meteorological variables (temperature, relative humidity, wind speed, wind direction, mean sea-level pressure) were recorded at the meteorological stations (Irish meteorological service) of Dublin airport. The time resolution is 1 h for meteorological data.

PBL height was calculated with a ceilometer (CL31) model from Vaisala at Casement, Dublin, which is ~15 km away from the UCD site. The time resolution for CL31 is 1 min. The PBL is defined by dynamic processes leading to movement of heat and air; however, with a ceilometer, we can only see surrogates such as aerosols. Hence, by observing the vertical aerosol abundance and how it changes with time, this proxy elucidates the stability structure and the contribution of a mixing layer, if present, to the location and extent of the PBL[55].

The ACSM was operated following the recommendation on calibration and data analysis provided by the ACSM manufacturer (Aerodyne Research) and Ng et al.[25]. Briefly, the ambient air was drawn into the cyclone with a size cut-off of 2.5 µm at a flow rate of 3 l min^{-1} to remove coarse mode particles. The resulting flow was dried by passing through a Nafion dryer before reaching the ACSM inlet. In the ACSM, the dried aerosol particles were focused into a narrow beam by the aerodynamic lens (~2 torrs) and entered a vacuum chamber where they were vaporized, ionized and analysed by a quadrupole mass spectrometer. A response factor of 2.72×10^{-11} with a standard deviation of 15% and relative ionization efficiencies of 5.56 for ammonium and 0.76 for sulfate were adopted based on ammonium nitrate and ammonium sulfate calibrations.

ACSM data were analysed by the software of ACSM_local (version 1.6.0.3). OA, sulfate, nitrate, ammonium and chloride mass concentrations were extracted from aerosol mass spectra data using the fragmentation table[56]. A collection efficiency of 1 was used for ACSM data. This was supported by the comparison between PM_1 and SMPS volume (Supplementary Fig. 9), as well as PM_1 and $PM_{2.5}$ mass concentrations (Supplementary Fig. 1). The estimated PM_1 volume was calculated by assuming a composition-dependent density of the ACSM species and AE-33 eBC. The slope was 1.05 ± 0.01.

The operation of AE-33 followed the recommendation of its manufacturer (Magee Scientific)[26]. The aerosol attenuation was measured at seven different wavelengths (370, 470, 520, 590, 660, 880 and 950 nm) with a time resolution of 1 min. The optical properties of aerosol and eBC concentrations were retrieved from the change in the light attenuation. Mass absorption coefficients (b_{abs}) at 880 nm were used to calculate the eBC concentration using the mass absorption cross-section 7.77 $m^2 g^{-1}$.

OA source apportionment. The preparation of organic matter data and its related uncertainty followed the recommendation of Ulbrich et al.[57]. Data points with a low signal-to-noise ratio (SNR < 0.2) were removed, whereas data with a SNR in the range of 0.2–2 were downweighted by a factor of 2. PMF was run in a robust mode. In this study, organic fragments with $m/z \leq 100$ were analysed. Higher m/z ratios were not included because of the low SNR.

PMF does not require any prior information but may have a substantial degree of rotational ambiguity[27]. The rotational ambiguity may result in fewer factors or inaccurate factor attributions when some factors have similar temporal variation. To reduce rotational ambiguity, a priori information such as factor profile can be used to constrain the PMF model.

The multilinear engine (ME-2) is a solver of PMF. ME-2 can partly constrain the factors based on a priori information such as factor profiles (used in this study) and time series. The so-called a-value approach within ME-2 was used, where the a value represents the extent to which the reference profiles are allowed to vary (for example, an a value of 0.1 allows a variability of 10%). The interface of SoFi (Source Finder)[29] was used to run ME-2. a values from 0 to 0.6 with a step of 0.1 were used to constrain the refence profiles of oil, peat, coal and wood, leaving one unconstrained factor[31].

eBC source apportionment. Light absorption of the aerosol samples was measured at seven wavelengths from the near-infrared (950 nm) to the near-ultraviolet (370 nm). The light absorption of traffic-related eBC particles shows a low dependence on wavelength while biomass burning eBC particles feature enhanced light absorption at shorter wavelengths[47]. Increases in optical absorption in the near-ultraviolet and blue parts of the light spectrum indicate a possible emission from biomass burning.

A linear regression model was used to perform eBC source apportionment into biomass burning eBC (eBC_{bb}) and fossil fuel burning eBC (eBC_{ff}). The detailed description of eBC source apportionment is given by Sandradewi et al[32]. Aerosol absorption coefficients (b_{abs}) follow the relationship

$$\frac{b_{abs}(\lambda)}{b_{abs}(\lambda_0)} = \left(\frac{\lambda}{\lambda_0}\right)^{-\alpha} \quad (1)$$

$$b_{abs}(\lambda) = b_{abs}(\lambda)_{ff} + b_{abs}(\lambda)_{bb} \quad (2)$$

where λ is the wavelength and α is the absorption Ångström exponent. b_{abs} at 470 nm and 880 nm were used. An α of 1 was used for fossil fuel ($\alpha_{ff} = 1$) and 2 for biomass ($\alpha_{bb} = 2$) (Magee Scientific).

The Ångström exponent model assumed constant α_{ff} and α_{bb} values. However, α_{ff} and α_{bb} are highly variable and have been shown to be dependent on variables such as combustion efficiency[58] and the type of fuel[32], ranging at least from 0.9 to 1.1 and from 1.8 to 2.2 (refs [44–46]), respectively. In our previous fingerprinting experiment (C.L. et al., manuscript in preparation), AE-33 was used to measure the light absorption of eBC from peat, wood and coal burning directly from a stove typical for Irish households. Aerosol particles emitted from both peat and wood burning show strong absorption at the near-ultraviolet wavelength with α in the range of 1.4–3.8 (10th–90th percentile) for wood burning and 2.0–4.0 for peat burning aerosol. The eBC source-apportionment model is capable of separating eBC into eBC_{ff} and eBC_{bb}. However, due to the similarity in α values for wood and peat burning aerosol, the model is not capable of separating eBC_{bb} further into peat burning or wood burning eBC. The same is true for coal and oil due to similar α values (that is, 1.1–1.4 for coal and 0.9– 1.1 for oil).

Data availability. The data that support the findings of this study are available from the corresponding author on request.

Received: 9 February 2018; Accepted: 30 July 2018;
Published online: 14 September 2018

References

1. Dockery, D. W. et al. An association between air pollution and mortality in Six U.S. cities. *N. Eng. J. Med.* **329**, 1753–1759 (1993).
2. Pope, C. A. III & Dockery, D. W. Health effects of fine particulate air pollution: lines that connect. *J. Air Waste Manag. Assoc.* **56**, 709–742 (2006).
3. Lelieveld, J., Evans, J. S., Fnais, M., Giannadaki, D. & Pozzer, A. The contribution of outdoor air pollution sources to premature mortality on a global scale. *Nature* **525**, 367–371 (2015).
4. WHO *Air Quality Guidelines: Global Update 2005* (World Health Organization, 2006).
5. Harrison, R. M. & Yin, J. Particulate matter in the atmosphere: Which particle properties are important for its effects on health? *Sci. Total Environ.* **249**, 85–101 (2000).
6. Hao, J., Wang, L., Shen, M., Li, L. & Hu, J. Air quality impacts of power plant emissions in Beijing. *Environ. Pollut.* **147**, 401–408 (2007).
7. Zhou, Y. et al. The impact of transportation control measures on emission reductions during the 2008 Olympic Games in Beijing, China. *Atmos. Environ.* **44**, 285–293 (2010).
8. Minguillón, M. C. et al. Effect of ceramic industrial particulate emission control on key components of ambient PM_{10}. *J. Environ. Manage.* **90**, 2558–2567 (2009).
9. Carvalho, V. S. B. et al. Air quality status and trends over the Metropolitan Area of São Paulo, Brazil as a result of emission control policies. *Environ. Sci. Policy* **47**, 68–79 (2015).
10. Johnson, T. V. Diesel emission control in review. *SAE Int. J. Fuels Lubr.* **1**, 68–81 (2009).
11. Mohr, M., Forss, A.-M. & Lehmann, U. Particle emissions from diesel passenger cars equipped with a particle trap in comparison to other technologies. *Environ. Sci. Technol.* **40**, 2375–2383 (2006).
12. DeWitt, H. L. et al. Near-highway aerosol and gas-phase measurements in a high-diesel environment. *Atmos. Chem. Phys.* **15**, 4373–4387 (2015).
13. Decarlo, P. F. et al. Investigation of the sources and processing of organic aerosol over the Central Mexican Plateau from aircraft measurements during MILAGRO. *Atmos. Chem. Phys.* **10**, 5257–5280 (2010).
14. Mohr, C. et al. Identification and quantification of organic aerosol from cooking and other sources in Barcelona using aerosol mass spectrometer data. *Atmos. Chem. Phys.* **12**, 1649–1665 (2012).
15. Liu, J. et al. Air pollutant emissions from Chinese households: a major and underappreciated ambient pollution source. *Proc. Natl Acad. Sci. USA* **113**, 7756–7761 (2016).
16. Lu, Z., Zhang, Q. & Streets, D. G. Sulfur dioxide and primary carbonaceous aerosol emissions in China and India, 1996–2010. *Atmos. Chem. Phys.* **11**, 9839–9864 (2011).
17. Smith, K. R. et al. Millions dead: how do we know and what does it mean? Methods used in the comparative risk assessment of household air pollution. *Annu. Rev. Public Health* **35**, 185–206 (2014).
18. Crippa, M. et al. Wintertime aerosol chemical composition and source apportionment of the organic fraction in the metropolitan area of Paris. *Atmos. Chem. Phys.* **13**, 961–981 (2013).
19. Allan, J. D. et al. Contributions from transport, solid fuel burning and cooking to primary organic aerosols in two UK cities. *Atmos. Chem. Phys.* **10**, 647–668 (2010).

20. Xu, L. et al. Wintertime aerosol chemical composition, volatility, and spatial variability in the greater London area. *Atmos. Chem. Phys.* **16**, 1139–1160 (2016).
21. Young, D. E. et al. Investigating a two-component model of solid fuel organic aerosol in London: processes, PM_1 contributions, and seasonality. *Atmos. Chem. Phys.* **15**, 2429–2443 (2015).
22. Young, D. E. et al. Investigating the annual behaviour of submicron secondary inorganic and organic aerosols in London. *Atmos. Chem. Phys.* **15**, 6351–6366 (2015).
23. Solomon, P. A. et al. U.S. national $PM_{2.5}$ chemical speciation monitoring networks-CSN and IMPROVE: description of networks. *J. Air Waste Manag. Assoc.* **64**, 1410–1438 (2014).
24. Grigas, T. et al. Sophisticated clean air strategies required to mitigate against particulate organic pollution. *Sci. Rep.* **7**, 44737 (2017).
25. Ng, N. L. et al. An aerosol chemical speciation monitor (ACSM) for routine monitoring of the composition and mass concentrations of ambient aerosol. *Aerosol Sci. Technol.* **45**, 780–794 (2011).
26. Drinovec, L. et al. The "dual-spot" aethalometer: an improved measurement of aerosol black carbon with real-time loading compensation. *Atmos. Meas. Tech.* **8**, 1965–1979 (2015).
27. Paatero, P. The multilinear engine-a table-driven, least squares program for solving multilinear problems, including the *n*-way parallel factor analysis model. *J. Comput. Graph. Stat.* **8**, 854–888 (1999).
28. Paatero, P. Least squares formulation of robust non-negative factor analysis. *Chemom. Intell. Lab. Syst.* **37**, 23–35 (1997).
29. Canonaco, F., Crippa, M., Slowik, J. G., Baltensperger, U. & Prévôt, A. S. H. SoFi, an IGOR-based interface for the efficient use of the generalized multilinear engine (ME-2) for the source apportionment: ME-2 application to aerosol mass spectrometer data. *Atmos. Meas. Tech.* **6**, 3649–3661 (2013).
30. Lanz, V. A. et al. Source attribution of submicron organic aerosols during wintertime inversions by advanced factor analysis of aerosol mass spectra. *Environ. Sci. Tech.* **42**, 214–220 (2008).
31. Lin, C. et al. Characterization of primary organic aerosol from domestic wood, peat, and coal burning in Ireland. *Environ. Sci. Tech.* **51**, 10624–10632 (2017).
32. Sandradewi, J. et al. Using aerosol light absorption measurements for the quantitative determination of wood burning and traffic emission contributions to particulate matter. *Environ. Sci. Tech.* **42**, 3316–3323 (2008).
33. *2011 Population Census Data* (Central Statistics Office, accessed on 1 June 2017); https://www.cso.ie
34. *2010 Population Census Data* (National Bureau of Statistics of China; accessed on 1 May 2018); http://www.stats.gov.cn/english/Statisticaldata/CensusData/
35. Ramanathan, V., & Carmichael, G. Global and regional climate changes due to black carbon. *Nat. Geosci.* **1**, 221–227 (2008).
36. Bond, T. C. & Bergstrom, R. W. Light absorption by carbonaceous particles: an investigative review. *Aerosol Sci. Technol.* **40**, 27–67 (2006).
37. Haslett, S. L. et al. Highly controlled, reproducible measurements of aerosol emissions from combustion of a common African biofuel source. *Atmos. Chem. Phys.* **18**, 385–403 (2018).
38. Ng, N. L. et al. Real-time methods for estimating organic component mass concentrations from aerosol mass spectrometer data. *Environ. Sci. Tech.* **45**, 910–916 (2011).
39. Alfarra, M. R. et al. Identification of the mass spectral signature of organic aerosols from wood burning emissions. *Environ. Sci. Tech.* **41**, 5770–5777 (2007).
40. Ryer, T. A., & Langer, A. W. Thickness change involved in the peat-to-coal transformation for a bituminous coal of Cretaceous age in central Utah. *J. Sediment. Res.* **50**, 987–992 (1980).
41. Ng, N. L. et al. Organic aerosol components observed in Northern Hemispheric datasets from aerosol mass spectrometry. *Atmos. Chem. Phys.* **10**, 4625–4641 (2010).
42. Jimenez, J. L. et al. Evolution of organic aerosols in the atmosphere. *Science* **326**, 1525–1529 (2009).
43. Tiitta, P. et al. Transformation of logwood combustion emissions in a smog chamber: formation of secondary organic aerosol and changes in the primary organic aerosol upon daytime and nighttime aging. *Atmos. Chem. Phys.* **16**, 13251–13269 (2016).
44. Favez, O. et al. Inter-comparison of source apportionment models for the estimation of wood burning aerosols during wintertime in an Alpine city (Grenoble, France). *Atmos. Chem. Phys.* **10**, 5295–5314 (2010).
45. Crilley, L. R. et al. Sources and contributions of wood smoke during winter in London: assessing local and regional influences. *Atmos. Chem. Phys.* **15**, 3149–3171 (2015).
46. Mohr, C. et al. Contribution of nitrated phenols to wood burning brown carbon light absorption in Detling, United Kingdom during winter time. *Environ. Sci. Technol.* **47**, 6316–6324 (2013).
47. Zotter, P. et al. Evaluation of the absorption Ångström exponents for traffic and wood burning in the aethalometer-based source apportionment using radiocarbon measurements of ambient aerosol. *Atmos. Chem. Phys.* **17**, 4229–4249 (2017).
48. Clancy, L., Goodman, P., Sinclair, H. & Dockery, D. W. Effect of air-pollution control on death rates in Dublin, Ireland: an intervention study. *Lancet* **360**, 1210–1214 (2002).
49. Goodman, P. G., Rich, D. Q., Zeka, A., Clancy, L. & Dockery, D. W. Effect of air pollution controls on black smoke and sulfur dioxide concentrations across Ireland. *J. Air Waste Manag. Assoc.* **59**, 207–213 (2009).
50. *Directive 2009/28/EC of the European Parliament and of the Council of 23 April 2009* (European Union, 2009); https://eur-lex.europa.eu/eli/dir/2009/28/oj
51. Driving Europe's transition to a low-carbon economy. *European Commission* (20 July 2016).
52. *Global Wood Pellet Industry and Trade Study 2017* (International Energy Agency Bioenergy, accessed on 1 June 2017).
53. *Biomass for Electricity and Heating* (European Parliament, 2015).
54. *Global Energy Data* (International Energy Agency, accessed on 1 June 2017); http://www.iea.org
55. Martucci, G., Milroy, C. & O'Dowd, C. D. Detection of cloud-base height using Jenoptik CHM15K and Vaisala CL31 ceilometers. *J. Atmos. Ocean. Tech.* **27**, 305–318 (2010).
56. Allan, J. D. et al. A generalised method for the extraction of chemically resolved mass spectra from Aerodyne aerosol mass spectrometer data. *J. Aerosol Sci.* **35**, 909–922 (2004).
57. Ulbrich, I. M., Canagaratna, M. R., Zhang, Q., Worsnop, D. R. & Jimenez, J. L. Interpretation of organic components from positive matrix factorization of aerosol mass spectrometric data. *Atmos. Chem. Phys.* **9**, 2891–2918 (2009).
58. Garg, S. et al. Limitation of the use of the absorption Angstrom exponent for source apportionment of equivalent black carbon: a case study from the North West Indo-Gangetic Plain. *Environ. Sci. Tech.* **50**, 814–824 (2016).

Acknowledgements

This work was funded by the Irish Environmental Protection Agency (AEROSOURCE, 529 2016-CCRP-MS-31; SAPPHIRE, 2013-EH-MS-15), Science Foundation Ireland (MaREI award 14-SP-2740), the European Commission, the National Natural Science Foundation of China 530 (NSFC) under grant no. 91644219, China Scholarship Council (CSC, no. 201506310020) 531 and the Irish Research Council (GOIPG/2015/3051). We also acknowledge Met Éireann for ceilometer and meteorological data.

Author contributions

J.O., D.C., M.R., M.C.F., J.W., R.-J.H. and C.O'D. conceived and designed the experiments; C.L., J.O., D.C. and P.B. performed the experiments; C.L., R.-J.H., J.O., P.B., J.P. and C.O'D. analysed the data; C.L. and C.O'D. wrote the paper with input from all co-authors.

Competing interests

The authors declare no competing interests.

Additional information

Supplementary information is available for this paper at https://doi.org/10.1038/s41893-018-0125-x.

Reprints and permissions information is available at www.nature.com/reprints.

Correspondence and requests for materials should be addressed to R.-J.H. or C.O'D.

Publisher's note: Springer Nature remains neutral with regard to jurisdictional claims in published maps and institutional affiliations.

Environmental Science & Technology

Article

pubs.acs.org/est

Characterization of Primary Organic Aerosol from Domestic Wood, Peat, and Coal Burning in Ireland

Chunshui Lin,[†,‡] Darius Ceburnis,[†] Stig Hellebust,[§] Paul Buckley,[§] John Wenger,[§] Francesco Canonaco,[∥] André Stephan Henry Prévôt,[∥] Ru-Jin Huang,[*,†,‡,∥] Colin O'Dowd,[*,†] and Jurgita Ovadnevaite[†]

[†]School of Physics and Centre for Climate and Air Pollution Studies, Ryan Institute, National University of Ireland Galway, University Road, H91CF50 Galway, Ireland

[‡]State Key Laboratory of Loess and Quaternary Geology and Key Laboratory of Aerosol Chemistry and Physics, Institute of Earth Environment, Chinese Academy of Sciences, 710061 Xi'an, China

[§]Department of Chemistry and Environmental Research Institute, University College Cork, T23XE10 Cork, Ireland

[∥]Laboratory of Atmospheric Chemistry, Paul Scherrer Institute (PSI), 5232 Villigen, Switzerland

Supporting Information

ABSTRACT: An aerosol chemical speciation monitor (ACSM) was deployed to study the primary nonrefractory submicron particulate matter emissions from the burning of commercially available solid fuels (peat, coal, and wood) typically used in European domestic fuel stoves. Organic mass spectra (MS) from burning wood, peat, and coal were characterized and intercompared for factor analysis against ambient data. The reference profiles characterized in this study were used to estimate the contribution of solid fuel sources, along with oil combustion, to ambient pollution in Galway, Ireland using the multilinear engine (ME-2). During periods influenced by marine air masses, local source contribution had dominant impact and nonsea-spray primary organic emissions comprised 88% of total organic aerosol mass, with peat burning found to be the greatest contributor (39%), followed by oil (21%), coal (17%), and wood (11%). In contrast, the resolved oxygenated organic aerosol (OOA) dominated the aerosol composition in continental air masses, with contributions of 50%, compared to 12% in marine air masses. The source apportionment results suggest that the use of domestic solid fuels (peat, wood, and coal) for home heating is the major source of evening and night-time particulate pollution events despite their small use.

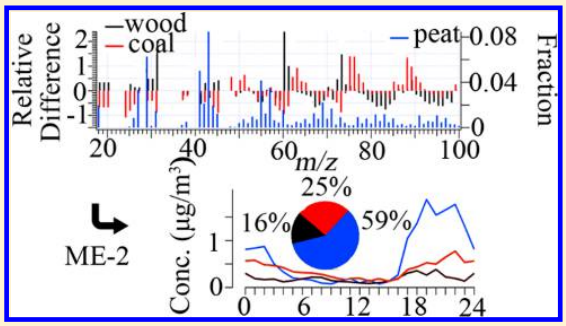

1. INTRODUCTION

Ambient particulate matter (PM) adversely affects human health[1,2] and has been credited with a more positive effect on climate through directly scattering or absorbing solar radiation and indirectly acting as cloud condensation nuclei,[3] both leading to a partial negation of global warming induced by greenhouse gas emissions. In Ireland, domestic coal burning was the cause of numerous air pollution events in the 1980s, which led to increased mortality rates.[4] The introduction of the ban on marketing, sale, and distribution of bituminous (smoky) coal in Dublin in 1990, which was subsequently extended to urban areas with a population over 15 000, resulted in significant reductions in black smoke concentrations and in noticeable improvements in air quality.[5,6] However, a recent study in the city of Cork, Ireland,[7] using polar organic compounds to estimate the contribution of domestic solid fuel (DSF) combustion indicates that, despite the ban on bituminous coal, DSF is still the major source of $PM_{2.5}$ organic carbon (0.6−23.7 $\mu g/m^3$; OC) during the winter (contributing around 75% to total $PM_{2.5}$). Thus, the ban on bituminous coal alone may not be sufficient because peat and wood emit similar or higher amounts of PM when burned. In fact, according to the report from International Energy Agency (2013),[8] the annual consumption of bituminous coal in Ireland was 404 kt in 2013, while annual peat consumption was 611 kt, which makes peat one of the most commonly used solid fuels. In contrast, the annual consumption of wood for domestic heating was only 34 kt in 2015. Different types of DSF have different emissions factors that are dependent on the type of fuel and burning conditions.[9−11] However, developing a way to identify and evaluate the contribution of DSF burning to particulate matter with high time resolution is limited.

Received: April 13, 2017
Revised: July 25, 2017
Accepted: August 17, 2017
Published: August 17, 2017

DOI: 10.1021/acs.est.7b01926
Environ. Sci. Technol. 2017, 51, 10624−10632

The identification of specific marker compounds in aerosol particles produced from different solid fuels, and the use of markers for subsequent evaluation of the DSF contribution to airborne pollution has been reported by Kourtchev et al.[7] Polar organic maker compounds (i.e., levoglucosan, galactosan, and mannosan) determined by gas chromatography−mass spectrometry (GC/MS) and the levoglucosan-to-OC ratio derived from combustion experiments of coal, peat, and wood were used to identify and evaluate their contributions to ambient PM.[7] However, GC/MS suffers from low time resolution (6 h), and the levoglucosan-to-OC ratio might differ greatly under different burning conditions that limit this tracer approach. Recently, the aerosol mass spectrometer (AMS), which determines the chemical composition and concentration of submicron aerosols online and at high time resolution, has proven to be a robust tool for evaluating the contribution of various sources.[12−17] Based on thermal vaporization and electron impact, AMS classifies organic aerosols (OAs) by mass spectrometric fingerprint rather than individual specific marker compounds.[18] Several major components of OA have been identified through positive matrix factorization (PMF) analysis of AMS mass spectra such as hydrocarbon-like (HOA), biomass burning (BBOA), oxygenated (OOA), and several other primary OA.[19−21] Direct AMS measurement of OA from various primary emissions can help understand the MS signatures of different primary OA sources and thus help the interpretation of AMS data. Emissions from motor vehicles,[22,23] meat cooking,[24] and solid fuels[10,25,26] have been intensively studied and compared in terms of their AMS mass spectral signatures. However, the source profiles may differ with fuel types and combustion conditions, and relevant studies are very scarce, hindering the efforts for a better apportionment of sources with PMF-AMS. Healy et al.[25] and Dall'Osto et al.[26] carried out a series of experiments on wood, smokeless coal, and peat burning in an open-door grate using aerosol time-of-flight mass spectrometer (ATOFMS) and high-resolution time-of-flight aerosol mass spectrometer (HR-ToF-AMS), respectively, which provides high-mass-resolution characterization of emitted PM. Wang et al.[9] characterized OA formation during pulverized coal combustion in a drop-tube furnace. Zhou et al.[11] studied the evolution of OA from burning different types of coal in a typical Chinese stove using an aerosol chemical speciation monitor (ACSM, a compact version of AMS).[27] However, to the best of our knowledge, direct Q-ACSM measurements and comparison of domestic wood, peat, and coal burning have not been reported, which should get more attention for their significant impacts on air quality in Ireland and other places (e.g., the United Kingdom and Finland) where these fuels are popular for domestic heating.[6,7,25,26]

In this study, seven solid fuel samples including dry wood (15%−20% moisture, DW), wet wood (>20% moisture, WW), dry raw peat (DP), wet raw peat (WP), peat briquettes (PB), bituminous (smoky) coal (SC), and ovoids (smokeless, based on anthracite) coal (SLC) were burned in a typical residential stove in Ireland. Characterization of PM emitted from burning these samples was conducted using an ACSM. OA was found to be the major contributor to the total submicron nonrefractory ($NR\text{-}PM_1$) aerosol particles. Mass spectral signatures of OA from each fuel type were obtained at unit mass resolution and compared. These signatures were used to apportion ambient OA measured by ACSM in Galway, Ireland to estimate the relative contribution of each type of fuel to air pollution and characterize their emission and formation process by comparing the influence of continental and marine air masses.

2. EXPERIMENTAL SECTION

Solid Fuel Types. Wood (oak), raw peat, peat briquettes, bituminous (smoky) coal, and smokeless coal ovoids were purchased locally in County (Co.) Tipperary, where the burning experiments were performed. Peat products are locally produced, and smoky coal is imported from Colombia (78% of the coal in Ireland is imported from Colombia in 2014; SEAI 2016). Smokeless coal (ovoids) is purchased from ArignaBiofuels (based in Ireland) where coal is roasted, blended with other biomass products, and briquetted as ovoids. Stored, dried wood had a moisture content less than 20%. Wet wood had a moisture content from 20% up to 40%. Peat is an accumulation of partially decayed vegetation and is the first step for the formation of coal. Raw peat is cut from peatlands, and peat briquettes are compressed peat.[28] Raw peat was dry when purchased and was exposed to the outdoor atmosphere to achieve wet raw peat. Smoky coal and smokeless coal were directly burned because they are more water resistant.

Fingerprinting Experiment Setup. The solid fuel burning experiments were performed using a solid fuel stove located in a cottage in Co. Tipperary from January 16 to 21 2016 with an average ambient temperature of 6 ± 3 °C and RH of 92 ± 5%. A schematic of the stove and sampling system is provided in Scheme S1. Each type of sampling fuel was continuously burned for at least 1 h with a total use of each type of fuel >5 kg. The stove was cleared of residue following combustion of each fuel sample. An ACSM device (Aerodyne Research Inc.) was used to characterize the chemical composition of the $NR\text{-}PM_1$ and obtain unique mass spectral signatures of aerosols produced from burning each of the solid fuels. In the ACSM,[27] nafion dried submicron particles sampled through the inlet are deposited on the heated surface (600 °C), and only the $NR\text{-}PM_1$ are vaporized and ionized by the ion source. The resulting ions are analyzed by quadrupole mass spectrometer. Black carbon and other refractory components are not analyzed by ACSM. The time resolution of ACSM for ambient measurement is usually set at ∼15−30 min due to the low concentration, while in this direct fuel combustion measurement, it was set at ∼1 min (1 set of sample and filter cycle) for the high aerosol emission (10−500 $\mu g/m^3$) during the sampling period. The emissions from the 1 h burning were averaged to get the relative mass contribution and mass spectral signatures of OA for each type of fuel.

Ambient Aerosol Measurements in Galway. The ambient aerosol measurements were conducted in the National University of Ireland Galway's Center of Climate and Air Pollution Studies (53.28° N and 9.06° W) from October 17th to November 23rd, 2015. This site is located adjacent to and east off the main urban residential area and at least 200 m away from the main road to avoid the direct influence from traffic. Ambient air was drawn from a height of around 6 m above the ground through a tube at a flow rate at 3 LPM. A substream of ∼85 mL/min was analyzed by ACSM at a time resolution of 30 min. Meteorological data recorded at the engineering building (1 km from the monitoring site) was used to compare and analyze the origin and transport of aerosol in this study.

Data Analysis. In this study, we employ ME-2[29−31] within the SoFi software package (version 6.1), an Igor-based software, for source apportionment. A detailed description of ME-2 and the software package can be found in Canonaco et al.[29] Briefly,

DOI: 10.1021/acs.est.7b01926
Environ. Sci. Technol. 2017, 51, 10624−10632

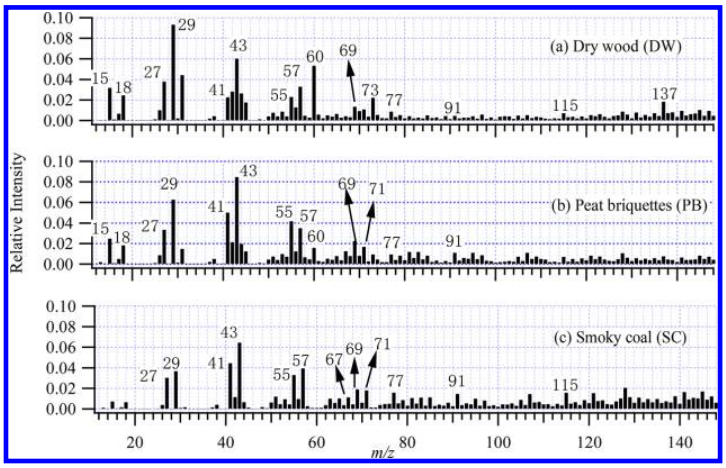

Figure 1. Normalized mass spectra of organics from the combustion of (a) dry wood, (b) peat briquettes, and (c) smoky coal.

in a typical PMF algorithm in which a measured matrix X can be deconvolved into two matrices (G and F) and the remaining residue matrix (E), multiple combinations of G and F due to rotational ambiguity can lead to mathematically meaningful but not interpretable PMF solutions especially when factors show temporal covariations. An *a*-value approach within ME-2 has been successfully used to explore the rotational ambiguity for online and offline data set in which users can direct the algorithm toward environmentally reasonable rotations by constraining reference factor profiles (currently the case) or time series based on priori information.[17,32,33] The *a* value determines the extent to which a reference profile is allowed to vary (e.g., an *a* value of 0.1 allows a variability of 10%). In this study, the pollution events mostly happened during evening or night-time, indicating their emission sources from domestic heating. Thus, we conducted the source apportionment by constraining the primary components, i.e., oil (HOA), peat, coal, and wood using the *a*-value approach and allowed for one additional free factor representing OOA. The HOA reference profile, taken from Crippa et al.,[21] usually represents emission profile from traffic.[34,35] However, oil burning has similar particulate emissions to that of traffic emission in terms of mass spectra as indicated in the diesel burning work by Schneider et al.[23] and the vehicles chase study by Canagaratna et al.[22] Actually, oil burning for domestic heating is quite popular in Galway, Ireland (around 85% of the non-natural gas and nonelectricity households) based on the census data from Central Statistics Office on the households by the type of central heating (CSO)[36] (Figure S1). The night-time peaks of HOA (Figure 4a,b) indicates its source from domestic heating; HOA is, therefore, denoted as oil burning thereafter. The *a* value of 0.1 (an *a* value of 0−0.2 was explored, and more information is provided in the OA Source Apportionment section) was used for all primary factors (oil, peat, coal, and wood).

3. RESULTS AND DISCUSSION

Relative Fraction of Solid-Fuel Burning NR-PM_1 Emissions. Organics constitute the largest fraction of total NR-PM_1 emissions from burning fuels (e.g., ∼98% for dry wood, ∼91% for peat briquettes, and ∼94% smoky coal) except for the smokeless coal (∼26%) (Figure S2). For the latter, chloride is the major component of the aerosol particles, with a value of about 53%, followed by organics (26%), sulfate (11%), and ammonium (8%). Burning conditions have minor effects on the relative contribution of ACSM species by comparing dry and wet wood and dry and wet raw peat. In contrast, the compositions of fuel type result in differences in contributions to NR-PM_1 mass between different types of fuels. For example, wood burning emissions contain little sulfate and little ammonium (∼0.3%), while all types of peat burning emissions have higher levels of sulfate, with around 5% of the total NR-PM_1 mass being sulfate for peat briquettes.

ACSM Mass Spectra Profiles of Different Fuels. Averaged normalized ACSM unit mass resolution (UMR) mass spectra (MS) of OA particles obtained for dry wood, peat, and coal are shown in Figure 1. All three MS are dominated by C_nH_{2n+1} (29, 43, 57, 71···) and C_nH_{2n-1} (27, 41, 55, 69···), indicating the large contribution from saturated alkanes, alkenes, and also possible cycloalkanes in the primary OA emissions from wood, peat, and coal. However, the MS profile patterns and signals at specific *m*/*z* (e.g., *m*/*z* 60) of different fuels vary significantly corresponding to the composition of the fuels. For example, the most prominent ion in wood burning aerosol MS profile is the signal at *m*/*z* (mass to charge ratio) 29, followed by *m*/*z* 43, while *m*/*z* 43 is the most abundant ion in peat emissions, followed by *m*/*z* 29. In contrast, *m*/*z* 43 and *m*/*z* 41 are the most abundant ions in coal emissions MS. In addition, there was a relatively higher contribution from heavier ions (>100) in the coal emission spectra most likely from PAH emissions if compared to the peat and wood spectra.

Wood. The prominent signals at *m*/*z* 29 and 43 in wood emissions (Figure 1a) are consistent with the previous reports using HR-ToF-AMS.[24] The large presence of CHO^+ and $C_2H_3O^+$ in HR-ToF-AMS are found to be responsible for the high signal at *m*/*z* 29 and *m*/*z* 43, respectively.[24] Mass fragments at *m*/*z* 60 are often regarded as marker fragments for wood burning aerosols,[37] which mainly arise from the thermal decomposition of cellulose, the pyrolysis of which produces levoglucosan. The electron impact ionization of levoglucosan shows intense signals at *m*/*z* 60.[26] Fragment *m*/*z* 44 (CO_2^+, strongly influenced by di or poly(carboxylic acid)s), a marker for OOA,[38] which arises together with *m*/*z* 18 (which is set to equal to *m*/*z* 44 in the fragmentation table as in the Q-AMS) contributes to around 2% of total BBOA signal.[39,40] Fragment

DOI: 10.1021/acs.est.7b01926
Environ. Sci. Technol. 2017, 51, 10624−10632

m/z 29 has the highest fraction of the signal in the dry wood profile. However, it is not a unique marker for wood burning due to its presence in all other fuel profiles. These characteristics are consistent with other UMR MS of OA from pine burning and PMF results of ambient OA data.[10,37] Wet wood profile shows a higher contribution from larger m/z fragments especially at m/z 137 (Figure S3), which may be due to the fact that wet wood has a lower burning temperature that leads to incomplete combustion. Despite the differences between dry wood and wet wood profile, wood marker fragments m/z 60, 73, and 137 are still prominent. The MS signal fractions of m/z > 80 for dry wood are 31%, which implies that primary OA from wood burning contains high-molecular-weight organic compounds. This high fraction is consistent with the previous fingerprinting experiment reported by He et al.[24] in which high signal fractions of m/z > 100 could reach 13%. However, the absolute amount is strongly influenced by the transmission function applied in the ACSM in which small errors in the higher m/z range can cause the behavior of slowly increasing calculated signal at m/z above 100.

Peat. Mass spectrometry of primary OA from peat shows the highest signal fraction at m/z 43 (Figure 1b), which is consistent with the HR-ToF-AMS measurement of open-grate peat burning[26] and the ToF-ACSM measurement of peat burning in closed chamber.[41] Ions at m/z 43 are dominated by $C_3H_7^+$ in peat emissions, while $C_2H_3O^+$ dominate the same nominal ions in wood emissions in HR-ToF-AMS.[26] $C_xH_y^+$-type ions make up 71% of peat MS, which implies a high fraction of hydrocarbon in peat emissions.[26] In addition, typical aromatic ion series at m/z 77 and 91 are present in the peat MS and are more prominent than that in wood MS. The presence of m/z 60 in peat MS profiles is due to the incomplete decay of vegetation, which contains cellulose.[42] Cellulose is one of the most common chemical substances that exist in peat.[42] Although these ion series in peat profile are not as prominent as in the wood profile, ions at m/z 60 are enough to distinguish the peat MS profile from coal and oil whose formation involves a complete decay of vegetation. For example, HOA from traffic typically has the most prominent peak at m/z 57, characteristic of saturated hydrocarbons but no signal at m/z 60.[20,43] High similarity in MS profiles for dry, wet raw peat and peat briquettes (R^2 > 0.95) can be observed, which suggests that the state of the peat (raw, wet, shredded, and compressed into briquettes) does not make a difference to the OA mass spectra (Figure S4). The MS signal fractions of m/z > 80 for peat are 34%, which is slightly higher than wood, indicating that high-molecular-weight compounds are forming in peat.

Coal. The burning of smoky coal visibly produces a larger amount of black carbon than smokeless coal. However, the mass spectral signatures of smoky and smokeless coal appear very similar (Figure S5), both with large contribution from heavier ions. The similarity in MS patterns between smoky and smokeless coal indicates that the compositions in ovoids responsible for the emission of primary OA are similar to that of smoky coal. The strongest peak in coal MS is the signal at m/z 43, followed by m/z 41 (Figure 1c). This is similar to peat and consistent with a previous HR-ToF-AMS measurement of emissions from open-grate coal burning.[26] $C_xH_y^+$-type ions dominate the MS of coal with a fraction of 71%, which is the same as peat MS profile.[26] Coal is formed through a process called "coalification"[44] when peat is physically and chemically altered as a result of bacterial decay, compaction, heat and time. No signal at m/z 60 was observed for smoky coal MS (Figure 1c), which might be due to the complete decomposition of cellulose in the formation of coal. In contrast, m/z 60 is slightly elevated in ovoids MS, which might be due to its complex composition that contains biomass. The absence of m/z 60 distinguishes smoky coal MS from contemporary biomass burning. In addition, the signal at m/z 57 is slightly higher than m/z 55 in coal profile, while the opposite is the case for peat, indicating that coal has more saturated hydrocarbon than peat. Further, fragments at m/z 77, 91, and 115 are stronger in coal MS than in peat MS likely due to the high fraction of aromatic compounds in coal. The signal fractions of m/z > 80 are 51%, which is significantly higher than wood and peat.

Differences between ACSM Profiles and Implications for PMF Analysis. The differences between the MS shown in Figure 1 are compared by plotting the relative differences of individual m/z values compared to peat (i.e., ($f(m/z$, wood and coal) − $f(m/z$, peat))/$f(m/z$, peat); see Figure S6). The peat MS was chosen as the reference MS due to the fact peat is the middle evolution state between wood and coal. Wood and peat MS show moderate similarity with the correlation value R^2 of 0.69 (Table S2). Differences at values of m/z 29, 31, 41, 60, 73, 83, 96, and 137 are mainly responsible for the discrepancy. Higher values of m/z 29, 31, 60, 73, and 137 (positive relative difference for wood) are observed for wood, while higher values of m/z 41, 83, and 96 (negative relative difference) are observed for peat. Coal and peat MS also show moderate similarity, with R^2 being 0.77. Higher values at m/z 29, 31, 45, 60, and 73 for peat and higher values at m/z > 115 for coal contribute mainly to the discrepancy. The differences in intensities at the m/z values mentioned above are expected to play an important role in PMF to separate OA emissions from wood, peat, and coal.

For the comparison between MS profiles of all the burning sources in this study and PMF factors of ambient measurement from literature, R^2 values were calculated and summarized in Table S2. The dry and wet raw peat MS shows a good intercorrelation with R^2 being 0.98, which was higher than that between dry wood and wet wood (R^2 = 0.91), indicating that wood burning emissions are more influenced by moisture. Smoky coal and smokeless coal show the poorest intercorrelation (R^2 = 0.78), which is in part due to the production process of smokeless coal from smoky coal that leaves out most of the volatile content in smoky coal responsible for the high smoke output. In fact, the signal fractions in the range m/z > 80 for smokeless coal MS are 40.9%, which is less than that of smoky coal (51.3%). The discrepancy in the MS between smoky coal and smokeless coal can also be explained by complicated compositions of ovoids that are blended with biomass (www.arignabiofuels.ie). This might also be the reason that the correlation coefficient between smokeless coal and peat could reach 0.92. In this regard, it is hard to separate peat and smokeless coal in factor analysis of the ambient data set. Peat briquettes MS is better correlated with PMF factor BBOA (taken from Ng et al.[43]) (mean R^2 = 0.88) than dry wood (R^2 = 0.77), which implies that in areas where peat is widely used (e.g., Ireland and the United Kingdom), extreme care is required to separate peat and BBOA because they have similar MS and usually show temporal covariation as domestic heating fuels. Peat shows moderate correlation (mean R^2 = 0.8) with HOA (taken from Crippa et al.),[21] but an elevated signal at m/z 60 for peat should be enough to distinguish them in PMF analysis. Wood and HOA shows a bad correlation (mean R^2 =

DOI: 10.1021/acs.est.7b01926
Environ. Sci. Technol. 2017, 51, 10624−10632

0.25), which means that wood-burning emissions can be easily separated from HOA in factor analysis of the ambient data set.

Ambient Measurement of NR-PM$_1$ in Galway, Ireland. An overview of the NR-PM$_1$ components (organics, nitrate, sulfate, and ammonium) in Galway during early winter (from October 17th to November 23rd, 2015) is shown in Figure 2 as well as meteorological parameters (wind direction, wind speed, relative humidity, and temperature). During the measurement period, the temperatures were mild, with an average of 10.6 ± 2.6 °C ranging from 3 to 16 °C. The ambient relative humidity had a mean value of 90.8 ± 8.8%, ranging from 56% to 100%. The wind mainly blew from the southwest (46% of the time) with a mean wind velocity of 3.1 ± 1.6 m/s ranging from 0.4 to 9.2 m/s. The ACSM yielded a range of NR-PM$_1$ concentrations from 0.1 to 43.5 μg/m^3, with a low mean value of 3.4 ± 4.5 μg/m^3 mainly due to the frequent influence of clean marine air masses. However, under certain meteorological conditions of continental air masses (periods S1 and S2) and low wind speed (<2 m/s), a high concentration of NR-PM$_1$ can build up throughout the day, with an average of 7.8 μg/m^3 and 11.2 μg/m^3 for S1 and S2, respectively. Even with marine air masses and associated low wind speed (M3), high peak NR-PM$_1$ concentration (34 μg/m^3, 10 times mean NR-PM$_1$ value) can be seen in the evening and night-time, indicating the large emissions from domestic heating in Galway. A very low background concentration of lower than 1 μg/m^3 was observed during the daytime of the period M3 despite high pollution at night. Thus, it is insightful to analyze the composition during different periods.

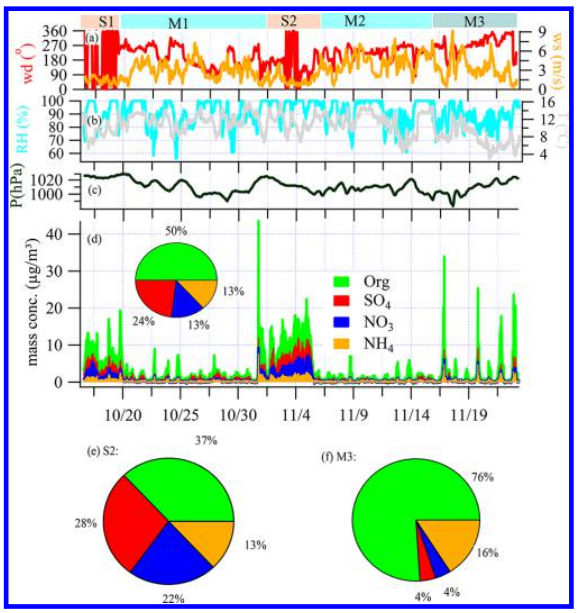

Figure 2. Time series of (a) wind direction (wd) and wind speed (ws); (b) relative humidity (RH) and temperature (T); (c) pressure (P); and (d) submicron species, i.e., organics, sulfate, ammonium, and nitrate. The inset pie chart shows average composition for the entire study the and pie chart contribution of submicron species during selected periods (e) S2 and (f) M3. The colors and characters on the top of the graph represent the different air masses classifications: light red, stagnant continental (S1 and S2); light green, marine with high wind speed (M1 and M2); dark green, marine with low wind speed (M3). Back-trajectory analysis for the whole periods is shown in Figure S11.

On average, the NR-PM$_1$ mass mainly composed of OA (50%), followed by sulfate (24%), ammonium (13%), and nitrate (13%) for the entire measurement period in Galway (Figure 2d). However, under different meteorological conditions, their fractions vary significantly. During stagnant time periods (S2) with continental air masses, the pollution levels were elevated throughout the day and the fraction of secondary inorganic aerosols (sulfate, nitrate, and ammonium) increased to around 63% (Figure 2e), indicating a regional source. In contrast, during marine time periods, OA alone accounts for 76% of total NR-PM$_1$ mass (Figure 2f). The recurring evening and night-time pollution events, with OA being the dominant component, underline the importance of source apportionment of OA.

OA Source Apportionment. For source apportionment of OA, we take advantage of ME-2, which can direct the PMF analysis to environmentally reasonable solutions by constraining the a priori ACSM-derived source profiles of peat, coal, and wood as well as oil (HOA) from Crippa et al.[21] An *a* value of 0.1 (i.e., 10% variation in profile) was applied due to the fact that most primary OA was freshly emitted, with peak concentrations occurring at the early nighttime and thus should have small variation from the ACSM derived fingerprints. Due to the lack of possible tracer marker for each type of domestic fuel combustions, the best *a* value will be further investigated as indicated in Elser et al.[17] As illustrated in Figure 3a, a five-factor solution including four constrained primary factors and one additional unconstrained OOA is found to be the environmentally reasonable solution. Further increase of the number of factors leads to uninterpretable factors (Figure S7). The time series of four primary factors (Figure 3b) show similar temporal variation due to the similar emission time from domestic heating activities during the evening, which was also the reason why ME-2 is necessary to separate preconstrained factors to estimate the contribution of candidate sources. Otherwise, highly mixed and non-meaningful factors would be achieved with a totally unconstrained PMF (Figure S8) and, thus, an unconstrained PMF would be unable to estimate the contribution of the different combustion fuels to the air pollution. In contrast, the OOA could be easily resolved both in constrained and unconstrained PMF due to its time series distinct from primary factors. OOA is characterized with a prominent signal at m/z 44 and has a high correlation with sulfate (R^2 = 0.83). The OOA time series show a relatively constant high level during periods S1 and S2, indicating the importance of OOA formation under these conditions. However, during periods M1, M2, and M3, some evening peaks of OOA can also be observed, indicating an additional contribution from a more local and evening and night-time production process. Unlike OOA, the resulting time series of primary factors only show elevated evening and night-time pollution levels, corresponding to emission time.

When running ME-2 using the *a*-value approach on ACSM data sets, the selection of best *a* value is critical. An *a* value that is too small (i.e., very tightly constrained) might not give enough freedom to the unconstrained factor (e.g., OOA), while a large *a* value might lead to interfactor mixing. Thus, an optimized *a* value need to be explored in ME-2. Previous work by Elser et al.[17] suggests the selection criteria of using factor-tracer correlation to find the best *a* value corresponding solution that best describes the organic aerosols. A combination

DOI: 10.1021/acs.est.7b01926
Environ. Sci. Technol. 2017, 51, 10624−10632

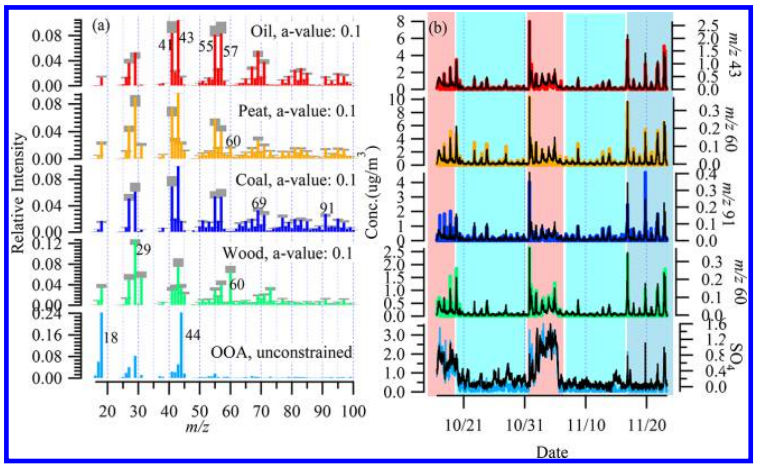

Figure 3. (a) Factor profiles (mass spectra) of 5-factor ME-2 solution. The a-value method within SoFi was applied (matrix with m/z up to 100 was used for PMF). Oil-burning profile is from ambient data PMF-derived hydrocarbon-like organic aerosol (HOA).[21] Peat, wood, and coal reference profiles are from previous fingerprinting experiments. Gray bar in the back represents reference profile employed. (b) The factor time series (color-coded with the same periods of S1, M1, S2, M2, and M3 as in Figure 2) of source apportionment and comparison of primary factors with typical ACSM fragments (HOA vs m/z 43 (R^2 = 0.88); peat vs m/z 60 (R^2 = 0.84); coal vs m/z 91 (R^2 = 0.63); wood vs m/z 60 (R^2 = 0.79)) and a comparison of secondary factors (OOA) with an external source of sulfate (R^2 = 0.83).

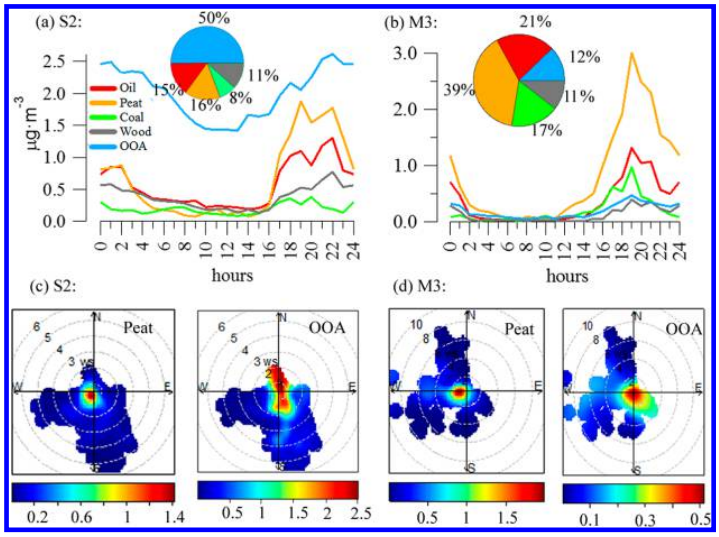

Figure 4. Diurnal cycle of resolved factors (i.e., oil, peat, coal, wood, and OOA) during (a) periods of relatively stagnant and continental air masses (S2) and (b) marine air masses (M3) (insets are relative contribution of the resolved OA factors). Polar plot of hourly averaged major component of OA (i.e., peat and OOA; color-coded based on concentration of each species in $\mu g/m^3$) as a function of wind speed (radial axis) and wind direction during periods (c) S2 and (d) M3. Polar-plot figures were generated with OpenAir software.[48]

of different a values for a specific factor can be derived using this method. However, in cases in which the constrained factors' corresponding tracer data are not available, we assume a same a value for all constrained factors. To explore the influence of a value, a value of 0, 0.05, 0.1, and 0.2 were run in ME-2. The constrained factors' relative fraction and the correlation between the unconstrained OOA and sulfate are found to be affected by a value differently (Figure S10). The factors' relative contribution to total OA for oil, coal, and wood burning remain nearly unchanged for this a value range (0–0.2). In contrast, OOA fraction decreases sharply from 45% to 35% as a value of increases from 0 to 0.1 but slowly from 35% to 34% as a value increases from 0.1 to 0.2, while peat burning fraction increases from 21% (a value of 0) to 32% (a value of 0.1) and decreases to 28% (a value of 0.2). R^2 between the OOA and sulfate increases from 0.71 to 0.83 as the a value increases from 0 to 0.1 and starts to level off after 0.1. Thus, 0.1 is found to be the most-optimized a value because it can give enough freedom to OOA and prevent further mixing between factors by increasing the a value. It is also important to note that peat is always the largest primary fraction with the same a value.

Local versus Regional OA Sources. During the measurement periods, the frequent marine air masses bring a very clean

DOI: 10.1021/acs.est.7b01926
Environ. Sci. Technol. 2017, 51, 10624–10632

background OA level (<0.1 $\mu g/m^3$) that provides a perfect chance to study the anthropogenic pollutants especially for the local sources. In addition, occasional continental air masses bring the opportunity to study the regional OA sources from the United Kingdom and mainland Europe. The relationship between resolved OA factors and meteorology is, therefore, demonstrated by comparing two distinct pollution patterns corresponding to continental and marine air masses (Figure S11). Continental air masses and marine air masses alternated during the measurement period and led to different contributions of OA factors as well as diurnal patterns, especially for OOA. As shown in Figure 4a, OOA is the major component of OA in continental air masses (S2; 50%), and its diurnal cycle shows higher concentration during the night than day, which might be due to the influence of planetary boundary layer that is shallower during night and higher during the day. Wind roses of OOA during S2 show that higher OOA concentrations are related to air masses from the north and southeast side rather than the west side of measurement location, indicating that its origin might come from mainland Europe or the United Kingdom rather than the ocean (Figure 4c). In contrast, in the marine air masses (i.e., M3 period), OOA only comprises 12% of total OA (Figure 4b), and its diurnal cycle shows a peak at evening and night-time, which coincides with primary factors, indicating a possible night-time OOA formation process of the condensation of semivolatile organic matter emitted from fuel combustion.[47] In addition, the wind roses of OOA (Figure 4d) during M3 show no preference for wind direction but for low wind speed, which might be required for the formation process as semivolatile organic matter dissipate more quickly with high wind speed. The wind rose of OOA between S2 and M3 shows a clear different pattern indicating the difference in transport and formation of OOA under different meteorological conditions. Similarly, inorganic aerosols (sulfate, nitrate, and ammonium) also show obvious peaks during M3 nighttime, which should also come from primary emissions or fast night-time formation (Figure 2).

Unlike OOA, all primary factors (oil, peat, coal, and wood burning), show peak concentrations at early night (at around 19:00) and very low concentrations (<0.5 $\mu g/m^3$) during the day (8:00−16:00, sunrise at around 8:00 and sunset at around 16:00 during the measurement period), corresponding to their emission time and locally produced nature. Primary OA contributes around 50% during S2 and 88% during M3, indicating its importance for air pollution over the wintertime, especially during marine periods. Peat burning contributes 39% during M3 and 16% during S2 (Figure 4a,b), making it the largest primary contributor to the total ambient OA during cold winter nights in Galway. This is in great contrast to the relatively small usage of peat, as indicated by the census data (Figure S1) from Central Statistics Office, which shows only around 10% of the non-natural gas and non-electricity households use peat for heating. However, the emission-factor profile (Table S1),[45] which indicates a large emission factor and a low net calorific value for peat can help explain the dominance of peat. Similarly, smoky coal has a large emission factor and claim for 17% of total OA mass during M3 when less than 1% of the households report the use of smoky coal for heating probably due to the ban on coal in Galway. In contrast, most households use oil for heating (around 85%) but, due to the low emission factor for oil burning, a relatively small fraction (21% during M3) is observed. HOA is usually used to quantify the traffic emissions.[21] However, the time series of HOA in this study show a huge early evening peak (at around 19:00) and the absence of a morning rush hour peak (Figure 4a,b), which points to its major source from domestic heating activities rather than traffic as reported by previous papers.[34,35] It is possible that the interference from oil burning due to their similar mass spectra[22,23] and the low mass resolution of ACSM leads to the difficulties in resolving the traffic factor with a low contribution (e.g., <5%), particularly when it co-varies with a source with higher emissions. Previous work by Ulbrich et al. suggests that true components with <5% of the mass are difficult to retrieve accurately using PMF.[46] In contrast to OOA, the wind roses of major primary factor (i.e., peat burning) always show an origin from the west of the measurement site during both the S2 and the M3 periods, which is consistent with the location of the residential area.

■ ASSOCIATED CONTENT

Supporting Information

The Supporting Information is available free of charge on the ACS Publications website at DOI: 10.1021/acs.est.7b01926.

A scheme showing combustion and sampling system. Tables showing the emission factors and caloric values for oil, peat, coal, and wood and correlation coefficients between ACSM profiles of different sources and PMF factors. Figures showing the relative fraction of ACSM measured species, the mass spectra of each type of fuel under different states, the relative difference of dry wood and smoky coal MS profile compared to peat at each m/z, the time series and mass spectra of PMF solutions, the relative contribution of the resolved factors and correlation between OOA and sulfate, and the back trajectory during the measurement period in Galway Ireland. (PDF)

■ AUTHOR INFORMATION

Corresponding Authors

*Phone: +86-(0)29-6233-6275; e-mail: rujin.huang@ieecas.cn.
*Phone: +353-91-49-3306; e-mail: colin.odowd@nuigalway.ie.

ORCID

Chunshui Lin: 0000-0003-3175-6778

Notes

The authors declare no competing financial interest.

■ ACKNOWLEDGMENTS

This work was supported by EPA-Ireland (AEROSOURCE, 2016-CCRP-MS-31), the National Natural Science Foundation of China (NSFC) under grant no. 91644219, and Chinese Scholarship Council (CSC, no. 201506310020). We also thank Harry Arndt for allowing us to use the cottage in County Tipperary for the burning experiments and especially for providing valuable input into the design and construction of the sampling system. The team from University College Cork acknowledge support from the Environmental Protection Agency and Department of Environment Community and Local Government in Ireland through the SAPPHIRE project (2013-EH-MS.15).

■ REFERENCES

(1) Pope, C. A., III; Burnett, R. T.; Thun, M. J. Lung cancer, cardiopulmonary mortality, and long-term exposure to fine particulate air pollution. *JAMA* **2002**, *287* (9), 1132−1141.

DOI: 10.1021/acs.est.7b01926
Environ. Sci. Technol. 2017, 51, 10624−10632

(2) Sandström, T.; Nowak, D.; van Bree, L. Health effects of coarse particles in ambient air: messages for research and decision-making. *Eur. Respir. J.* **2005**, *26* (2), 187−188.
(3) O'Dowd, C. D.; Facchini, M. C.; Cavalli, F.; Ceburnis, D.; Mircea, M.; Decesari, S.; Fuzzi, S.; Yoon, Y. J.; Putaud, J.-P. Biogenically driven organic contribution to marine aerosol. *Nature* **2004**, *431* (7009), 676−680.
(4) Kelly, I.; Clancy, L. Mortality in a general hospital and urban air pollution. *Irish Med. J.* **1984**, *77* (10), 322−324.
(5) Clancy, L.; Goodman, P.; Sinclair, H.; Dockery, D. W. Effect of air-pollution control on death rates in Dublin, Ireland: an intervention study. *Lancet* **2002**, *360* (9341), 1210−1214.
(6) Goodman, P. G.; Rich, D. Q.; Zeka, A.; Clancy, L.; Dockery, D. W. Effect of Air Pollution Controls on Black Smoke and Sulfur Dioxide Concentrations across Ireland. *J. Air & Waste Manage* **2009**, *59* (2), 207−213.
(7) Kourtchev, I.; Hellebust, S.; Bell, J. M.; O'Connor, I. P.; Healy, R. M.; Allanic, A.; Healy, D.; Wenger, J. C.; Sodeau, J. R. The use of polar organic compounds to estimate the contribution of domestic solid fuel combustion and biogenic sources to ambient levels of organic carbon and PM2.5 in Cork Harbour, Ireland. *Sci. Total Environ.* **2011**, *409* (11), 2143−2155.
(8) International Energy Agency. Energy balance for Ireland. http://www.iea.org/statistics/statisticssearch/ (accessed December 8, 2016).
(9) Wang, X.; Williams, B.; Wang, X.; Tang, Y.; Huang, Y.; Kong, L.; Yang, X.; Biswas, P. Characterization of organic aerosol produced during pulverized coal combustion in a drop tube furnace. *Atmos. Chem. Phys.* **2013**, *13* (21), 10919−10932.
(10) Weimer, S.; Alfarra, M. R.; Schreiber, D.; Mohr, M.; Prévôt, A. S. H.; Baltensperger, U. Organic aerosol mass spectral signatures from wood-burning emissions: Influence of burning conditions and type. *J. Geophys. Res.* **2008**, *113* (10), 304−305.
(11) Zhou, W.; Jiang, J.; Duan, L.; Hao, J. Evolution of Submicrometer Organic Aerosols during a Complete Residential Coal Combustion Process. *Environ. Sci. Technol.* **2016**, *50* (14), 7861−7869.
(12) Jayne, J. T.; Leard, D. C.; Zhang, X.; Davidovits, P.; Smith, K. A.; Kolb, C. E.; Worsnop, D. R. Development of an aerosol mass spectrometer for size and composition analysis of submicron particles. *Aerosol Sci. Technol.* **2000**, *33* (1−2), 49−70.
(13) Canagaratna, M. R.; Jayne, J. T.; Jimenez, J. L.; Allan, J. D.; Alfarra, M. R.; Zhang, Q.; Onasch, T. B.; Drewnick, F.; Coe, H.; Middlebrook, A.; Delia, A.; Williams, L. R.; Trimborn, A. M.; Northway, M. J.; DeCarlo, P. F.; Kolb, C. E.; Davidovits, P.; Worsnop, D. R. Chemical and microphysical characterization of ambient aerosols with the aerodyne aerosol mass spectrometer. *Mass Spectrom. Rev.* **2007**, *26* (2), 185−222.
(14) Middlebrook, A. M.; Bahreini, R.; Jimenez, J. L.; Canagaratna, M. R. Evaluation of Composition-Dependent Collection Efficiencies for the Aerodyne Aerosol Mass Spectrometer using Field Data. *Aerosol Sci. Technol.* **2012**, *46* (3), 258−271.
(15) Carbone, S.; Saarikoski, S.; Frey, A.; Reyes, F.; Reyes, P.; Castillo, M.; Gramsch, E.; Oyola, P.; Jayne, J.; Worsnop, D.; Hillamo, R. Chemical characterization of submicron Aerosol particles in Santiago de Chile. *Aerosol Air Qual. Res.* **2013**, *13* (2), 462−473.
(16) Canonaco, F.; Slowik, J. G.; Baltensperger, U.; Prévôt, A. S. H. Seasonal differences in oxygenated organic aerosol composition: Implications for emissions sources and factor analysis. *Atmos. Chem. Phys.* **2015**, *15* (12), 6993−7002.
(17) Elser, M.; Huang, R. J.; Wolf, R.; Slowik, J. G.; Wang, Q.; Canonaco, F.; Li, G.; Bozzetti, C.; Daellenbach, K. R.; Huang, Y.; Zhang, R.; Li, Z.; Cao, J.; Baltensperger, U.; El-Haddad, I.; Prevot, A. S. H. New insights into PM2.5 chemical composition and sources in two major cities in China during extreme haze events using aerosol mass spectrometry. *Atmos. Chem. Phys.* **2016**, *16* (5), 3207−3225.
(18) Zhang, Q.; Jimenez, J. L.; Canagaratna, M. R.; Ulbrich, I. M.; Ng, N. L.; Worsnop, D. R.; Sun, Y. Understanding atmospheric organic aerosols via factor analysis of aerosol mass spectrometry: A review. *Anal. Bioanal. Chem.* **2011**, *401* (10), 3045−3067.
(19) Jimenez, J. L.; Canagaratna, M. R.; Donahue, N. M.; Prevot, A. S. H.; Zhang, Q.; Kroll, J. H.; DeCarlo, P. F.; Allan, J. D.; Coe, H.; Ng, N. L.; Aiken, A. C.; Docherty, K. S.; Ulbrich, I. M.; Grieshop, A. P.; Robinson, A. L.; Duplissy, J.; Smith, J. D.; Wilson, K. R.; Lanz, V. A.; Hueglin, C.; Sun, Y. L.; Tian, J.; Laaksonen, A.; Raatikainen, T.; Rautiainen, J.; Vaattovaara, P.; Ehn, M.; Kulmala, M.; Tomlinson, J. M.; Collins, D. R.; Cubison, M. J. E.; Dunlea, J.; Huffman, J. A.; Onasch, T. B.; Alfarra, M. R.; Williams, P. I.; Bower, K.; Kondo, Y.; Schneider, J.; Drewnick, F.; Borrmann, S.; Weimer, S.; Demerjian, K.; Salcedo, D.; Cottrell, L.; Griffin, R.; Takami, A.; Miyoshi, T.; Hatakeyama, S.; Shimono, A.; Sun, J. Y.; Zhang, Y. M.; Dzepina, K.; Kimmel, J. R.; Sueper, D.; Jayne, J. T.; Herndon, S. C.; Trimborn, A. M.; Williams, L. R.; Wood, E. C.; Middlebrook, A. M.; Kolb, C. E.; Baltensperger, U.; Worsnop, D. R. Evolution of Organic Aerosols in the Atmosphere. *Science* **2009**, *326* (5959), 1525−1529.
(20) Lanz, V. A.; Prevot, A. S. H.; Alfarra, M. R.; Weimer, S.; Mohr, C.; Decarlo, P. F.; Gianini, M. F. D.; Hueglin, C.; Schneider, J.; Favez, O.; D'Anna, B.; George, C.; Baltensperger, U. Characterization of aerosol chemical composition with aerosol mass spectrometry in Central Europe: An overview. *Atmos. Chem. Phys.* **2010**, *10* (21), 10453−10471.
(21) Crippa, M.; Decarlo, P. F.; Slowik, J. G.; Mohr, C.; Heringa, M. F.; Chirico, R.; Poulain, L.; Freutel, F.; Sciare, J.; Cozic, J.; Di Marco, C. F.; Elsasser, M.; Nicolas, J. B.; Marchand, N.; Abidi, E.; Wiedensohler, A.; Drewnick, F.; Schneider, J.; Borrmann, S.; Nemitz, E.; Zimmermann, R.; Jaffrezo, J. L.; Prévôt, A. S. H.; Baltensperger, U. Wintertime aerosol chemical composition and source apportionment of the organic fraction in the metropolitan area of Paris. *Atmos. Chem. Phys.* **2013**, *13* (2), 961−981.
(22) Canagaratna, M. R.; Jayne, J. T.; Ghertner, D. A.; Herndon, S.; Shi, Q.; Jimenez, J. L.; Silva, P. J.; Williams, P.; Lanni, T.; Drewnick, F.; Demerjian, K. L.; Kolb, C. E.; Worsnop, D. R. Chase Studies of Particulate Emissions from in-use New York City Vehicles. *Aerosol Sci. Technol.* **2004**, *38* (6), 555−573.
(23) Schneider, J.; Weimer, S.; Drewnick, F.; Borrmann, S.; Helas, G.; Gwaze, P.; Schmid, O.; Andreae, M. O.; Kirchner, U. Mass spectrometric analysis and aerodynamic properties of various types of combustion-related aerosol particles. *Int. J. Mass Spectrom.* **2006**, *258* (1−3), 37−49.
(24) He, L. Y.; Lin, Y.; Huang, X. F.; Guo, S.; Xue, L.; Su, Q.; Hu, M.; Luan, S. J.; Zhang, Y. H. Characterization of high-resolution aerosol mass spectra of primary organic aerosol emissions from Chinese cooking and biomass burning. *Atmos. Chem. Phys.* **2010**, *10* (23), 11535−11543.
(25) Healy, R. M.; Hellebust, S.; Kourtchev, I.; Allanic, A.; O'Connor, I. P.; Bell, J. M.; Healy, D. A.; Sodeau, J. R.; Wenger, J. C. Source apportionment of PM2.5 in Cork Harbour, Ireland using a combination of single particle mass spectrometry and quantitative semi-continuous measurements. *Atmos. Chem. Phys.* **2010**, *10* (19), 9593−9613.
(26) Dall'Osto, M.; Ovadnevaite, J.; Ceburnis, D.; Martin, D.; Healy, R. M.; O'Connor, I. P.; Kourtchev, I.; Sodeau, J. R.; Wenger, J. C.; O'Dowd, C. Characterization of urban aerosol in Cork city (Ireland) using aerosol mass spectrometry. *Atmos. Chem. Phys.* **2013**, *13* (9), 4997−5015.
(27) Ng, N. L.; Herndon, S. C.; Trimborn, A.; Canagaratna, M. R.; Croteau, P. L.; Onasch, T. B.; Sueper, D.; Worsnop, D. R.; Zhang, Q.; Sun, Y. L.; Jayne, J. T. An Aerosol Chemical Speciation Monitor (ACSM) for Routine Monitoring of the Composition and Mass Concentrations of Ambient Aerosol. *Aerosol Sci. Technol.* **2011**, *45* (7), 780−794.
(28) Eaton, J. M.; McGoff, N. M.; Byrne, K. A.; Leahy, P.; Kiely, G. Land cover change and soil organic carbon stocks in the Republic of Ireland 1851−2000. *Clim. Change* **2008**, *91* (3−4), 317−334.
(29) Canonaco, F.; Crippa, M.; Slowik, J. G.; Baltensperger, U.; Prévôt, A. S. H. SoFi, an IGOR-based interface for the efficient use of the generalized multilinear engine (ME-2) for the source apportionment: ME-2 application to aerosol mass spectrometer data. *Atmos. Meas. Tech.* **2013**, *6* (12), 3649−3661.

DOI: 10.1021/acs.est.7b01926
Environ. Sci. Technol. 2017, 51, 10624−10632

(30) Paatero, P. Least squares formulation of robust non-negative factor analysis. *Chemom. Intell. Lab. Syst.* **1997**, *37* (1), 23−35.
(31) Paatero, P.; Eberly, S.; Brown, S. G.; Norris, G. A. Methods for estimating uncertainty in factor analytic solutions. *Atmos. Meas. Tech.* **2014**, *7* (3), 781−797.
(32) Lanz, V. A.; Alfarra, M. R.; Baltensperger, U.; Buchmann, B.; Hueglin, C.; Prévôt, A. S. H. Source apportionment of submicron organic aerosols at an urban site by factor analytical modelling of aerosol mass spectra. *Atmos. Chem. Phys.* **2007**, *7* (6), 1503−1522.
(33) Crippa, M.; Canonaco, F.; Lanz, V. A.; Äijälä, M.; Allan, J. D.; Carbone, S.; Capes, G.; Ceburnis, D.; Dall'Osto, M.; Day, D. A.; DeCarlo, P. F.; Ehn, M.; Eriksson, A.; Freney, E.; Hildebrandt Ruiz, L.; Hillamo, R.; Jimenez, J. L.; Junninen, H.; Kiendler-Scharr, A.; Kortelainen, A. M.; Kulmala, M.; Laaksonen, A.; Mensah, A. A.; Mohr, C.; Nemitz, E.; O'Dowd, C.; Ovadnevaite, J.; Pandis, S. N.; Petäjä, T.; Poulain, L.; Saarikoski, S.; Sellegri, K.; Swietlicki, E.; Tiitta, P.; Worsnop, D. R.; Baltensperger, U.; Prévôt, A. S. H. Organic aerosol components derived from 25 AMS data sets across Europe using a consistent ME-2 based source apportionment approach. *Atmos. Chem. Phys.* **2014**, *14* (12), 6159−6176.
(34) Petit, J. E.; Favez, O.; Sciare, J.; Canonaco, F.; Croteau, P.; Močnik, G.; Jayne, J.; Worsnop, D.; Leoz-Garziandia, E. Submicron aerosol source apportionment of wintertime pollution in Paris, France by double positive matrix factorization (PMF2) using an aerosol chemical speciation monitor (ACSM) and a multi-wavelength Aethalometer. *Atmos. Chem. Phys.* **2014**, *14* (24), 13773−13787.
(35) Poulain, L.; Iinuma, Y.; Müller, K.; Birmili, W.; Weinhold, K.; Brüggemann, E.; Gnauk, T.; Hausmann, A.; Löschau, G.; Wiedensohler, A.; Herrmann, H. Diurnal variations of ambient particulate wood burning emissions and their contribution to the concentration of Polycyclic Aromatic Hydrocarbons (PAHs) in Seiffen, Germany. *Atmos. Chem. Phys.* **2011**, *11* (24), 12697−12713.
(36) Central Statistical Office. Private Households in Permanent Housing Units by Type of Central Heating, Aggregate Town or Rural Area, Period in which Built, Province County or City and CensusYear - StatBank - data and statistics. http://www.cso.ie/px/pxeirestat/Statire/SelectVarVal/Define.asp?Maintable=CDD41&Planguage=0 (accessed December 8, 2016).
(37) Alfarra, M. R.; Prevot, A. S. H.; Szidat, S.; Sandradewi, J.; Weimer, S.; Lanz, V. A.; Schreiber, D.; Mohr, M.; Baltensperger, U. Identification of the mass spectral signature of organic aerosols from wood burning emissions. *Environ. Sci. Technol.* **2007**, *41* (16), 5770−5777.
(38) Duplissy, J.; DeCarlo, P. F.; Dommen, J.; Alfarra, M. R.; Metzger, A.; Barmpadimos, I.; Prevot, A. S. H.; Weingartner, E.; Tritscher, T.; Gysel, M.; Aiken, A. C.; Jimenez, J. L.; Canagaratna, M. R.; Worsnop, D. R.; Collins, D. R.; Tomlinson, J.; Baltensperger, U. Relating hygroscopicity and composition of organic aerosol particulate matter. *Atmos. Chem. Phys.* **2011**, *11* (3), 1155−1165.
(39) Allan, J. D.; Delia, A. E.; Coe, H.; Bower, K. N.; Alfarra, M. R.; Jimenez, J. L.; Middlebrook, A. M.; Drewnick, F.; Onasch, T. B.; Canagaratna, M. R.; Jayne, J. T.; Worsnop, D. R. A generalised method for the extraction of chemically resolved mass spectra from Aerodyne aerosol mass spectrometer data. *J. Aerosol Sci.* **2004**, *35* (7), 909−922.
(40) Allan, J. D.; Jimenez, J. L.; Williams, P. I.; Alfarra, M. R.; Bower, K. N.; Jayne, J. T.; Coe, H.; Worsnop, D. R. Quantitative sampling using an Aerodyne aerosol mass spectrometer 1. Techniques of data interpretation and error analysis. *J. Geophys. Res-Atmos.* **2003**, *108* (D3), 4090−4091.
(41) Budisulistiorini, S. H.; Riva, M.; Williams, M.; Chen, J.; Itoh, M.; Surratt, J. D.; Kuwata, M. Light-Absorbing Brown Carbon Aerosol Constituents from Combustion of Indonesian Peat and Biomass. *Environ. Sci. Technol.* **2017**, *51* (8), 4415−4423.
(42) Szajdak, L.; Brandyk, T.; Szatylowicz, J. Chemical properties of different peat-moorsh soils from the Biebrza River Valley. *Agronomy Res.* **2007**, *5* (2), 165−174.
(43) Ng, N. L.; Canagaratna, M. R.; Zhang, Q.; Jimenez, J. L.; Tian, J.; Ulbrich, I. M.; Kroll, J. H.; Docherty, K. S.; Chhabra, P. S.; Bahreini, R.; Murphy, S. M.; Seinfeld, J. H.; Hildebrandt, L.; Donahue, N. M.; DeCarlo, P. F.; Lanz, V. A.; Prévôt, A. S. H.; Dinar, E.; Rudich, Y.; Worsnop, D. R. Organic aerosol components observed in Northern Hemispheric datasets from Aerosol Mass Spectrometry. *Atmos. Chem. Phys.* **2010**, *10* (10), 4625−4641.
(44) Ibarra, J.; Munoz, E.; Moliner, R. FTIR study of the evolution of coal structure during the coalification process. *Org. Geochem.* **1996**, *24* (6), 725−735.
(45) TNO. 2001: TNO Web: CEPMEIP Database. http://www.air.sk/tno/cepmeip (accessed December 8, 2016).
(46) Ulbrich, I. M.; Canagaratna, M. R.; Zhang, Q.; Worsnop, D. R.; Jimenez, J. L. Interpretation of organic components from Positive Matrix Factorization of aerosol mass spectrometric data. *Atmos. Chem. Phys.* **2009**, *9* (9), 2891−2918.
(47) Tiitta, P.; Leskinen, A.; Hao, L.; Yli-Pirilä, P.; Kortelainen, M.; Grigonyte, J.; Tissari, J.; Lamberg, H.; Hartikainen, A.; Kuuspalo, K.; Kortelainen, A. M.; Virtanen, A.; Lehtinen, K. E. J.; Komppula, M.; Pieber, S.; Prévôt, A. S. H.; Onasch, T. B.; Worsnop, D. R.; Czech, H.; Zimmermann, R.; Jokiniemi, J.; Sippula, O. Transformation of logwood combustion emissions in a smog chamber: formation of secondary organic aerosol and changes in the primary organic aerosol upon daytime and nighttime aging. *Atmos. Chem. Phys.* **2016**, *16* (20), 13251−13269.
(48) Carslaw, D. C.; Ropkins, K. openair — An R package for air quality data analysis. *Environ. Modell. Softw.* **2012**, *27*−*28*, 52−61.

DOI: 10.1021/acs.est.7b01926
Environ. Sci. Technol. 2017, 51, 10624−10632

atmosphere

MDPI

Article

Summertime Aerosol over the West of Ireland Dominated by Secondary Aerosol during Long-Range Transport

Chunshui Lin [1,2,3], Darius Ceburnis [1], Ru-Jin Huang [1,2,3,*], Francesco Canonaco [4], André Stephan Henry Prévôt [4], Colin O'Dowd [1,*] and Jurgita Ovadnevaite [1]

1 School of Physics, Ryan Institute's Centre for Climate and & Pollution Studies, and Marine Renewable Energy Ireland, National University of Ireland Galway, University Road, Galway H91 CF50, Ireland; c.lin7@nuigalway.ie (C.L.); darius.ceburnis@nuigalway.ie (D.C.); jurgita.ovadnevaite@nuigalway.ie (J.O.)
2 State Key Laboratory of Loess and Quaternary Geology and Key Laboratory of Aerosol Chemistry and Physics, Institute of Earth Environment, Chinese Academy of Sciences, Xi'an 710061, China
3 Center for Excellence in Quaternary Science and Global Change, Institute of Earth Environment, Chinese Academy of Sciences, Xi'an 710061, China
4 Laboratory of Atmospheric Chemistry, Paul Scherrer Institute (PSI), 5232 Villigen, Switzerland; francesco.canonaco@psi.ch (F.C.); andre.prevot@psi.ch (A.S.H.P.)
* Correspondence: rujin.huang@ieecas.cn (R.-J.H.); colin.odowd@nuigalway.ie (C.O.); Tel.: +86-(0)29-6233-6275 (R.-J.H.); +353-91-49-3306 (C.O.)

Received: 18 January 2019; Accepted: 28 January 2019; Published: 1 February 2019

Abstract: The chemical composition and sources of non-refractory submicron aerosol (NR-PM_1) on Galway, a west coast city of Ireland, were characterized using an aerosol chemical speciation monitor during summertime in June 2016. Organic aerosol (OA) was found to be the major part of NR-PM_1 (54%), followed by secondary inorganic sulfate (25%), ammonium (11%), and nitrate (10%). Factor analysis revealed that oxygenated OA (OOA) was the dominant OA factor, on average accounting for 84% of the total OA. The remaining 16% of OA was attributed to primary peat burning associated with domestic heating activities. As a result, secondary organic and inorganic aerosol together accounted for 91% of the total NR-PM_1, pointing to an aged aerosol population originating from secondary formation during long-range transport. Concentration-weighted trajectory analysis indicated that these secondary aerosols were mainly associated with easterly long-range transport from the UK and/or France.

Keywords: PM_1; ACSM; air pollution sources; organic aerosol; source apportionment

1. Introduction

Atmospheric aerosol has a significant impact on visibility and air quality both locally and regionally, and plays an important role in climate by scattering and absorbing solar radiation, or by acting as a nucleus for cloud condensation [1–4]. It also has a serious impact on human health, increasing the risk of respiratory and cardiovascular diseases and even decreasing life expectancy [5–8]. Aerosol particles can be directly emitted from primary sources (e.g., traffic, domestic heating, wild fires, and volcano emissions) or be formed via gas-to-particle formation. These are known as primary and secondary aerosols, respectively. In order to design effective mitigation strategies for improving the air quality, knowledge of emission sources affecting the urban aerosol population has to be expanded.

With the advent of aerosol mass spectrometry (AMS) [9–13], chemical characterization and source apportionment of submicron aerosol has significantly improved [14–16]. AMS can provide near real-time measurements of non-refractory submicron aerosol species (NR-PM_1): Organic aerosol

(OA), sulfate, nitrate, ammonium, and chloride [17–22]. In addition, the application of positive matrix factorization (PMF) on the AMS OA matrix has demonstrated its source apportionment potential which could result in different sets of OA factors depending on the site [23–29]. These OA factors include primary OA (POA) and secondary OA (SOA) corresponding to specific sources and processes [30]. For example, hydrocarbon-like OA (HOA) factor is primary and is usually associated with traffic emission [31]. Oxygenated OA (OOA) is more related to secondary processes or aging primary and could be associated with both regional transport and local secondary production [32].

Galway city, located on the west coast of Ireland, with a population of ~80,000, has been designated as the 2020 European Capital of Culture. However, the knowledge of particulate matter (PM) components in Galway is very limited [33]. Our winter campaign has indicated that pollution events, with peak NR-PM_1 concentration >20 μg m^{-3}, were mainly caused by local domestic heating sources [33]. However, sources dominating PM concentrations during summer remain unknown.

In this study, the chemical composition of NR-PM_1 in June 2016 was characterized using an aerosol chemical speciation monitor (ACSM) and OA source apportionment was performed using both PMF and multi-linear engine (ME-2). Finally, the possible geographic origins of the NR-PM_1 components were analyzed through examination of the influence of air mass trajectories.

2. Methods

2.1. Aerosol Measurements

Non-refractory submicron (NR-PM_1) aerosol species including organics, sulfate, nitrate, and ammonium were measured *in situ* at the same location as Lin et al. [33] (i.e., at the National University of Ireland, Galway (53.28° N and 9.06° W)) from 1 to 22 June 2016. The measurement site is representative of the regional background conditions over the region of Galway, on the west coast of Ireland. The aerosol sampling setup and the ACSM operation in this study were also the same as those in Lin et al. [33]. Briefly, the ambient air was drawn from a height of around 6 m above the ground at a flow rate of 3 L/min with a sub-stream of 85 mL/min being drawn into the ACSM. In the ACSM, the NR-PM_1 was vaporized at 600 °C with a standard vaporizer and subsequently ionized by electron impact. The resulting ions were analyzed by quadrupole mass analyzer. The time resolution of ACSM in this study was set to 30 min.

ACSM standard data analysis software (v 1.6.0.3) was used to process the mass concentrations of organics, sulfate, nitrate, and ammonium. Chloride accounted for a minor fraction (<1%) of the total NR-PM_1 and was not included in the discussion. A collection efficiency (CE) of 1 was applied for all species, which provides a lower limit for ACSM-measured mass concentration. This CE was validated against a collocated scanning mobility particle sizer (SMPS) in our previous study with the same instrument [29]. The sum of the calculated ACSM volume and black carbon (BC) volume correlated well with the PM_1 volume from the SMPS, with a slope close to unity and correlation coefficient r = 0.96 [29]. It is worthy to note that changes in CE will not affect the relative contribution of chemical species, since the same CE was applied to all measured species. OA mass spectra matrix and error matrix were also extracted using this software for subsequent PMF analysis.

2.2. OA Source Apportionment

A PMF model was used to analyze the ACSM organic mass spectra to separate OA into different factors in terms of their mass spectra and time series. The PMF model is defined as

$$X_{ij} = \sum_{k=1}^{p} G_{ik} F_{kj} + E_{ij}, \quad (1)$$

where X represents the ACSM OA matrix, F represents the profile (or mass spectra) of this factor, G represents the time series of this factor, and E represents the residue. Column i corresponds to time,

and j to m/z. p is the number of factors of the chosen solution. PMF requires non-negative entries for G and F to be physically meaningful. PMF uses a least squares algorithm that iteratively minimizes the objective function Q, defined as

$$Q^m = \sum_{i=1}^{m} \sum_{j=1}^{n} \left(\frac{e_{ij}}{\sigma_{ij}} \right), \quad (2)$$

where σ_{ij} represents measurement uncertainty. The preparation of organic and uncertainty matrix followed the recommendation of Ulbrich et al. [34]. Data points with a low signal-to-noise ratio (SNR; < 0.2) were removed, whereas data with SNR in the range of 0.2–2 were down-weighted by a factor of 2. PMF was run with a robust mode. In this study, organic fragments with $m/z \leq 100$ were analyzed. Higher m/z values were not included because of the low SNR.

PMF does not require any prior information but may have a substantial degree of rotational ambiguity [35]. The rotational ambiguity may result in fewer factors or inaccurate factor attributions when some factors have similar temporal variation. To reduce rotational ambiguity, a priori information, such as factor profile, can be used to constrain the PMF model.

Multi-linear engine (ME-2) is a solver of PMF. ME-2 can partly constrain the factors based on a priori information such as factor profiles (used in this study) and time series. The so-called a value approach within ME-2 was used, where a value represents the extent to which the reference profiles are allowed to vary (e.g., an a value of 0.05 allows a variability of 5%). The interface of Source Finder (SoFi) [27] was used to run both PMF and ME-2.

2.3. Back Trajectory Analysis

Air mass back trajectories were calculated using the Hybrid Single-Particle Lagrangian Integrated Trajectory (HYSPLIT), a transport and dispersion model developed by the NOAA Air Resources Laboratory [36]. The back trajectories were calculated every 6 h for an arrival height of 500 m and length of 72 h.

The concentration-weighted trajectory (CWT) approach was used to investigate the potential transport of pollution [37] on the interface of ZeFir [38]. CWT couples concentration data with air mass history to identify potential source regions that may be responsible for high concentrations observed at the receptor site. A weighing function was added to the CWT calculation to down-weight cells associated with a low count of trajectory endpoints. The setup of the different weights is empirical, and our setup followed the recommendation of Petit et al., [37]. The weighing function was based on the trajectory density; the weighing coefficients were relative to the maximum of this density.

3. Results

3.1. Mass Concentration and Chemical Composition

Time series of the OA, sulfate, nitrate, and ammonium, as well as meteorological parameters (temperature, wind speed, wind direction, relative humidity, pressure, and precipitation), are presented in Figure 1. Over the measurement period, the average temperature was 15.4 ± 3.4 °C (± standard deviation) varying from 4.5 to 23.3 °C. The ambient relative humidity had a mean value of 79 ± 14%, ranging from 39% to 97%. Westerly and easterly winds alternated during the measurement period, with a mean wind velocity of 2.2 ± 1.6 m/s ranging from 0.5 to 8.0 m/s. The median and mean value of total NR-PM_1 mass were 2.3 and 2.7 ± 2.3 μg m^{-3} (ranging from <0.5 to 14.4 μg m^{-3}), respectively. These values were much lower than the ones reported for summer in Paris (with a mean NR-PM_1 of ~4.0 μg m^{-3}) [15] and London (with a mean NR-PM_1 of ~9.0 μg m^{-3}) [39]. The mean value was also lower than that measured at the same site in winter (winter mean NR-PM_1 = 3.4 μg m^{-3}) [33]. Overall, NR-PM_1 was dominated by OA, which accounted for 54% of the total mass, followed by sulfate (25%), ammonium (11%), and nitrate (10%). The absolute NR-PM_1 concentration was dependent on specific meteorological parameters. For example, high NR-PM_1 concentrations (4–9 June) were mainly

associated with easterly winds and relatively low wind speed. In contrast, low NR-PM_1 concentrations (12–14 June) were mainly associated with westerly winds and relatively high wind speed.

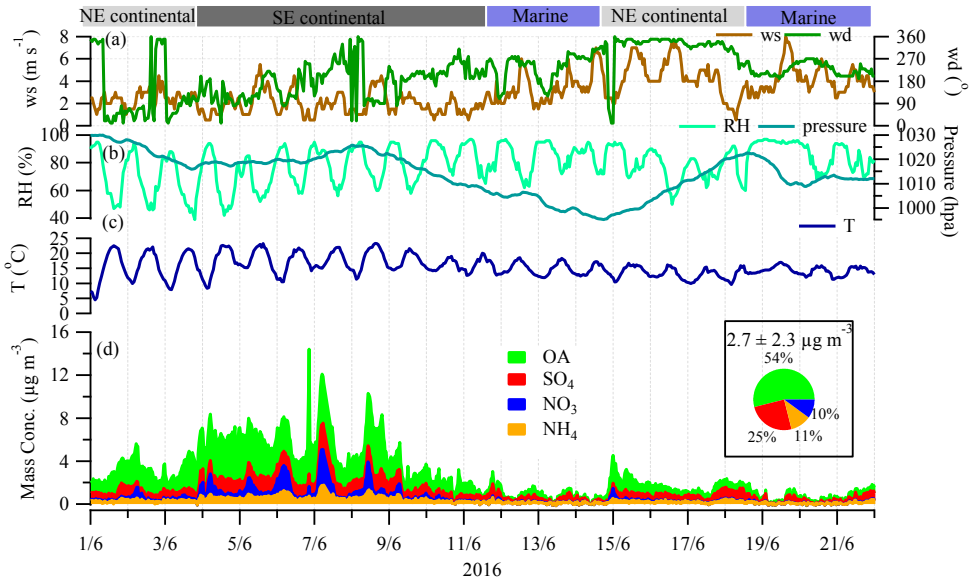

Figure 1. Time series of (**a**) wind speed (ws) and wind direction (wd); (**b**) relative humidity (RH) and pressure; (**c**) temperature; and (**d**) organics (OA), sulfate (SO_4), ammonium (NH_4), and nitrate (NO_3) during 1–22 June 2016. Inset pie chart shows the relative contribution over the whole period. The value above the pie chart is the mean NR-PM_1 concentration ± 1 standard deviation. Meteorology data were obtained from the Irish National Meteorological Service (Met Éireann) with 1 h resolution. OA, sulfate, ammonium, and nitrate were measured by an aerosol chemical speciation monitor (ACSM) with 30 min resolution. The bars above the figure highlight the different periods under the influence of different air masses for further discussion. The three periods include northeast (NE) continental (light gray), southeast (SE) continental (dark gray), and marine (light blue) air masses. See Section 3.3 for the classification of air masses.

Average diurnal cycles of OA, sulfate, nitrate, and ammonium over the three periods in different air masses are shown in Figure 2. OA was flat throughout the day, with a slight increase in the midday and in the evening in southeast (SE) continental air masses (Figure 2a), indicating that the measurement site was not influenced by any strong local emission. OA remained at the level of around 2.7 µg m^{-3}, more than 2 times higher than other species. Sulfate and ammonium showed a similar pattern, with no obvious trend. However, nitrate presented in relatively higher concentrations during the night (with a maximum at 5:00 am, local time) and lower concentrations during the day (with a minimum at 16:00), suggesting strong influences from evaporative loss and gas–aerosol partitioning. As discussed in Section 3.4, the major source of nitrate was from regional transport. Therefore, the diurnal variation of nitrate was driven solely by evaporative loss and gas-to-particle partitioning. In northeast (NE) continental air masses, none of the NR-PM_1 species showed any obvious trend and all were relatively flat except for OA, which showed a slight drop in the evening (Figure 2b). The concentrations of NR-PM_1 species were 1.6–3.6 times lower in NE continental air masses than in SE continental air masses. In marine air masses, all the NR-PM_1 concentrations were the lowest among the three studied periods (Figure 2c). OA and sulfate showed a similar trend, with an increase from ~13:00 until 20:00, indicating a similar source or an aging process.

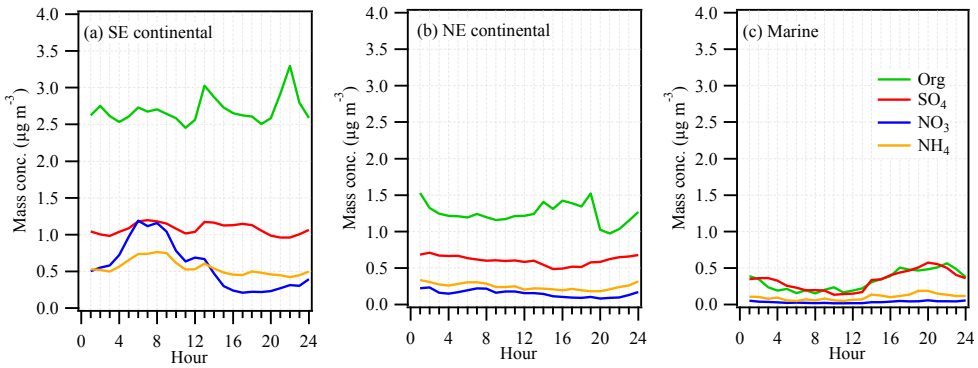

Figure 2. The diurnal variation of NR-PM_1 species (OA, sulfate, nitrate, and ammonium) over the period influenced by (**a**) SE continental; (**b**) NE continental; and (**c**) marine air masses.

3.2. OA Source Apportionment

Unconstrained PMF (or free PMF) identified two factors: peat-like factors and OOA factors (Figures S1–S4 and Table S1). No other physically meaningful factors could be identified even by increasing the number of factors. However, the profile of peat-like factor contained no mass to charge ratio (m/z) 44 fraction (f44) and higher than expected f29 when compared to a reference peat profile [33], compromising its attribution. Therefore, multilinear engine (ME-2) was utilized by constraining the reference peat profile with the a value approach [27,33]. Sensitivity analysis by varying the a value showed that the relative contribution did not vary significantly (only by a few percent) within the considered a value (Figure S5). Having analyzed the residual, the ME-2 solution was mathematically acceptable and represented the dataset well (Figure S6).

Figure 3 shows the mass spectra and temporal variations of peat and oxygenated OA (OOA) at an a value of 0.1. Peat was classified as primary OA and was associated with peat burning activities. The peat profile shows prominent peaks at mass to charge ratios (m/z) 41, 43, 55, and 57, characteristic of aliphatic hydrocarbons. It was also characterized by higher contribution at m/z 60 compared to traffic-related hydrocarbon-like OA factor (known as HOA). m/z 60 was associated with fragments of sugars, such as levoglucosan, which is produced by cellulose pyrolysis [40]. The time series of peat correlates well with that m/z 60 (R = 0.81). Most of the time, peat factor shows low concentrations (< 0.2 μg m^{-3}) but with few pollution spikes (> 1 μg m^{-3}) observed during the evening. As shown in Figure 1c, the temperature during summer in Galway could drop below 10 °C during the evening, so it is likely that some peat burning could occur during these cold summer evenings. On the other hand, the profile of OOA shows a high f44, arising mainly from CO_2^+, which is associated with aerosol aging or secondary formation. The time series of OOA shows a good correlation with sulfate (R = 0.83), pointing to secondary and/or regional sources.

The average diurnal cycles of peat and OOA factors over the three periods in different air masses are presented in Figure 4. In the three studied periods, OOA showed a dominant contribution over peat factor, on average accounting for ~84% (or 1.0–2.2 μg m^{-3}) of the total OA in the continental air masses (Table 1) and 72% (or 0.2 μg m^{-3}) in the marine air masses, suggesting the strong influence of secondary formation. The strong influence of secondary formation on urban PM levels have also been reported in summer in Paris [41] and London [39], where ~50% of the total OA was found to be OOA in both cities. As will be discussed in Section 3.4, France and the UK were potential geographic origins of the secondary aerosol observed in Galway. The higher OOA fraction in Galway than in London or Paris suggests an aging process during long-range transport. In addition, peat burning accounted for a minor fraction of the total OA (16–28%, or 0.09–0.4 μg m^{-3}) of the total OA, suggesting a relatively low influence from local sources. As shown in Figure 1a, peat had an increased concentration during the evening (at ~22:00, local time) which was mainly associated with emissions from domestic heating

activities coupled with the shallower planetary boundary layer in the evening. In addition, a slight peak at noon (at ~13:00) was also observed, which might be due to emission from peat burning for barbecues.

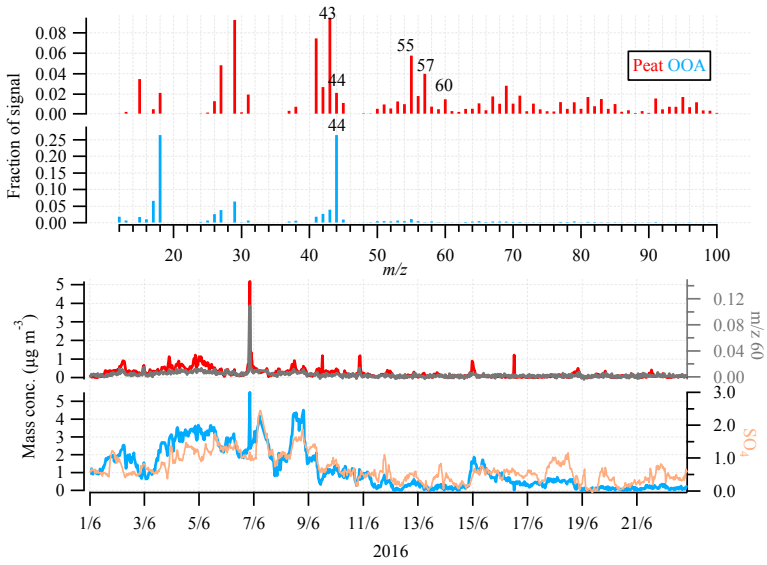

Figure 3. Profile (at *a* value of 0.1) and time series of peat and OOA (oxygenated organic aerosol). Also shown are the time series of m/z 60 and sulfate.

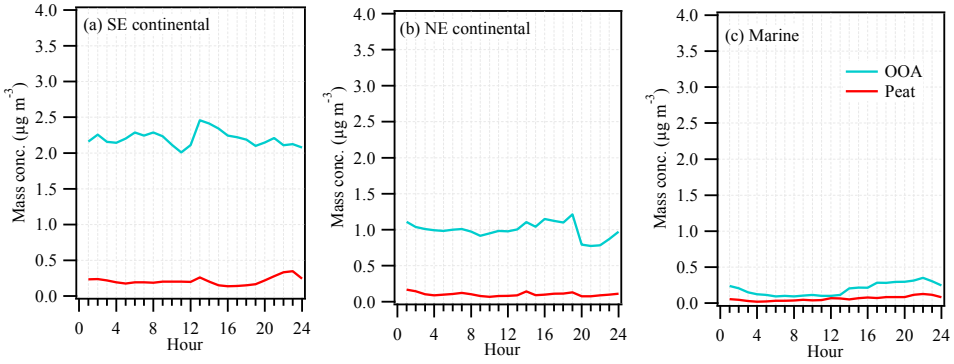

Figure 4. The average diurnal cycle of OOA and peat over the period influenced by (**a**) SE continental; (**b**) NE continental; and (**c**) marine air masses.

It is important to note that traffic-related factor, HOA, was not identified, probably due to its low contribution and/or mixing with peat-like factor. To evaluate the upper limit of the contribution from traffic emission, a reference HOA profile [25] was forced to be constrained in ME-2, along with a reference peat profile (Figures S7–S8). As expected, HOA comprised a small fraction of total OA (~4%). Furthermore, the diurnal cycle of HOA was relatively flat, and no morning or evening rush hour peaks could be observed, indicating very little influence from local traffic (Figure S9). The low contribution of HOA was consistent with low concentration of NOx, with an average morning rush hour (8:00, local time) peak concentration of ~3 ppb (Figure S10). Nevertheless, OOA was still the dominant factor, accounting for 85% of OA, followed by peat (11%). What's more, the resulting peat and OOA time series were well correlated with the 2-factor ME-2 solution, with R = 0.91–1 and slope = 0.9–0.97

(Figure S11). Thus, constraining HOA and peat in the ME-2 analysis did not affect the attribution of peat and OOA significantly, and only by 3–10%. In conclusion, the upper limit of the contribution of traffic emission to OA at the urban background site was small (only 4%).

Table 1. NR-PM_1 chemical compositions in different air masses (μg m^{-3}).

	Continental (SE)					Continental (NE)					Marine				
	N	**Mean**	**Median**	**SD**	**%**	***N***	**Mean**	**Median**	**SD**	**%**	**N**	**Mean**	**Median**	**SD**	**%**
OA	184	2.7	2.6	1.3	55	159	1.3	1.1	0.8	55	156	0.3	0.3	0.2	41
SO_4		1.1	1.1	0.4	22		0.6	0.6	0.2	27		0.3	0.3	0.2	42
NO_3		0.6	0.4	0.6	12		0.2	0.1	0.2	7		0.03	0.03	0.03	4
NH_4		0.6	0.5	0.3	11		0.2	0.2	0.1	11		0.1	0.1	0.1	13
Total		4.9					2.3					0.8			
OA factors															
Peat		0.4	0.3	0.4	14		0.1	0.08	0.2	14		0.09	0.06	0.08	28
OOA		2.2	2.3	1.1	86		1.0	0.9	0.6	86		0.20	0.2	0.2	72

N stands for number of data points. One data point corresponds to one-hourly-averaged data. % is calculated from the means. SD stands for one standard deviation.

3.3. Continental versus Marine Air Masses Impacts

Continental and marine air masses alternatively arrived at the measurement site, featuring different NR-PM_1 chemical compositions and OA factors. Figure 5 presents the back trajectory (BT) clusters of air mass at an arrival height of 500 m above the ground at intervals of 6 h (00:00, 06:00, 12:00, etc.) using the HYSPLIT model [36]. Using a nonhierarchical clustering algorithm [36], the BTs were classified into three clusters of air masses based on their spatial distribution during the measurement period. The three clusters included southeasterly (SE) continental BTs, northeasterly (NE) continental BTs, and marine BTs. Continental (SE) air masses originated over mainland Europe (e.g., France), the UK, and southeast Ireland (Figure 5a), while continental (NE) air masses advected over Scotland and Northern Ireland (Figure 5b). Finally, marine air masses had nearly 3 days of no contact with land but advected over the rural area on the west coast of Ireland before arriving at the measurement site (Figure 5c). It is worth noting that the total number of the calculated BTs were nearly evenly distributed into the three clusters (Figure S12): 37% for continental (SE), 32% for continental (NE), and 31% for marine, providing unbiased results for the subsequent analysis of chemical composition and OA factor contribution in each air mass cluster (Table 1).

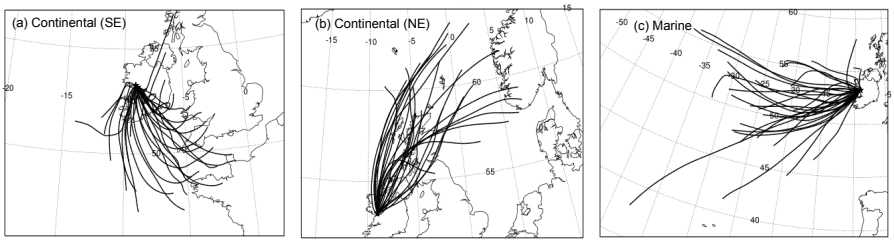

Figure 5. Classification of air mass back trajectories (BTs): (**a**) Southeasterly (SE) continental BTs; (**b**) northeasterly (NE) continental BTs; (**c**) marine BTs. The BTs (black lines) were calculated every 6 h, and the length is 72 h.

Speciated aerosol mass concentration, fractional contribution, and OA factors associated with different air mass clusters are presented in Table 1. The NR-PM_1 concentrations were higher during continental events, especially with SE air mass origins. The average NR-PM_1 concentration was 4.9 μg m^{-3} for continental (SE) air masses, which was 2.1 times higher than that for continental (NE) air masses (2.3 μg m^{-3}) and 6.1 times higher than that for marine air masses (0.8 μg m^{-3}). Also, the NR-PM_1 chemical composition was affected by air mass origins. Continental air masses

featured higher nitrate contribution (7–12%, or 0.2–0.6 μg m^{-3}) whereas marine air masses contained a very low contribution of nitrate to the total NR-PM_1 (4%, or 0.03 μg m^{-3}). Low nitrate contribution during marine events was due to the absence of marine sources of particulate nitrate [21,41]. For OA factors, continental OOA concentration was 5–11 times higher for continental air masses (1.0–2.2 μg m^{-3}) than for marine air masses (0.2 μg m^{-3}). However, fractional contributions of OOA during continental (86% of OA) and marine (72%) events were similarly high, indicating the aerosols were highly aged in both cases. Note that although peat had a higher contribution in marine air masses (28%) than in continental air masses (~14%), its absolute concentration was lower in marine air masses (0.09 μg m^{-3}) than in continental air masses (0.1–0.4 μg m^{-3}).

3.4. Geographic Origins of Major NR-PM_1 Components

The potential geographic origins (Figure 6) of the sulfate, nitrate, and OOA were investigated by coupling the concentration data with back trajectories using the CWT approach [38]. The CWT results for sulfate, nitrate, and OOA show that long-range transport from the UK and France were responsible for the high NR-PM_1 concentrations (>0.8 μg m^{-3} for OOA) observed in Galway. Only very low concentrations of sulfate (<0.3 μg m^{-3}) and OOA (<0.2 μg m^{-3}) could be associated with marine regions. CWT uses residence time information to geographically identify air parcels that may be responsible for high concentrations observed at the receptor site. Secondary aerosol (i.e., OOA, nitrate, and sulfate) concentrations were relatively high in the southeast continental air masses (Table 1). The cluster of SE continental air masses had originated over France and the UK but advected over southeast Ireland before reaching the measurement site. Therefore, the CWT result shows that southeast Ireland was also a potential geographic source of secondary aerosols, in addition to France and the UK. The formation of secondary aerosols involves the photochemical reactions of their precursors (e.g., VOC, NO_x, and SO_2). As shown in Figure S10, the local nitrate precursor concentration of NOx was very low even during the morning rush hour peak (~3 ppb on average). Some small cities are located in southeast Ireland and, similarly, low levels of precursor emissions are expected. Therefore, we believe most of the precursors of secondary aerosol were from other countries, and their photochemical reactions formed the secondary aerosol during transport, which was subsequently observed at the measurement site. Peat is a primary OA factor, and its diurnal cycle shows peaks in the evening, indicating a local source emission from nearby households. One of the disadvantages of CWT and other wind analysis tools are their inability to analyse local sources. This is because the wind speed cannot be directly related to a distance, leading to a risk of misinterpreting plotted results on top of a map [38]. Therefore, Peat–OA was not included in the CWT plot.

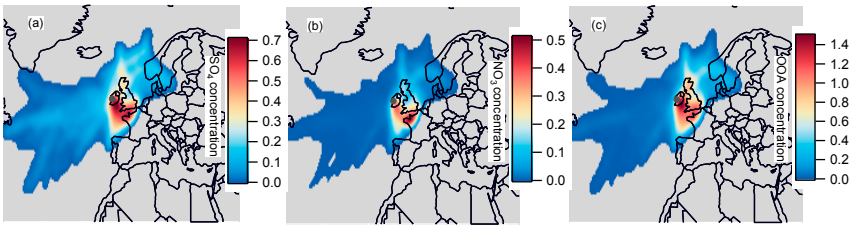

Figure 6. CWT results of hourly averaged (**a**) sulfate (SO_4), (**b**) nitrate (NO_3), and (**c**) OOA; color-coded based on the concentration of each species in μg m^{-3}. The CWT were plotted using ZeFir [38].

Galway city is located on the west coast of Ireland, facing the northern Atlantic Ocean. The sampling site in Galway provides a good opportunity to study arriving aerosol from both the ocean and other European countries as marine air masses and continental air masses alternatively arrive at the sampling site. Our measurement is representative of the cases in western European countries, especially in similarly sized cities in the UK and western France, with similar air mass back trajectories in summer.

4. Conclusions

An aerosol chemical speciation monitor (ACSM) was used to measure non-refractory submicron particles at the urban background site of Galway city, on the west coast of Ireland, during summer 2016. PMF was conducted on OA mass spectra to investigate the OA sources. The results show that the summertime average NR-PM_1 concentration of 2.7 $\pm$ 2.3 μg m^{-3} in Galway is lower than that observed in other European cities (e.g., London and Paris), and lower than that observed in winter at the same location. On average, 54% of the NR-PM_1 was comprised of organic aerosol, 84% of which was attributed to secondary production (OOA factor), which shows a good time series correlation with sulfate (R = 0.83), and only 16% of which was coming from primary peat burning. Together with secondary inorganic species (sulfate (25%), nitrate (10%), and ammonium (11%)), 91% of NR-PM_1 was of secondary origin and only 9% was coming from primary sources. Concentration-weighted trajectory analysis points to long-range transport from the UK and France being the major source of the secondary organic and inorganic species. Paris and London are much larger than Galway; however, the comparison of the factor contribution shows that higher a OOA fraction (84% of total OA) was found in Galway than in London or Paris (50%), suggesting aerosol aging during long-range transport.

Supplementary Materials: The following are available online at http://www.mdpi.com/2073-4433/10/2/59/s1, Figure S1: Q/Qexp as a function of number of factors, Figure S2: The mass spectra of the free PMF solutions, Figure S3: The time series of OOA-like and peat-like factor from the free PMF solution. Figure S4: The diurnal cycle and the relative contribution of the peat and OOA to the total OA, Figure S5: Relative contribution of the resolved peat and OOA as a function of a values from 0 to 0.9 with ME-2, Figure S6: Residual of the ME-2 solution, Figure S7: Relative contribution of HOA, peat, and OOA as a function of *a* value from 0 to 0.2, Figure S8: Profile (at *a* value of 0.1) and time series of hydrocarbon-like OA (HOA), Peat, and OOA (oxygenated organic aerosol), Figure S9: The diurnal cycle and the relative contribution of the HOA, peat, and OOA to the total OA at *a* value of 0.1, Figure S10: Diurnal cycle of NOx, Figure S11: Linear correlation between the time series of ME-2 solution and free PMF solution, Table S1: The correlation coefficient between the 2-factor solution factor profiles in free PMF and the reference factor profile from literature.

Author Contributions: J.O., D.C., and C.O. conceived and designed the experiments; C.L., J.O., and D.C. performed the experiments; C.L., R.-J.H., J.O., F.C., and A.S.H.P. helped analyze the data; C.L. and J.O. wrote the paper.

Acknowledgments: This work was supported by the EPA-Ireland (AEROSOURCE, 2016-CCRP-MS-31), the National Natural Science Foundation of China (NSFC) under grant No. 91644219, and Chinese Scholarship Council (CSC, No. 201506310020). The authors would also like to acknowledge the contribution of the COST Action CA16109 (COLOSSAL) and MaREI (Center for Marine and Renewable Energy).

Conflicts of Interest: The authors declare no conflict of interest.

References

1. Albrecht, B.A. Aerosols, cloud microphysics, and fractional cloudiness. *Science* **1989**, *245*, 1227–1231. [CrossRef] [PubMed]
2. Tegen, I.; Lacis, A.A.; Fung, I. The influence on climate forcing of mineral aerosols from disturbed soils. *Nature* **1996**, *380*, 419–422. [CrossRef]
3. Huang, R.-J.; Zhang, Y.; Bozzetti, C.; Ho, K.-F.; Cao, J.-J.; Han, Y.; Daellenbach, K.R.; Slowik, J.G.; Platt, S.M.; Canonaco, F.; et al. High secondary aerosol contribution to particulate pollution during haze events in China. *Nature* **2014**, *514*, 218. [CrossRef] [PubMed]
4. Deng, X.; Tie, X.; Wu, D.; Zhou, X.; Bi, X.; Tan, H.; Li, F.; Jiang, C. Long-term trend of visibility and its characterizations in the Pearl River Delta (PRD) region, China. *Atmos. Environ.* **2008**, *42*, 1424–1435. [CrossRef]
5. Pope, C.A., III; Burnett, R.T.; Thun, M.J.; Calle, E.E.; Krewski, D.; Ito, K.; Thurston, G.D. Lung cancer, cardiopulmonary mortality, and long-term exposure to fine particulate air pollution. *JAMA* **2002**, *287*, 1132–1141. [CrossRef] [PubMed]
6. Clancy, L.; Goodman, P.; Sinclair, H.; Dockery, D.W. Effect of air-pollution control on death rates in Dublin, Ireland: An intervention study. *Lancet* **2002**, *360*, 1210–1214. [CrossRef]
7. Pope, C.A.; Ezzati, M.; Dockery, D.W. Fine-Particulate Air Pollution and Life Expectancy in the United States. *N. Engl. J. Med.* **2009**, *360*, 376–386. [CrossRef] [PubMed]

8. Lelieveld, J.; Evans, J.S.; Fnais, M.; Giannadaki, D.; Pozzer, A. The contribution of outdoor air pollution sources to premature mortality on a global scale. *Nature* **2015**, *525*, 367–371. [CrossRef] [PubMed]
9. DeCarlo, P.F.; Kimmel, J.R.; Trimborn, A.; Northway, M.J.; Jayne, J.T.; Aiken, A.C.; Gonin, M.; Fuhrer, K.; Horvath, T.; Docherty, K.S.; et al. Field-Deployable, High-Resolution, Time-of-Flight Aerosol Mass Spectrometer. *Anal. Chem.* **2006**, *78*, 8281–8289. [CrossRef] [PubMed]
10. Drewnick, F.; Hings, S.S.; DeCarlo, P.; Jayne, J.T.; Gonin, M.; Fuhrer, K.; Weimer, S.; Jimenez, J.L.; Demerjian, K.L.; Borrmann, S.; et al. A new time-of-flight aerosol mass spectrometer (TOF-AMS)—Instrument description and first field deployment. *Aerosol Sci. Technol.* **2005**, *39*, 637–658. [CrossRef]
11. Canagaratna, M.R.; Jayne, J.T.; Jimenez, J.L.; Allan, J.D.; Alfarra, M.R.; Zhang, Q.; Onasch, T.B.; Drewnick, F.; Coe, H.; Middlebrook, A.; et al. Chemical and microphysical characterization of ambient aerosols with the Aerodyne aerosol mass spectrometer. *Mass Spectrom. Rev.* **2007**, *26*, 185–222. [CrossRef] [PubMed]
12. Ng, N.L.; Herndon, S.C.; Trimborn, A.; Canagaratna, M.R.; Croteau, P.L.; Onasch, T.B.; Sueper, D.; Worsnop, D.R.; Zhang, Q.; Sun, Y.L.; et al. An Aerosol Chemical Speciation Monitor (ACSM) for routine monitoring of the composition and mass concentrations of ambient aerosol. *Aerosol Sci. Technol.* **2011**, *45*, 780–794. [CrossRef]
13. Fröhlich, R.; Cubison, M.J.; Slowik, J.G.; Bukowiecki, N.; Prévôt, A.S.H.; Baltensperger, U.; Schneider, J.; Kimmel, J.R.; Gonin, M.; Rohner, U.; et al. The ToF-ACSM: A portable aerosol chemical speciation monitor with TOFMS detection. *Atmos. Meas. Tech.* **2013**, *6*, 3225–3241. [CrossRef]
14. Sun, Y.; Wang, Z.; Dong, H.; Yang, T.; Li, J.; Pan, X.; Chen, P.; Jayne, J.T. Characterization of summer organic and inorganic aerosols in Beijing, China with an Aerosol Chemical Speciation Monitor. *Atmos. Environ.* **2012**, *51*, 250–259. [CrossRef]
15. Petit, J.E.; Favez, O.; Sciare, J.; Crenn, V.; Sarda-Estève, R.; Bonnaire, N.; Močnik, G.; Dupont, J.C.; Haeffelin, M.; Leoz-Garziandia, E. Two years of near real-time chemical composition of submicron aerosols in the region of Paris using an Aerosol Chemical Speciation Monitor (ACSM) and a multi-wavelength Aethalometer. *Atmos. Chem. Phys.* **2015**, *15*, 2985–3005. [CrossRef]
16. Zhang, Y.J.; Tang, L.L.; Wang, Z.; Yu, H.X.; Sun, Y.L.; Liu, D.; Qin, W.; Canonaco, F.; Prévôt, A.S.H.; Zhang, H.L.; et al. Insights into characteristics, sources, and evolution of submicron aerosols during harvest seasons in the Yangtze River Delta region, China. *Atmos. Chem. Phys.* **2015**, *15*, 1331–1349. [CrossRef]
17. Elser, M.; Huang, R.J.; Wolf, R.; Slowik, J.G.; Wang, Q.; Canonaco, F.; Li, G.; Bozzetti, C.; Daellenbach, K.R.; Huang, Y.; et al. New insights into $PM_{2.5}$ chemical composition and sources in two major cities in China during extreme haze events using aerosol mass spectrometry. *Atmos. Chem. Phys.* **2016**, *16*, 3207–3225. [CrossRef]
18. Li, Y.J.; Sun, Y.; Zhang, Q.; Li, X.; Li, M.; Zhou, Z.; Chan, C.K. Real-time chemical characterization of atmospheric particulate matter in China: A review. *Atmos. Environ.* **2017**, *158*, 270–304. [CrossRef]
19. Minguillón, M.C.; Ripoll, A.; Pérez, N.; Prévôt, A.S.H.; Canonaco, F.; Querol, X.; Alastuey, A. Chemical characterization of submicron regional background aerosols in the western Mediterranean using an Aerosol Chemical Speciation Monitor. *Atmos. Chem. Phys.* **2015**, *15*, 6379–6391. [CrossRef]
20. Ovadnevaite, J.; O'Dowd, C.; Dall'Osto, M.; Ceburnis, D.; Worsnop, D.R.; Berresheim, H. Detecting high contributions of primary organic matter to marine aerosol: A case study. *Geophys. Res. Lett.* **2011**, *38*. [CrossRef]
21. Ovadnevaite, J.; Ceburnis, D.; Leinert, S.; Dall'Osto, M.; Canagaratna, M.; O'Doherty, S.; Berresheim, H.; O'Dowd, C. Submicron NE Atlantic marine aerosol chemical composition and abundance: Seasonal trends and air mass categorization. *J. Geophys. Res. Atmos.* **2014**, *119*, 11850–11863. [CrossRef]
22. Crenn, V.; Sciare, J.; Croteau, P.L.; Verlhac, S.; Fröhlich, R.; Belis, C.A.; Aas, W.; Äijälä, M.; Alastuey, A.; Artiñano, B.; et al. ACTRIS ACSM intercomparison—Part 1: Reproducibility of concentration and fragment results from 13 individual Quadrupole Aerosol Chemical Speciation Monitors (Q-ACSM) and consistency with co-located instruments. *Atmos. Meas. Tech.* **2015**, *8*, 5063–5087. [CrossRef]
23. Fröhlich, R.; Crenn, V.; Setyan, A.; Belis, C.A.; Canonaco, F.; Favez, O.; Riffault, V.; Slowik, J.G.; Aas, W.; Aijälä, M.; et al. ACTRIS ACSM intercomparison—Part 2: Intercomparison of ME-2 organic source apportionment results from 15 individual, co-located aerosol mass spectrometers. *Atmos. Meas. Tech.* **2015**, *8*, 2555–2576. [CrossRef]
24. Crippa, M.; Canonaco, F.; Lanz, V.A.; Äijälä, M.; Allan, J.D.; Carbone, S.; Capes, G.; Ceburnis, D.; Dall'Osto, M.; Day, D.A.; et al. Organic aerosol components derived from 25 AMS data sets across Europe using a consistent ME-2 based source apportionment approach. *Atmos. Chem. Phys.* **2014**, *14*, 6159–6176. [CrossRef]

25. Crippa, M.; Decarlo, P.F.; Slowik, J.G.; Mohr, C.; Heringa, M.F.; Chirico, R.; Poulain, L.; Freutel, F.; Sciare, J.; Cozic, J.; et al. Wintertime aerosol chemical composition and source apportionment of the organic fraction in the metropolitan area of Paris. *Atmos. Chem. Phys.* **2013**, *13*, 961–981. [CrossRef]
26. Paatero, P. Least squares formulation of robust non-negative factor analysis. *Chemom. Intell. Lab. Syst.* **1997**, *37*, 23–35. [CrossRef]
27. Canonaco, F.; Crippa, M.; Slowik, J.G.; Baltensperger, U.; Prévôt, A.S.H. SoFi, an IGOR-based interface for the efficient use of the generalized multilinear engine (ME-2) for the source apportionment: ME-2 application to aerosol mass spectrometer data. *Atmos. Meas. Tech.* **2013**, *6*, 3649–3661. [CrossRef]
28. Canonaco, F.; Slowik, J.G.; Baltensperger, U.; Prévôt, A.S.H. Seasonal differences in oxygenated organic aerosol composition: Implications for emissions sources and factor analysis. *Atmos. Chem. Phys.* **2015**, *15*, 6993–7002. [CrossRef]
29. Lin, C.; Huang, R.-J.; Ceburnis, D.; Buckley, P.; Preissler, J.; Wenger, J.; Rinaldi, M.; Facchini, M.C.; O'Dowd, C.; Ovadnevaite, J. Extreme air pollution from residential solid fuel burning. *Nat. Sustain.* **2018**, *1*, 512–517. [CrossRef]
30. Jimenez, J.L.; Canagaratna, M.R.; Donahue, N.M.; Prevot, A.S.H.; Zhang, Q.; Kroll, J.H.; DeCarlo, P.F.; Allan, J.D.; Coe, H.; Ng, N.L.; et al. Evolution of Organic Aerosols in the Atmosphere. *Science* **2009**, *326*, 1525–1529. [CrossRef]
31. Canagaratna, M.R.; Jayne, J.T.; Ghertner, D.A.; Herndon, S.; Shi, Q.; Jimenez, J.L.; Silva, P.J.; Williams, P.; Lanni, T.; Drewnick, F.; et al. Chase Studies of Particulate Emissions from in-use New York City Vehicles. *Aerosol Sci. Technol.* **2004**, *38*, 555–573. [CrossRef]
32. Zhang, Q.; Jimenez, J.L.; Canagaratna, M.R.; Ulbrich, I.M.; Ng, N.L.; Worsnop, D.R.; Sun, Y. Understanding atmospheric organic aerosols via factor analysis of aerosol mass spectrometry: A review. *Anal. Bioanal. Chem.* **2011**, *401*, 3045–3067. [CrossRef] [PubMed]
33. Lin, C.; Ceburnis, D.; Hellebust, S.; Buckley, P.; Wenger, J.; Canonaco, F.; Prévôt, A.S.H.; Huang, R.-J.; O'Dowd, C.; Ovadnevaite, J. Characterization of primary organic aerosol from domestic wood, peat, an coal burning in Ireland. *Environ. Sci. Technol.* **2017**, *51*, 10624–10632. [CrossRef] [PubMed]
34. Ulbrich, I.M.; Canagaratna, M.R.; Zhang, Q.; Worsnop, D.R.; Jimenez, J.L. Interpretation of organic components from Positive Matrix Factorization of aerosol mass spectrometric data. *Atmos. Chem. Phys.* **2009**, *9*, 2891–2918. [CrossRef]
35. Paatero, P. The multilinear engine-a table-driven, least squares program for solving multilinear problems, including the n-way parallel factor analysis model. *J. Comput. Graph. Stat.* **1999**, *8*, 854–888.
36. Stein, A.F.; Draxler, R.R.; Rolph, G.D.; Stunder, B.J.B.; Cohen, M.D.; Ngan, F. NOAA's HYSPLIT Atmospheric Transport and Dispersion Modeling System. *Bull. Am. Meteorol. Soc.* **2015**, *96*, 2059–2077. [CrossRef]
37. Fleming, Z.L.; Monks, P.S.; Manning, A.J. Review: Untangling the influence of air-mass history in interpreting observed atmospheric composition. *Atmos. Res.* **2012**, *104–105*, 1–39. [CrossRef]
38. Petit, J.E.; Favez, O.; Albinet, A.; Canonaco, F. A user-friendly tool for comprehensive evaluation of the geographical origins of atmospheric pollution: Wind and trajectory analyses. *Environ. Model. Softw.* **2017**, *88*, 183–187. [CrossRef]
39. Young, D.E.; Allan, J.D.; Williams, P.I.; Green, D.C.; Flynn, M.J.; Harrison, R.M.; Yin, J.; Gallagher, M.W.; Coe, H. Investigating the annual behaviour of submicron secondary inorganic and organic aerosols in London. *Atmos. Chem. Phys.* **2015**, *15*, 6351–6366. [CrossRef]
40. Alfarra, M.R.; Prevot, A.S.H.; Szidat, S.; Sandradewi, J.; Weimer, S.; Lanz, V.A.; Schreiber, D.; Mohr, M.; Baltensperger, U. Identification of the mass spectral signature of organic aerosols from wood burning emissions. *Environ. Sci. Technol.* **2007**, *41*, 5770–5777. [CrossRef]
41. Crippa, M.; El Haddad, I.; Slowik, J.G.; Decarlo, P.F.; Mohr, C.; Heringa, M.F.; Chirico, R.; Marchand, N.; Sciare, J.; Baltensperger, U.; et al. Identification of marine and continental aerosol sources in Paris using high resolution aerosol mass spectrometry. *J. Geophys. Res. Atmos.* **2013**, *118*, 1950–1963. [CrossRef]

Atmos. Chem. Phys., 19, 2283–2298, 2019
https://doi.org/10.5194/acp-19-2283-2019

Atmospheric Chemistry and Physics
Open Access
EGU

Primary emissions versus secondary formation of fine particulate matter in the most polluted city (Shijiazhuang) in North China

Ru-Jin Huang[1,2], Yichen Wang[1,2], Junji Cao[1,2], Chunshui Lin[1,2,3], Jing Duan[1,2], Qi Chen[4], Yongjie Li[5], Yifang Gu[1,2], Jin Yan[1,2], Wei Xu[1,2,3], Roman Fröhlich[6], Francesco Canonaco[6], Carlo Bozzetti[6], Jurgita Ovadnevaite[3], Darius Ceburnis[3], Manjula R. Canagaratna[7], John Jayne[7], Douglas R. Worsnop[7], Imad El-Haddad[6], André S. H. Prévôt[6], and Colin D. O'Dowd[3]

[1]Key Laboratory of Aerosol Chemistry and Physics, State Key Laboratory of Loess and Quaternary Geology, Institute of Earth Environment, Chinese Academy of Sciences, Xi'an 710061, China
[2]CAS Center for Excellence in Quaternary Science and Global Change, Chinese Academy of Sciences, Xi'an 710061, China
[3]School of Physics and Centre for Climate and Air Pollution Studies, National University of Ireland Galway, Galway, Ireland
[4]State Key Joint Laboratory of Environmental Simulation and Pollution Control, College of Environmental Sciences and Engineering, Peking University, Beijing 100871, China
[5]Department of Civil and Environmental Engineering, Faculty of Science and Technology, University of Macau, Taipa, Macau, China
[6]Laboratory of Atmospheric Chemistry, Paul Scherrer Institute (PSI), 5232 Villigen, Switzerland
[7]Aerodyne Research, Inc., Billerica, MA, USA

Correspondence: Ru-Jin Huang (rujin.huang@ieecas.cn)

Received: 24 July 2018 – Discussion started: 26 July 2018
Revised: 16 January 2019 – Accepted: 6 February 2019 – Published: 21 February 2019

Abstract. Particulate matter (PM) pollution is a severe environmental problem in the Beijing–Tianjin–Hebei (BTH) region in North China. PM studies have been conducted extensively in Beijing, but the chemical composition, sources, and atmospheric processes of PM are still relatively less known in nearby Tianjin and Hebei. In this study, fine PM in urban Shijiazhuang (the capital of Hebei Province) was characterized using an Aerodyne quadrupole aerosol chemical speciation monitor (Q-ACSM) from 11 January to 18 February in 2014. The average mass concentration of non-refractory submicron PM (diameter $< 1\,\mu m$, NR-PM_1) was $178 \pm 101\,\mu g\,m^{-3}$, and it was composed of 50 % organic aerosol (OA), 21 % sulfate, 12 % nitrate, 11 % ammonium, and 6 % chloride. Using the multilinear engine (ME-2) receptor model, five OA sources were identified and quantified, including hydrocarbon-like OA from vehicle emissions (HOA, 13 %), cooking OA (COA, 16 %), biomass burning OA (BBOA, 17 %), coal combustion OA (CCOA, 27 %), and oxygenated OA (OOA, 27 %). We found that secondary formation contributed substantially to PM in episodic events, whereas primary emissions were dominant (most significant) on average. The episodic events with the highest NR-PM_1 mass range of 300–360 $\mu g\,m^{-3}$ were comprised of 55 % of secondary species. On the contrary, a campaign-average low OOA fraction (27 %) in OA indicated the importance of primary emissions, and a low sulfur oxidation degree (F_{SO_4}) of 0.18 even at RH > 90 % hinted at insufficient oxidation. These results suggested that in Shijiazhuang in wintertime fine PM was mostly from primary emissions without sufficient atmospheric aging, indicating opportunities for air quality improvement by mitigating direct emissions. In addition, secondary inorganic and organic (OOA) species dominated in pollution events with high-RH conditions, most likely due to enhanced aqueous-phase chemistry, whereas primary organic aerosol (POA) dominated in pollution events with low-RH and stagnant conditions. These results also highlighted the importance of meteorological conditions for PM pollution in this highly polluted city in North China.

Published by Copernicus Publications on behalf of the European Geosciences Union.

1 Introduction

Particulate pollution in China is a serious environmental problem, influencing air quality, regional and global climate, and human health. Especially during recent winters, large-scale and severe haze pollution has brought China's particulate pollution at the forefront of world-wide media and has evoked great scientific interest in air pollution studies. Measurements at a number of major cities showed that the wintertime daily average mass concentrations of $PM_{2.5}$ (particulate matter with an aerodynamic diameter $< 2.5\,\mu m$) are approximately 1–2 orders of magnitude higher than those observed in urban areas in the US and Europe (Huang et al., 2014). Severe particulate pollution is often accompanied by extremely poor visibility and poor air quality leading to a sharp increase in respiratory diseases. Long-term exposure to high levels of particulate pollution was estimated to have resulted in 1.1 million deaths in China in 2015, ranking China first in the world with respect to air-pollution-related mortality (Cohen et al., 2017).

The Beijing–Tianjin–Hebei (BTH) region is one of the important city clusters in China, but also suffers from serious air pollution. Seven cities in this region ranked the top 10 most polluted cities in China in the year 2014–2015 (http://www.zhb.gov.cn, last acces: 7 February 2017). The urgent need for an air quality improvement in this region has been recognized by central and local governments as well as the public, which has led to mitigating actions being undertaken by the authorities. In particular, various emission control measures have been implemented in this region to clean Beijing's air, e.g., during the 2014 Asia-Pacific Economic Cooperation (APEC) summit. These temporal measures include the odd–even ban on vehicles and shutdowns of factories and construction sites, which have led to serious side effects on daily life and economic growth. Therefore, the identification of the major sources and atmospheric processes producing airborne particles is required for implementing targeted and optimized emission control strategies.

The first step for quantifying PM sources requires the measurement of inorganic and organic tracers and/or mass spectrometric fingerprints of ambient PM samples. This can be realized by online ambient measurements using aerosol mass spectrometric (AMS) techniques to determine aerosol composition (Jimenez et al., 2009; Ng et al., 2011b; Elser et al., 2016b). In particular, the quadrupole aerosol chemical speciation monitor (Q-ACSM) and, recently, the time-of-flight aerosol chemical speciation monitor (TOF-ACSM) have been developed for long-term continuous measurements of non-refractory submicron aerosols (Ng et al., 2011a; Fröhlich et al., 2013). Aerosol sources have been successfully identified from AMS measurements using positive matrix factorization (PMF) analysis (Ulbrich et al., 2009; Crippa et al., 2013; Elser et al., 2016a). In terms of Q-ACSM data sets, the use of PMF often fails to resolve sources with similar mass spectral profiles, e.g., the mixing of cooking organic aerosol with traffic organic aerosol in Nanjing (Zhang et al., 2015), or those present in low contributions, e.g., the lack of success in resolving a factor related to biomass burning in Beijing (Jiang et al., 2015). It has also been pointed out that PMF cannot separate the aerosol sources of temporal covariations driven by low temperature and periods of strong inversions (Canonaco et al., 2013; Reyes-Villegas et al., 2016). Several source apportionment studies (in which PMF did not find optimal results) have utilized the multilinear engine (ME-2) solver, which enables the constraint of the factor profiles/time series, providing a superior separation of the PM sources (e.g., Canonaco et al., 2013, 2015; Fröhlich et al., 2015a, b; Minguillón et al., 2015; Petit et al., 2015; Ripoll et al., 2015; Reyes-Villegas et al., 2016; Bressi et al., 2016; Schlag et al., 2016; Wang et al., 2017; Zhu et al., 2018). However, studies using ME-2 to resolve OA sources from the ACSM measurements are scarce in the BTH region.

Apart from the lack of applications of ME-2 for OA source apportionment, most field studies have mainly focused on the aerosol pollution in Beijing (Sun et al., 2013, 2014, 2016; Jiang et al., 2015; Xu et al., 2015; Elser et al., 2016a; Hu et al., 2016a). These and related studies have clearly shown that Beijing is sensitive to the regional transport of aerosols from its surrounding areas (Xu et al., 2008; Zhang et al., 2012; P. Li et al., 2015). For example, Guo et al. (2010) estimated that the regional pollutants accounted for 69 % of PM_{10} and 87 % of $PM_{1.8}$ on average in Beijing during summer, with sulfate, ammonium, and oxalate mostly formed regionally (regional contributions > 87 %). Sun et al. (2014) reported that 66 % of NR-PM_1 was from regional transport in Beijing during the 2013 winter haze event. Among the surrounding areas of Beijing, the Hebei Province is the main source area leading to high aerosol loadings in Beijing (Chen et al., 2007; Xu et al., 2008; Lang et al., 2013; P. Li et al., 2015).

Shijiazhuang, the capital of Hebei Province, is located ~ 270 km south of Beijing and has a population approximately half that of Beijing. P. Zhao et al. (2013) and P. S. Zhao et al. (2013) characterized the spatial and seasonal variations of the $PM_{2.5}$ chemical composition in the BTH region, and Shijiazhuang was selected as the representative of the polluted cities in Hebei Province. The off-line analysis results showed that organic carbon (OC) and elemental carbon (EC) concentrations in Shijiazhuang were lower in the spring and summer than those in the autumn and winter. The sum of secondary inorganic species (SO_4^{2-}, NO_3^-, and NH_4^+) was highest in the autumn. However, the temporal profiles of PM composition cannot be captured by off-line analyses, hindering more detailed study of the sources and formation of PM. In this work, we present for the first time the 30 min time resolved NR-PM_1 measurements in Shijiazhuang during the winter heating season. The characteristics of NR-PM_1 are analyzed, which include the following: (1) time series, mass fraction, and diurnal variation of NR-PM_1 species; (2) multilinear engine (ME-2)-resolved OA sources and their mass fraction as well as their diurnal variation; and (3) the char-

acteristics and atmospheric evolution of aerosol composition and sources under different aerosol loadings and meteorological conditions.

2 Methods

2.1 Sampling site

Shijiazhuang, the capital of Hebei Province, is located ∼ 270 km south of Beijing. In 2014, ∼ 10 million residents and 2.1 million vehicles were reported in this city. It is often ranked first on the list of the top 10 most polluted cities in China, especially during wintertime heating periods (from 15 November to 15 March of the next year). For example, the average concentration of $PM_{2.5}$ was 226.5 $\mu g\,m^{-3}$ with a peak hourly concentration of 933 $\mu g\,m^{-3}$ during the 2013–2014 wintertime heating period, largely exceeding the Chinese air pollution limit of 75 $\mu g\,m^{-3}$. In this study, we performed an intensive field measurement campaign at an urban site in Shijiazhuang to investigate the chemical composition, sources, and atmospheric processes of fine particles. The campaign was carried out from 11 January to 18 February 2014 on the building roof (15 m) of the Institute of Genetics and Developmental Biology, Chinese Academy of Sciences (38°2′3″ N, 114°32′29″ E), a site located in a residential–business mixed zone.

2.2 Instrumentation

NR-PM_1 was measured using an Aerodyne quadrupole aerosol chemical speciation monitor (Q-ACSM), which can provide quantitative mass concentration and mass spectra of non-refractory species including organics, sulfate, nitrate, ammonium, and chloride. The operation principles of Q-ACSM can be found elsewhere (Ng et al., 2011a). The ambient aerosol was drawn through a Nafion dryer (Perma Pure PD-50T-24SS) following a URG cyclone (model: URG-2000-30ED) with a cutoff size of 2.5 µm to remove coarse particles. The sampling flow was ∼ 3 $L\,min^{-1}$, of which ∼ 85 $mL\,min^{-1}$ was isokinetically sampled into the Q-ACSM. The residence time in the sampling tube was ∼ 5 s. The Q-ACSM was operated with a time resolution of 30 min and scanned from m/z 10 to 150 at 200 ms amu^{-1}. Dry monodispersed 300 nm ammonium nitrate and ammonium sulfate particles (selected by a differential mobility analyzer, DMA, TSI model 3080) were nebulized from a custom-built atomizer and sampled into the Q-ACSM and a condensation particle counter (CPC, TSI model 3772) calibrating ionization efficiency (IE). Therefore, IE can be determined by comparing the response factors of Q-ACSM to the mass calculated with the known particle size and the number concentration from the CPC.

Ozone (O_3) was measured by a Thermo Scientific Model 49i ozone analyzer, CO by a Thermo Scientific Model 48i carbon monoxide analyzer, SO_2 by an Ecotech EC 9850 sulfur dioxide analyzer, and NO_2 by a Thermo Scientific Model 42i NO–NO_2–NO_x analyzer. The meteorological data, including temperature, relative humidity (RH), precipitation, wind speed, and wind direction, were measured by an automatic weather station (MAWS201, Vaisala, Vantaa, Finland) and a wind sensor (Vaisala Model QMW101-M2).

2.3 Data analysis

2.3.1 Q-ACSM data analysis

The mass concentrations and composition of NR-PM_1 were analyzed with the standard Q-ACSM data analysis software written in Igor Pro (WaveMetrics, Inc., OR, USA). Standard relative ionization efficiencies (RIEs) were used for organics, nitrate, and chloride (i.e., 1.4 for organics, 1.1 for nitrate, and 1.3 for chloride) (Ng et al., 2011a), and RIEs for ammonium (6.0) and sulfate (1.2) were derived from the IE calibrations. The particle collection efficiency (CE) was applied to correct for the particle loss at the vaporizer due to particle bounce, which is influenced by aerosol acidity, composition, and the aerosol water content. Given that aerosol was dried before entering into Q-ACSM and that the ammonium nitrate mass fraction (ANMF) during the observation period was lower than 0.4, the composition dependent CE was estimated following the method described in Middlebrook et al. (2012).

2.3.2 The multilinear engine (ME-2)

PMF is a bilinear receptor model that represents an input data matrix as a linear combination of a set of factor profiles and their time-dependent concentrations (Paatero and Tapper, 1994). Factors typically correspond to unique sources and/or processes. This allows for a quantitative apportionment of bulk mass spectral time series into several factors through the minimization of a quantity Q, which is the sum of the squares of the error-weighted residuals of the model. The PMF-AMS/ACSM analyses have been widely used for apportioning the sources of organic aerosol. However, in conventional PMF analyses, rotational ambiguity with limited rotational controls can lead to unclear factor resolution, especially in China where the emission sources are very complex and covariant during haze events. In contrast, the multilinear engine (ME-2), used in this study, enables efficient exploration of the entire solution space and can direct the apportionment towards an environmentally meaningful solution through the constraints of a subset of a priori factor profiles or time series using the a value approach (Canonaco et al., 2013). The a value can vary between 0 and 1. An a value of 0.1 accounts for maximum ±10 % variability of each m/z signal of the final solution spectra that may differ from the anchor, implying that some m/z signals might increase while some might decrease.

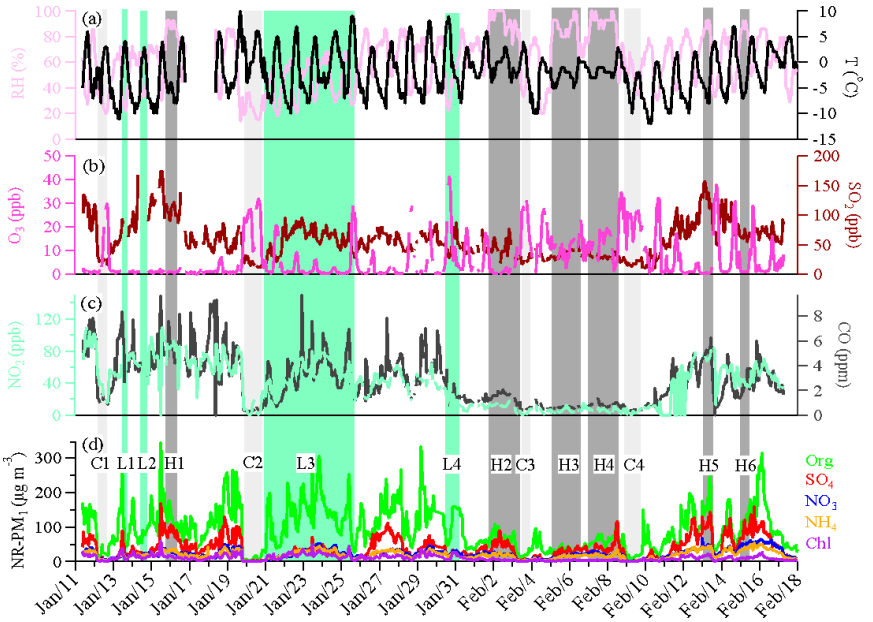

Figure 1. Time series of relative humidity and temperature **(a)**, O_3 and SO_2 **(b)**, NO_2 and CO **(c)**, and the NR-PM_1 species **(d)** during the observation period. Six high-RH (> 80 %) polluted episodes (H1–H6), four low-RH (< 60 %) polluted episodes (L1–L4), and four clean episodes (C1–C4) are marked for further discussion.

The source finder (SoFi, Canonaco et al., 2013) tool version 4.9 for Igor Pro was used for ME-2 input preparation and result analysis. The number of factors resolved is determined by the user and the solutions of the model are not mathematically unique due to rotational ambiguity. Therefore, it is critical to study other parameters, e.g., the chemical fingerprint of the factor profiles, diurnal cycles, and time series of factors and external measurements, to support factor identification and interpretation (Canonaco et al., 2013; Crippa et al., 2014; Elser et al., 2016b).

3 Results and discussion

3.1 Concentration and chemical composition of NR-PM_1

Figure 1 shows the time series of NR-PM_1 species, trace gases, and meteorological conditions during the entire measurement period. The measured mass concentrations of NR-PM_1 for the entire campaign period ranged from a few to 508.4 $\mu g\,m^{-3}$, with an average of $178 \pm 101\,\mu g\,m^{-3}$. That was much higher than the wintertime/summertime concentrations measured in many other cities (see Table 1). The mass concentration of NR-PM_1 correlated strongly with that of $PM_{2.5}$ ($R^2 = 0.76$) with a regression slope of 0.72, indicating that NR-PM_1 represents a majority of $PM_{2.5}$ mass. The NR-PM_1 concentrations exceeded the Chinese $PM_{2.5}$ limit of 75 $\mu g\,m^{-3}$ for 90 % of days during the measurement period, showing the severity of particulate air pollution at Shijiazhuang.

Similar to measurements at other urban sites, OA was the dominant fraction of NR-PM_1, with an average of 50 % (31 %–80 %), followed by 21 % of sulfate (4 %–36 %), 12 % of nitrate (2 %–26 %), 11 % of ammonium (4 %–21 %), and 6 % of chloride (2 %–20 %). The dominant contribution of organics in NR-PM_1 is also consistent with measurements from other urban sites in the BTH region during winter heating seasons (see Table 1). Sulfate was the second largest contributor to NR-PM_1. The large fraction of sulfate was likely associated with the large consumption of coal in Hebei Province, i.e., 296 million tons was used in coal-fired power plants and steel industry (producing ∼ 11 % of global steel output) in 2014. The enhancement of chloride fraction from > 1 % to 4 % in other Chinese cities in summer (see Table 1) to 6 % in Shijiazhuang in winter (within the range of > 2 %–7 % in other Chinese cities in winter, see Table 1) can be attributed to the substantial emissions from coal and/or biomass burning activities.

Figure 2a shows the diurnal variations of NR-PM_1 components, which were affected by the evolution of the planetary boundary layer (PBL) height that governed the vertical dispersion of pollutants and by the diurnal cycle of the emissions and atmospheric processes. The concentrations of pollutants increased at night as a result of enhanced emissions from residential heating (in particular, for organics and chloride) and a progressively shallower PBL. During daytime the

Table 1. The fine PM mass concentrations and fractional contribution of different compositions at different locations.

City	Season	NR-PM_1 ($\mu g\,m^{-3}$)	OA %	SO_4^{2-} %	NO_3^- %	NH_4^+ %	Cl^- %	Ref.
Beijing	Winter, 2010	60	54	14	11	12	9	Hu et al. (2016a)
Beijing	Winter, 2011	59	51	13	17	14	5	Sun et al. (2015)
Beijing	Winter, 2012	66.8	52	14	16	13	5	Sun et al. (2013)
Beijing	Winter, 2012	79	52	17	14	10	7	Wang et al. (2015)
Beijing	Winter, 2013	77	50	19	16	12	3	Sun et al. (2014)
Beijing	Winter, 2013	13.0	52	17	14	10	7	Jiang et al. (2015)
Beijing	Winter, 2013	64	60	15	11	8	6	Sun et al. (2016)
Beijing	Winter, 2014	75*	56	16	10	7	11	Elser et al. (2016a)
Beijing	Summer, 2011	80	32	28	21	17	2	Hu et al. (2016a)
Beijing	Summer, 2012	52	41	14	25	17	3	Sun et al. (2015)
Lanzhou	Winter, 2014	57.3	55	13	18	11	3	Xu et al. (2016)
Lanzhou	Summer, 2012	24	53	18	11	13	5	Xu et al. (2014)
Ziyang	Winter, 2012	60	40	24	15	17	4	Hu et al. (2016b)
Handan	Winter, 2015	178	47	16	15	13	9	Li et al. (2017)
Shenzhen	Autumn, 2009	38.3	46	29	12	11	2	He et al. (2011)
Shanghai	Summer, 2010	27	31	36	17	14	2	Huang et al. (2012)
Nanjing	Summer, 2013	36.8	42	14	24	19	1	Zhang et al. (2015)
Hong Kong	Winter, 2012	14.5	33	40	10	16	1	Y. J. Li et al. (2015)
Hong Kong	Summer, 2011	8.7	26	56	3	15	0.1	Y. J. Li et al. (2015)
Paris	Winter, 2010	16.7	35	16	33	15	1	Crippa et al. (2013)
Fresno, California	Winter, 2010	11.8	67	3	20	8	2	Ge et al. (2012)
Shijiazhuang	Winter, 2014	178	50	21	12	11	6	This study

* NR-$PM_{2.5}$

PBL height was developed by solar radiation; thus, the pollutants became diluted resulting in the decrease of organics, sulfate, ammonium, and chloride in the afternoon. In contrast, the concentrations of nitrate increased after sunrise but then remained rather constant throughout the afternoon, suggesting a strong source or production of nitrate which offsets the dilution from PBL development. To minimize the effects of PBL heights, data were normalized by ΔCO. CO is often used as an emission tracer to account for dilution on timescales of hours to days because of its relatively long lifetime against oxidation by OH radicals (approximately 1 month) (DeCarlo et al., 2010). After offsetting the PBL dilution effect, sulfate, nitrate, and ammonium showed clear increases from 07:00 to 15:00 LT (local time; Fig. 2c), indicating the efficient daytime production of these secondary inorganic species. It should be noted that the increase of nitrate (about 2 times, from ~ 6 to $\sim 12\,\mu g\,m^{-3}\,ppm^{-1}$) is slightly larger than that of sulfate (about 1.6 times, from ~ 11 to $\sim 17.5\,\mu g\,m^{-3}\,ppm^{-1}$), indicating more efficient photochemical production of nitrate than sulfate, given that the loss rate of sulfate could not be higher than that of nitrate as nitric acid is semi-volatile and may be further lost by evaporation. Furthermore, the continuous increase of organics after sunrise suggested efficient photochemical production of secondary organic aerosol (SOA).

3.2 Sources of organic aerosol

From the PMF analysis, we first examined a range of solutions with three to eight factors. The solution that best represents the data is the five-factor solution (Fig. S1 in the Supplement). The solutions with factor numbers more than five provide no new meaningful factors (see Fig. S2 and more details in the Supplement).

Although the five-factor solution can reasonably represent the data, HOA is still mixed with BBOA because the HOA profile contains a higher than expected contribution from m/z 60. In addition, COA contains no signal at m/z 44, which might indicate a suboptimal splitting between the contributing sources. To better separate HOA from BBOA, we constrained the HOA profile from Ng et al. (2011b), which is an average profile over 15 cities from China, Japan, Europe, and the US. Although gasoline vehicles dominate in China while diesel vehicles dominate in Europe, HOA mass spectra do not show significant variability when compared to different sites in China and Europe (Ng et al., 2011b; Reyes-Villegas et al., 2016; Bozzetti et al., 2017), indicating that traffic emissions from different types of vehicles have similar profiles. To avoid the influences of other sources on COA, the COA profile from Paris (Crippa et al., 2013) was used as a constraint because high similarities were found between the COA profile from Paris and four COA profiles from dif-

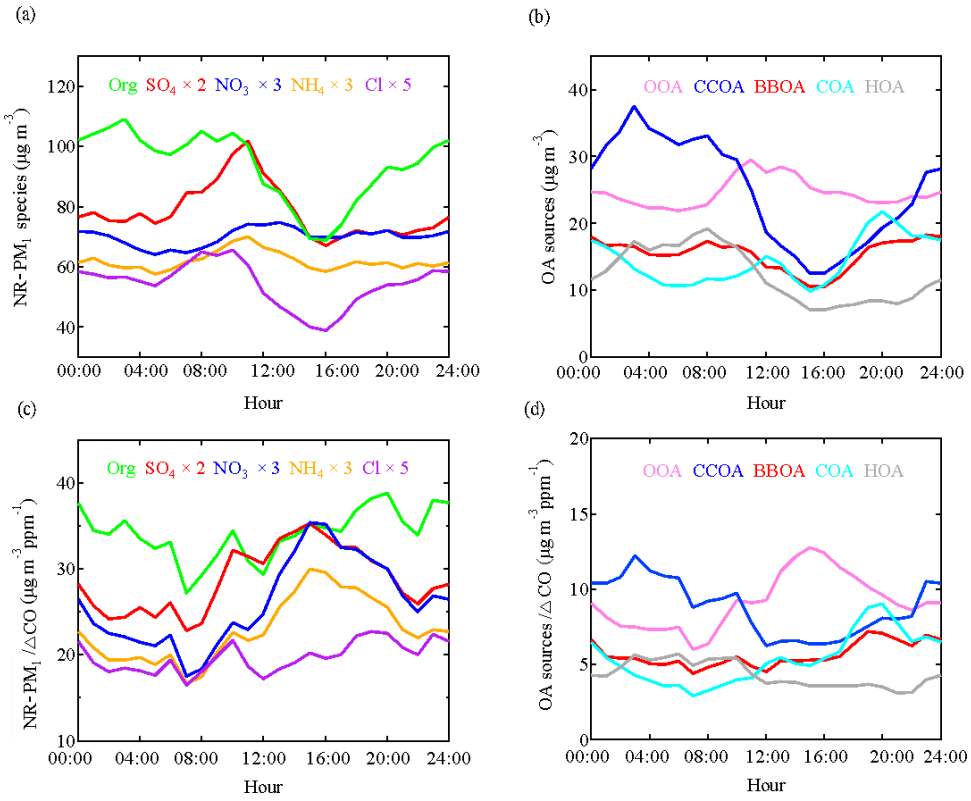

Figure 2. Diurnal variations of NR-PM_1 composition **(a)**, OA sources **(b)**, NR-PM_1 species/ΔCO **(c)**, and OA sources/ΔCO **(d)**.

ferent types of Chinese cooking activities (He et al., 2010; Crippa et al., 2013). However, the constraint on HOA and COA profiles still seems to sub-optimally resolve the apportionment of BBOA from CCOA, as one unconstrained factor contains high contributions from both m/z 60 and PAH-related m/z's (m/z 77, 91, and 115, as shown in Fig. S3) which indicates the mixing between BBOA and CCOA. To separate BBOA and CCOA, we constrained BBOA using the average of BBOA profiles from the five-factor unconstrained PMF solutions.

To explore the solution space, an a value of 0–0.5 with an interval of 0.1 was used to constrain both the HOA and COA reference profiles from literature while BBOA was constrained with an a value of 0 because the BBOA profile was resolved from an unconstrained PMF solution which is not expected to vary significantly. Thirty-six possible results were obtained by limiting the range of a values. Three criteria for optimizing OA source appointment are as follows:

1. *The diurnal pattern of COA*. The diurnal cycle of COA should have higher concentrations during mealtimes.
2. *Minimization of m/z 60 in HOA*. The upper limit of m/z 60 in the HOA profile is 0.006, which is the maximal fractional contribution derived from multiple ambient data sets in different regions (mean $+2\sigma$) (Ng et al., 2011b).
3. *The rationality of unconstrained factors*. OOA should have abundant signal at m/z 44 and should contain much lower signals at PAH-related ion peaks compared with CCOA.

Nine solutions match the criteria above. Therefore, the final time series and mass spectra are the averages of these nine solutions. The diurnal variations of mass concentrations of the OA factors and their PBL-corrected results are shown in Fig. 2b and d, respectively. The mass spectra and time series of the OA factors and their correlation with external tracers are shown in Fig. 3. The relative contributions of each OA source to the m/z's are shown in Fig. S4. Potential source contribution function (PSCF) analysis was also performed and the result is shown in Fig. S5.

OOA is characterized by high signals at m/z 44 (CO_2^+) and m/z 43 ($C_3H_7^+$ or $C_2H_3O^+$) and accounts for 85 % of m/z 44 signal, which is much higher than other OA sources. The time series of OOA is highly correlated with that of sulfate ($R^2 = 0.70$), nitrate ($R^2 = 0.75$), and ammonium ($R^2 = 0.76$), confirming the secondary nature of this factor. The diurnal cycle of OOA shows an increase from

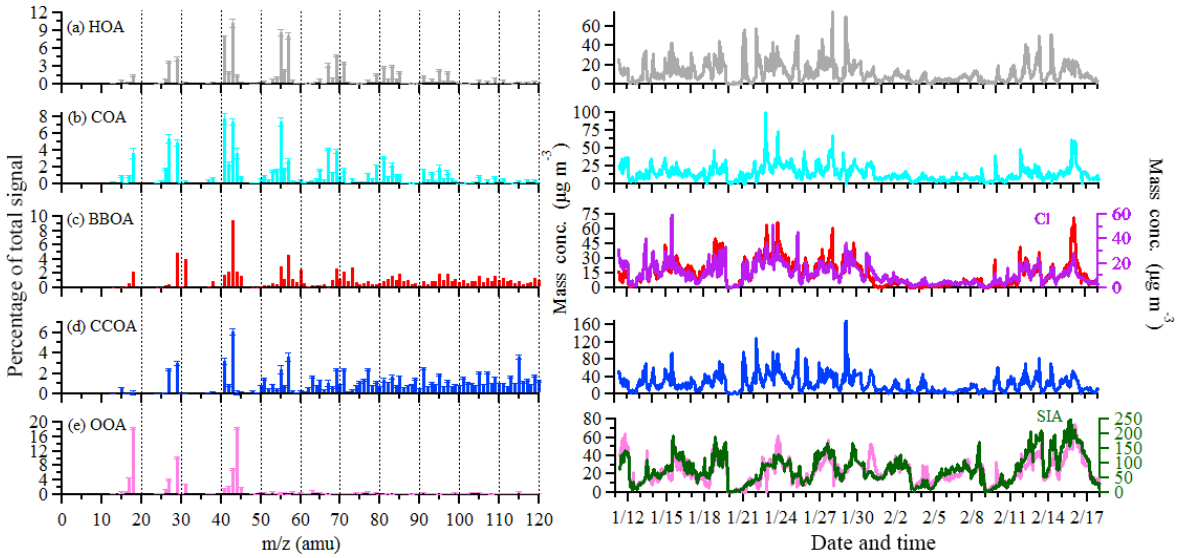

Figure 3. Mass spectrums (left) and time series (right) of five OA sources. Error bars of the mass spectrums represent the standard deviation of each m/z over all accepted solutions.

07:00 to 11:00 LT, followed by a decrease in the afternoon due to the PBL evolution effect. After normalizing the PBL effect, OOA increased continuously from 07:00 to 15:00 LT, indicating the importance of photochemical oxidation. This diurnal feature in combination with the PSCF results indicated that a large fraction of OOA was produced locally and/or produced from the highly populated and industrialized surrounding areas, consistent with the sulfate production discussed below.

The mass spectrum of CCOA is featured by prominent contributions of unsaturated hydrocarbons, particularly PAH-related ion peaks (e.g., 77, 91, and 115). The CCOA profile shows a weaker signal at m/z 44 than that observed in Beijing (Hu et al., 2016a) and Lanzhou (Xu et al., 2016). This difference can be caused by the difference in coal types, burning conditions, and aging processes (Zhou et al., 2016). CCOA accounts for 42 %–66 % of PAH-related ion peaks, much higher than those in other OA sources. This result suggested that the major source of PAHs was coal combustion in Shijiazhuang in wintertime. The campaign-averaged mass concentration of CCOA was 23.2 $\mu g\,m^{-3}$, which is higher than that in Xi'an (10.1 $\mu g\,m^{-3}$) but is similar to that in Beijing (23.5 $\mu g\,m^{-3}$) observed in the same winter (Elser et al., 2016a). Nevertheless, during haze extremes, the average CCOA concentration was 77.5 $\mu g\,m^{-3}$ in Shijiazhuang, much higher than that in Beijing (48.2 $\mu g\,m^{-3}$, Elser et al., 2016a). CCOA showed distinct diurnal variations with low concentrations (down to 12.6 $\mu g\,m^{-3}$) during the day and high concentrations (up to 37.6 $\mu g\,m^{-3}$) at night, corresponding to 19 % and 35 % of OA, respectively. The elevated CCOA concentrations at night suggested a large emission from residential heating activities using coal as the fuel compounded by the shallow PBL. The average contribution of CCOA to the total OA was 27 %, which is consistent with studies in Beijing and Handan ($\sim$ 160 km south to Shijiazhuang) where CCOA was found to be the dominant primary OA (Elser et al., 2016a; Sun et al., 2016; Li et al., 2017). Given this large fraction of OA from coal combustion, mitigating residential coal combustion is of significant importance for improving air quality in the BTH regions.

The BBOA mass spectrum is featured by prominent m/z 60 (mainly $C_2H_4O_2^+$) and 73 (mainly $C_3H_5O_2^+$) signals (He et al., 2010). These two ions ($C_2H_4O_2^+$ and $C_3H_5O_2^+$) are fragments of anhydrous sugars produced from the incomplete combustion and pyrolysis of cellulose and hemicelluloses (Alfarra et al., 2007; Lanz et al., 2007; Mohr et al., 2009). Consistently, BBOA accounts for 50 % of m/z 60 and 56 % of m/z 73, which is much higher than those in other sources. In addition, BBOA accounts for 9 %–27 % of the PAH-related m/z's (i.e., m/z 77, 91, and 115), which is lower than those in CCOA but higher than those in other primary OA sources. This suggested that BBOA was also an important PAH source in Shijiazhuang in wintertime. A high correlation was found between the time series of BBOA and that of chloride ($R^2 = 0.75$), the latter of which was suggested to be one of the tracers of biomass burning. BBOA accounted for 17 % of OA on average, which is higher than those (9 %–12 %) observed in Beijing during wintertime heating seasons (Elser et al., 2016a; Hu et al., 2016a; Sun et al., 2016). The higher BBOA contribution in Shijiazhuang in wintertime is likely associated with the widespread use of wood and crop

residuals for heating and cooking in Shijiazhuang and surrounding areas, as supported by the PSCF results (Fig. S5).

The COA profile is characterized by a high m/z 55/57 ratio of 2.7, which is much higher than that in non-cooking POA (0.6–1.1) but within the range of 2.2–2.8 in COA profiles reported by Mohr et al. (2012). COA shows a clear diurnal cycle with distinct peaks at lunchtime (between 11:00 and 13:00 LT) and dinnertime (between 19:00 and 21:00 LT). A small peak was also observed in the morning between 06:00 and 07:00 LT, consistent with breakfast time. COA accounted for 16 % of total OA on average with the highest contribution of 24 % during dinnertime.

The HOA mass spectrum is dominated by hydrocarbon ion series of $[C_nH_{2n+1}]^+$ and $[C_nH_{2n-1}]^+$ (Canagaratna et al., 2004; Mohr et al., 2009). The diurnal variation of HOA is featured by a high concentration at night, likely due to enhanced truck emissions (only allowed to drive on the road between 23:00 and 06:00 LT) and a shallow PBL at night. Similar diurnal cycles were found in Beijing and Xi'an in wintertime (Sun et al., 2016; Elser et al., 2016a). HOA, on average, accounted for 13 % of total OA for the entire observation period, which was higher than that in Beijing (9 %–10 %) but lower than that in Xi'an (15 %) measured in the same winter (Elser et al., 2016a; Sun et al., 2016).

3.3 Chemical nature and sources at different PM levels

Figure 4 shows the mass fractions of NR-PM_1 species and OA sources on reference days and extremely polluted days. Here, the days with a NR-PM_1 daily average mass concentration higher than the 75th percentile (i.e., $\geq 238\,\mu g\,m^{-3}$) are denoted as extremely polluted days and the rest of days are as designated as reference days. The average concentration of NR-PM_1 was $310\,\mu g\,m^{-3}$ during extremely polluted days, about 2 times higher than that during reference days ($162\,\mu g\,m^{-3}$). The average concentration of secondary inorganic aerosol was $65\,\mu g\,m^{-3}$ (40 % of NR-PM_1 mass) during reference days and increased to $143\,\mu g\,m^{-3}$ (46 % of NR-PM_1 mass) during extremely polluted days. Secondary organic aerosol also increased from $19\,\mu g\,m^{-3}$ (22 % of OA) during reference days to $40\,\mu g\,m^{-3}$ (26 % of OA) during extremely polluted days. The enhanced mass concentrations (~ 2 times) of both secondary inorganic aerosol and secondary organic aerosol during extremely pollution days suggested strong secondary aerosol production during pollution events. Such enhancement was likely confounded by stagnant weather conditions (e.g., average wind speed of $0.9\,m\,s^{-1}$) and a high RH of 69.4 % which facilitated the production and accumulation of secondary aerosol. Note that it was already very polluted during the reference days with an average NR-PM_1 concentration of $162\,\mu g\,m^{-3}$, which may explain the relatively small increase in the fractional contribution of secondary aerosol from reference days to extremely polluted days.

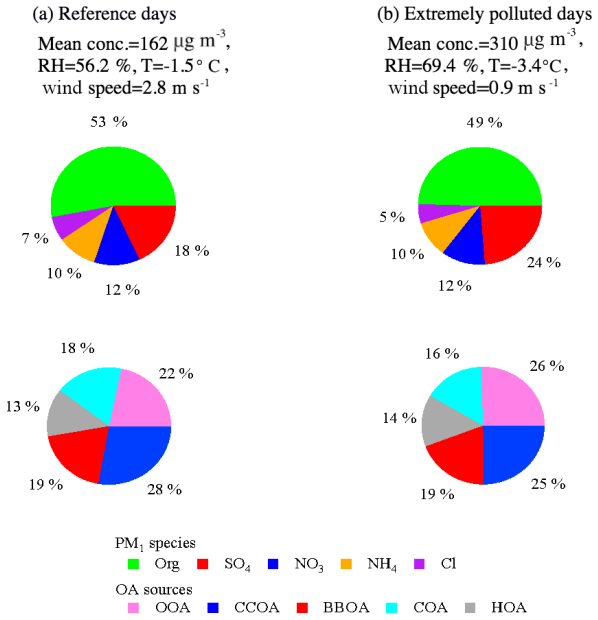

Figure 4. Relative contributions of NR-PM_1 species and OA sources (OOA, CCOA, BBOA, COA, and HOA) on reference days **(a)** and extremely polluted days **(b)**. Extremely polluted days are defined as days with a NR-PM_1 daily average mass concentration higher than the 75th percentile ($237.3\,\mu g\,m^{-3}$), and the remaining days are referred to the reference days. Data collected during the Chinese Spring Festival are excluded to eliminate the influence of the change in emission patterns during the holiday.

Figure 5a and b show the factors driving the pollution events by binning the fractional contribution of each chemical species and OA source to total NR-PM_1 and OA mass, respectively. The data clearly show that high pollution events are characterized by an increasing secondary fraction, reaching ~ 55 % at the highest NR-PM_1 mass bin (300–$360\,\mu g\,m^{-3}$). In particular, from the lowest NR-PM_1 bin to the highest NR-PM_1 bin, the fractional contribution increases from 14 % to 25 % for sulfate in NR-PM_1 and from 18 % to 25 % for OOA in OA, demonstrating the importance of secondary aerosol formation in driving particulate air pollution (Huang et al., 2014; Elser et al., 2016a; Wang et al., 2017). To investigate the oxidation degree of sulfur at different NR-PM_1 mass, the sulfur oxidation ratio (F_{SO_4}) was calculated according to Eq. (1):

$$F_{SO_4^{2-}} = \frac{n[SO_4^{2-}]}{n[SO_4^{2-}] + n[SO_2]}, \quad (1)$$

where n is the molar concentration. As can be seen from Fig. 6, F_{SO_4} shows a clear increasing trend with NR-PM_1 mass, climbing from 0.08 in the lowest mass bin to 0.21 in the highest mass bin. However, the highest F_{SO_4} value is still much lower than that reported in previous studies, e.g., 0.62

in Xi'an (Elser et al., 2016a), suggesting a low atmospheric oxidative capacity during the measurement period in Shijiazhuang. This may also explain the relatively low OOA fraction (see Fig. 5b). Certainly, it should be noted that the mass concentration of sulfate may also be affected by other parameters, including aerosol liquid water content, aerosol, or cloud water pH, besides atmospheric oxidative capacity.

3.4 Evolution of aerosol composition and sources at different RH levels

Figure 7a and b show the mass concentrations of the NR-PM_1 species and of the OA sources as a function of RH, with RH bins of 10 % increments. The absolute mass concentrations of secondary inorganic species increased as RH increased from 60 %, whereas chloride showed a decreasing trend. Among the OA sources, OOA and HOA were enhanced with RH – increasing from < 60 % to 90 % – whereas other OA sources did not show a clear trend. As RH increased gradually with the decrease in wind speed (Fig. 6a), the development of stagnant weather conditions (including a shallower PBL) promoted both the accumulation of pollutants and the formation of secondary aerosol (Tie et al., 2017). To minimize the effects of PBL variations, the NR-PM_1 species and OA fractions were normalized by the sum of the POA, as a surrogate of secondary aerosol precursors. The resulting ratios were further normalized by the values at the first RH bin (< 60 %) for better visualization. As shown in Fig. 7c, when RH increased from 60 % to 100 %, the normalized sulfate increased by a factor of $\sim$ 1.7, suggesting the importance of aqueous-phase SO_2 oxidation in the formation of sulfate at high RH. The enhancements for nitrate and ammonium were slightly lower ($\sim$ 1.2) compared to that of sulfate, because NH_4NO_3 is thermally labile and its gas–particle partitioning is affected by both temperature and RH. The importance of aqueous-phase chemistry is further supported by the increase of F_{SO_4} as a function of RH (Fig. 6b). At RH < 60 %, F_{SO_4} was rather constant, with an average of 0.09, indicating a low sulfur oxidation degree. At RH > 60 %, F_{SO_4} increased rapidly with the increase in RH, reaching a maximal average of 0.18 at the last RH bin (90 %–100 %). Note that the sulfur oxidation degree at high RH (> 60 %) was much lower compared with those measured in Xi'an during the same winter (average F_{SO_4} 0.62 at a RH of 90 %–100 %, Elser et al., 2016a). The low sulfur oxidation degree observed in Shijiazhuang (i.e., > 80 % of sulfur is still not oxidized) indicated insufficient atmospheric processing and also suggested a large fraction of pollutants in Shijiazhuang was likely emitted locally and/or transported from the heavily populated and industrialized surrounding areas. With a longer atmospheric processing time in the downwind region, e.g., Beijing, higher secondary aerosol fractions are expected, as observed in previous studies (e.g., Huang et al., 2014). Similar to sulfate, the normalized OOA increased by a factor of $\sim$ 1.2 when RH increased from 60 % to 100 % (Fig. 7d). The mass fraction of OOA increased from 29 % to 41 % when RH increased from 70 % to 100 %, whereas POA contribution decreased correspondingly from 71 % to 59 % (Fig. 6d). These results support the above discussion that aqueous-phase chemistry also plays an important role in the formation of OOA under high-RH conditions during haze pollution episodes.

3.5 Primary emissions versus secondary formation

Frequent changes between clean and polluted episodes were observed in this study. To get a better insight into aerosol sources and atmospheric processes, four clean periods (C1–C4) with a daily average NR-PM_1 mass concentration lower than the 25th percentile, six high-RH (> 80 %) polluted episodes (H1–H6), and four low-RH (< 60 %) polluted episodes (L1–L4) with daily average NR-PM_1 mass concentration higher than the 75th percentile were selected for further analysis. As shown in Fig. 8, the chemical composition and sources differed during different episodes. The contributions of organics showed a decreasing trend, from 54 %–64 % during C1–C4 to 49 %–58 % during L1–L4, and to 35 %–44 % during H1–H6, while the corresponding contributions of secondary inorganic species increased. This indicated a notable production and accumulation of secondary inorganic aerosol during severe haze pollution events. For example, the mass fraction of sulfate in NR-PM_1 was much higher during high-RH pollution events (H1–H6, 27 %–30 %) compared to those during low-RH pollution events (L1–L4, 11 %–18 %) and clean events (C1–C4, 11 %–17 %). OOA also showed a much higher contribution to OA during high-RH pollution events (H1–H6, 29 %–50 %) than during low-RH pollution events (L1–L3, 17 %–26 %) and clean events (C1–C4, 10 %–34 %). Interestingly, when comparing high-RH and low-RH pollution events of similar PM levels (Fig. 8), secondary inorganic species and OOA dominated the particulate pollution during high-RH pollution events, which was likely due to enhanced secondary formation, similar to previous studies (e.g., Wang et al., 2017), whereas POA dominated the particulate pollution at low RH and under stagnant conditions. The concentrations of POA are determined by both emissions and meteorological conditions. The different significance of primary aerosol and secondary aerosol in low- and high-RH pollution events highlights the importance of meteorological conditions in driving particulate pollution.

Figure 9 shows the evolution of aerosol species in two cases with different RH levels. The first case had an average RH < 50 % from 20 to 24 January (C2 and L3 episodes). The high wind speed (> 6 $m\,s^{-1}$) from the northwest before the L3 episode led to a significant reduction of air pollutants (the C3 episode, a clean-up period). When the wind direction switched from northwest to the 90–270° sector and the wind speed decreased to < 3 $m\,s^{-1}$, the measured pollutants (except O_3 which was reacted out by increasing NO emissions) started to build up. Specifically, NR-PM_1 showed a dramatic increase by a factor of 19 over the first 11 h (from 20 January

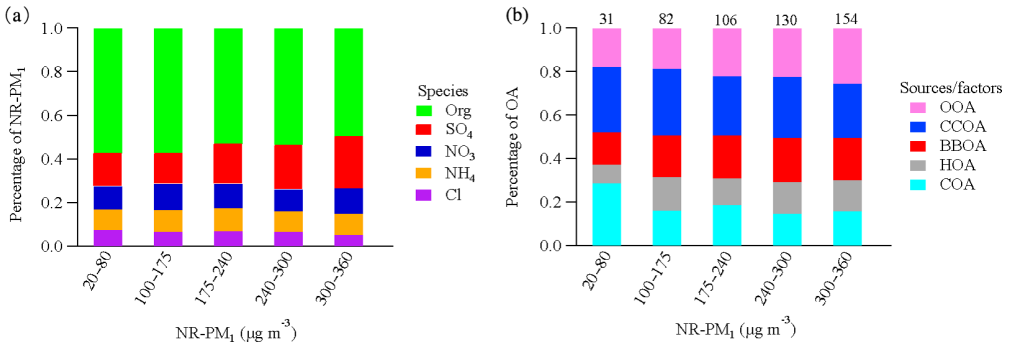

Figure 5. Relative contributions of NR-PM_1 species **(a)** and OA sources **(b)** as a function of the daily average NR-PM_1 mass concentrations. The numbers above the bars refer to the OA mass concentration ($\mu g\,m^{-3}$). Data collected during the Chinese Spring Festival are excluded to eliminate the influence of the change in emission patterns during the holiday.

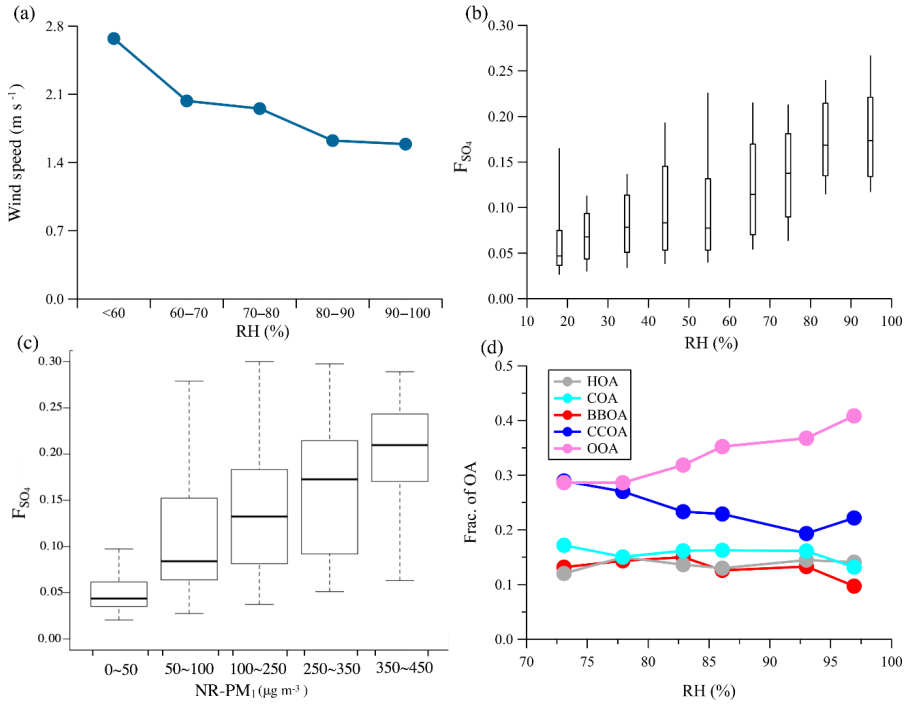

Figure 6. Variations of wind speed as a function of RH **(a)**, F_{SO_4} as a function of RH **(b)** and of the NR-PM_1 mass concentrations **(c)**, and the mass fraction of OA as a function of RH **(d)**.

16:00 to 21 January 03:00 LT) from 12 to 233 $\mu g\,m^{-3}$. During this process POA contributed to an average 69 % of NR-PM_1 mass. The other three processes were also characterized by a rapid increase of NR-PM_1 mass (39–50 $\mu g\,m^{-3}\,h^{-1}$) and a high contribution of POA, i.e., from 22 January 00:00–03:00, 22 January 16:00–20:00, and 23 January 12:00–19:00 LT. Such rapid increases in NR-PM_1 mass under low RH were associated with stagnant weather conditions (e.g., low wind speed) which promoted the accumulation of pollutants. The second case had an average RH > 80 % from 5 to 8 February (H3 and H4 episodes). In this case, the wind speed was low ($< 3\,m\,s^{-1}$) throughout the 4-day period. Under these very stagnant weather conditions, POA accumulated continuously (Fig. 9). However, unlike from the low-RH case, the concentration of secondary species also showed continuous increases in this high-RH case. The enhancement of secondary aerosol formation was likely driven by aqueous-phase chemistry at high-RH levels (Elser et al., 2016a; Wang et al., 2017)

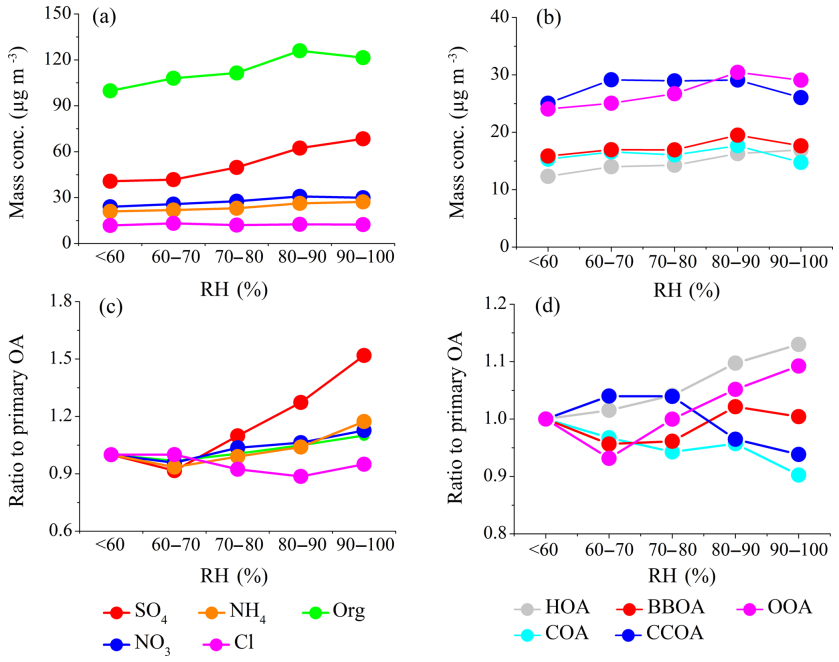

Figure 7. The average mass concentration of NR-PM_1 species **(a)** and OA sources **(b)** as a function of RH. The average mass concentration of NR-PM_1 species **(c)** and OA sources **(d)** normalized to the sum of primary sources (HOA, COA, BBOA, and CCOA) as a function of RH. All ratios are further normalized to the values at the first RH bin (< 60 %) for better illustration.

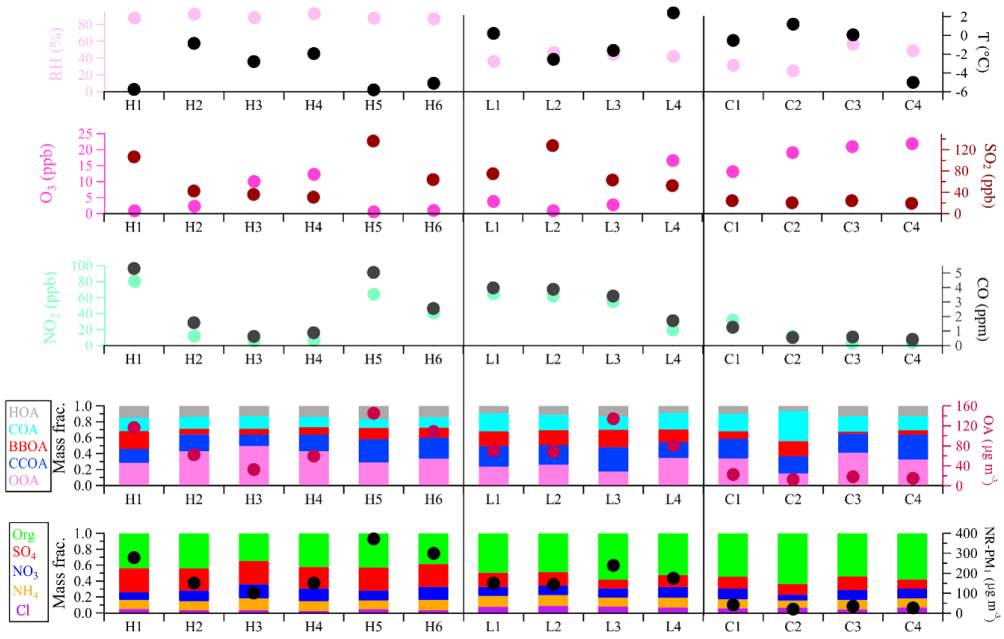

Figure 8. Summary of relative humidity and temperature, gaseous species, organic sources, and NR-PM_1 chemical composition for high-RH (H1–H6) polluted, low-RH (L1–L4) polluted, and clean (C1–C4) episodes.

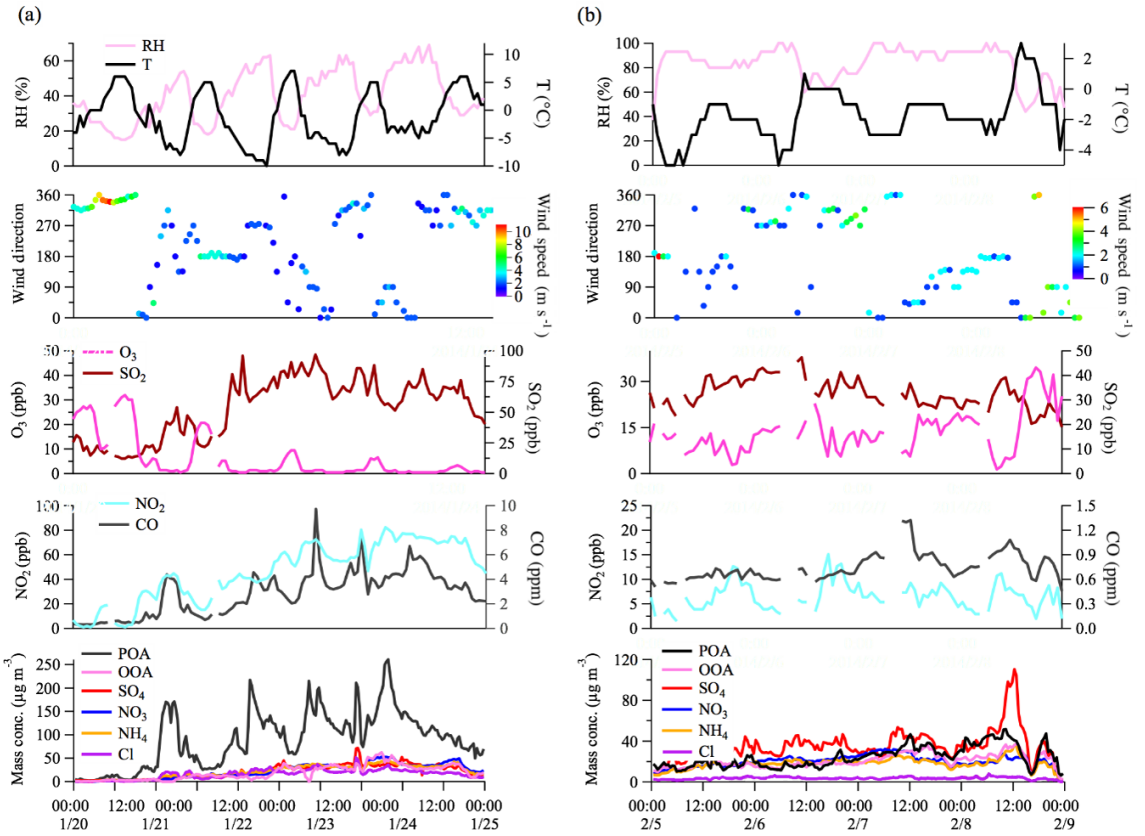

Figure 9. Time series of meteorological factors (relative humidity, temperature, wind speed, and wind direction), gaseous species, OA factors, and NR-PM_1 chemical composition for the first period (average RH < 50 %) **(a)** and the second period (average RH > 80 %) **(b)**.

and the accumulation of pollutants under stagnant weather conditions (Tie et al., 2017) which further promoted the formation of secondary species.

4 Conclusions

The chemical nature, sources, and atmospheric processes of wintertime fine particles in Shijiazhuang were investigated. The mass fractions of secondary inorganic species and SOA increased with the increase of NR-PM_1 mass, suggesting the importance of secondary formation in driving PM pollution. However, the low sulfur oxidation degree and low OOA fraction indicated an insufficient atmospheric oxidation capacity. Together with the diurnal variations and PSCF results, these observations suggested that a large fraction of pollutants in Shijiazhuang was most likely produced locally and/or transported from the heavily populated and industrialized surrounding areas without sufficient atmospheric aging. Two different regimes were found to be responsible for the high PM pollution in Shijiazhuang. At low RH under stagnant weather conditions, the accumulation of primary emissions was the main culprit. In contrast, at high RH, the enhanced formation of secondary aerosol through aqueous-phase chemistry was the main issue. To conclude, we found that in this highly polluted city in North China, (1) secondary formation is important in high-PM episodes, (2) primary emissions are still important on an average basis, and (3) meteorological conditions play an key role in pollutant accumulation and transformation. Thus, the findings from this study suggest that (a) there are still opportunities for air pollution mitigation by controlling direct emissions such as coal combustion, and (b) control on precursors (e.g., NO_x, SO_2, and volatile organic compounds) for secondary formation, especially during high-PM episodes with unfavorable meteorological conditions, can ease the situation substantially.

Data availability. All data needed to evaluate the conclusions presented in this study are present in the paper and the Supplement. Additional data related to this paper are available upon request from the corresponding author.

Supplement. The supplement related to this article is available online at: https://doi.org/10.5194/acp-19-2283-2019-supplement.

Author contributions. RJH and JC designed the study. YW and RJH performed the measurements. RJH, YW, CL, JD, QC, and YL analyzed and interpreted the data. RJH, YW, and JD wrote the paper with contributions from all co-authors.

Competing interests. The authors declare that they have no conflict of interest.

Acknowledgements. This research is supported by the National Science Foundation of China (grant nos. 91644219, 41877408, and 41675120), the National Key Research and Development Program of China (grant no. 2017YFC0212701), and EPA-Ireland (AEROSOURCE, 2016-CCRP-MS-31).

Edited by: Jianping Huang
Reviewed by: two anonymous referees

References

Alfarra, M. R., Prévôt, A. S. H., Szidat, S., Sandradewi, J.,Weimer, S., Schreiber, D., Mohr, M., and Baltensperger, U.: Identification of the mass spectral signature of organic aerosols from wood burning emissions, Environ. Sci. Technol., 41, 5770–5777, 2007.

Bozzetti, C., El Haddad, I., Salameh, D., Daellenbach, K. R., Fermo, P., Gonzalez, R., Minguillón, M. C., Iinuma, Y., Poulain, L., Elser, M., Müller, E., Slowik, J. G., Jaffrezo, J.-L., Baltensperger, U., Marchand, N., and Prévôt, A. S. H.: Organic aerosol source apportionment by offline-AMS over a full year in Marseille, Atmos. Chem. Phys., 17, 8247–8268, https://doi.org/10.5194/acp-17-8247-2017, 2017.

Bressi, M., Cavalli, F., Belis, C. A., Putaud, J.-P., Fröhlich, R., Martins dos Santos, S., Petralia, E., Prévôt, A. S. H., Berico, M., Malaguti, A., and Canonaco, F.: Variations in the chemical composition of the submicron aerosol and in the sources of the organic fraction at a regional background site of the Po Valley (Italy), Atmos. Chem. Phys., 16, 12875–12896, https://doi.org/10.5194/acp-16-12875-2016, 2016.

Canagaratna, M. R., Jayne, J. T., Ghertner, D. A., Herndon, S., Shi, Q., Jimenez, J. L., Silva, P. J., Williams, P., Lanni, T., Drewnick, F., Demerjian, K. L., Kolb, C. E., and Worsnop, D. R.: Chase studies of particulate emissions from in-use New York City vehicles, Aerosol Sci. Tech., 38, 555–573, 2004.

Canonaco, F., Crippa, M., Slowik, J. G., Baltensperger, U., and Prévôt, A. S. H.: SoFi, an IGOR-based interface for the efficient use of the generalized multilinear engine (ME-2) for the source apportionment: ME-2 application to aerosol mass spectrometer data, Atmos. Meas. Tech., 6, 3649–3661, https://doi.org/10.5194/amt-6-3649-2013, 2013.

Canonaco, F., Slowik, J. G., Baltensperger, U., and Prévôt, A. S. H.: Seasonal differences in oxygenated organic aerosol composition: implications for emissions sources and factor analysis, Atmos. Chem. Phys., 15, 6993–7002, https://doi.org/10.5194/acp-15-6993-2015, 2015.

Chen, D. S., Cheng, S. Y., Liu, L., Chen, T., and Guo, X. R.: An integrated MM5-CMAQ modeling approach for assessing transboundary PM_{10} contribution to the host city of 2008 Olympic summer games-Beijing, China, Atmos. Environ., 41, 1237–1250, 2007.

Cohen, A. J., Brauer, M., Burnett, R., Anderson, H. R., Frostad, J., Estep, K., Balakrishnan, K., Brunekreef, B., Dandona, L., Dandona, R., Feigin, V., Freedman, G., Hubbell, B., Jobling, A., Kan, H. D., Knibbs, L., Liu, Y., Martin, R., Morawska, L., Pope III, C. A., Shin, H., Straif, K., Shaddick, G., Thomas, M., van Dingenen, R., van Donkelaar, A., Vos, T., Murray, C. J. L., and Forouzanfar, M. H.: Estimates and 25-year trends of the global burden of disease attributable to ambient air pollution: an analysis of data from the Global Burden of Diseases Study 2015, Lancet, 389, 1907–1918, 2017.

Crippa, M., DeCarlo, P. F., Slowik, J. G., Mohr, C., Heringa, M. F., Chirico, R., Poulain, L., Freutel, F., Sciare, J., Cozic, J., Di Marco, C. F., Elsasser, M., Nicolas, J. B., Marchand, N., Abidi, E., Wiedensohler, A., Drewnick, F., Schneider, J., Borrmann, S., Nemitz, E., Zimmermann, R., Jaffrezo, J.-L., Prévôt, A. S. H., and Baltensperger, U.: Wintertime aerosol chemical composition and source apportionment of the organic fraction in the metropolitan area of Paris, Atmos. Chem. Phys., 13, 961–981, https://doi.org/10.5194/acp-13-961-2013, 2013.

Crippa, M., Canonaco, F., Lanz, V. A., Äijälä, M., Allan, J. D., Carbone, S., Capes, G., Ceburnis, D., Dall'Osto, M., Day, D. A., DeCarlo, P. F., Ehn, M., Eriksson, A., Freney, E., Hildebrandt Ruiz, L., Hillamo, R., Jimenez, J. L., Junninen, H., Kiendler-Scharr, A., Kortelainen, A.-M., Kulmala, M., Laaksonen, A., Mensah, A. A., Mohr, C., Nemitz, E., O'Dowd, C., Ovadnevaite, J., Pandis, S. N., Petäjä, T., Poulain, L., Saarikoski, S., Sellegri, K., Swietlicki, E., Tiitta, P., Worsnop, D. R., Baltensperger, U., and Prévôt, A. S. H.: Organic aerosol components derived from 25 AMS data sets across Europe using a consistent ME-2 based source apportionment approach, Atmos. Chem. Phys., 14, 6159–6176, https://doi.org/10.5194/acp-14-6159-2014, 2014.

DeCarlo, P. F., Ulbrich, I. M., Crounse, J., de Foy, B., Dunlea, E. J., Aiken, A. C., Knapp, D., Weinheimer, A. J., Campos, T., Wennberg, P. O., and Jimenez, J. L.: Investigation of the sources and processing of organic aerosol over the Central Mexican Plateau from aircraft measurements during MILAGRO, Atmos. Chem. Phys., 10, 5257–5280, https://doi.org/10.5194/acp-10-5257-2010, 2010.

Elser, M., Huang, R.-J., Wolf, R., Slowik, J. G., Wang, Q., Canonaco, F., Li, G., Bozzetti, C., Daellenbach, K. R., Huang, Y., Zhang, R., Li, Z., Cao, J., Baltensperger, U., El-Haddad, I., and Prévôt, A. S. H.: New insights into $PM_{2.5}$ chemical composition and sources in two major cities in China during extreme haze events using aerosol mass spectrometry, Atmos. Chem. Phys., 16, 3207–3225, https://doi.org/10.5194/acp-16-3207-2016, 2016a.

Elser, M., Bozzetti, C., El-Haddad, I., Maasikmets, M., Teinemaa, E., Richter, R., Wolf, R., Slowik, J. G., Baltensperger, U., and Prévôt, A. S. H.: Urban increments of gaseous and aerosol pollutants and their sources using mobile aerosol mass spectrometry measurements, Atmos. Chem. Phys., 16, 7117–7134, https://doi.org/10.5194/acp-16-7117-2016, 2016b.

Fröhlich, R., Cubison, M. J., Slowik, J. G., Bukowiecki, N., Prévôt, A. S. H., Baltensperger, U., Schneider, J., Kimmel, J. R., Gonin, M., Rohner, U., Worsnop, D. R., and Jayne, J. T.: The ToF-ACSM: a portable aerosol chemical speciation monitor with TOFMS detection, Atmos. Meas. Tech., 6, 3225–3241, https://doi.org/10.5194/amt-6-3225-2013, 2013.

Fröhlich, R., Crenn, V., Setyan, A., Belis, C. A., Canonaco, F., Favez, O., Riffault, V., Slowik, J. G., Aas, W., Aijälä, M., Alastuey, A., Artiñano, B., Bonnaire, N., Bozzetti, C., Bressi, M., Carbone, C., Coz, E., Croteau, P. L., Cubison, M. J., Esser-Gietl, J. K., Green, D. C., Gros, V., Heikkinen, L., Herrmann, H., Jayne, J. T., Lunder, C. R., Minguillón, M. C., Mocnik, G., O'Dowd, C. D., Ovadnevaite, J., Petralia, E., Poulain, L., Priestman, M., Ripoll, A., Sarda-Estève, R., Wiedensohler, A., Baltensperger, U., Sciare, J., and Prévôt, A. S. H.: ACTRIS ACSM intercomparison – Part 2: Intercomparison of ME-2 organic source apportionment results from 15 individual, co-located aerosol mass spectrometers, Atmos. Meas. Tech., 8, 2555–2576, https://doi.org/10.5194/amt-8-2555-2015, 2015a.

Fröhlich, R., Cubison, M. J., Slowik, J. G., Bukowiecki, N., Canonaco, F., Croteau, P. L., Gysel, M., Henne, S., Herrmann, E., Jayne, J. T., Steinbacher, M., Worsnop, D. R., Baltensperger, U., and Prévôt, A. S. H.: Fourteen months of on-line measurements of the non-refractory submicron aerosol at the Jungfraujoch (3580 m a.s.l.) – chemical composition, origins and organic aerosol sources, Atmos. Chem. Phys., 15, 11373–11398, https://doi.org/10.5194/acp-15-11373-2015, 2015b.

Ge, X., Zhang, Q., Sun, Y. L., Ruehl, C. R., and Setyan, A.: Effect of aqueous-phase processing on aerosol chemistry and size distributions in Fresno, California, during wintertime, Environ. Chem., 9, 221–235, https://doi.org/10.1071/EN11168, 2012.

Guo, S., Hu, M., Wang, Z. B., Slanina, J., and Zhao, Y. L.: Size-resolved aerosol water-soluble ionic compositions in the summer of Beijing: implication of regional secondary formation, Atmos. Chem. Phys., 10, 947–959, https://doi.org/10.5194/acp-10-947-2010, 2010.

He, L.-Y., Lin, Y., Huang, X.-F., Guo, S., Xue, L., Su, Q., Hu, M., Luan, S.-J., and Zhang, Y.-H.: Characterization of high-resolution aerosol mass spectra of primary organic aerosol emissions from Chinese cooking and biomass burning, Atmos. Chem. Phys., 10, 11535–11543, https://doi.org/10.5194/acp-10-11535-2010, 2010.

He, L.-Y., Huang, X.-F., Xue, L., Hu, M., Lin, Y., Zheng, J., Zhang, R., and Zhang, Y.-H.: Submicron aerosol analysis and organic source apportionment in an urban atmosphere in Pearl River Delta of China using high-resolution aerosol mass spectrometry, J. Geophys. Res., 116, D12304, https://doi.org/10.1029/2010JD014566, 2011.

Hu, W., Hu, M., Hu, W., Jimenez, J. L., Yuan, B., Chen, W., Wang, M., Wu, Y., Chen, C., Wang, Z., Peng, J., Zeng, L., and Shao, M.: Chemical composition, sources and aging process of submicron aerosols in Beijing: contrast between summer and winter, J. Geophys. Res., 121, 1955–1977, https://doi.org/10.1002/2015JD024020, 2016a.

Hu, W., Hu, M., Hu, W.-W., Niu, H., Zheng, J., Wu, Y., Chen, W., Chen, C., Li, L., Shao, M., Xie, S., and Zhang, Y.: Characterization of submicron aerosols influenced by biomass burning at a site in the Sichuan Basin, southwestern China, Atmos. Chem. Phys., 16, 13213–13230, https://doi.org/10.5194/acp-16-13213-2016, 2016b.

Huang, R. J., Zhang, Y., Bozzetti, C., Ho, K. F., Cao, J. J., Han, U., Daellenbach, K. R., Slowik, J. G., Platt, S. M., Canonaco, F., Zotter, P., Wolf, R., Pieber, S. M., Bruns, E. A., Crippa, M., Ciarelli, G., Piazzalunga, A., Schwikowski, M., Abbaszade, G., Schnelle-Kreis, J., Zimmermann, R., An, Z., Szidat, S., Baltensperger, U., El Haddad, I., and Prévôt, A. S. H.: High secondary aerosol contribution to particulate pollution during haze events in China, Nature, 514, 218–222, 2014.

Huang, X.-F., He, L.-Y., Xue, L., Sun, T.-L., Zeng, L.-W., Gong, Z.-H., Hu, M., and Zhu, T.: Highly time-resolved chemical characterization of atmospheric fine particles during 2010 Shanghai World Expo, Atmos. Chem. Phys., 12, 4897–4907, https://doi.org/10.5194/acp-12-4897-2012, 2012.

Jiang, Q., Sun, Y. L., Wang, Z., and Yin, Y.: Aerosol composition and sources during the Chinese Spring Festival: fireworks, secondary aerosol, and holiday effects, Atmos. Chem. Phys., 15, 6023–6034, https://doi.org/10.5194/acp-15-6023-2015, 2015.

Jimenez, J. L., Canagaratna, M. R., Donahue, N. M., Prévôt, A. S. H., Zhang, Q., Kroll, J. H., DeCarlo, P. F., Allan, J. D., Coe, H., Ng, N. L., Aiken, A. C., Docherty, K. S., Ulbrich, I. M., Grieshop, A. P., Robinson, A. L., Duplissy, J., Smith, J. D., Wilson, K. R., Lanz, V. A., Hueglin, C., Sun, Y. L., Tian, J., Laaksonen, A., Raatikainen, T., Rautiainen, J., Vaattovaara, P., Ehn, M., Kulmala, M., Tomlinson, J. M., Collins, D. R., Cubison, M. J., E, Dunlea, J., Huffman, J. A., Onasch, T. B., Alfarra, M. R., Williams, P. I., Bower, K., Kondo, Y., Schneider, J., Drewnick, F., Borrmann, S., Weimer, S., Demerjian, K., Salcedo, D., Cottrell, L., Griffin, R., Takami, A., Miyoshi, T., Hatakeyama, S., Shimono, A., Sun, J. Y., Zhang, Y. M., Dzepina, K., Kimmel, J. R., Sueper, D., Jayne, J. T., Herndon, S. C., Trimborn, A. M., Williams, L. R., Wood, E. C., Middlebrook, A. M., Kolb, C. E., Baltensperger, U., and Worsnop, D. R.: Evolution of organic aerosols in the atmosphere, Science, 326, 1525–1529, 2009.

Lang, J. L., Cheng, S. Y., Li, J. B., Chen, D. S., Zhou, Y., Wei, X., Han, L. H., and Wang, H. Y.: A monitoring and modeling study to investigate regional transport and characteristics of $PM_{2.5}$ pollution, Aerosol Air Qual. Res., 13, 943–956, 2013.

Lanz, V. A., Alfarra, M. R., Baltensperger, U., Buchmann, B., Hueglin, C., and Prévôt, A. S. H.: Source apportionment of submicron organic aerosols at an urban site by factor analytical modelling of aerosol mass spectra, Atmos. Chem. Phys., 7, 1503–1522, https://doi.org/10.5194/acp-7-1503-2007, 2007.

Li, H., Zhang, Q., Zhang, Q., Chen, C., Wang, L., Wei, Z., Zhou, S., Parworth, C., Zheng, B., Canonaco, F., Prévôt, A. S. H., Chen, P., Zhang, H., Wallington, T. J., and He, K.: Wintertime aerosol chemistry and haze evolution in an extremely polluted city of the North China Plain: significant contribution from coal and biomass combustion, Atmos. Chem. Phys., 17, 4751–4768, https://doi.org/10.5194/acp-17-4751-2017, 2017.

Li, P., Yan, R., Yu, S., Wang, S., Liu, W., and Bao, H.: Reinstate regional transport of $PM_{2.5}$ as a major cause of severe haze in Beijing, P. Natl. Acad. Sci. USA, 112, E2739–E2740, https://doi.org/10.1073/pnas.1502596112, 2015.

Li, Y. J., Lee, B. P., Su, L., Fung, J. C. H., and Chan, C. K.: Seasonal characteristics of fine particulate matter (PM) based on high-resolution time-of-flight aerosol mass spectrometric (HR-ToF-AMS) measurements at the HKUST Supersite in Hong Kong,

Atmos. Chem. Phys., 15, 37-53, https://doi.org/10.5194/acp-15-37-2015, 2015.

Middlebrook, A. M., Bahreini, R., Jimenez, J. L., and Canagaratna, M. R.: Evaluation of Composition-Dependent Collection Efficiencies for the Aerodyne Aerosol Mass Spectrometer using Field Data, Aerosol Sci. Tech., 46, 258–271, 2012.

Minguillón, M. C., Ripoll, A., Pérez, N., Prévôt, A. S. H., Canonaco, F., Querol, X., and Alastuey, A.: Chemical characterization of submicron regional background aerosols in the western Mediterranean using an Aerosol Chemical Speciation Monitor, Atmos. Chem. Phys., 15, 6379–6391, https://doi.org/10.5194/acp-15-6379-2015, 2015.

Mohr, C., Huffman, J. A., Cubison, M. J., Aiken, A. C., Docherty, K. S., Kimmel, J. R., Ulbrich, I. M., Hannigan, M., and Jimenez, J. L.: Characterization of primary organic aerosol emissions from meat cooking, trash burning, and motor vehicles with High-Resolution Aerosol Mass Spectrometry and comparison with ambient and chamber observations, Environ. Sci. Technol., 43, 2443–2449, https://doi.org/10.1021/es8011518, 2009.

Mohr, C., DeCarlo, P. F., Heringa, M. F., Chirico, R., Slowik, J. G., Richter, R., Reche, C., Alastuey, A., Querol, X., Seco, R., Peñuelas, J., Jiménez, J. L., Crippa, M., Zimmermann, R., Baltensperger, U., and Prévôt, A. S. H.: Identification and quantification of organic aerosol from cooking and other sources in Barcelona using aerosol mass spectrometer data, Atmos. Chem. Phys., 12, 1649–1665, https://doi.org/10.5194/acp-12-1649-2012, 2012.

Ng, N. L., Herndon, S. C., Trimborn, A., Canagaratna, M. R., Croteau, P. L., Onasch, T. B., Sueper, D., Worsnop, D. R., Zhang, Q., Sun, Y. L., and Jayne, J. T.: An Aerosol Chemical Speciation Monitor (ACSM) for Routine Monitoring of the Composition and Mass Concentrations of Ambient Aerosol, Aerosol Sci. Tech., 45, 770–784, 2011a.

Ng, N. L., Canagaratna, M. R., Jimenez, J. L., Zhang, Q., Ulbrich, I. M., and Worsnop, D. R.: Real-time methods for estimating organic component mass concentrations from aerosol mass spectrometer data, Environ. Sci. Technol., 45, 910–916, 2011b.

Paatero, P. and Tapper, U., Positive Matrix Factorization: A Non-Negative Factor Model with Optimal Utilization of Error Estimates of Data Values, Environmetrics, 5, 111–126, https://doi.org/10.1002/env.3170050203, 1994.

Petit, J.-E., Favez, O., Sciare, J., Crenn, V., Sarda-Estève, R., Bonnaire, N., Mocnik, G., Dupont, J.-C., Haeffelin, M., and Leoz-Garziandia, E.: Two years of near real-time chemical composition of submicron aerosols in the region of Paris using an Aerosol Chemical Speciation Monitor (ACSM) and a multi-wavelength Aethalometer, Atmos. Chem. Phys., 15, 2985–3005, https://doi.org/10.5194/acp-15-2985-2015, 2015.

Reyes-Villegas, E., Green, D. C., Priestman, M., Canonaco, F., Coe, H., Prévôt, A. S. H., and Allan, J. D.: Organic aerosol source apportionment in London 2013 with ME-2: exploring the solution space with annual and seasonal analysis, Atmos. Chem. Phys., 16, 15545–15559, https://doi.org/10.5194/acp-16-15545-2016, 2016.

Ripoll, A., Minguillón, M. C., Pey, J., Jimenez, J. L., Day, D. A., Sosedova, Y., Canonaco, F., Prévôt, A. S. H., Querol, X., and Alastuey, A.: Long-term real-time chemical characterization of submicron aerosols at Montsec (southern Pyrenees, 1570 m a.s.l.), Atmos. Chem. Phys., 15, 2935–2951, https://doi.org/10.5194/acp-15-2935-2015, 2015.

Schlag, P., Kiendler-Scharr, A., Blom, M. J., Canonaco, F., Henzing, J. S., Moerman, M., Prévôt, A. S. H., and Holzinger, R.: Aerosol source apportionment from 1-year measurements at the CESAR tower in Cabauw, the Netherlands, Atmos. Chem. Phys., 16, 8831–8847, https://doi.org/10.5194/acp-16-8831-2016, 2016.

Sun, Y. L., Wang, Z. F., Fu, P. Q., Yang, T., Jiang, Q., Dong, H. B., Li, J., and Jia, J. J.: Aerosol composition, sources and processes during wintertime in Beijing, China, Atmos. Chem. Phys., 13, 4577–4592, https://doi.org/10.5194/acp-13-4577-2013, 2013.

Sun, Y. L., Jiang, Q., Wang, Z., Fu, P., Li, J., Yang, T., and Yin, Y.: Investigation of the sources and evolution processes of severe haze pollution in Beijing in January 2013, J. Geophys. Res., 119, 4380–4398, https://doi.org/10.1002/2014JD021641, 2014.

Sun, Y. L., Wang, Z. F., Du, W., Zhang, Q., Wang, Q. Q., Fu, P. Q., Pan, X. L., Li, J., Jayne, J., and Worsnop, D. R.: Long-term real-time measurements of aerosol particle composition in Beijing, China: seasonal variations, meteorological effects, and source analysis, Atmos. Chem. Phys., 15, 10149–10165, https://doi.org/10.5194/acp-15-10149-2015, 2015.

Sun, Y., Du, W., Fu, P., Wang, Q., Li, J., Ge, X., Zhang, Q., Zhu, C., Ren, L., Xu, W., Zhao, J., Han, T., Worsnop, D. R., and Wang, Z.: Primary and secondary aerosols in Beijing in winter: sources, variations and processes, Atmos. Chem. Phys., 16, 8309–8329, https://doi.org/10.5194/acp-16-8309-2016, 2016.

Tie, X., Huang, R. J., Cao, J. J., Zhang, Q., Cheng, Y. F., Su, H., Chang, D., Pöschl, U., Hoffmann, T., Dusek, U., Li, G. H., Worsnop, D. R., and O'Dowd, C. D.: Severe pollution in China amplified by atmospheric moisture, Sci. Rep.-UK, 7, 15760, https://doi.org/10.1038/s41598-017-15909-1, 2017.

Ulbrich, I. M., Canagaratna, M. R., Zhang, Q., Worsnop, D. R., and Jimenez, J. L.: Interpretation of organic components from Positive Matrix Factorization of aerosol mass spectrometric data, Atmos. Chem. Phys., 9, 2891–2918, https://doi.org/10.5194/acp-9-2891-2009, 2009.

Wang, Q., Sun, Y., Jiang, Q., Du, W., Sun, C., Fu, P., and Wang, Z.: Chemical composition of aerosol particles and light extinction apportionment before and during the heating season in Beijing, China, J. Geophys. Res.-Atmos., 120, 12708–12722, 2015.

Wang, Y. C., Huang, R. J., Ni, H. Y., Chen, Y., Wang, Q. Y., Li, G. H., Tie, X. X., Shen, Z. X., Huang, Y., Liu, S. X., Dong, W. M., Xue, P., Frohlich, R., Canonaco, F., Elser, M., Daellenbach, K. R., Bozzetti, C., El Haddad, I., and Prevot, A. S. H.: Chemical composition, sources and secondary processes of aerosols in Baoji city of northwest China, Atmos. Environ., 158, 128–137, 2017.

Xu, J., Zhang, Q., Chen, M., Ge, X., Ren, J., and Qin, D.: Chemical composition, sources, and processes of urban aerosols during summertime in northwest China: insights from high-resolution aerosol mass spectrometry, Atmos. Chem. Phys., 14, 12593–12611, https://doi.org/10.5194/acp-14-12593-2014, 2014.

Xu, J., Shi, J., Zhang, Q., Ge, X., Canonaco, F., Prévôt, A. S. H., Vonwiller, M., Szidat, S., Ge, J., Ma, J., An, Y., Kang, S., and Qin, D.: Wintertime organic and inorganic aerosols in Lanzhou, China: sources, processes, and comparison with the results during summer, Atmos. Chem. Phys., 16, 14937–14957, https://doi.org/10.5194/acp-16-14937-2016, 2016.

Xu, W. Q., Sun, Y. L., Chen, C., Du, W., Han, T. T., Wang, Q. Q., Fu, P. Q., Wang, Z. F., Zhao, X. J., Zhou, L. B., Ji, D. S., Wang, P. C., and Worsnop, D. R.: Aerosol composition, oxidation properties, and sources in Beijing: results from the 2014 Asia-Pacific Economic Cooperation summit study, Atmos. Chem. Phys., 15, 13681–13698, https://doi.org/10.5194/acp-15-13681-2015, 2015.

Xu, X., Barsha, N. A. F., and Li, J.: Analyzing Regional Influence of Particulate Matter on the City of Beijing, China, Aerosol Air Qual. Res., 8, 78–93, 2008.

Zhang, J. P., Zhu, T., Zhang, Q. H., Li, C. C., Shu, H. L., Ying, Y., Dai, Z. P., Wang, X., Liu, X. Y., Liang, A. M., Shen, H. X., and Yi, B. Q.: The impact of circulation patterns on regional transport pathways and air quality over Beijing and its surroundings, Atmos. Chem. Phys., 12, 5031–5053, https://doi.org/10.5194/acp-12-5031-2012, 2012.

Zhang, Y. J., Tang, L. L., Wang, Z., Yu, H. X., Sun, Y. L., Liu, D., Qin, W., Canonaco, F., Prévôt, A. S. H., Zhang, H. L., and Zhou, H. C.: Insights into characteristics, sources, and evolution of submicron aerosols during harvest seasons in the Yangtze River delta region, China, Atmos. Chem. Phys., 15, 1331–1349, https://doi.org/10.5194/acp-15-1331-2015, 2015.

Zhao, P., Dong, F., Yang, Y., He, D., Zhao, X., Zhang, W., Yao, Q., and Liu, H.: Characteristics of carbonaceous aerosol in the region of Beijing, Tianjin, and Hebei, China, Atmos. Environ., 71, 389–398, 2013.

Zhao, P. S., Dong, F., He, D., Zhao, X. J., Zhang, X. L., Zhang, W. Z., Yao, Q., and Liu, H. Y.: Characteristics of concentrations and chemical compositions for $PM_{2.5}$ in the region of Beijing, Tianjin, and Hebei, China, Atmos. Chem. Phys., 13, 4631–4644, https://doi.org/10.5194/acp-13-4631-2013, 2013.

Zhou, W., Jiang, J., Duan, L., and Hao, J.: Evolution of submicron organic aerosols during a complete residential coal combustion process, Environ. Sci. Technol., 50, 7861–7869, 2016.

Zhu, Q., Huang, X.-F., Cao, L.-M., Wei, L.-T., Zhang, B., He, L.-Y., Elser, M., Canonaco, F., Slowik, J. G., Bozzetti, C., El-Haddad, I., and Prévôt, A. S. H.: Improved source apportionment of organic aerosols in complex urban air pollution using the multilinear engine (ME-2), Atmos. Meas. Tech., 11, 1049–1060, https://doi.org/10.5194/amt-11-1049-2018, 2018.

Environmental Science & Technology

Article

Cite This: Environ. Sci. Technol. 2018, 52, 10967−10974

pubs.acs.org/est

Source-Specific Health Risk Analysis on Particulate Trace Elements: Coal Combustion and Traffic Emission As Major Contributors in Wintertime Beijing

Ru-Jin Huang,[*,†] Rui Cheng,[†] Miao Jing,[‡] Lu Yang,[†] Yongjie Li,[§] Qi Chen,[∥] Yang Chen,[⊥] Jin Yan,[†] Chunshui Lin,[†,#] Yunfei Wu,[▽] Renjian Zhang,[▽] Imad El Haddad,[○] Andre S. H. Prevot,[○] Colin D. O'Dowd,[#] and Junji Cao[†]

[†]Key Laboratory of Aerosol Chemistry and Physics, State Key Laboratory of Loess and Quaternary Geology, Institute of Earth and Environment, Chinese Academy of Sciences, Xi'an 710061, P. R. China

[‡]COE Lab of Thermofisher Scientific Technology, Shanghai 201206, P. R. China

[§]Department of Civil and Environmental Engineering, Faculty of Science and Technology, University of Macau, Taipa 999078, Macau

[∥]State Key Joint Laboratory of Environmental Simulation and Pollution Control, College of Environmental Sciences and Engineering, Peking University, Beijing 100871, P. R. China

[⊥]Chongqing Institute of Green and Intelligent Technology, Chinese Academy of Sciences, Chongqing 400714, P. R. China

[#]School of Physics and Centre for Climate and Air Pollution Studies, Ryan Institute, National University of Ireland Galway, University Road, Galway H91CF50, Ireland

[▽]RCE-TEA, Institute of Atmospheric Physics, Chinese Academy of Sciences, Beijing 100029, P. R. China

[○]Laboratory of Atmospheric Chemistry, Paul Scherrer Institute (PSI), 5232 Villigen, Switzerland

Supporting Information

ABSTRACT: Source apportionment studies of particulate matter (PM) link chemical composition to emission sources, while health risk analyses link health outcomes and chemical composition. There are limited studies to link emission sources and health risks from ambient measurements. We show such an attempt for particulate trace elements. Elements in $PM_{2.5}$ were measured in wintertime Beijing, and the total concentrations of 14 trace elements were 1.3−7.3 times higher during severe pollution days than during low pollution days. Fe, Zn, and Pb were the most abundant elements independent of the PM pollution levels. Chemical fractionation shows that Pb, Mn, Cd, As, Sr, Co, V, Cu, and Ni were present mainly in the bioavailable fraction. Positive matrix factorization was used to resolve the sources of particulate trace elements into dust, oil combustion, coal combustion, and traffic-related emissions. Traffic-related emission contributed 65% of total mass of the measured elements during low pollution days. However, coal combustion dominated (58%) during severe pollution days. By combining element-specific health risk analyses and source apportionment results, we conclude that traffic-related emission dominates the health risks by particulate trace elements during low pollution days, while coal combustion becomes equally or even more important during moderate and severe pollution days.

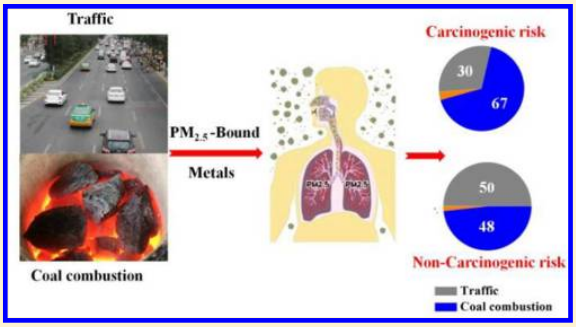

INTRODUCTION

Atmospheric fine particulate matter ($PM_{2.5}$ with an aerodynamic diameter less than 2.5 μm) in urban areas has profound effects on human health. Particularly, trace elements such as Cd, Cr, Cu, Fe, Mn, Ni, Pb, and Zn in $PM_{2.5}$ can lead to an array of short-term or long-term adverse health effects, including pulmonary and heart diseases, and potentially premature death.[1,2] However, there are very few studies that directly link metals associated with $PM_{2.5}$ to human health outcomes. Toxicological studies have revealed some mechanisms of the toxicity of those trace elements. For example, particulate trace elements can catalyze the formation of reactive oxygen species (ROS), leading to oxidative stress and consequently inflammation in respiratory tract epithelium.[3−7] Therefore, the link between particulate trace elements

Received: April 19, 2018
Revised: August 20, 2018
Accepted: September 5, 2018
Published: September 6, 2018

DOI: 10.1021/acs.est.8b02091
Environ. Sci. Technol. 2018, 52, 10967−10974

and health risk constitutes an important health issue. The adverse health effects induced by trace elements were determined by their bioavailability and toxicity.[8−10] Bioavailability of an element is a measure of the degree to which this element binds with active sites, such as the pharyngeal and tracheal region and the alveolar region of lungs, indicating the extent and rate of its absorption by a living system.[11,12] Soluble metals are more readily bioactivated and bioavailable than less soluble components in the alveoli of lung tissues.[12,13] The solubility of an element is dependent on the aerosol surface property, the aerosol-element bonds, the solvent media, and the chemical form of the element.[12] Therefore, for risk assessment, it is important to investigate the chemical fraction (e.g., those soluble fractions) of particulate trace elements instead of their total contents.

A four-step Tessier's method modified by Espinosa et al. classifies the heavy metals into four chemical fractions: soluble and exchangeable metals (F1: exchangeable fraction); carbonates, oxides and reducible metals (F2: reducible fraction); metals bound to organic matter, oxidizable and sulphidic (F3: oxidizable fraction); and residual metals (F4: residual fraction).[8,14] The exchangeable fraction and reducible fraction are highly soluble in the aqueous phase, often regarded as the bioavailable fraction.[15,16] Many recent studies have investigated the bioavailable fraction and its associated health risk. For example, Balasubramanian et al. showed a significant influence of the size-resolved particulate-bound heavy metals on the human health.[17] Li et al. showed that Cd, Cr, Cu, Pb, and Zn constitute a large proportion of the exchangeable fraction in ambient aerosol in a haze episode in wintertime Nanjing, China.[18]

The haze pollution has become a severe environmental problem in China in recent winters, characterized with poor air quality, high aerosol mass concentration, and high health risk. A majority of studies have been focused on the chemical nature and sources of the main components such as sulfate, nitrate, ammonium, and organic compounds.[19−21] Studies on trace elements, however, are limited. A few studies on trace elements mainly focused on the total concentration of individual elements,[17,22] or on the speciated/fractionated concentrations and associated health risk without considering their sources.[15,18,23] There are, however, limited studies on the relationships between the emission sources and health risks of particulate trace elements.

In this study, we investigate the trace elements in $PM_{2.5}$ samples collected in Beijing during winter. The concentration and fractionation of 14 elements on low pollution days, moderate pollution days, and severe pollution days are characterized. The sources of these particulate trace elements are then quantified using a positive matrix factorization (PMF) receptor model. The bioavailability and the carcinogenic and noncarcinogenic health risks of these elements are evaluated and contributions from each source are quantified.

MATERIALS AND METHODS

Aerosol Samples Collection. Daily (from 1st to 25th January 2014) 24-h integrated $PM_{2.5}$ samples were collected on prebaked (780 °C, 3 h) quartz-fiber filters (8 × 10 in^2). Samples were collected using a high-volume sampler (Model TE-6070VFC, Tisch Environmental Inc., Ohio, U.S.A.) at a flow rate of 1.13 m^3 min^{-1}. The sampling site was at the campus of the Institute of Atmospheric Physics, Chinese Academy of Sciences in Beijing (116°20′ E, 39°59′ N), which is typical of urban site surrounded by residential, commercial, and education areas. Samples were taken on the roof of a building, about 10 m above the ground. An overview of the sampling site is shown in Figure S1 in the Supporting Information (SI). The samples were stored at −20 °C until analysis.

Sequential Extraction and Analysis. A four-step sequential extraction procedure was used for chemical fractionation of trace elements in $PM_{2.5}$.[8] This approach can separate the elements into four fractions: exchangeable fraction; reducible fraction; oxidizable fraction; and residual fraction. After extraction, 14 elements (i.e., Ti, V, Cr, Mn, Fe, Co, Ni, Cu, Zn, As, Sr, Cd, Ba, and Pb) in the extracts were quantified using an inductively coupled plasma mass spectrometer (ICP-MS, iCAP Q, ThermoFisher Scientific, Waltham, MA, U.S.A.). More details about the sequential extraction and quality control of analysis are shown in the SI (also see Tables S1−S3).

Source Apportionment. A positive matrix factorization (PMF) receptor model was used to identify and quantify the main sources of these elements. The receptor model requires two inputs to run PMF, namely concentration and its uncertainty. Different source numbers were tested by applying a trial to determine the optimal solutions. The identification of sources was conducted based on major marker species. More details are described in SI (PMF analysis).

Health Risk Assessment. The carcinogenic and noncarcinogenic risks posed by airborne metals via direct inhalation of $PM_{2.5}$ were calculated using US Environmental Protection Agency human health risk assessment models, which mainly involve exposure assessment and risk characterization.[24,25] The bioavailable concentrations (exchangeable fraction and reducible fraction) of particulate trace elements, instead of total concentrations, were used for the carcinogenic and noncarcinogenic risks characterization. Details of health risk assessment of trace elements and emission sources are described in the SI (Health risk assessment).

RESULTS AND DISCUSSION

Total Concentrations of Particulate Trace Elements. The daily mean concentrations of $PM_{2.5}$ ranged from 27.6 to 319.0 $\mu g\ m^{-3}$ with an average of 112.3 $\mu g\ m^{-3}$ during the entire measurement campaign, which is much higher than the WHO standard for daily mean $PM_{2.5}$ concentration (25 $\mu g\ m^{-3}$). We categorized the 25 measurement days into low, moderate and severe pollution days according to the Chinese national ambient air quality standard (NAAQS) of 75 $\mu g\ m^{-3}$ (daily concentration) and the mean + σ (170 $\mu g\ m^{-3}$), that is, low pollution days ($PM_{2.5} \leq 75\ \mu g\ m^{-3}$, 8 days), moderate pollution days ($75 \leq PM_{2.5} \leq 170\ \mu g\ m^{-3}$, 13 days), and severe pollution days ($PM_{2.5} \geq 170\ \mu g\ m^{-3}$, 4 days) (see Figure S2a). The average concentrations of $PM_{2.5}$ are approximately 2 and 5 times higher during moderate pollution days (112.1 $\mu g\ m^{-3}$) and severe pollution days (241.4 $\mu g\ m^{-3}$) than during low pollution days (51.2 $\mu g\ m^{-3}$), respectively. Figure S2b shows the meteorological data during the measurement period. The temperature was rather stable (around 0 °C) during the entire measurement period. The wind speed was generally lower during moderate and severe pollution days compared to low pollution days as low wind speed favors the development of stagnant weather conditions. The relative humidity (RH) was also generally higher during moderate and severe pollution days than during low pollution days. The high RH favors the

DOI: 10.1021/acs.est.8b02091
Environ. Sci. Technol. 2018, 52, 10967−10974

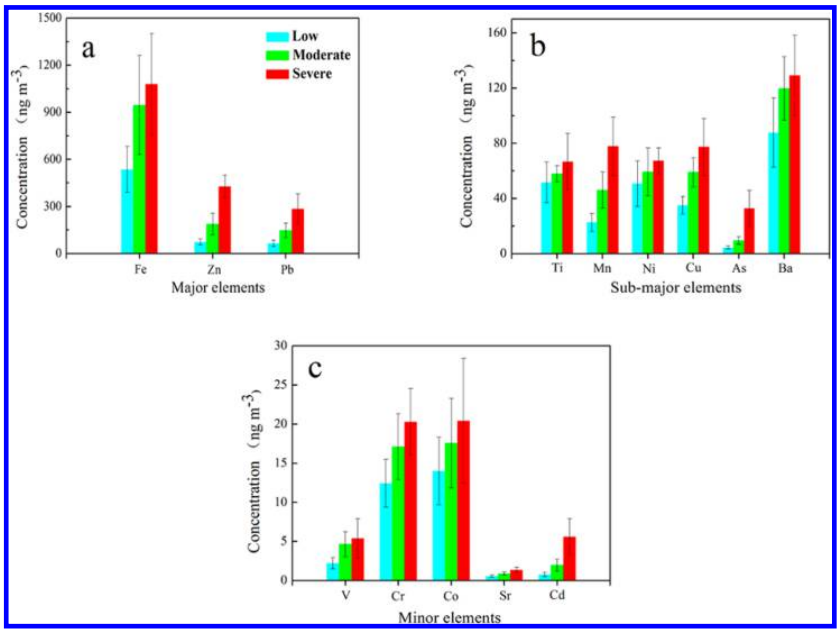

Figure 1. Concentration distribution of trace elements in $PM_{2.5}$: (a) major elements, (b) submajor elements, and (c) minor elements during low pollution days, moderate pollution days, and severe pollution days.

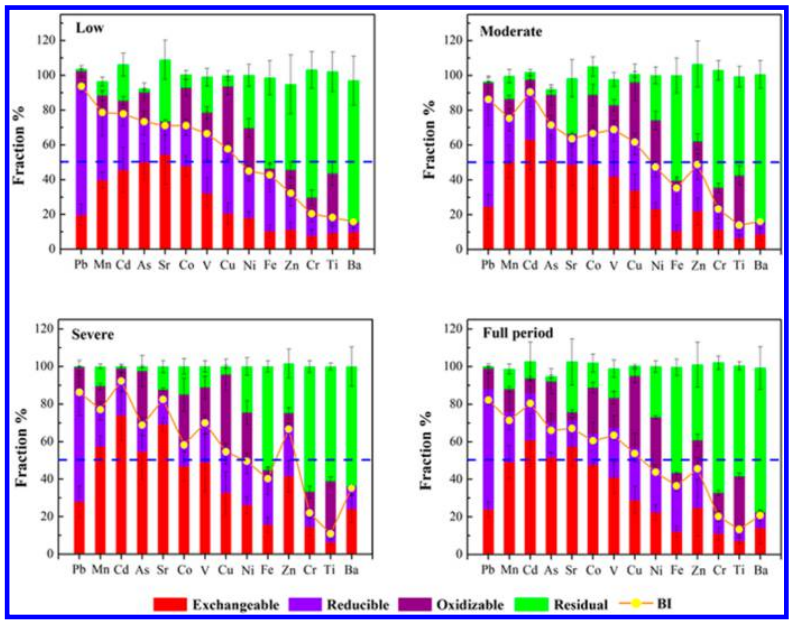

Figure 2. Exchangeable, reducible, oxidizable, and residual fraction of trace elements in $PM_{2.5}$ during low pollution days, moderate pollution days, severe pollution days, and full period. Blue dashed line represents 50% bioavailability index (BI).

decrease of planetary boundary layer (PBL) height and therefore the accumulation of aerosol.[26]

There are two main considerations for the selection of those 14 elements. On the one hand, these elements are frequently used to determine health risks in previous studies.[18,23] On the other hand, they are commonly used in source apportionment studies because of their source specificity and significant relative abundance allowing their precious quantification.[20,27] The average concentrations of these elements are shown in Table S4 for different pollution conditions. The total concentrations of all measured elements constituted 0.9%, 2.2%, 3.3%, and 2.1% of $PM_{2.5}$ mass during severe pollution days, moderate pollution days, low pollution days, and the entire measurement period, respectively. The percentages are consistent with previous studies. For example, measurements in Beijing in winter 2006 showed that these 14 elements

DOI: 10.1021/acs.est.8b02091
Environ. Sci. Technol. 2018, 52, 10967−10974

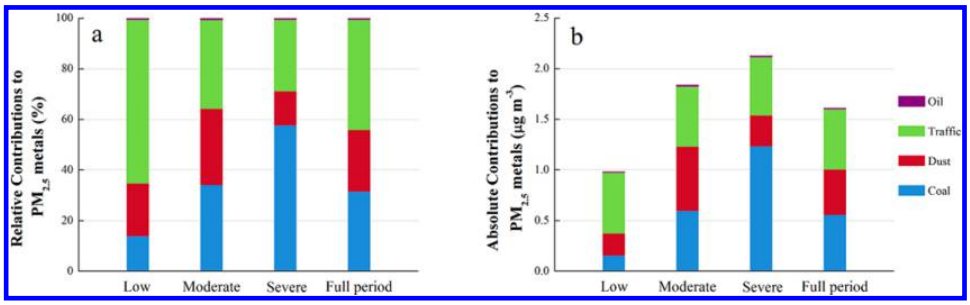

Figure 3. Relative (a) and absolute (b) source contributions to the measured trace elements in $PM_{2.5}$ during low, moderate, and severe pollution days and entire measurement period, respectively.

constituted about 1.9% of the $PM_{2.5}$ mass.[20] Another study showed the total concentration of Fe, Zn, Pb, Ti, Mn, Ni, Cu, As, Ba, V, and Cr constituted approximately 3.1% of $PM_{2.5}$ mass in Beijing in December 2010.[19] In Lanzhou, the capital of the Gansu Province in China, the total concentration of these elements (except Fe) constituted 1.6% (haze days) and 2.0% (nonhaze days) of the $PM_{2.5}$ mass in winter 2012.[21] The percentage of particulate trace elements is dependent on the mass of other chemical composition, particularly sulfate, nitrate, ammonium, and carbonaceous matter. The decrease of the elemental fraction with the increase of pollution levels could be attributed to the enhanced formation of secondary inorganic aerosol and secondary organic aerosol during pollution days.[27]

Figure 1 shows the total concentrations of individual particulate trace elements during low pollution, moderate pollution and severe pollution days. Fe, Zn, and Pb are the most abundant elements (major elements), followed by a submajor group (including Ba, Mn, Cu, Ni, Ti, and As) and a minor group (including Co, Cr, V, Cd, and Sr). The concentrations of each measured element increased as pollution levels increased. Statistically significant difference between the concentrations of the elements during severe pollution days and low pollution days can be observed for all elements, except for Ti and Sr (t-test, $p < 0.05$). The concentrations of trace elements are 1.1−2.5 times higher during moderate pollution days and 1.3−7.3 times higher during severe pollution days than those during low pollution days (see Table S4), indicating a significant accumulation of the particulate trace elements during pollution days. Among all elements, the concentrations of carcinogenic elements including As, Cd, and Pb increased most significantly by a factor of 4.4−7.3 from low pollution days to severe pollution days. Therefore, it is crucial to understand the sources of these elements and whether the sources and their contribution change with the pollution levels.

Chemical Fractionation and Bioavailability Index of Trace Elements in $PM_{2.5}$. Figure 2 shows the fractionation distribution of individual elements under different pollution conditions. Fe, Zn, Cr, Ti, and Ba were present mainly in residual fraction (>50%). The percentage of this fraction was rather constant from low pollution days to moderate and severe pollution days (4−8% difference) except for Zn and Ba which show larger decrease from low pollution days to severe pollution days (from 49% to 27% for Zn and 81% to 64% for Ba). The constitution of Ni was rather constant under different pollution conditions, i.e., about 24% of exchangeable fraction, 23% of reducible fraction, 27% of oxidizable fraction, and 26% of residual fraction. The characteristics of Ni, Fe, and Zn are consistent with previous studies in Guangzhou and Nanjing.[15] Pb existed predominantly in the reducible fraction (64%) at different pollution levels, indicating a large potential in transformation to exchangeable fraction. Mn and V present mainly in exchangeable fraction (49% for Mn, 41% for V) and reducible fraction (27% for both Mn and V). Cd, As, Sr, and Co were presented mainly in exchangeable fraction, which were consistent with results reported by Schleicher et al.[10] Cu was found mainly in exchangeable fraction (29%), reducible fraction (28%), and oxidizable fraction (38%), but little in residual fraction (5%). This observation could be attributed to its strong ability in combining with organic matter.[28]

As discussed above, the distribution pattern of these four fractions determines the bioavailability of an element and therefore the health risk. The exchangeable fraction is readily dissolved and penetrates to the bloodstream through lung fluids, and thus represents a high bioavailability.[15] The reducible fraction is thermodynamically unstable and susceptible to pH changes and redox conditions. This fraction can become bioavailable and causes a potential risk to human health under anoxic conditions.[29] The exchangeable and reducible fraction together can lead to "direct effect" on human health through biochemical reactions within cells and the formation of reactive oxygen species that can cause cellular imbalance and oxidative stress.[15,16,18] The exchangeable and reducible fraction of an element is represented as a bioavailability index (BI) to estimate its potential bioavailability.[15,16] The values of BI < 30%, 30% < BI < 50%, and BI > 50% represent low, medium, and high bioavailability, respectively.[30] As shown in Figure 2, the BI values of Cr, Ti, and Ba were lower than 30% representing low health risk. The BI values of Ni, Fe, and Zn were between 30% and 50%, while the BI values of Pb, Cd, Mn, Sr, As, V, Co, and Cu were larger than 50% indicating high bioavailability and toxicity. It should be noted that the BI values of Fe, Mn, Ti, Pb, As, Cu, Co, Cr, and Ni were rather constant at different pollution levels. However, the BI values of Cd, Sr, V, Zn, and Ba enhanced significantly in the severe pollution days, compared to those in low pollution days ($p < 0.05$). In particular, the largest transformation of Zn was observed from low pollution days (BI = 31%) to severe pollution days (BI = 66%), suggesting a higher risk of some particulate heavy metals to human health in pollution days than in low pollution days.

Sources of Trace Elements. A receptor model (PMF) has been widely used for source apportionment of particulate matter, and it was used to identify and quantify the main sources of elements measured in this study. Figures S3 and S5

DOI: 10.1021/acs.est.8b02091
Environ. Sci. Technol. 2018, 52, 10967−10974

provide details regarding the estimated source profiles, indicating the relative intensity of element to each factor and the fraction of the total predicted concentration for a given element, which can be useful for qualitative identification of the sources. In Figure S4 we show the correlation (R^2) of each element with each source identified by PMF. Four factors were identified, including oil combustion, dust, traffic-related, and coal combustion emissions. The first factor is characterized by a high contribution of vanadium (~50%), often used as a tracer for oil combustion in many previous studies in China.[31−35] It should be noted that the composition of the emissions might be different depending on the country of origin. For example, vanadium may not be a good tracer of oil combustion in some countries depending on quality and country of origin of the oil. Selenium is a good tracer for coal combustion emission in the U.S., but not the case in China.[36] Therefore, attention should be paid to the difference in emission signature for source identification. The second factor is dominated by crustal elements, e.g., Ti and Fe.[18] This factor represents crustal materials, mainly from unpaved road and/or construction activities, and constitutes 13.5−30.1% of the total mass of measured elements (Figure 3a). The third factor is characterized by high contributions of Ni, Ba, Cr, and Cu, which have been considered to be from tire abrasion, brake linings, lubricants, and corrosion of vehicular parts.[19,37,38] The relative contributions of this factor to Cr and Ni are >70%, most likely from brake wear as reported in Visser et al.[38] Also for this factor, Fe constitutes ~45% of the total mass of measured elements, consistent with previous results that traffic-related emissions are dominated by Fe.[38] The fourth factor contributes more than 80% to As, Cd, and Pb, and ~50% to Mn, Co, and Zn. As, Pb, and Cd are found in the exhaust from the activities associated with coal burning processes and smelting furnace and have been used as tracers for coal combustion emissions.[35]

The relative contribution of each factor to the total mass concentration of measured elements is shown in Figure 3a. Oil combustion was a negligible source, contributing <1% of total mass of elements measured in Beijing, irrespective of the pollution level. Traffic-related emission was the dominant source during low pollution days, contributing 65% of total mass of the measured elements, followed by dust emission (21%) and coal combustion (14%). During moderate pollution days, the contribution of traffic-related emission decreased significantly to 35%, and the contribution of dust (30%) and coal combustion (34%) increased to around one-third, respectively. During severe pollution days, the coal combustion emission increased to be the dominant contribution (58%), followed by traffic-related (28%) and dust emission (14%). Figure 3b shows the absolute contribution of each factor to the mass concentrations of trace elements in $PM_{2.5}$ at different pollution levels. With increasing pollution level, the absolute contribution of coal combustion increased dramatically (from 0.15 to 1.24 $\mu g\ m^{-3}$). However, traffic emissions remained rather stable (~0.6 $\mu g\ m^{-3}$). The observed differences in both relative and absolute source contributions highlight the changes in emissions and/or accumulation at different pollution levels.

Health Risk Assessment. The health risk from inhalation of particulate trace elements in wintertime 2014 in Beijing is assessed. The calculated values of exposure concentration (EC), inhalation reference concentration (RfC) and inhalation unit risk (IUR) are shown in Table S5. Mn (10.8 ng m^{-3} for both children and adults) and Pb (3.16 ng m^{-3} for children and 12.6 ng m^{-3} for adults) are found to have the highest exposure concentrations among the noncarcinogenic and carcinogenic elements, respectively. The carcinogenic risks of inhaling particulate Cd, Co, and Ni are lower than the precautionary criterion (10^{-6}) both for children and adults. The carcinogenic risks of Pb and As are higher than 10^{-6} for adults only, but the carcinogenic risks of Cr for children and adults both exceed the precautionary criterion (Table S6). Furthermore, the combined carcinogenic risks from these trace elements are 2.85×10^{-6} for children and 1.14×10^{-5} for adults, both higher than the precautionary criterion, indicating that for every million children and million adults living in local environment, approximately 3 children and 12 adults may develop cancer from inhaling these particulate trace elements during their lifetime. The noncarcinogenic health risks via inhalation of particulate As, Cd, Co, Cr, Mn, Ni, and V are all lower than the safe limit (i.e., hazard quotient (HQ) < 1) for both children and adults (Table S6). However, the sum of HQ values from these trace elements is 1.14, indicating accumulative noncarcinogenic risks.

In combination with the source profiles resolved by PMF, the element-specific risk is then translated into source-specific risk. The results in Table S7 show that coal combustion has the highest carcinogenic risk (5.31×10^{-6} for adults and 1.33×10^{-6} for children), followed by traffic-related emissions (4.84×10^{-6} for adults and 1.21×10^{-6} for children). The carcinogenic risk of dust (1.05×10^{-6}) is slightly higher than the precautionary criterion (10^{-6}) for adults only. As for the noncarcinogenic health risk, the HQ value of individual emission sources identified in this study is lower than the safe limit (HQ < 1), but the accumulative HQ values from these emission sources are higher than 1 for both children and adults.

The contribution of each source to health risk is finally calculated by combining the source-specific risk and the PMF source apportionment results. For carcinogenic risk, traffic-related emission was the dominant source (76.6%) during low pollution days. This percentage decreased to 44.4% during moderate pollution days and contribution from coal combustion increased from 18.1% to 47.3%. The contribution from coal combustion increased further to 67% during severe pollution days (Figure 4). These results suggest that significant carcinogenic risks can result from coal combustion and traffic-related emission in wintertime Beijing. The contribution patterns for noncarcinogenic risks are somewhat different from those for carcinogenic risks (Figure 4). Traffic-related emission was the major contributor, but had a higher contribution (88.6%) during low pollution days. During moderate pollution days, the traffic-related contribution decreased to 65.3% and coal combustion increased to 30.2%. The contribution from coal combustion increased further to around 50%, showing importance equal to traffic-related emission. The difference in health risks may be due to difference in the source composition of $PM_{2.5}$ at different pollution levels. Furthermore, the large contribution from these two sources is associated with the high normalized health risk (i.e., carcinogenic or noncarcinogenic risk normalized by element mass) of Cr, Co, Cd, As, and Ni from vehicular emission and coal combustion (see Figure S6).

The results are in agreement with previous work on source apportionment that used actual mortality data from six U.S. cities.[39] Our work further extends to source-specific health risk

DOI: 10.1021/acs.est.8b02091
Environ. Sci. Technol. 2018, 52, 10967−10974

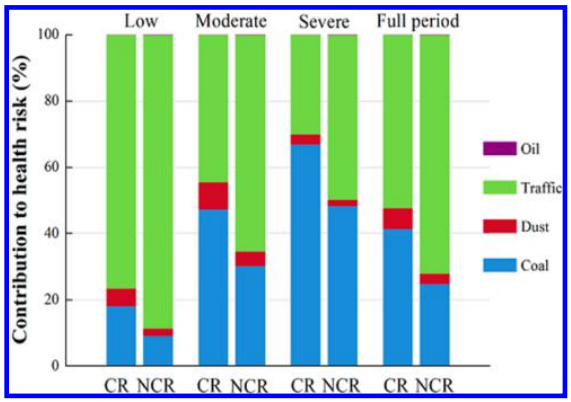

Figure 4. Contribution of each source to carcinogenic risks (CR) and noncarcinogenic risks (NCR) via inhalation exposure to $PM_{2.5}$-bound trace elements on low, moderate, severe pollution days, and full period in wintertime Beijing.

assessment from the concentration- and/or component-response risk assessment.[40,41] In addition, other studies relate specific particulate matter source apportionment with actual health data (e.g., hospital admissions, or mortality).[42−44] For example, Ozkaynak and Thurston showed that particles from industrial sources (e.g., from iron/steel emissions) and coal combustion were more significant contributors to human mortality than soil-derived particles.[42] Ostro et al. found that several sources of $PM_{2.5}$, including vehicle exhaust, fuel oil combustion, secondary nitrate/organics, minerals, secondary sulfate/organics, and road dust, had statistically significant associations ($p < 0.05$) with cardiovascular risks.[43] The results of Bell et al. suggested that some particle sources and constituents are more harmful than others and that in the Connecticut/Massachusetts region the most harmful particles include black carbon, calcium, and road dust $PM_{2.5}$.[44] In our work, traffic-related emission is the dominant contributor for both carcinogenic and noncarcinogenic risks during low pollution days, while coal combustion becomes equally or even more important contributor during moderate and severe pollution days.

Limitations of the Risk Assessment. The carcinogenic and noncarcinogenic risks through direct inhalation of particulate trace elements were calculated using US Environmental Protection Agency (US EPA) human health risk assessment models (US EPA 2009).[24] In this study, we extend such chemical component-response health risk assessment to source-specific risk assessment by combining with source apportionment analysis. This assessment was made by a number of assumptions, including the assessment models used, reference toxic data, default exposure parameters, and population characteristic parameters. Other exposure routes, including ingestion of atmospheric particulates after deposition, dermal absorption of particles adhered to exposed skin, and atmospheric particle exposure indoors, were not considered. Notwithstanding, inhalation is regarded as the most efficient administration route of particulate matter into the human blood. Other important toxic constituents in $PM_{2.5}$, e.g., atmospheric mercury, elemental carbon, and polycyclic aromatic hydrocarbons, were not considered. Therefore, health risk assessments presented here are only limited to trace elements. Nevertheless, the four sources identified through trace elements in this study are widespread in China and therefore estimates are relevant on a regional scale. It should also be noted that the source-related risks derived may differ from the sum of the risks from each constitute as the actual risks of the mixtures may be synergetic. Despite uncertainties related with the absolute risk assessments provided in this study, they may serve as useful (although untested here) indices for comparing our results with previous and future work aiming at the determination of health risks associated with the chemical composition and sources of particulate matter.[15,30,45,46] In particular, the risk indices determined in this study should be validated in future studies against direct measurements of health impact.

■ ASSOCIATED CONTENT

Supporting Information

The Supporting Information is available free of charge on the ACS Publications website at DOI: 10.1021/acs.est.8b02091.

Tables S1−S7 and Figures S1−S6 with addition experimental procedures and results as described in the text (PDF)

■ AUTHOR INFORMATION

Corresponding Author

*E-mail: rujin.huang@ieecas.cn (R.-J.H.).

ORCID

Ru-Jin Huang: 0000-0002-4907-9616
Chunshui Lin: 0000-0003-3175-6778
Imad El Haddad: 0000-0002-2461-7238
Andre S. H. Prevot: 0000-0002-9243-8194

Notes

The authors declare no competing financial interest.

■ ACKNOWLEDGMENTS

This work was supported by the National Key Research and Development Program of China (No. 2017YFC0212701), the National Natural Science Foundation of China (NSFC) under Grant No. 91644219, 41877408, and 91544107.

■ REFERENCES

(1) Cakmak, S.; Dales, R.; Kauri, L. M.; Mahmud, M.; Van Ryswyk, K.; Vanos, J.; Liu, L.; Kumarathasan, P.; Thomson, E.; Vincent, R. Metal composition of fine particulate air pollution and acute changes in cardiorespiratory physiology. *Environ. Pollut.* **2014**, *189*, 208−214.

(2) Lu, S.-l.; Yao, Z.-k.; Chen, X.-h.; Wu, M.-h.; Sheng, G.-y.; Fu, J.-m.; Daly, P. The relationship between physicochemical characterization and the potential toxicity of fine particulates ($PM_{2.5}$) in Shanghai atmosphere. *Atmos. Environ.* **2008**, *42* (31), 7205−7214.

(3) Bollati, V.; Marinelli, B.; Apostoli, P.; Bonzini, M.; Nordio, F.; Hoxha, M.; Pegoraro, V.; Motta, V.; Tarantini, L.; Cantone, L. Exposure to metal-rich particulate matter modifies the expression of candidate microRNAs in peripheral blood leukocytes. *Environ. Health Perspect.* **2010**, *118* (6), 763−768.

(4) Gerlofs-Nijland, M. E.; Rummelhard, M.; Boere, A. J. F.; Leseman, D. L.; Duffin, R.; Schins, R. P.; Borm, P. J.; Sillanpaa, M.; Salonen, R. O.; Cassee, F. R. Particle induced toxicity in relation to transition metal and polycyclic aromatic hydrocarbon contents. *Environ. Sci. Technol.* **2009**, *43* (13), 4729−4736.

(5) Carter, J. D.; Ghio, A. J.; Samet, J. M.; Devlin, R. B. Cytokine production by human airway epithelial cells after exposure to an air pollution particle is metal-dependent. *Toxicol. Appl. Pharmacol.* **1997**, *146* (2), 180−188.

DOI: 10.1021/acs.est.8b02091
Environ. Sci. Technol. 2018, 52, 10967−10974

(6) Ghio, A. J.; Stonehuerner, J.; Dailey, L. A.; Carter, J. D. Metals associated with both the water-soluble and insoluble fractions of an ambient air pollution particle catalyze an oxidative stress. *Inhalation Toxicol.* **1999**, *11* (1), 37−49.
(7) Wilson, M. R.; Lightbody, J. H.; Donaldson, K.; Sales, J.; Stone, V. Interactions between ultrafine particles and transition metals in vivo and in vitro. *Toxicol. Appl. Pharmacol.* **2002**, *184* (3), 172−179.
(8) Espinosa, A. J. F.; Rodríguez, M. T.; de la Rosa, F. J. B.; Sánchez, J. C. J. A chemical speciation of trace metals for fine urban particles. *Atmos. Environ.* **2002**, *36* (5), 773−780.
(9) Pérez, G.; López-Mesas, M.; Valiente, M. Assessment of heavy metals remobilization by fractionation: comparison of leaching tests applied to roadside sediments. *Environ. Sci. Technol.* **2008**, *42* (7), 2309−2315.
(10) Schleicher, N. J.; Norra, S.; Chai, F.; Chen, Y. Z.; Wang, S. L.; Cen, K.; Yu, Y.; Stüben, D. Temporal variability of trace metal mobility of urban particulate matter from Beijing−A contribution to health impact assessments of aerosols. *Atmos. Environ.* **2011**, *45* (39), 7248−7265.
(11) Mukhtar, A.; Limbeck, A. Recent developments in assessment of bio-accessible trace metal fractions in airborne particulate matter: a review. *Anal. Chim. Acta* **2013**, *774*, 11−25.
(12) Smichowski, P.; Polla, G.; Gómez, D. Metal fractionation of atmospheric aerosols via sequential chemical extraction: a review. *Anal. Bioanal. Chem.* **2005**, *381* (2), 302−316.
(13) Fernandez-Espinosa, A. J.; Ternero-Rodríguez, M. Study of traffic pollution by metals in Seville (Spain) by physical and chemical speciation methods. *Anal. Bioanal. Chem.* **2004**, *379* (4), 684−699.
(14) Tessier, A.; Campbell, P. G. C.; Bisson, M. Sequential extraction procedure for the speciation of particulate trace metals. *Anal. Chem.* **1979**, *51* (7), 844−851.
(15) Feng, X. D.; Dang, Z.; Huang, W.; Yang, C. Chemical speciation of fine particle bound trace metals. *Int. J. Environ. Sci. Technol.* **2009**, *6*, 337−346.
(16) Sun, Y. Y.; Hu, X.; Wu, J. C.; Lian, H. Z.; Chen, Y. J. Fractionation and health risks of atmospheric particle-bound As and heavy metals in summer and winter. *Sci. Total Environ.* **2014**, *493*, 487−494.
(17) Behera, S. N.; Betha, R.; Huang, X.; Balasubramanian, R. Characterization and estimation of human airway deposition of size-resolved particulate-bound trace elements during a recent haze episode in Southeast Asia. *Environ. Sci. Pollut. Res.* **2015**, *22* (6), 4265−4280.
(18) Li, H. M.; Wang, Q. G.; Shao, M.; Wang, J. H.; Wang, C.; Sun, Y. X.; Qian, X.; Wu, H. F.; Yang, M.; Li, F. Y. Fractionation of airborne particulate-bound elements in haze-fog episode and associated health risks in a megacity of southeast China. *Environ. Pollut.* **2016**, *208*, 655−662.
(19) Yu, L. D.; Wang, G. F.; Zhang, R. J.; Zhang, L. M.; Song, Y.; Wu, B. B.; Li, X. F.; An, K.; Chu, J. H. Characterization and Source Apportionment of $PM_{2.5}$ in an Urban Environment in Beijing. *Aerosol Air Qual. Res.* **2013**, *13*, 574−583.
(20) Tan, J. H.; Duan, J. C.; Zhen, N. J.; He, K. B.; Hao, J. M. Chemical characteristics and source of size-fractionated atmospheric particle in haze episode in Beijing. *Atmos. Res.* **2016**, *167*, 24−33.
(21) Tan, J.; Zhang, L.; Zhou, X.; Duan, J.; Li, Y.; Hu, J.; He, K. Chemical characteristics and source apportionment of $PM_{2.5}$ in Lanzhou, China. *Sci. Total Environ.* **2017**, *601−602*, 1743−1752.
(22) Chen, R.; Cheng, J.; Lv, J.; Wu, L.; Wu, J. Comparison of chemical compositions in air particulate matter during summer and winter in Beijing, China. *Environ. Geochem. Health* **2017**, *39* (4), 913−921.
(23) Betha, R.; Behera, S. N.; Balasubramanian, R. 2013 Southeast Asian smoke haze: fractionation of particulate-bound elements and associated health risk. *Environ. Sci. Technol.* **2014**, *48* (8), 4327−4335.
(24) US EPA (U.S. Environmental Protection Agency). 2009. Risk Assessment Guidance for Superfund (RAGS), Volume I Human Health Evaluation Manual (Part F, Supplemental Guidance for Inhalation Risk Assessment). EPA-540-R-070−002, OSWER 9285.7−82, January. http://www.epa.gov/swerrims/riskassessment/ragsf/index.htm.
(25) US EPA (U.S. Environmental Protection Agency). 2013. User's Guide/technical Background Document for US EPA Region 9's RSL (Regional Screening Levels) Tables. http://www.epa.gov/region9/superfund/prg/.
(26) Tie, X. X.; Huang, R. J.; Cao, J. J.; Zhang, Q.; Cheng, Y. F.; Su, H.; Chang, D.; Poschl, U.; Hoffmann, T.; Dusek, U.; Li, G. H.; Worsnop, D. R.; O'Dowd, C. D. Severe Pollution in China Amplifed by Atmospheric Moisture. *Sci. Rep.* **2017**, *7* (1), 15760.
(27) Huang, R. J.; Zhang, Y.; Bozzetti, C.; Ho, K. F.; Cao, J. J.; Han, Y.; Daellenbach, K. R.; Slowik, J. G.; Platt, S. M.; Canonaco, F.; Zotter, P.; Wolf, R.; Pieber, S. M.; Bruns, E. A.; Crippa, M.; Ciarelli, G.; Piazzalunga, A.; Schwikowski, M.; Abbaszade, G.; Schnelle-Kreis, J.; Zimmermann, R.; An, Z.; Szidat, S.; Baltensperger, U.; Haddad, I. E.; Prevot, A. S. H. High secondary aerosol contribution to particulate pollution during haze events in China. *Nature* **2014**, *514* (7521), 218−222.
(28) Illera, V.; Walter, I.; Souza, P.; Cala, V. Short-term effects of biosolid and municipal solid waste applications on heavy metals distribution in a degraded soil under a semi-arid environment. *Sci. Total Environ.* **2000**, *255* (1−3), 29−44.
(29) Fuentes, A.; Lloréns, M.; Sáez, J.; Isabel Aguilar, M. A.; Ortuño, J. F.; Meseguer, V. F. Comparative study of six different sludges by sequential speciation of heavy metals. *Bioresour. Technol.* **2008**, *99* (3), 517−525.
(30) Li, H. M.; Wang, J. H.; Wang, Q. G.; Qian, X.; Qian, Y.; Yang, M.; Li, F. Y.; Lu, H.; Wang, C. Chemical fractionation of arsenic and heavy metals in fine particle matter and its implications for risk assessment: A case study in Nanjing, China. *Atmos. Environ.* **2015**, *103*, 339−346.
(31) Song, Y.; Tang, X. Y.; Xie, S. D.; Zhang, Y. H.; Wei, Y. J.; Zhang, M. S.; Zeng, L. M.; Lu, S. H. Source apportionment of $PM_{2.5}$ in Beijing in 2004. *J. Hazard. Mater.* **2007**, *146* (1−2), 124−130.
(32) Mazzei, F.; D'Alessandro, A.; Lucarelli, F.; Nava, S.; Prati, P.; Valli, G.; Vecchi, R. Characterization of particulate matter sources in an urban environment. *Sci. Total Environ.* **2008**, *401* (1−3), 81−89.
(33) Minguillón, M. C.; Cirach, M.; Hoek, G.; Brunekreef, B.; Tsai, T.; de Hoogh, K.; Jedynska, A.; Kooter, I. M.; Nieuwenhuijsen, M.; Querol, X. Spatial variability of trace elements and sources for improved exposure assessment in Barcelona. *Atmos. Environ.* **2014**, *89*, 268−281.
(34) Moreno, T.; Querol, X.; Alastuey, A.; Reche, C.; Cusack, M.; Amato, F.; Pandolfi, M.; Pey, J.; Richard, A. T.; Prevot, A. S. H.; Furger, M.; Gibbons, W. Variations in time and space of trace metal aerosol concentrations in urban areas and their surroundings. *Atmos. Chem. Phys.* **2011**, *11* (17), 9415−9430.
(35) Duan, J. C.; Tan, J. H. Atmospheric heavy metals and arsenic in China: situation, sources and control policies. *Atmos. Environ.* **2013**, *74*, 93−101.
(36) Yudovich, Y.; Ketris, M. Selenium in coal: A review. *Int. J. Coal Geol.* **2006**, *67*, 112−126.
(37) Mooibroek, D.; Schaap, M.; Weijers, E. P.; Hoogerbrugge, R. Source apportionment and spatial variability of $PM_{2.5}$ using measurements at five sites in the Netherlands. *Atmos. Environ.* **2011**, *45* (25), 4180−4191.
(38) Visser, S.; Slowik, J. G.; Furger, M.; Zotter, P.; Bukowiecki, N.; Canonaco, F.; Flechsig, U.; Appel, K.; Green, D. C.; Tremper, A. H.; Young, D. E.; Williams, P. I.; Allan, J. D.; Coe, H.; Williams, L. R.; Mohr, C.; Xu, l.; Ng, N. L.; Barlow, J. F.; Halios, C. H.; Fleming, Z. L.; Baltensperger, U.; Prevot, A. S. H.; Nemitz, E. Advanced source apportionment of size-resolved trace elements at multiple sites in London during winter. *Atmos. Chem. Phys.* **2015**, *15* (19), 11291−11309.
(39) Lepeule, J.; Laden, F.; Dockery, D.; Schwartz, J. Chronic exposure to fine particles and mortality: An extended follow-up of the Harvard Six Cities Study from 1974 to 2009. *Environ. Health Perspect.* **2012**, *120*, 965−970.

DOI: 10.1021/acs.est.8b02091
Environ. Sci. Technol. 2018, 52, 10967−10974

(40) Pope, C. A., III; Cropper, M.; Coggins, J.; Cohen, A. Health benefits of air pollution abatement policy: Role of the shape of the concentration−response function. *J. Air Waste Manage. Assoc.* **2015**, *65* (5), 516−522.
(41) Marshall, J. D.; Apte, J. S.; Coggins, J. S.; Goodkind, A. L. Blue skies bluer? *Environ. Sci. Technol.* **2015**, *49*, 13929−13936.
(42) Ozkaynak, H.; Thurston, G. Associations Between 1980 U. S. Mortality Rates and Alternative Measures of Airborne Particle Concentration. *Risk Anal.* **1987**, *7*, 449−460.
(43) Ostro, B.; Tobias, A.; Querol, X.; Alastuey, A.; Amato, F.; Pey, J.; Perez, N.; Sunyer, J. The Effects of Particulate Matter Sources on Daily Mortality: A Case-Crossover Study of Barcelona, Spain. *Environ. Health Perspect.* **2011**, *119* (12), 1781−1787.
(44) Bell, M. L.; Ebisu, K.; Leaderer, B. P.; Gent, J. F.; Lee, H. J.; Koutrakis, P.; Wang, Y.; Dominici, F.; Peng, R. D. Associations of $PM_{2.5}$ Constituents and Sources with Hospital Admissions: Analysis of Four Counties in Connecticut and Massachusetts (USA) for Persons ≥ 65 Years of Age. *Environ. Health Perspect.* **2014**, *122* (2), 138−144.
(45) Jan, R.; Roy, R.; Yadav, S.; Satsangi, P. G. Chemical fractionation and health risk assessment of particulate matter-bound metals in Pune, India. *Environ. Geochem. Health* **2018**, *40*, 255−270.
(46) Taner, S.; Pekey, B.; Pekey, H. Fine particulate matter in the indoor air of barbeque restaurants: elemental compositions, sources and health risks. *Sci. Total Environ.* **2013**, *454*−*455*, 79−87.

DOI: 10.1021/acs.est.8b02091
Environ. Sci. Technol. 2018, 52, 10967−10974

Atmos. Meas. Tech., 11, 3447–3456, 2018
https://doi.org/10.5194/amt-11-3447-2018

Atmospheric Measurement Techniques
Open Access
EGU

Organosulfates in atmospheric aerosol: synthesis and quantitative analysis of $PM_{2.5}$ from Xi'an, northwestern China

Ru-Jin Huang[1,2], Junji Cao[1], Yang Chen[3], Lu Yang[1], Jincan Shen[4], Qihua You[2], Kai Wang[1,5], Chunshui Lin[1,6], Wei Xu[1,6], Bo Gao[1], Yongjie Li[7], Qi Chen[8], Thorsten Hoffmann[5], Colin D. O'Dowd[6], Merete Bilde[9], and Marianne Glasius[9]

[1]Key Laboratory of Aerosol Chemistry and Physics, State Key Laboratory of Loess and Quaternary Geology, Institute of Earth and Environment, Chinese Academy of Sciences, Xi'an, 710061, China
[2]Centre for Atmospheric and Marine Sciences, Xiamen Huaxia University, Xiamen 361024, China
[3]Key Laboratory of Reservoir Aquatic Environment of CAS, Chongqing Institute of Green and Intelligent Technology, Chinese Academy of Sciences, Chongqing 400714, China
[4]Food Inspection & Quarantine Center of Shenzhen Entry-Exit Inspection and Quarantine Bureau, Shenzhen Key Laboratory of Detection Technology R&D on Food Safety, Shenzhen 518045, China
[5]Institute of Inorganic and Analytical Chemistry, Johannes Gutenberg University of Mainz, Duesbergweg 10–14, 55128 Mainz, Germany
[6]School of Physics and Centre for Climate and Air Pollution Studies, Ryan Institute, National University of Ireland Galway, University Road, Galway, Ireland
[7]Department of Civil and Environmental Engineering, Faculty of Science and Technology, University of Macau, Taipa, Macau, China
[8]State Key Joint Laboratory of Environmental Simulation and Pollution Control, College of Environmental Sciences and Engineering, Peking University, Beijing 100871, China
[9]Department of Chemistry, Aarhus University, Langelandsgade 140, 8000 Aarhus C, Denmark

Correspondence: Ru-Jin Huang (rujin.huang@ieecas.cn)

Received: 2 April 2018 – Discussion started: 6 April 2018
Revised: 2 June 2018 – Accepted: 7 June 2018 – Published: 18 June 2018

Abstract. The sources, formation mechanism and amount of organosulfates (OS) in atmospheric aerosol are not yet well understood, partly due to the lack of authentic standards for quantification. In this study, we report an improved robust procedure for the synthesis of organosulfates with different functional groups. Nine authentic organosulfate standards were synthesized and four standards (benzyl sulfate, phenyl sulfate, glycolic acid sulfate, and hydroxyacetone sulfate) were used to quantify their ambient concentrations. The authentic standards and ambient aerosol samples were analyzed using an optimized ultra performance liquid chromatography–electrospray ionization-tandem mass spectrometric method (UPLC–ESI–MS/MS). The recovery ranged from 80.4 to 93.2 %, the limits of detection and limits of quantification obtained were 1.1–16.7 and 3.4–55.6 pg m^{-3}, respectively. Measurements of ambient aerosol particle samples collected in winter 2013/2014 in urban Xi'an, northwestern China, show that glycolic acid sulfate (77.3 ± 49.2 ng m^{-3}) is the most abundant species of the identified organosulfates followed by hydroxyacetone sulfate (1.3 ± 0.5 ng m^{-3}), phenyl sulfate (0.14 ± 0.09 ng m^{-3}), and benzyl sulfate (0.04 ± 0.01 ng m^{-3}). Except for hydroxyacetone sulfate, which seems to form mainly from biogenic emissions in this region, the organosulfates quantified during winter in Xi'an show an increasing trend with an increase in the mass concentrations of organic carbon indicating their anthropogenic origin.

Published by Copernicus Publications on behalf of the European Geosciences Union.

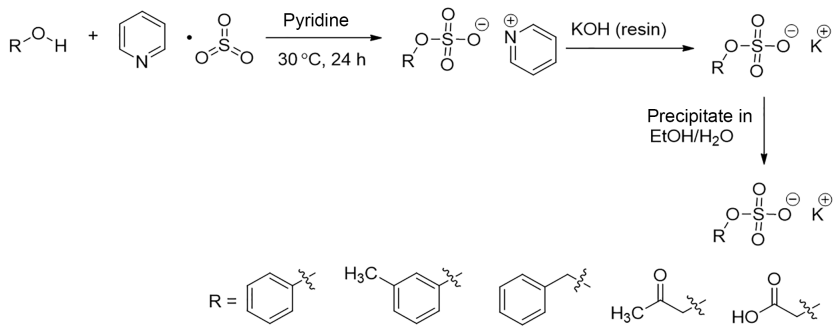

Figure 1. General scheme for the synthesis of organosulfate, modified from Staudt et al. (2014) and Hettiyadura et al. (2015).

1 Introduction

Atmospheric aerosol particles represent a highly complex blend of inorganic and organic matter originating from a wide variety of both natural and anthropogenic sources. The organic fraction typically constitutes 20–90 % of the total submicron aerosol mass and is much less constrained in terms of chemical composition than the inorganic fraction (Jimenez et al., 2009; Hallquist et al., 2009). Only ∼ 10–30 % of the particulate organic matter has been identified as specific compounds despite years of effort and the use of the most sophisticated techniques available (Hoffmann et al., 2011). The insufficient knowledge of the composition of organic aerosol particles at the molecular level hinders a better understanding of the sources, formation and atmospheric processes of organic aerosol as well as their physicochemical properties and effects on climate and human health (Noziere et al., 2015).

Organosulfates are ubiquitous in atmospheric aerosol and have been detected in ambient aerosol particles from America, Europe, Asia and the Arctic during the last decade (e.g., Surratt et al., 2008; Iinuma et al., 2007; Stone et al., 2012; Hansen et al., 2014; Kourtchev et al., 2016; Surratt et al., 2007). Due to the presence of the deprotonated functional group R–O–SO_3^-, organosulfates are acidic and highly water soluble and thus can enhance the aerosol hygroscopicity. These characteristics, together with the light-absorbing property of organosulfates, lead to potential impacts on climate (Lin et al., 2014).

Organosulfates are tracers of secondary organic aerosol (SOA) formation and have been demonstrated to be produced from heterogeneous and multiphase reactions (e.g., Surratt et al., 2008; Iinuma et al., 2007; Chan et al., 2011; Zhang et al., 2012). Chamber studies have found that the oxidation of biogenic volatile organic compounds (BVOCs) including isoprene, monoterpenes and sesquiterpenes can form organosulfates on acidified sulfate particles (e.g., Surratt et al., 2008; Iinuma et al., 2007; Chan et al., 2011; Zhang et al., 2012). A very recent study revealed a previously unrecognized pathway for organosulfate formation through the heterogeneous reaction of SO_2 with the unsaturated bond in oleic acid (Shang et al., 2016). A number of biogenic organosulfates have been observed in ambient aerosol, in particular, isoprene-derived organosulfates (e.g., Kristensen et al., 2011; He et al., 2014; Liao et al., 2015; Budisulistiorini et al., 2015). A recent study reported the formation of aromatic organosulfates by photochemical oxidation of polycyclic aromatic hydrocarbons (PAHs) in the presence of sulfate seed particles (Riva et al., 2016). Aromatic organosulfates have also recently been observed in urban aerosol from different locations in Asia. The presence of aromatic organosulfates was first suggested by Stone et al. (2012) based on analysis of aerosol samples collected at four sites in Asia. Kundu et al. (2013) quantified benzyl sulfate ($C_7H_7SO_4^-$) and identified its homologous series with increasing number of methylene groups ($C_8H_9SO_4^-$ and $C_9H_{11}SO_4^-$) in Lahore, Pakistan. Furthermore, Staudt et al. (2014) synthesized phenyl sulfate, benzyl sulfate, 3- and 4-methylphenyl sulfate and 2-, 3-, and 4-methylbenzyl sulfate and quantified them in aerosols collected in urban samples from Lahore and Pasadena, USA as well as Nepal. Ma et al. (2014) reported the contribution up to 64 % from aromatic organosulfates to the sum of identified organosulfates during winter in Shanghai, while Wang et al. (2016) found aromatic organosulfates to constitute less than 22 % of the detected number of organosulfates in Shanghai, Nanjing and Wuhan.

Organosulfates have been estimated to contribute 5–10 % of the organic mass in fine particles in the USA (Tolocka and Turpin, 2012). However, quantification of organosulfates is a challenging task due to the lack of authentic standards and incomplete understanding of the sources, precursors and formation processes of organosulfates. To date, many studies of organosulfates have remained at the qualitative level, although a limited number of studies have provided quantitative or semi-quantitative analysis of certain organosulfates (e.g., Kundu et al., 2013; Staudt et al., 2014; Ma et al., 2014; Olson et al., 2011; Hettiyadura et al., 2017). Moreover, several studies show that organosulfates are present as a wide range of species with individual species such as the

organosulfate derived from isoprene epoxydiols (IEPOXs) contributing 0.2–1.4 % of the total organic aerosol mass (Liao et al., 2015). This further complicates the quantification of organosulfates. A few organosulfate standards have been synthesized for quantification purposes. For example, Olsen et al. (2011) measured 0.4–3.8 ng m^{-3} lactic acid sulfate and 1.9–11.3 ng m^{-3} glycolic acid sulfate in samples of $PM_{2.5}$ (particulate matter with an aerodynamic diameter $< 2.5\,\mu m$) from the US, Mexico City, and Pakistan. Kundu et al. (2013) measured monthly average concentrations of benzyl sulfate ranging from 0.05 to 0.5 ng m^{-3} in $PM_{2.5}$ samples from Lahore, Pakistan. Staudt et al. (2014) quantified benzyl sulfate ranging from 4 to 90 pg m^{-3} in $PM_{2.5}$ samples from Lahore (Pakistan), Godavari (Nepal), and Pasadena (California), while methylbenzyl sulfates, phenyl sulfate, and methylphenyl sulfates were observed intermittently in these three locations. Furthermore, Hettiyadura et al. (2015) developed a hydrophilic interaction liquid chromatography method using an amide stationary phase providing excellent retention of carboxy-organosulfates and isoprene-derived organosulfates, which was validated using six model organosulfates including aliphatic and aromatic organosulfates.

Previous field studies focusing on organosulfates were conducted mainly in Europe (e.g., Iinuma et al., 2007; Kristensen et al., 2011; Gómez-González et al., 2008, 2012; Nguyen et al., 2014; Martinsson et al., 2017), North America (e.g., Surratt et al., 2007; Nguyen et al., 2012; Worton et al., 2011) and a few in China (He et al., 2014; Ma et al., 2014). The particulate air pollution has been a serious environmental problem during recent winters in China, characterized by high secondary aerosol concentrations including sulfate and SOA (e.g., Huang et al., 2014; Elser et al., 2016; Wang et al., 2017). As organosulfates are tracers for SOA, more studies on organosulfates will help to better understand and constrain the SOA formation mechanisms in highly polluted regions (e.g., China) and to reconcile the underestimation of particle-phase organic carbon in atmospheric models.

In this study, nine organosulfate standards (phenyl sulfate, 3-methylphenyl sulfate, benzyl sulfate, 2-methyl benzyl sulfate, 3-methyl benzyl sulfate, 2, 4-dimethyl benzyl sulfate, 3, 5-dimethyl benzyl sulfate, hydroxyacetone sulfate and glycolic acid sulfate) were synthesized using an approach modified from Staudt et al. (2014) and Hettiyadura et al. (2015). These authentic standards were used to optimize an ultra performance liquid chromatography electrospray ionization-tandem mass spectrometric method (UPLC–ESI–MS/MS) for the quantification of organosulfates. The presence and concentration of four of these organosulfates, namely, benzyl sulfate, phenyl sulfate, glycolic acid sulfate and hydroxyacetone sulfate, were determined in ambient $PM_{2.5}$ collected in urban air in Xi'an, China. The rest five organosulfates were not quantified in ambient $PM_{2.5}$ because the standards were synthesized at a later stage of the study.

2 Material and methods

2.1 Chemicals and synthesis

The chemicals used for the synthesis of organosulfates included hydroxyacetone (99 %, Sigma Aldrich), glycolic acid (99 %, Sigma Aldrich), phenol (99.5 %, Tic), benzyl alcohol (99.8 %, Aladdin, Shanghai, China), m-cresol (99 %, Sigma Aldrich), sulfur trioxide pyridine complex (98 %, Sigma Aldrich), pyridine (99.9 %, Sigma Aldrich) and Dowex® 50WX8 (hydrogen form, 100–200 mesh, Sigma Aldrich). MilliQ water (18.2 MΩ) was used, and all other reagents were analytical grade and used without further purification.

The organosulfate standards were synthesized using a general approach modified from Staudt et al. (2014) and Hettiyadura et al. (2015). Figure 1 shows the reaction scheme. In general, alcohol (7.0 mmol) and sulfur trioxide pyridine complex (1.2 equiv.) was dissolved in dry pyridine (10 mL) in an oven-dried, three-necked flask provided with magnetic stirring under nitrogen. The reaction mixture was stirred at 30 °C for 24 h, and then the solvent was removed via distillation under vacuum at 50 °C. The residue was redissolved in distilled water (10 mL) and titrated with 0.9 M KOH until pH was above 12. Neat ethanol (40 mL, 65 °C) was added to the aqueous solution. The resulting solution was heated to reflux followed by a quick vacuum filtration to remove the stark white precipitate. The mother liquor was then placed in a freezer (−25 °C) overnight. The potassium salts of organosulfate formed in the mother liquor were collected by vacuum filtration, rinsed with cold ethanol three times and dried to obtain the target product. The synthesized organosulfate standards were stored in refrigerator (∼ 4 °C) and no decomposition was observed after 2 years as confirmed by nuclear magnetic resonance (NMR) analysis.

2.2 Characterization

The synthesized products were characterized with NMR and ESI–MS. ^{1}H NMR and ^{13}C NMR spectra were recorded on a Bruker Advance-III 40 MHz spectrometer at 400 and 100 MHz, respectively using trimethylsilane (TMS) as an internal standard. Chemical shifts are reported in ppm downfield from the internal reference. The NMR spectra are shown in Supplement. The following abbreviations are used for the multiplicities: s = singlet, m = multiplet. The yield for phenyl sulfate was 45 %, ^{1}H NMR (400 MHz, D_2O): δ/ppm 7.29–7.43 (m, 5H), ^{13}C NMR (100 MHz, D_2O): δ/ppm 121.6, 126.4, 129.8 and 151.2. The yield for benzyl sulfate was 70 %, ^{1}H NMR (400 MHz, DMSO-*d*6): δ/ppm 7.25–7.40 (m, 5 H), 4.76 (s, 2 H), ^{13}C NMR (100 MHz, DMSO-*d*6): δ/ppm 67.9, 127.8, 128.0, 128.6 and 138.4. The yield for hydroxyacetone sulfate was 45 %, ^{1}H NMR (400 MHz, DMSO-*d*6): δ/ppm 4.22 (s, 2 H), 2.11 (s, 3 H), ^{13}C NMR (100 MHz, DMSO-*d*6): δ/ppm 26.9, 71.4 and 207.0. The yield for glycolic acid sulfate was 35 %, ^{1}H NMR

Table 1. The optimized ESI-MS/MS parameters and UPLC retention time of measured organosulfates.

Organosulfate	Deprotonate molecule (m/z)	Product ion (m/z)	Cone voltage (V)	Collision energy (eV)	Retention time (min)
Phenyl sulfate	$C_6H_5SO_4^-$ (173)	SO_3^- (80) $C_6H_5O^-$ (93)	41	20 21	0.86 ± 0.02
Benzyl sulfate	$C_7H_7SO_4^-$ (187) (187)	HSO_3^- (81) SO_4^- (96)	42	19 22	0.96 ± 0.02
Hydroxyacetone sulfate	$C_3H_5SO_5^-$ (153)	SO_3^- (80) HSO_4^- (97)	32	18 20	1.10 ± 0.02
Glycolic acid sulfate	$C_2H_3SO_6^-$ (155)	$C_2H_3O_3^-$ (75) HSO_4^- (97)	26	18 14	5.78 ± 0.03

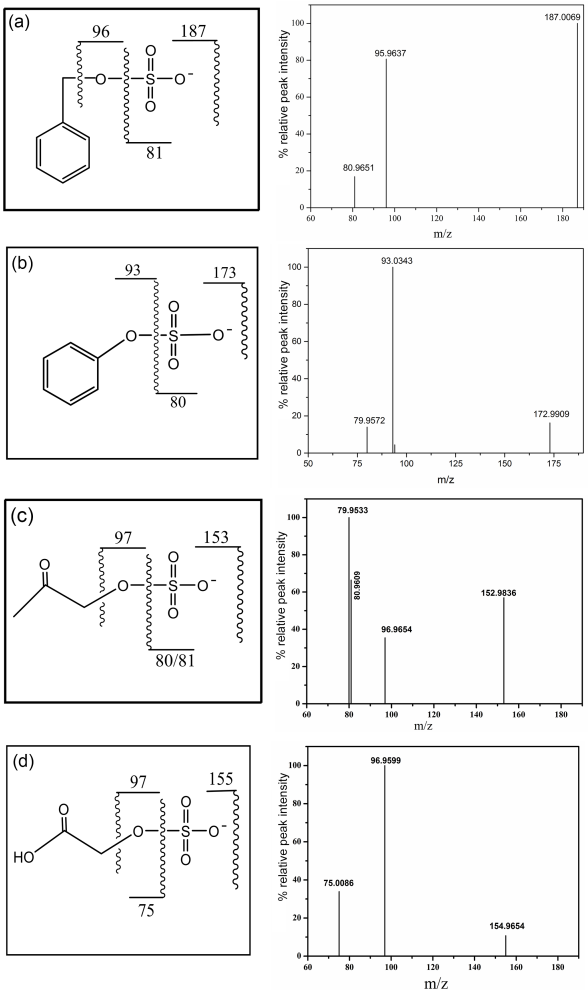

Figure 2. The fragmentation (left) and mass spectra (right) of benzyl sulfate **(a)**, phenyl sulfate **(b)**, hydroxyacetone sulfate **(c)** and glycolic acid sulfate **(d)**.

(400 MHz, DMSO-$d6$): δ/ppm 4.07 (s, 2 H) and ^{13}C NMR (100 MHz, DMSO-$d6$): δ/ppm 65.0, 173.1. The organosulfate standards were recrystallized in ethanol for purification and purity of these synthesized standards is >95 %, confirmed by NMR analysis. Exact mass spectra were recorded on a high-resolution mass spectrometer (HR–MS, Q Exactive Plus, Thermo Scientific, USA) equipped with an ESI source in the negative ion mode (ESI-). The ESI conditions were as follows: spray voltage −3.2 kV, collision energy (CE) 40 V for benzyl sulfate and 45 V for hydroxyacetone sulfate, 3-methylphenyl sulfate, glycolic acid sulfate and phenyl sulfate, capillary temperature 350 °C, aux gas heater temperature 320 °C, sheath gas flow rate 35 and aux gas flow rate 10. The mass resolving power was 70 000. Data acquisition was performed with m/z ranging from 50 to 200.

2.3 $PM_{2.5}$ samples

The 24 h integrated $PM_{2.5}$ samples were collected on pre-baked (780 °C, 3 h) quartz-fiber filters (8 × 10 inch, Whatman, QM-A, USA) using a high-volume sampler (Tisch, Cleveland, OH, USA) at a flow rate of 1.05 m^3 min^{-1} from 18 December 2013 to 17 February 2014. After collection, the filter samples were immediately wrapped in pre-baked aluminum foil and stored in a freezer (below −20 °C) until analysis. The sampling site was located on the rooftop of the Institute of Earth and Environment (∼ 10 m above the ground), Chinese Academy of Sciences (IEECAS, 34.23° N, 108.88° E), which is surrounded by residential, commercial and trafficked areas.

2.4 Sample analysis

A portion of the filter (6 × 0.526 cm^2 punch) taken from each sample was sonicated for 25 min in 9 mL of acetonitrile (ACN)/water mixture (95 : 5, V/V). The extracts were filtered through a 0.22 µm polypropylene membrane syringe filter to remove insoluble material. The eluate was concentrated almost to dryness with a gentle stream of purified nitrogen (99.999 %) at 45 °C using an evaporation system (TurboVap® LV, biotage), then redissolved in 500 µL of ace-

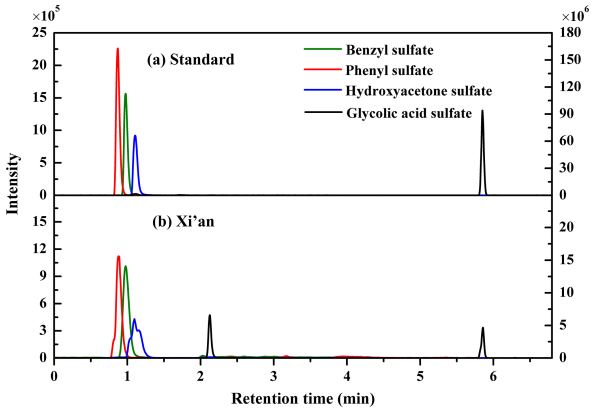

Figure 3. Typical chromatograms of organosulfates from the mixture of authentic standard solution and ambient $PM_{2.5}$ samples, measured with the UPLC–ESI–MS/MS method. Note, the intensity of benzyl sulfate and phenyl sulfate refers to the left *y* axis, and the intensity of hydroxyacetone sulfate and glycolic acid sulfate refers to right *y* axis.

tonitrile/water mixture (V/V, 95 : 5). The prepared samples were stored at 4 °C in the refrigerator and analyzed within 24 h. The separation and quantification were realized using a ACQUITY UPLC system (equipped with a quaternary pump, autosampler, and thermostated column compartment) coupled to a tandem mass spectrometer (Xevo TQ MS, Waters, USA). The separation was carried out using a BEH amide column (2.1 mm × 100 mm, 1.7 µm particle size, Waters, USA) equipped with a pre-column. The column was maintained at 35 °C and the flow rate of mobile phase was 0.25 mL min^{-1}. A 5 µL injection volume was used for quantitative analysis of samples and standards. The optimized mobile phase A (organic) consisted of ammonium acetate buffer (5 mM, pH 8.5) in ACN and ultra-pure water (95 : 5, V/V) and mobile phase B (aqueous) consisted of ammonium acetate buffer (5 mM, pH 9) in ultra-pure water. A mobile phase gradient was used: mobile phase A was maintained at 98 % for 2 min, then decreased to 60 % from 2 to 5 min and then held there for 2 min; from 7 to 12 min mobile phase A was returned to 98 %. Organosulfates were detected by a TQ MS equipped with an ESI source in the negative ion mode. The mass spectrometer was operated in multiple reaction monitoring (MRM) mode. Optimized MS conditions for the four organosulfates chosen for the field studies (e.g., cone voltages and collision energies) are listed in Table 1. The capillary voltage was 2.7 kV, source temperature was 150 °C, desolvation temperature was 350 °C, desolvation gas (N_2) flow rate at 800 L h^{-1}, cone gas (N_2) flow rate was 150 L h^{-1}, and collision gas (Ar) flow rate was 0.16 mL min^{-1}. All data were acquired and processed using MassLynx software (version 4.1). All samples and standard spectra were background subtracted.

2.5 Quality control

For every 10 analyses, a procedural blank and a spiked sample, real ambient samples spiked with known amounts of a standard solution of organosulfates to be quantified, were measured to check for interference and cross-contamination. The external standard method was used for quantitative determination of the analytes. The limits of detection are defined as the minimum detectable peaks of individual species with a signal-to-noise (S/N) ratio of 3 : 1. The recoveries were determined by the analysis of the spiked samples: we first measured a filter punch without spike and then measured the second punch from the identical filter spiked with known amounts of a standard solution of organosulfates. The differences between these two measurements were divided by the amounts of organosulfates spiked to calculate the recoveries of individual organosulfates. This recovery test also provides an indication of potential matrix effect. The reproducibility (relative standard deviation, RSD) was determined by measuring five identical samples that were subjected to the same pretreatment procedure. The field blank samples were collected and analyzed, and the data reported here were corrected for the field blanks.

3 Results and discussion

3.1 Mass spectral fragmentation and UPLC separation

Each synthesized organosulfate was analyzed by high resolution tandem MS (MS/MS). The molecular ion for each organosulfate was assigned to the deprotonated molecule (R–O–SO_3^-). Major sulfur-containing product ions included the sulfite ion radical ($\cdot SO_3^-$, m/z 80) that is formed from the homolytic cleavage of the O–S bond, the sulfate ion radical ($\cdot SO_4^-$, m/z 96) that is formed from the homolytic cleavage of the C–O bond, the bisulfite anion (HSO_3^-, m/z 81) that is formed from hydrogen abstraction followed by the heterolytic cleavage of the O–S bond, and the bisulfate anion (HSO_4^-, m/z 97). Phenyl sulfate, 3-methylphenyl sulfate, and glycolic acid sulfate produce phenoxide ($C_6H_5O^-$, m/z 93), 3-methylphenoxide ($C_7H_7O^-$, m/z 107) and glycolate ($C_2H_3O_3^-$, m/z 75) anions, respectively, formed from neutral loss of SO_3. The mass spectra of these compounds are shown in Fig. 2. The mass spectrum of phenyl sulfate is similar to that reported by Staudt et al. (2014), the mass spectra of hydroxy acetone sulfate and glycolic acid sulfate are similar to those reported by Hettiyadura et al. (2015) and the spectrum of benzyl sulfate is similar to that reported by Kundu et al. (2013), confirming the identity of the compounds.

The ESI-MS/MS in MRM mode is applied for the quantification of individual organosulfates. This can greatly enhance the selectivity and sensitivity by monitoring a transition pair of precursor and product ions and thus eliminating potential interferences from the complex aerosol matrix. Ta-

Table 2. Analytical performance of the UPLC-ESI-MS/MS method for organosulfate analysis.

Organosulfate	Linear range ($ng\,mL^{-1}$)	Linearity (R^2)	Recovery %	LOD (pg), injection volume (5 µL)	LOQ (pg), injection volume (5 µL)	LOD* ($pg\,m^{-3}$)	LOQ* ($pg\,m^{-3}$)
Phenyl sulfate	0.1–40	0.998	80.4	0.13	0.43	1.1	3.5
Benzyl sulfate	0.1–40	0.998	89.6	0.13	0.43	1.1	3.4
Hydroxyacetone sulfate	0.3–120	0.997	93.2	2.1	6.9	16.7	55.6
Glycolic acid sulfate	2–800	0.995	92.0	0.27	0.88	2.1	7.1

* For analyzing 6×0.526 cm punches of filters collected with high-volume samplers (sampling at $1.13\,m^3\,min^{-1}$ for 24 h on 8" × 10" filters).

Table 3. The quantification of organosulfates at Xi'an and comparison with data reported in the literature.

Location	Date	$PM_{2.5}$ $\mu g\,m^{-3}$	OC $\mu g\,m^{-3}$	Organosulfate $ng\,m^{-3}$				Ref.
				benzyl sulfate	phenyl sulfate	hydroxyacetone sulfate	glycolic acid sulfate	
Riverside, CA	27/07/05	16.5	7.6	–	–	–	3.3	Olson et al. (2011)
Mexico City (T0)	26/03/06	40	8.5	–	–	–	4.1	
Mexico City (T1)	26/03/06	33	5.2	–	–	–	7.0	
Cleveland, OH	15/07/07	12.7	3.9	–	–	–	1.9	
Bakersfield, CA	16–18/06/10	11.1–12.0	4.0-4.8	–	–	–	4.5–5.4	
Lahore, Pakistan	02/11/07	327.5	174.7	–	–	–	11.3	
Lahore, Pakistan	12/01/2007–13/01/2008	–	–	0.05–0.50	–	–	–	Kundu et al. (2013)
Lahore, Pakistan	Mar/07	177.1	44.6	0.09	0.004	–	–	Staudt et al. (2014)
Godavari, Nepal	Feb/07	42.0	4.7	0.004	ND	–	–	
Pasadena, CA	5–6/06/10	41.8–44.1	7.3–7.6	0.006–0.007	ND	–	–	
Centreville, AL	10–11/07/13	–	–	ND	ND	2.7–5.8	9–14	Hettiyadura et al. (2015)
Shanghai	5–7/04/12 12–14/07/12 27–29/10/12 14–16/01/13	–	–	0.3–0.8	–	–	–	Ma et al. (2014)
Xi'an ($n = 10$)	18/12/13–17/02/14	94.7–314.5	14.9–68.5	0.03–0.06	0.04–0.31	0.9–2.6	18.1–155.5	This study

ble 1 shows the optimized ESI- conditions and the transition pairs for each organosulfate studied. The organosulfate standards were separated by UPLC using a BEH amide column that retains extremely polar compounds through ionic, hydrogen bonding and dipole interactions. A gradient elution procedure was applied and the aqueous portion of the mobile phase increased from 7–43 %, leading to the baseline separation of four organosulfates within 6 min (Fig. 3a). The retention time was 0.86 min for phenyl sulfate, 0.96 min for benzyl sulfate, 1.10 min for hydroxyacetone sulfate and 5.78 min for glycolic acid sulfate, respectively. The mobile phase was buffered to slightly basic pH to maintain the deprotonated state of the organosulfates, which favors the separation. The amide functionalization of the BEH stationary phase introduces hydrogen bonding and strengthens interaction with organosulfates particularly for those containing carboxyl and hydroxyl functional groups. It should be noted that the chromatographic peak-broadening occurred particularly for phenyl sulfate and hydroxyacetone sulfate when analyzing the ambient samples (Fig. 3b). This might be explained by matrix effects due to the complex samples, which can influence the partitioning of analyte between the stationary phase and mobile phase, particularly for those analytes with weak retention on the column. However, the quantification of organosulfates is not affected by the peak broadening because the transition pair of precursor and product ions used in the MRM mode of the mass spectrometer guarantees selectivity and accuracy.

3.2 Method validation

Table 2 shows the analytical performance of the method under optimized UPLC and MS/MS conditions. The calibration curves of each organosulfate are highly linear ($R^2 \geq 0.995$), ranging from 0.1–40 $ng\,mL^{-1}$ for phenyl sulfate and benzyl sulfate, from 0.3–120 $ng\,mL^{-1}$ for hydroxyacetone sulfate, and 2.0–800 $ng\,mL^{-1}$ for glycolic acid sulfate. The recoveries, determined by analyzing ambient samples spiked with known amounts of organosulfate standards, ranging from 80.4–93.2 %. The good recoveries indicate high extraction efficiency, low sample matrix effect and low error from sample pretreatment and the UPLC-MS measurement. The

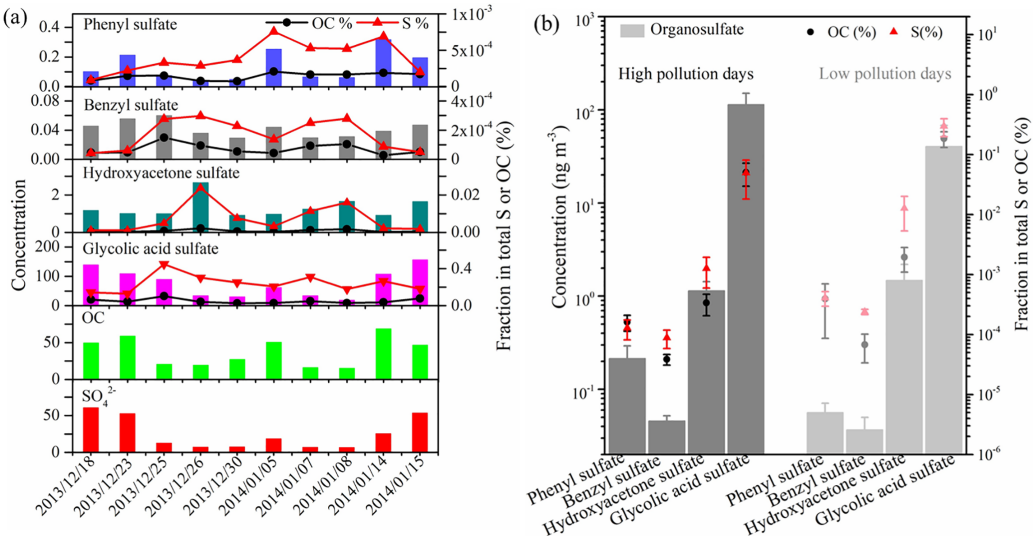

Figure 4. Time series of organosulfates (ng m^{-3}), OC (µg m^{-3}), SO_4^{2-} (µg m^{-3}) and the fraction of individual organosulfates in total sulfur and OC **(a)**. The average concentrations of individual organosulfates and the fractional contribution in total sulfur and OC during high and low pollution days are also shown **(b)**.

limit of detection (LOD, S/N = 3) and limit of quantification (LOQ, S/N = 10) ranged from 0.03 to 0.42 ng mL^{-1} and 0.09 to 1.4 ng mL^{-1} of the extracts, respectively. This corresponds to LODs of 1.1 to 16.7 pg m^{-3} and LOQs of 3.4 to 55.6 pg m^{-3}, respectively, using the current set-up (see experimental section).

3.3 Quantification of organosulfates in ambient aerosol

Ambient $PM_{2.5}$ samples were extracted and analyzed by UPLC-MS/MS following the same procedure as the OS standards. The four selected organosulfates were identified according to the transition pairs of precursor and product ions of individual compounds on the MS/MS as well as the UPLC retention time. Table 3 shows the concentrations of phenyl sulfate, benzyl sulfate, hydroxyacetone sulfate, and glycolic acid sulfate in $PM_{2.5}$ samples collected at Xi'an (this work), together with concentrations reported in the literature from other locations worldwide for comparison. In our samples from Xi'an glycolic acid sulfate (average 77.3 ± 49.2 ng m^{-3}, range 18.1–155.5 ng m^{-3}) was the most abundant species of the identified organosulfate followed by hydroxyacetone sulfate (average 1.3 ± 0.5 ng m^{-3}, range 0.9–2.6 ng m^{-3}), phenyl sulfate (average 0.14 ± 0.09 ng m^{-3}, range 0.04–0.31 ng m^{-3}) and benzyl sulfate (average 0.04 ± 0.01 ng m^{-3}, range 0.03–0.06 ng m^{-3}).

The concentration of glycolic acid sulfate quantified in this study is about one order of magnitude higher than those reported in the literature (see Table 3), indicating the substantial formation of this secondary organic compound in polluted urban Xi'an. Glycolic acid sulfate can form efficiently from glycolic acid relative to glyoxal in the presence of acidic sulfate particles (Olson et al., 2011). While both organic precursors (glycolic acid and glyoxal) have biogenic and anthropogenic origins, they form mainly from the oxidation of anthropogenic emissions during winter in Xi'an. The concentrations of particle-phase glyoxal and glycolic acid measured at Xi'an during winter have been reported to be significantly higher compared to other studied regions (e.g., Kawamura and Yasui, 2005; Miyazaki et al., 2009; Cheng et al., 2013), which thus may explain the elevated glycolic acid sulfate. The concentration of the other three organosulfates quantified in this study was much lower, but falling into the ranges measured in other regions.

It is noted that the time series of glycolic acid sulfate, phenyl sulfate and benzyl sulfate is similar to that of organic carbon (OC) and SO_4^{2-}, while the concentration of hydroxyacetone sulfate did not show an increasing trend when the concentrations of OC increased (Fig. 4a). Hydroxyacetone sulfate can form from photochemical oxidation of isoprene and/or isoprene ozonolysis in the presence of acidic sulfate aerosols (Surratt et al., 2008; Riva et al., 2015), although hydroxyacetone was also suggested to originate from anthropogenic emissions (e.g., biomass burning and fossil fuel combustion) (Hansen et al., 2014). Also, the formation rate of biogenic hydroxyacetone sulfate and anthropogenic hydroxyacetone sulfate may different. This may explain the lack of correlation between hydroxyacetone sulfate and OC during winter in Xi'an. The average concentrations of glycolic acid sulfate, phenyl sulfate and benzyl sulfate were 1.3–3.2× higher during high pollution

days ($PM_{2.5}$ range of 293.7–314.5 $\mu g\,m^{-3}$ with an average of 300.6 $\mu g\,m^{-3}$) than during low pollution days ($PM_{2.5}$ range of 94.7–121.2 $\mu g\,m^{-3}$ with an average of 106.4 $\mu g\,m^{-3}$), while the average concentrations of hydroxyacetone sulfate were rather similar between high pollution days and low pollution days (Fig. 4b). These four organosulfates together account for 0.25 % of total sulfur and 0.05 % of OC, respectively.

4 Conclusions

Nine authentic organosulfate standards, including phenyl sulfate, 3-methylphenyl sulfate, benzyl sulfate, 2-methyl benzyl sulfate, 3-methyl benzyl sulfate, 2, 4-dimethyl benzyl sulfate, 3, 5-dimethyl benzyl sulfate, hydroxyacetone sulfate and glycolic acid sulfate, were synthesized in this study using an improved robust procedure. The synthesized compounds of benzyl sulfate, phenyl sulfate, glycolic acid sulfate, and hydroxyacetone sulfate were used as standards for quantification of these molecules in ambient $PM_{2.5}$ samples. The other five organosulfate standards were synthesized, but not used for quantification of ambient samples in this study. An improved UPLC-ESI-MS/MS method was developed and optimized for the quantification. The recovery ranges from 80.4–93.2 %, and the limits of detection and limits of quantification obtained are 1.1–16.7 and 3.4–55.6 $pg\,m^{-3}$, respectively. Measurements of $PM_{2.5}$ samples from Xi'an show that glycolic acid sulfate ($77.3 \pm 49.2\,ng\,m^{-3}$) is the most abundant organosulfate followed by hydroxyacetone sulfate ($1.3 \pm 0.5\,ng\,m^{-3}$), phenyl sulfate ($0.14 \pm 0.09\,ng\,m^{-3}$) and benzyl sulfate ($0.04 \pm 0.01\,ng\,m^{-3}$). Glycolic acid sulfate, phenyl sulfate and benzyl sulfate show an increasing trend with the increase of OC concentrations indicating their anthropogenic origin.

Data availability. Raw data used in this study are archived at the Institute of Earth Environment, Chinese Academy of Sciences, and are available on request by contacting the corresponding author.

The Supplement related to this article is available online at https://doi.org/10.5194/amt-11-3447-2018-supplement.

Competing interests. The authors declare that they have no conflict of interest.

Acknowledgements. This work was supported by the National Natural Science Foundation of China (NSFC) under grant No. 91644219, No. 41650110488, the Minjiang Scholar Program and the Carlsberg Foundation.

Edited by: Mingjin Tang
Reviewed by: two anonymous referees

References

Budisulistiorini, S. H., Li, X., Bairai, S. T., Renfro, J., Liu, Y., Liu, Y. J., McKinney, K. A., Martin, S. T., McNeill, V. F., Pye, H. O. T., Nenes, A., Neff, M. E., Stone, E. A., Mueller, S., Knote, C., Shaw, S. L., Zhang, Z., Gold, A., and Surratt, J. D.: Examining the effects of anthropogenic emissions on isoprene-derived secondary organic aerosol formation during the 2013 Southern Oxidant and Aerosol Study (SOAS) at the Look Rock, Tennessee ground site, Atmos. Chem. Phys., 15, 8871–8888, https://doi.org/10.5194/acp-15-8871-2015, 2015.

Chan, M. N., Surratt, J. D., Chan, A. W. H., Schilling, K., Offenberg, J. H., Lewandowski, M., Edney, E. O., Kleindienst, T. E., Jaoui, M., Edgerton, E. S., Tanner, R. L., Shaw, S. L., Zheng, M., Knipping, E. M., and Seinfeld, J. H.: Influence of aerosol acidity on the chemical composition of secondary organic aerosol from β-caryophyllene, Atmos. Chem. Phys., 11, 1735–1751, https://doi.org/10.5194/acp-11-1735-2011, 2011.

Cheng, C. L., Wang, G. H., Zhou, B. H., Meng, J. J., Li, J. J., Cao, J. J., and Xiao, S.: Comparison of Dicarboxylic Acids and Related Compounds in Aerosol Samples Collected in Xi'An, China During Haze and Clean Periods, Atmos. Environ., 81, 443–449, https://doi.org/10.1016/j.atmosenv.2013.09.013, 2013.

Elser, M., Huang, R.-J., Wolf, R., Slowik, J. G., Wang, Q., Canonaco, F., Li, G., Bozzetti, C., Daellenbach, K. R., Huang, Y., Zhang, R., Li, Z., Cao, J., Baltensperger, U., El-Haddad, I., and Prévôt, A. S. H.: New insights into $PM_{2.5}$ chemical composition and sources in two major cities in China during extreme haze events using aerosol mass spectrometry, Atmos. Chem. Phys., 16, 3207–3225, https://doi.org/10.5194/acp-16-3207-2016, 2016.

Gómez-González, Y., Surratt, J. D., Cuyckens, F., Szmigielski, R., Vermeylen, R., Jaoui, M., Lewandowski, M., Offenberg, J. H., Kleindienst, T. E., and Edney, E. O.: Characterization of Organosulfates From the Photooxidation of Isoprene and Unsaturated Fatty Acids in Ambient Aerosol Using Liquid Chromatography/(-)Electrospray Ionization Mass Spectrometry, J. Mass Spectrom., 43, 371–382, https://doi.org/10.1002/jms.1329, 2008.

Gómez-González, Y., Wang, W., Vermeylen, R., Chi, X., Neirynck, J., Janssens, I. A., Maenhaut, W., and Claeys, M.: Chemical characterisation of atmospheric aerosols during a 2007 summer field campaign at Brasschaat, Belgium: sources and source processes of biogenic secondary organic aerosol, Atmos. Chem. Phys., 12, 125–138, https://doi.org/10.5194/acp-12-125-2012, 2012.

Hallquist, M., Wenger, J. C., Baltensperger, U., Rudich, Y., Simpson, D., Claeys, M., Dommen, J., Donahue, N. M., George, C., Goldstein, A. H., Hamilton, J. F., Herrmann, H., Hoffmann, T., Iinuma, Y., Jang, M., Jenkin, M. E., Jimenez, J. L., Kiendler-Scharr, A., Maenhaut, W., McFiggans, G., Mentel, Th. F., Monod, A., Prévôt, A. S. H., Seinfeld, J. H., Surratt, J. D., Szmigielski, R., and Wildt, J.: The formation, properties and impact of secondary organic aerosol: current and emerging issues, Atmos. Chem. Phys., 9, 5155–5236, https://doi.org/10.5194/acp-9-5155-2009, 2009.

Hansen, A. M. K., Kristensen, K., Nguyen, Q. T., Zare, A., Cozzi, F., Nøjgaard, J. K., Skov, H., Brandt, J., Christensen, J. H., Ström, J., Tunved, P., Krejci, R., and Glasius, M.: Organosulfates and organic acids in Arctic aerosols: speciation, annual variation and concentration levels, Atmos. Chem. Phys., 14, 7807–7823, https://doi.org/10.5194/acp-14-7807-2014, 2014.

He, Q. F., Ding, X., Wang, X. M., Yu, J. Z., Fu, X. X., Liu, T. Y., Zhang, Z., Xue, J., Chen, D. H., and Zhong, L. J.: Organosulfates From Pinene and Isoprene Over the Pearl River Delta, South China: Seasonal Variation and Implicationin Formation Mechanisms, Environ. Sci. Technol., 48, 9236–9245, https://doi.org/10.1021/es501299v, 2014.

Hettiyadura, A. P. S., Stone, E. A., Kundu, S., Baker, Z., Geddes, E., Richards, K., and Humphry, T.: Determination of atmospheric organosulfates using HILIC chromatography with MS detection, Atmos. Meas. Tech., 8, 2347–2358, https://doi.org/10.5194/amt-8-2347-2015, 2015.

Hettiyadura, A. P. S., Jayarathne, T., Baumann, K., Goldstein, A. H., de Gouw, J. A., Koss, A., Keutsch, F. N., Skog, K., and Stone, E. A.: Qualitative and quantitative analysis of atmospheric organosulfates in Centreville, Alabama, Atmos. Chem. Phys., 17, 1343–1359, https://doi.org/10.5194/acp-17-1343-2017, 2017.

Hoffmann, T., Huang, R. J., and Kalberer, M.: Atmospheric analytical chemistry, Anal. Chem., 83, 4649–4664, 2011.

Huang, R. J., Zhang, Y. L., Bozzetti, C., Ho, K. F., Cao, J. J., Han, Y. M., Daellenbach, K. R., Slowik, J. G., Platt, S. M., and Canonaco, F.: High Secondary Aerosol Contribution to Particulate Pollution During Haze Events in China, Nature, 514, 218–222, https://doi.org/10.1038/nature13774, 2014.

Iinuma, Y., Müller, C., Berndt, T., Böge, O., Claeys, M., and Herrmann, H.: Evidence for the Existence of Organosulfates from β-Pinene Ozonolysis in Ambient Secondary Organic Aerosol, Environ. Sci. Technol., 41, 6678–6683, https://doi.org/10.1021/es070938t, 2007.

Jimenez, J. L., Canagaratna, M. R., Donahue, N. M., Prevot, A. S. H., Zhang, Q., Kroll, J. H., DeCarlo, P. F., Allan, J. D., Coe, H., and Ng, N. L.: Evolution of Organic Aerosols in the Atmosphere, Science, 326, 1525–1529, https://doi.org/10.1126/science.1180353, 2009.

Kawamura, K. and Yasui, O.: Diurnal Changes in the Distribution of Dicarboxylic Acids, Ketocarboxylic Acids and Dicarbonyls in the Urban Tokyo Atmosphere, Atmos. Environ., 39, 1945–1960, https://doi.org/10.1016/j.atmosenv.2004.12.014, 2005.

Kourtchev, I., Godoi, R. H. M., Connors, S., Levine, J. G., Archibald, A. T., Godoi, A. F. L., Paralovo, S. L., Barbosa, C. G. G., Souza, R. A. F., Manzi, A. O., Seco, R., Sjostedt, S., Park, J.-H., Guenther, A., Kim, S., Smith, J., Martin, S. T., and Kalberer, M.: Molecular composition of organic aerosols in central Amazonia: an ultra-high-resolution mass spectrometry study, Atmos. Chem. Phys., 16, 11899–11913, https://doi.org/10.5194/acp-16-11899-2016, 2016.

Kristensen, K. and Glasius, M.: Organosulfates and Oxidation Products From Biogenic Hydrocarbons in Fine Aerosols From A Forest in North West Europe During Spring, Atmos. Environ., 45, 4546–4556, https://doi.org/10.1016/j.atmosenv.2011.05.063, 2011.

Kundu, S., Quraishi, T. A., Yu, G., Suarez, C., Keutsch, F. N., and Stone, E. A.: Evidence and quantitation of aromatic organosulfates in ambient aerosols in Lahore, Pakistan, Atmos. Chem. Phys., 13, 4865–4875, https://doi.org/10.5194/acp-13-4865-2013, 2013.

Liao, J., Froyd, K. D., Murphy, D. M., Keutsch, F. N., Yu, G., Wennberg, P. O., St Clair, J. M., Crounse, J. D., Wisthaler, A., and Mikoviny, T.: Airborne Measurements of Organosulfates Over the Continental US, J. Geophys. Res.-Atmos., 120, 2990–3005, https://doi.org/10.1002/2014JD022378, 2015.

Lin, Y. H., Budisulistiorini, H., Chu, K., Siejack, R. A., Zhang, H. F., Riva, M., Zhang, Z. F., Gold, A., Kautzman, K. E., and Surratt, J. D.: Light-Absorbing Oligomer Formation in Secondary Organic Aerosol from Reactive Uptake of Isoprene Epoxydiols, Environ. Sci. Technol., 48, 12012–12021, https://doi.org/10.1021/es503142b, 2014.

Ma, Y., Xu, X. K., Song, W. H., Geng, F. H., and Wang, L.: Seasonal and Diurnal Variations of Particulate Organosulfates in Urban Shanghai, China, Atmos. Environ., 85, 152–160, https://doi.org/10.1016/j.atmosenv.2013.12.017, 2014.

Martinsson, J., Monteil, G., Sporre, M. K., Kaldal Hansen, A. M., Kristensson, A., Eriksson Stenström, K., Swietlicki, E., and Glasius, M.: Exploring sources of biogenic secondary organic aerosol compounds using chemical analysis and the FLEXPART model, Atmos. Chem. Phys., 17, 11025–11040, https://doi.org/10.5194/acp-17-11025-2017, 2017.

Miyazaki, Y., Aggarwal, S. G., Singh, K., Gupta, P. K., and Kawamura, K.: Dicarboxylic Acids and Water-Soluble Organic Carbon in Aerosols in New Delhi, India, in Winter: Characteristics and Formation Processes, J. Geophys. Res.-Atmos., 114, 1–12, https://doi.org/10.1029/2009JD011790, 2009.

Nguyen, T. B., Lee, P. B., Updyke, K. M., Bones, D. L., Laskin, J., Laskin, A., and Nizkorodov, S. A.: Formation of Nitrogen-And Sulfur-Containing Light-Absorbing Compounds Accelerated by Evaporation of Water from Secondary Organic Aerosols, J. Geophys. Res.-Atmos., 117, 1–14, https://doi.org/10.1029/2011JD016944, 2012.

Nguyen, Q. T., Kristensen, T. B., Hansen, A. M. K., Skov, H., Bossi, R., Massling, A., Sørensen, L. L., Bilde, M., Glasius, M., and Nøjgaard, J. K.: Characterization of Humic-Like Substances in Arctic Aerosols, J. Geophys. Res.-Atmos., 119, 5011–5027, https://doi.org/10.1002/2013JD020144, 2014.

Noziere, B., Kalberer, M., Claeys, M., Allan, J., D'Anna, B., Decesari, S., Finessi, E., Glasius, M., Grgic, I., and Hamilton, J. F.: The Molecular Identification of Organic Compounds in the Atmosphere: State of the Art and Challenges, Chem. Rev., 115, 3919–3983, https://doi.org/10.1021/cr5003485, 2015.

Olson, C. N., Galloway, M. M., Yu, G., Hedman, C. J., Lockett, M. R., Yoon, T., Stone, E. A., Smith, L. M., and Keutsch, F. N.: Hydroxycarboxylic Acid-Derived Organosulfates: Synthesis, Stability, and Quantification in Ambient Aerosol, Environ. Sci. Technol., 45, 6468–6474, https://doi.org/10.1021/es201039p, 2011.

Riva, M., Tomaz, S., Cui, T. Q., Lin, Y. H., Perraudin, E., Gold, A., Stone, E. A., Villenave, E., and Surratt, J. D.: Evidence for an Unrecognized Secondary Anthropogenic Source of Organosulfates and Sulfonates: Gas-Phase Oxidation of Polycyclic Aromatic Hydrocarbons in the Presence of Sulfate Aerosol, Environ. Sci. Technol., 49, 6654–6664, https://doi.org/10.1021/acs.est.5b00836, 2015.

Riva, M., Budisulistiorini, S. H., Zhang, Z. F., Gold, A., and Surratt, J. D.: Chemical Characterization of Secondary Or-

ganic Aerosol Constituents From Isoprene Ozonolysis in the Presence of Acidic Aerosol, Atmos. Environ., 130, 5–13, https://doi.org/10.1016/j.atmosenv.2015.06.027, 2016.

Shang, J., Passananti, M., Dupart, Y., Ciuraru, R., Tinel, L., Rossignol, S. P., Perrier, S. B., Zhu, T., and George, C.: SO_2 Uptake on Oleic Acid: A New Formation Pathway of Organosulfur Compounds in the Atmosphere, Environ. Sci. Tech. Let., 3, 67–72, https://doi.org/10.1021/acs.estlett.6b00006, 2016.

Staudt, S., Kundu, S., Lehmler, H. J., He, X. R., Cui, T. Q., Lin, Y. H., Kristensen, K., Glasius, M., Zhang, X. L., Weber, R. J., Surratt, J. D., and Stone, E. A.: Aromatic Organosulfates in Atmospheric Aerosols: Synthesis, Characterization, and Abundance, Atmos. Environ., 94, 366–373, https://doi.org/10.1016/j.atmosenv.2014.05.049, 2014.

Stone, E. A., Yang, L. M., Liya, E. Y., and Rupakheti, M.: Characterization of Organosulfates in Atmospheric Aerosols at Four Asian Locations, Atmos. Environ., 47, 323–329, https://doi.org/10.1016/j.atmosenv.2011.10.058, 2012.

Surratt, J. D., Kroll, J. H., Kleindienst, T. E., Edney, E. O., Claeys, M., Sorooshian, A., Ng, N. L., Offenberg, J. H., Lewandowski, M., and Jaoui, M.: Evidence for Organosulfates in Secondary Organic Aerosol, Environ. Sci. Technol., 41, 517–527, https://doi.org/10.1021/es062081q, 2007.

Surratt, J. D., Gómez-González, Y., Chan, A. W. H., Vermeylen, R., Shahgholi, M., Kleindienst, T. E., Edney, E. O., Offenberg, J. H., Lewandowski, M., and Jaoui, M.: Organosulfate Formation in Biogenic Secondary Organic Aerosol, J. Phys. Chem. A., 112, 8345–8378, https://doi.org/10.1021/jp802310p, 2008.

Tolocka, M. P. and Turpin, B.: Contribution of Organosulfur Compounds to Organic Aerosol Mass, Environ. Sci. Technol., 46, 7978–7983, https://doi.org/10.1021/es300651v, 2012.

Wang, X. K., Rossignol, S., Ma, Y., Yao, L., Wang, M. Y., Chen, J. M., George, C., and Wang, L.: Molecular Characterization of Atmospheric Particulate Organosulfates in Three Megacities at the Middle and Lower Reaches of the Yangtze River, Atmos. Chem. Phys., 16, 2285–2298, https://doi.org/10.5194/acp-16-2285-2016, 2016.

Wang, Y. C., Huang, R. J., Ni, H. Y., Chen, Y., Wang, Q. Y., Li, G. H., Tie, X. X., Shen, Z. X., Huang, Y., and Liu, S. X.: Chemical Composition, Sources and Secondary Processes of Aerosols in Baoji City of Northwest China, Atmos. Environ., 158, 128–137, https://doi.org/10.1016/j.atmosenv.2017.03.026, 2017.

Worton, D. R., Goldstein, A. H., Farmer, D. K., Docherty, K. S., Jimenez, J. L., Gilman, J. B., Kuster, W. C., de Gouw, J., Williams, B. J., Kreisberg, N. M., Hering, S. V., Bench, G., McKay, M., Kristensen, K., Glasius, M., Surratt, J. D., and Seinfeld, J. H.: Origins and composition of fine atmospheric carbonaceous aerosol in the Sierra Nevada Mountains, California, Atmos. Chem. Phys., 11, 10219–10241, https://doi.org/10.5194/acp-11-10219-2011, 2011.

Zhang, H. F., Worton, D. R., Lewandowski, M., Ortega, J., Rubitschun, C. L., Park, J. H., Kristensen, K., Campuzano-Jost, P., Day, D. A., and Jimenez, J. L.: Organosulfates as Tracers for Secondary Organic Aerosol (SOA) Formation From 2-Methyl-3-Buten-2-Ol (Mbo) in the Atmosphere, Environ. Sci. Technol., 46, 9437–9446, https://doi.org/10.1021/es301648z, 2012.

Environmental Science & Technology

Article

Cite This: Environ. Sci. Technol. 2018, 52, 6825−6833

pubs.acs.org/est

Brown Carbon Aerosol in Urban Xi'an, Northwest China: The Composition and Light Absorption Properties

Ru-Jin Huang,[*,†] Lu Yang,[†] Junji Cao,[†] Yang Chen,[‡] Qi Chen,[§] Yongjie Li,[⊥] Jing Duan,[†] Chongshu Zhu,[†] Wenting Dai,[†] Kai Wang,[†,¶] Chunshui Lin,[†,○] Haiyan Ni,[†,◆] Joel C. Corbin,[#] Yunfei Wu,[▽] Renjian Zhang,[▽] Xuexi Tie,[†] Thorsten Hoffmann,[¶] Colin O'Dowd,[○] and Uli Dusek[◆]

[†]Key Laboratory of Aerosol Chemistry and Physics, State Key Laboratory of Loess and Quaternary Geology, Institute of Earth and Environment, Chinese Academy of Sciences, Xi'an 710061, China

[‡]Chongqing Institute of Green and Intelligent Technology, Chinese Academy of Sciences, Chongqing 400714, China

[§]State Key Joint Laboratory of Environmental Simulation and Pollution Control, College of Environmental Sciences and Engineering, Peking University, Beijing 100871, China

[⊥]Department of Civil and Environmental Engineering, Faculty of Science and Technology, University of Macau, Taipa 000000, Macau China

[¶]Institute of Inorganic and Analytical Chemistry, Johannes Gutenberg University of Mainz, Duesbergweg 10−14, Mainz 55128, Germany

[○]School of Physics and Centre for Climate and Air Pollution Studies, Ryan Institute, National University of Ireland Galway, University Road, Galway H91CF50, Ireland

[▽]RCE-TEA, Institute of Atmospheric Physics, Chinese Academy of Sciences, Beijing 100029, China

[#]Laboratory of Atmospheric Chemistry, Paul Scherrer Institute (PSI), Villigen 5232, Switzerland

[◆]Centre for Isotope Research (CIO), Energy and Sustainability Research Institute Groningen (ESRIG), University of Groningen, Groningen 9747 AG The Netherlands

Supporting Information

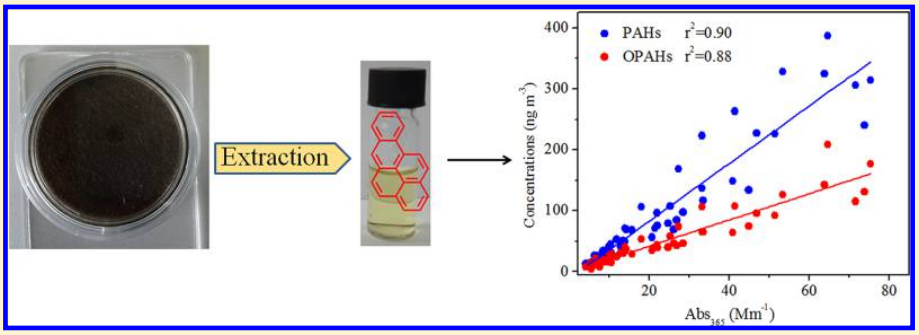

ABSTRACT: Light-absorbing organic carbon (i.e., brown carbon or BrC) in the atmospheric aerosol has significant contribution to light absorption and radiative forcing. However, the link between BrC optical properties and chemical composition remains poorly constrained. In this study, we combine spectrophotometric measurements and chemical analyses of BrC samples collected from July 2008 to June 2009 in urban Xi'an, Northwest China. Elevated BrC was observed in winter (5 times higher than in summer), largely due to increased emissions from wintertime domestic biomass burning. The light absorption coefficient of methanol-soluble BrC at 365 nm (on average approximately twice that of water-soluble BrC) was found to correlate strongly with both parent polycyclic aromatic hydrocarbons (parent-PAHs, 27 species) and their carbonyl oxygenated derivatives (carbonyl-OPAHs, 15 species) in all seasons (r^2 > 0.61). These measured parent-PAHs and carbonyl-OPAHs account for on average ∼1.7% of the overall absorption of methanol-soluble BrC, about 5 times higher than their mass fraction in total organic carbon (OC, ∼0.35%). The fractional solar absorption by BrC relative to element carbon (EC) in the ultraviolet range (300−400 nm) is significant during winter (42 ± 18% for water-soluble BrC and 76 ± 29% for methanol-soluble BrC), which may greatly affect the radiative balance and tropospheric photochemistry and therefore the climate and air quality.

INTRODUCTION

Carbonaceous aerosol, including organic carbon (OC) and black carbon (BC), constitutes a large fraction of atmospheric aerosol

Received: May 4, 2018
Accepted: May 25, 2018
Published: May 25, 2018

DOI: 10.1021/acs.est.8b02386
Environ. Sci. Technol. 2018, 52, 6825−6833

and influences Earth's climate directly by absorbing and scattering radiation. The importance of BC has been well documented over the past decades because of its strong light absorption coefficient.[1−4] However, only in recent years has the role of brown carbon (BrC) been recognized.[5−16] BrC is a group of light absorbing organic compounds with absorption increasing sharply from the visible (Vis) to ultraviolet (UV) range. Although the mass absorption efficiency of BrC is lower than that of BC, its contribution to the UV absorption of carbonaceous aerosol is potentially significant due to the much higher abundance of OC compared to BC in continental aerosol. In addition to the direct effect on solar radiation, BrC immersed in cloud droplets absorbs light and might facilitate water evaporation and cloud dispersion, which is an additional indirect effect that counteracts the cooling effect of cloud droplet nucleation by aerosol.[17]

The sources of BrC are not well characterized so far. Emissions from incomplete and smoldering combustion of biomass, including forest fires, burning of wood and agricultural waste, are known to be a main source of BrC.[18−22] Coal combustion is also recognized to be the source of BrC, particularly in areas with residential coal combustion.[23−25] BrC can also be produced from atmospheric processes other than direct combustion emissions. As summarized in a recent review paper,[15] "secondary BrC" can be formed from atmospheric multiphase reactions between the gas-phase, particle-phase, and cloud droplet constituents. The difference in BrC emission sources together with the formation of secondary BrC result in the complexity in BrC chemical composition and absorption properties. Additional complications stem from the dynamic evolution of BrC in its physicochemical properties as a consequence of atmospheric aging, which can either enhance or reduce light absorption by BrC.[26−29] It is therefore a challenging task to investigate the effect of the dynamically evolving BrC composition on its absorption properties.

Measurements of BrC absorption properties can be realized by spectrophotometric analysis of aerosol extracts. As solution extracts of aerosol do not contain BC or mineral dust, the light absorption of BrC contained in these extracts can be measured without interference of BC or mineral dust.[30] Spectrophotometric analysis of solution extracts can also provide highly spectrally resolved data over a wide wavelength range. Further, chemical analysis of individual chromophores in the solution extracts and their correlation with spectrophotometric measurements can provide a better understanding of the effects of BrC molecular composition and chemistry on its optical properties. Such correlation studies are still in their early stages but are of importance because recent evidence shows that the overall absorption properties of some BrC compounds may be determined by the very minor presence of highly absorbing chromophores with unique molecular structures and precursor-specific chemistry in their formation and evolution.[15,31]

Model studies show elevated BrC annual burden in the areas with large biomass burning activities, such as in Africa, India, and China.[32,33] High concentrations of BrC in China may greatly influence the visibility, air quality, climate, and the tropospheric photochemistry. However, BrC related studies are still very scarce in China, with very limited studies focusing on the light absorption properties in megacities, for example, Beijing.[34−36] Here, we extended the BrC studies to Xi'an, a megacity in northwest China experiencing severe particulate air pollution, especially in the wintertime domestic heating season due to enhanced biomass burning activities. The objectives of this study were to investigate (1) the concentrations and seasonal variations of BrC in urban Xi'an; (2) the correlation of BrC absorption with individual chromophores; and (3) the fractional solar absorption by BrC relative to EC.

EXPERIMENTAL SECTION

Ambient Sample Collection. 24-h integrated $PM_{2.5}$ samples were collected every 6 days on prebaked (780 °C, 3 h) quartz-fiber filters (8 × 10 in., Whatman, QM-A) using a Hi-Vol $PM_{2.5}$ air sampler (Tisch, Cleveland, OH) at a flow rate of 1.05 m^3 min^{-1} from 5 July 2008 to 27 June 2009. After collection, the filter samples were immediately wrapped in baked aluminum foils and stored in a freezer (below −10 °C) until analysis. The sampling site was located on the rooftop of the Institute of Earth and Environment (~10 m above the ground), Chinese Academy of Sciences (IEECAS), which was surrounded by residential, commercial and traffic area (see Supporting Information (SI) Figure S1).The seasonal division was made according to the meteorological characteristics, that is, the period from 15 November to 14 March was designated as winter, from 15 March to 31 May as spring, from 1 June to 31 August as summer and from 1 September to 14 November as Fall.[37] SI Figure S2 show the seasonal frequency distribution of wind speed and wind direction.

Filter Extraction and Absorption Spectra Analysis. A portion of filter (0.526 cm^2 punch) taken from each sample was sonicated for 1 h in 10 mL of ultrapure water (>18.2 MΩ) or methanol (J. T. Baker, HPLC grade). The extracts were then filtered with a 0.45 μm PTFE pore syringe filter to remove insoluble material. The extraction efficiencies were tested by analyzing the absorption (365 nm) of the second extracts of the same filters and the OC remained on the filter after the first extraction (see SI and Figure S3). Absorption spectra of the extracts (water or methanol) were measured using a Liquid Waveguide Capillary Cell (LWCC-3100, World Precision Instrument) equipped with a UV−vis spectrophotometer (300−700 nm), following the method established by Hecobian et al. (2010).[8] The extracts were diluted to the range where the Beer−Lambert law is valid before absorption spectra measurements. The spectra recorded were corrected for the filter blanks. The absorption data were converted to the absorption coefficient following eq 1

$$\mathrm{Abs}_\lambda = (A_\lambda - A_{700}) \frac{V_l}{V_a \times l} \times \ln(10) \quad (1)$$

where Abs_λ (Mm^{-1}) represents the absorption coefficient of filter extracts at wavelength of λ. A_λ (arbitrary unit) is the absorbance recorded. V_l (in mL) corresponds to the volume of solvent (water or methanol) used to extract the filter sample, and V_a (in m^3) is the volume of the air sampled through the filter punch. The optical length (l) of LWCC used here is 0.94 m and ln(10) converts the log base-10 (recorded by UV−vis spectrophotometer) to natural logarithm to provide base-e absorption coefficient. To account for baseline shift that may occur during analysis, absorption at all wavelengths below 700 nm are referenced to that of 700 nm where there is no absorption for ambient aerosol extracts. The average absorption coefficient between 360 and 370 nm (Abs_{365}) is used to represent BrC absorption in order to avoid interferences from nonorganic compounds (e.g., nitrate) and to maintain consistence with previous reported results.

The mass absorption efficiency (MAE) of the filter extract at wavelength of λ can be described as

$$\mathrm{MAE}_\lambda = \frac{\mathrm{Abs}_\lambda}{M} \quad (2)$$

where M (μgC m^{-3}) is the water-soluble organic carbon (WSOC) concentration for water extracts or methanol-soluble organic

DOI: 10.1021/acs.est.8b02386
Environ. Sci. Technol. 2018, 52, 6825−6833

carbon (MSOC) concentration for methanol extracts. Note that for methanol extracts the use of an organic solvent prohibits determining carbon mass and therefore the OC concentration measured by the thermal/optical carbon analyzer is used assuming OC is completely extracted by methanol. This assumption may lead to underestimate of the MAE of methanol extracted BrC, although previous studies show high OC extraction efficiencies by methanol (e.g., ~95% for biomass burning OC and ~85% for ambient OC in Beijing).[36,38]

The wavelength dependence for light absorption by chromophores in solution can be characterized by a power law equation:

$$\mathrm{Abs}_{\lambda} = K \cdot \lambda^{-\mathrm{AAE}} \quad (3)$$

where K is a constant related to chromophores concentration and AAE is termed the absorption Ångström exponent, which depends on the types of the chromophores in solution. The AAE of filter extracts is calculated by a linear regression of log Abs_{λ} versus log λ in the wavelength range of 330−550 nm. This range is chosen to (1) avoid interferences from nonorganic compounds at lower wavelength; (2) ensure sufficient signal-noise ratio for the investigate samples.

Chemical Analysis. OC and EC were measured by a DRI Model 2001 thermal/optical carbon analyzer following the IMPROVE-A temperature protocol. More details were described in previous studies.[39,40] WSOC concentration was determined by a TOC/TN analyzer (TOC−L, Shimadzu, Japan) and details were described elsewhere.[41] The concentrations of levoglucosan and water-soluble inorganic ions (NH_4^+, SO_4^{2-}, NO_3^-, Cl^-, Na^+, K^+, Ca^{2+}, Mg^{2+}) were determined with ion chromatography following procedures described by Zhang et al.[37] The concentrations of particulate polycyclic aromatic hydrocarbons (PAHs) and their oxygenated (OPAHs) and nitro derivatives, including 27 parent-PAHs, 15 carbonyl-OPAHs, 8 hydroxyl- and carboxyl-OPAHs, and 9 nitro-PAHs, were analyzed with a gas chromatography−mass spectrometer (GC−MS) following methods described by Wang et al.[42]

Direct Solar Absorption of Brown Carbon Relative to Element Carbon. The measurement of EC light absorption coefficient by thermal/optical carbon analyzer is similar to the determination of BC light absorption by Aethalometer, which measure the light attenuation through a particle-loaded and a particle-free reference quartz filter. Intercomparison between attenuation coefficient derived by the carbon analyzer and Aethalometer showed good agreement, indicating the equivalence of light absorption measurement by the two analytical methods.[43] The artifacts associated with the filter-based measurement of EC absorption coefficient were corrected following the method of Ram and Sarin[43] (see SI for more details). The direct solar absorption of brown carbon relative to EC was estimated by the approach similar to Kirchstetter and Thatcher[44] and Kirillova et al.[45] Briefly, light absorption by absorbing species x (BrC or EC herein) follows the Beer−Lambert's law as

$$\frac{I_0 - I}{I_0}(\lambda) = 1 - e^{-b_{\mathrm{ap},x,\lambda} \cdot h_{\mathrm{ABL}}} \quad (4)$$

where h_{ABL} corresponds to the boundary layer height (assuming 1000 m), $b_{\mathrm{ap},x,\lambda}$ for EC denotes the absorption coefficient derived from the thermal/optical carbon analysis described above, and for BrC $b_{\mathrm{ap},x,\lambda}$ represents the absorption coefficient of particulate BrC. Previous studies reported that the light absorption coefficient of particulate BrC is about 0.7−2.0 times that of BrC aerosol extract.[46,47] Here, a conversion factor of 1 is applied and the uncertainties are estimated. Then, the fraction of solar radiation absorbed by water- or methanol-soluble BrC aerosol relative to EC is given by

$$f = \frac{\int I_0(\lambda)\{1 - e^{-b_{ap,\,\mathrm{BrC(water/methanol)},\lambda} \cdot h_{ABL}}\}\mathrm{d}\lambda}{\int I_0(\lambda)\{1 - e^{-b_{ap,\mathrm{EC},\lambda} \cdot h_{ABL}}\}\mathrm{d}\lambda} \quad (5)$$

where $I_0(\lambda)$ is the clear sky Air Mass 1 Global Horizontal solar irradiance.[48] The fraction f is obtained by numerical integration of the above formula in the wavelength range of 300−2500 nm, 300−700 nm and 300−400 nm for each sample, respectively. This approximate estimation is based on the following assumptions (1) the ground measurement results represent the whole atmospheric boundary layer; (2) the light absorption coefficient of BrC aerosol extract is equal to that of particulate BrC.

RESULTS AND DISCUSSION

Light Absorption Properties of Soluble BrC. Figure 1 shows the seasonal average absorption spectra of WSOC and MSOC at the wavelengths between 300 and 700 nm, which exhibit the common characteristic of BrC with sharply increasing absorbance toward shorter wavelength and is obviously different from the absorption properties of BC which are only weakly wavelength dependent with an AAE close to 1. The seasonal average AAE of WSOC varies slightly between 5.7 and 6.1 with mean values of 5.9, within the range of previous studies in, for example, the New Delhi, Beijing and outflow from northern China.[35,45,49] The AAE of MSOC (6.0 ± 0.2) is comparable with that of WSOC, consistent with a previous study in urban Beijing during winter.[36] This feature is different from measurements in the Los Angeles Basin and the North American continental troposphere where the AAE values of MSOC are lower compared to AAE values of WSOC.[13,50] The difference in AAE between China and North America might reflect the difference in emission sources and atmospheric processes which determine the composition of BrC chromophores. Another evident feature of BrC absorption spectra shown in Figure 1 is that absorption coefficient of MSOC is always greater than that of WSOC across all measurement wavelengths, which is consistent with previous studies. This can be attributed to the difference in type and amount of chromophores extracted, i.e., more chromophores are extracted in methanol (e.g., PAHs from biomass burning and fossil fuel combustion) but not in water.[38,50] It should be noted that the change of pH from particles to water extracts may affect BrC absorption, as Phillips et al.[51] showed that the BrC absorption increases by 10% per pH unit from pH 2−12. We calculated the particle pH value of the NH_4^+-SO_4^{2-}-NO_3^--Cl^--Na^+-K^+-Ca^{2+}-Mg^{2+} system using the thermodynamic model ISORROPIA-II which was run in "forward" mode.[52] Our results show that the average particle pH during the entire measurement period was 5.97, similar to previous studies in Xi'an.[53] Therefore, the pH change from particle to water extracts is likely less than 1 pH unit and the effect on BrC absorption is less than 10%.

Figure 2a and b show the time series of absorption coefficient of WSOC and MSOC at 365 nm (i.e., $\mathrm{Abs}_{365,\mathrm{WSOC}}$ and $\mathrm{Abs}_{365,\mathrm{MSOC}}$) as well as the concentrations of WSOC, OC, levoglucosan, parent-PAHs and carbonyl-OPAHs. They all show clear seasonal variations with enhanced values in winter. The seasonal averages for all measured parameters peak in winter, decreasing in fall and spring and reaching the minimum in summer (see SI Table S1). It should be noted that $\mathrm{Abs}_{365,\mathrm{MSOC}}$ is approximately two times (1.7−2.1) higher than $\mathrm{Abs}_{365,\mathrm{WSOC}}$ in all seasons, indicating that MSOC provides a better estimation of BrC than WSOC. Figure 2c shows

DOI: 10.1021/acs.est.8b02386
Environ. Sci. Technol. 2018, 52, 6825−6833

Environmental Science & Technology Article

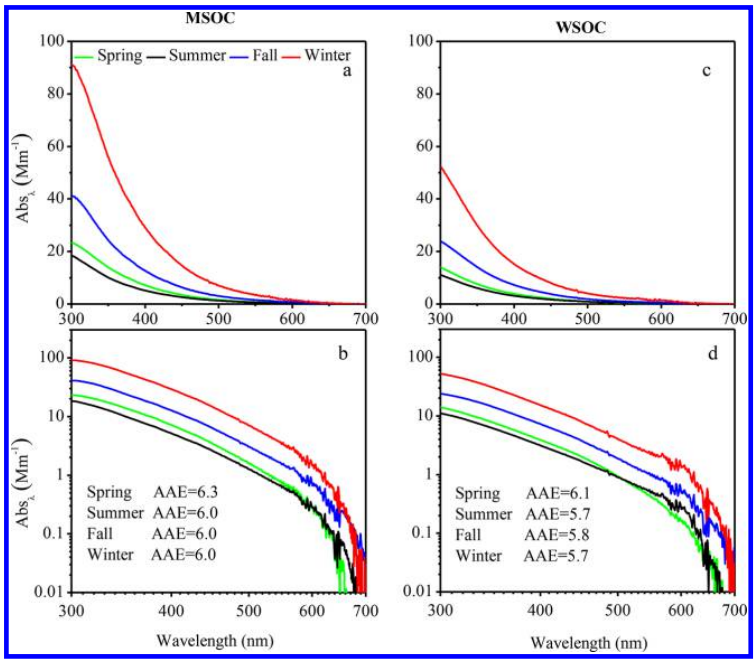

Figure 1. Seasonal average absorption spectra of MSOC (a and b) and WSOC (c and d) plotted on a linear (top) and logarithmic (bottom) scale. AAE is determined by a linear regression of $\log(\mathrm{Abs}_\lambda)$ versus $\log(\lambda)$ in the wavelength range of 330−550 nm.

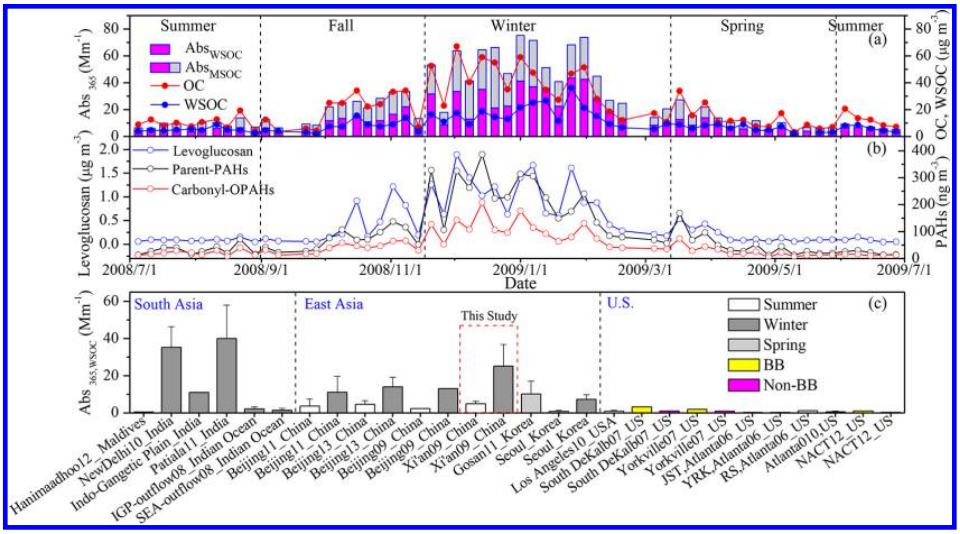

Figure 2. Time series of the light absorption coefficient of WSOC and MSOC at 365 nm ($\mathrm{Abs}_{365,WSOC}$ and $\mathrm{Abs}_{365,\ MSOC}$, respectively) as well as OC, WSOC (a) and levoglucosan, parent-PAHs, carbonyl-OPAHs concentrations (b) and comparison of $\mathrm{Abs}_{365,WSOC}$ in South Asia, East Asia, and the United States (c).

the comparison with previous studies in East Asia, South Asia, and the U.S. Note that $\mathrm{Abs}_{365,MSOC}$ was not measured in most previous studies and therefore only $\mathrm{Abs}_{365,WSOC}$ values are compared here. It can be seen from the figure that $\mathrm{Abs}_{365,WSOC}$ in the urban regions of South Asia and East Asia is much higher than that in the U.S., indicating the large difference in the composition and concentration of chromophores. The wintertime $\mathrm{Abs}_{365,WSOC}$ is significantly higher than the summertime $\mathrm{Abs}_{365,WSOC}$ in China ($P < 0.001$), which could be attributed to the enhanced emissions of BrC from residential heating in winter.

Figure 3a and b show the correlation between $\mathrm{Abs}_{365,WSOC}$ and WSOC and between $\mathrm{Abs}_{365,MSOC}$ and OC, respectively. The slopes represent the seasonal average of mass absorption efficiency at the wavelength of 365 nm (MAE_{365}), which follows the descending order of winter > fall > spring > summer for both WSOC and MSOC (see also SI Table S1). The seasonal difference in $\mathrm{MAE}_{365,WSOC}$ and $\mathrm{MAE}_{365,MSOC}$ indicates the seasonal difference

DOI: 10.1021/acs.est.8b02386
Environ. Sci. Technol. 2018, 52, 6825−6833

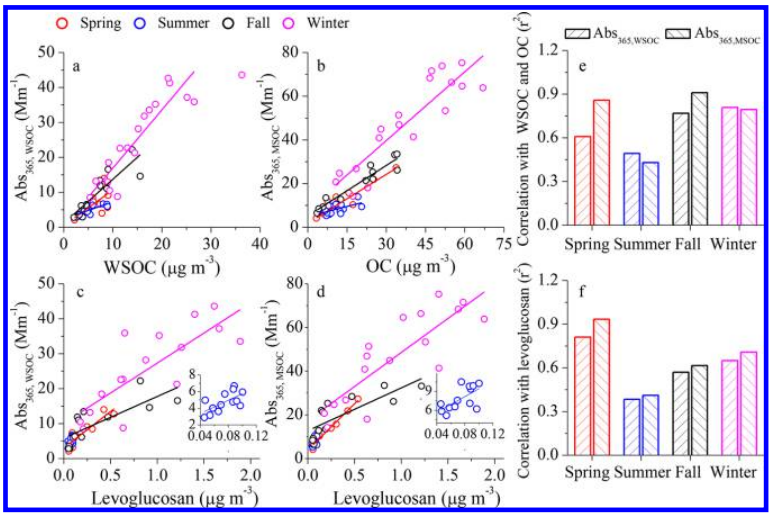

Figure 3. Scatter plots of $Abs_{365,WSOC}$ and $Abs_{365,MSOC}$ against WSOC and OC (a and b) and levoglucosan concentrations (c and d) and the corresponding linear correlation coefficients (e and f).

in the chemical composition and sources of BrC, the latter is further supported by the seasonal difference in correlation coefficient (r^2) of the linear regression. For example, a high correlation was observed in winter for both WSOC (r^2=0.81) and MSOC (r^2 = 0.79), which is consistent with the high correlation between $Abs_{365,WSOC}$ and levoglucosan (r^2 = 0.65) and between $Abs_{365,MSOC}$ and levoglucosan (r^2 = 0.71) in winter (Figure 3c and d), indicating that biomass burning emissions are the major source contributing to the absorption of BrC at Xi'an in winter (Biomass burning was found to be the dominant source of organic aerosol in Xi'an during winter[37,54]). Furthermore, the MAE values (average of 1.65 for WSOC and 1.33 for MSOC) in winter are within the range of MAE of biomass burning ((e.g., 1.3−1.8 for corn stalk,[55] 1.37 for rice straw,[56] ∼ 1.9 for BB smoke particles[57]), which further supports that biomass burning is the major BrC source in winter in Xi'an. In contrast to the wintertime case, a lower correlation was observed in summer for both WSOC (r^2 = 0.49) and MSOC (r^2 = 0.31) because more WSOC and MSOC in summer are derived from secondary organic aerosol (SOA) and many low molecular weight SOA compounds are colorless. The diversity in the sources of BrC in different seasons is further supported by the descending order of spring > winter > fall > summer for the correlation coefficient between $Abs_{365,WSOC}$ and levoglucosan and between $Abs_{365,MSOC}$ and levoglucosan (Figure 3c and d), and by the smaller correlation coefficient (except spring) between $Abs_{365,WSOC}$ and levoglucosan and between $Abs_{365,MSOC}$ and levoglucosan when compared to the corresponding correlation coefficient between $Abs_{365,WSOC}$ and WSOC and between $Abs_{365,MSOC}$ and OC. In other words, there existed other sources contributing to BrC in Xi'an in all seasons, particularly in summer (e.g., secondary BrC). Note that the high correlation suggests similar sources and lifetimes in the atmosphere and are not likely to be driven by changes in the boundary layer mixing volumes which are more like to promote changes in absolute concentration by a factor of ∼2 as we observed in Xi'an between winter and summer (The boundary layer heights were 600−700 m in winter and 1300−1500 m in summer, respectively[58]).

PAHs: An Efficient BrC Chromophore. PAHs are ubiquitous in atmospheric particles from incomplete combustion of biomass and coal. Data available in the literature show that some PAHs, due to the large conjugated polycyclic structure, are strongly light-absorbing compounds at near-UV wavelength range (i.e., 300−400 nm, also see SI Figure S4) and therefore have been suggested to be important BrC chromophores.[47,59,60] In order to understand the potential contribution of PAHs to BrC absorption, the relationships between light absorption of BrC and the concentrations of parent-PAHs and carbonyl-OPAHs are examined. Scatter plots of parent-PAHs and carbonyl−OPAHs against $Abs_{365,WSOC}$ and $Abs_{365,MSOC}$ are shown in Figure 4. In general, parent-PAHs and carbonyl-OPAHs are correlated well with $Abs_{365,MSOC}$ in all seasons (r^2 > 0.61). This result indicates that a significant part of BrC comes from a similar source as PAHs (i.e., incomplete combustion of biofuel or fossil fuel), or that PAHs are a significant fraction of BrC chromophores. Correlations of $Abs_{365,WSOC}$ with parent-PAHs and carbonyl-OPAHs are lower compared to corresponding correlations with $Abs_{365,MSOC}$ in all seasons. This is reasonable because parent-PAHs and carbonyl-OPAHs are organic solvent extractable (e.g., methanol) but mostly insoluble in water. Therefore, they contribute to methanol-soluble but not to water-soluble BrC absorption. The moderate correlation coefficient of $Abs_{365,WSOC}$ with parent-PAHs and carbonyl-OPAHs may be ascribed to the water-soluble chromophores that coemitted with parent-PAHs and carbonyl-OPAHs from sources such as biomass burning and coal combustion. Again the extremely low correlations between $Abs_{365,WSOC}$ and parent-PAHs and carbonyl-OPAHs in summer indicate that extra sources, not associated with PAHs (e.g., SOA), contribute to the light absorption of WSOC.

The potential contribution of PAHs to the bulk light absorption of BrC (300−700 nm) in ambient air is estimated following a method modified from Samburova et al.[60] who estimated the contribution of PAHs to BrC light absorption in biomass burning source emission. Here, the contribution was calculated based on two parameters: ambient mass concentrations of individual PAHs and its solar-spectrum-weighed light absorption efficiency−MAE_{PAH_av}. The latter was obtained by multiplying MAE of individual PAHs with the power distribution of the solar spectrum and spectrally integrated (see SI and Figure S5).[56] SI Table S2 summarizes the MAE_{PAH_av} of individual parent-PAHs and carbonyl-OPAHs studied here. The PAHs with

DOI: 10.1021/acs.est.8b02386
Environ. Sci. Technol. 2018, 52, 6825−6833

Environmental Science & Technology Article

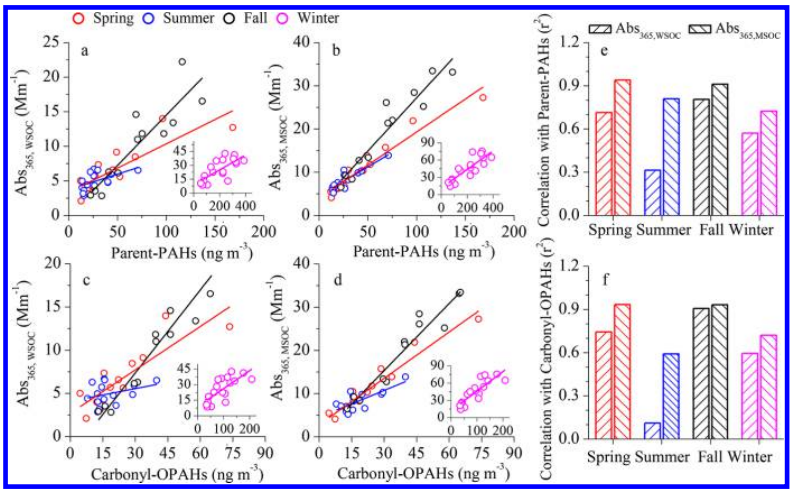

Figure 4. Scatter plots of $Abs_{365,WSOC}$ and $Abs_{365,MSOC}$ versus concentrations of parent-PAHs (a and b) and carbonyl-OPAHs (c and d) and the corresponding linear correlation coefficients (e and f).

Table 1. Annual Mean Contributions of Main BrC_PAHs Species to Methanol Extracted BrC Light Absorption

compounds	r^2 (conc.Vs $Abs_{365,MSOC}$)	MAE_{PAH_av} [a] ($m^2\ g^{-1}$)	concentration (ng m^{-3})	contribution to BrC light absorption (%)
indeno[1,2,3-cd]pyrene	0.804	1.0711	6.17	0.272
benzo[b+j+k]fluoranthenes	0.862	0.3475	18.04	0.244
benzo[a]pyrene	0.807	0.7709	8.6	0.241
benzo[e]pyrene	0.863	0.7709	7.94	0.240
pyrene	0.849	0.3530	7.97	0.082
perylene	0.787	1.7942	1.09	0.074
coronene	0.777	0.2774	6.93	0.073
benzo[ghi]perylene	0.759	0.1821	6.64	0.052
retene	0.736	0.1969	10.12	0.044
benzo[a]anthracene	0.786	0.2842	4.81	0.041
fluoranthene	0.867	0.2834	3.52	0.028
dibenzo[a,h]anthracene	0.840	0.2842	1.33	0.015
chrysene	0.887	0.0883	4.99	0.014
anthracene	0.788	0.2801	0.65	0.006
7H-Benz[d,e]anthracene-7-one	0.796	0.4385	9.01	0.138
5,12-naphthacenedione	0.773	0.3069	2.76	0.026
9,10-anthracenedione	0.864	0.1033	5.26	0.015
9-fluorenone	0.847	0.0920	1.79	0.083
total				1.688

[a] MAE_{PAH_av} of individual PAH is obtained by multiplying MAE of individual PAHs with the power distribution of the solar spectrum and spectrally integrated (see Supporting Information).

MAE_{PAH_av} > 0.1 $m^2\ g^{-1}$ are named BrC_PAHs, which have strong light absorption properties in the blue and near-UV spectral region. Individual BrC_PAHs shows good correlation with $Abs_{365,MSOC}$ (r^2 > 0.73, see Table 1), indicating further that these PAHs are likely a significant fraction of BrC chromophores. The contributions of individual BrC_PAHs to the BrC bulk light absorption (300−700 nm) are estimated by dividing solar-spectrum-weighed absorption coefficient of MSOC by that of BrC_PAHs ($MAE_{PAH,av}$ × PAH concentration). The overall annual average contribution of all BrC_PAHs listed in Table 1 to the BrC bulk light absorption is about 1.7%. This contribution is about 5 times of their mass contribution to organic carbon (~0.35%), indicating that even small amounts of light-absorbing compounds can have a disproportionately high impact on the light absorption properties of BrC. Besides PAHs, a few compounds have been identified as BrC chromophore. Laboratory study showed that N-heterocyclic PAHs (N-PAHs) with 4−6 aromatic rings emitted from biomass burning are likely important BrC chromophores but they absorb more solar radiation in the visible wavelength range (400−500 nm) than their corresponding PAHs.[61] Mohr et al.[62] quantified five nitrated phenol compounds which accounted for ~4% of BrC light absorption at 370 nm in ambient air in Detling, United Kingdom. Zhang et al.[50] identified eight nitro-aromatic compounds in aerosol extracts in Los Angeles Basin, which contributed to ~4% of water-soluble BrC light absorption at 365 nm. Teich et al.[63] determined eight nitrated aromatic compounds in aerosol samples collected in Germany and China. The mean contribution of these nitrated aromatic compounds to water-soluble BrC light absorption at 370 nm ranged from 0.1 to 1.3% under acidic condition and from 0.1 to 3.7% under alkaline condition. However, in cloudwater samples heavily affected by biomass burning collected at Mount Tai,

DOI: 10.1021/acs.est.8b02386
Environ. Sci. Technol. 2018, 52, 6825−6833

Table 2. Average Direct Solar Absorbance of BrC Relative to EC during Summer and Winter

	WSOC/EC			MSOC/EC		
	$f_{300-2500}$ nm (%)	$f_{300-700}$ nm (%)	$f_{300-400}$ nm (%)	$f_{300-2500}$ nm (%)	$f_{300-700}$ nm (%)	$f_{300-400}$ nm (%)
summer	2 ± 1	3 ± 1	9 ± 3	4 ± 1	5 ± 1	15 ± 3
winter	10 ± 4	15 ± 6	42 ± 18	18 ± 7	26 ± 10	76 ± 29

Desyaterik et al.[64] identified 16 major light-absorbing compounds (mainly nitrophenols and aromatic carbonyls compounds), which contributed to ~50% of BrC light absorption between 300 and 400 nm. In general, a large fraction of BrC chromophores are still not identified so far. More studies are therefore necessary to better understand the link between BrC light absorption properties and the chemical composition.

Direct Solar Absorption of Brown Carbon Relative to Element Carbon. The importance of BrC optical properties is evaluated by calculating the fractional solar absorption by BrC relative to EC following eq 5 and the results are shown in Table 2. In the whole range of solar spectrum (300−2500 nm), the amount of solar radiation absorbed by WSOC relative to EC is only 2 ± 1% and 10 ± 4% in summer and winter, respectively, which are similar to previous studies in Beijing (6 ± 3% in summer and 11 ± 3% in winter),[35] New Delhi (6 ± 3% in winter)[45] and Gosan, Korea (6 ± 2 in winter).[49] MOSC shows slightly higher contribution (i.e., 3 ± 1% in summer and 18 ± 7% in winter). However, when considering the UV range (300−400 nm) only, the fractional solar absorption by WSOC relative to EC increases to 9 ± 3% in summer and to 42 ± 18% in winter. The contribution from MSOC increases further to 15 ± 3% in summer and to 76 ± 29% in winter. It should be noted that these calculated results provide an approximate estimate of the relative climate effect of BrC relative to EC, which may be affected by the uncertainties associated with the assumptions (i.e., AAE of EC (AAE_{EC}) is set to 1 and the light absorption coefficient of particulate BrC is equal to that of BrC aerosol extract). When the upper limit value of AAE_{EC} (1.4) is applied, the fractional solar absorption by BrC relative to EC in the UV range is still significant (38 ± 16% for WSOC and 68 ± 26% for MSOC during winter) (see SI Table S3). Likewise, direct solar absorption of BrC relative to EC is significant when the conversion factor of light absorption coefficient between BrC aerosol extract and particulate BrC varies from 0.7 to 2.0 (see SI Table S4), although this estimate has its limitations derived from the simplifying assumptions, for example, the light absorption of aerosol extracts may not be directly translated into the absorption of ambient aerosol considering the size distribution of aerosol, the effects of internal mixing and the changes in absorption caused by dissolving the chromophores into methanol or water. Note that although a constant boundary layer height of 1000 m was used for the calculation, uncertainty analysis indicates that the change of boundary layer height from 500 to 1500 m has a minor effect on the results (<2%). These results indicate that although EC is the main light-absorbing carbonaceous species in the atmosphere, the effect of BrC should not be ignored, especially in the lower wavelength (i.e., below 400 nm) during winter season. In general, the strong absorption of solar radiation by BrC in the UV range may significantly affect the radiative balance and therefore the tropospheric photochemistry. For example, Jo et al.[65] estimated that the inclusion of BrC absorption (traditional scattering only) can lead to the decrease of annual NO_2 photolysis rate by up to ~8% in surface air over Asia and therefore 6% reduction of annual mean surface O_3 concentration. Hammer et al.[66] examined the effects of BrC absorption on the tropospheric OH photochemistry and found that OH concentrations decreased by ~5% over China in April 2007 due to BrC absorption. Therefore, future climate and air quality model should consider the effect of BrC absorption.

Despite the uncertainties derived from assumptions discussed above, our results show the significance of the direct solar absorption of BrC relative to EC. Understanding the BrC sources, molecular composition and chemistry as well as the links with optical properties are critical for better quantifying the implications of BrC, but is still in its early stages as discussed in a recent review paper.[15] Similar to nitrated phenols, nitrated aromatics,[50,62,63] the PAHs and carbonyl-OPAHs quantified here also only explain a small fraction of BrC light absorption but their concentrations are strongly correlated with MSOC absorption. Future studies of BrC chemical characterization should target the speciation of compounds coemitted with PAHs or the identification of common features (e.g., functional groups) and proxy compounds.

■ ASSOCIATED CONTENT

Supporting Information

The Supporting Information is available free of charge on the ACS Publications website at DOI: 10.1021/acs.est.8b02386.

Tables S1−S4 and Figures S1−S5 with addition experimental procedures and results as described in the text (PDF)

■ AUTHOR INFORMATION

Corresponding Author

*E-mail: rujin.huang@ieecas.cn.

ORCID

Chunshui Lin: 0000-0003-3175-6778

Notes

The authors declare no competing financial interest.

■ ACKNOWLEDGMENTS

This work was supported by the National Natural Science Foundation of China (NSFC) under Grant No. 91644219, No. 41673134, and No. 41650110488. We also acknowledge the grant KNAW (No. 530-5CDP30) from The Netherlands.

■ REFERENCES

(1) Jacobson, M. Z. Strong radiative heating due to the mixing state of black carbon in atmospheric aerosols. *Nature* **2001**, *409*, 695−697.

(2) Menon, S.; Hansen, J.; Nazarenko, L.; Luo, Y. F. Climate effects of black carbon aerosols in China and India. *Science* **2002**, *297*, 2250−2253.

(3) Derimian, Y.; Karnieli, A.; Kaufman, Y. J.; Andreae, M. O.; Andreae, T. W.; Dubovik, O.; Maenhut, W.; Koren, I. The role of iron and bclack carbon in aerosol light absorption. *Atmos. Chem. Phys.* **2008**, *8*, 3623−3637.

(4) Bond, T. C.; Doherty, S. J.; Fahey, D. W.; Forster, P. M.; Berntsen, T.; DeAngelo, B. J.; Flanner, M. G.; Ghan, S.; Kärcher, B.; Koch, D.; Kinne, S.; Kondo, Y.; Quinn, P. K.; et al. Bounding the role of black carbon in the climate system: A scientific assessment. *J. Geophys. Res.* **2013**, *118*, 5380−5552.

DOI: 10.1021/acs.est.8b02386
Environ. Sci. Technol. 2018, 52, 6825−6833

(5) Andreae, M. O.; Gelencser, A. Black carbon or brown carbon? The nature of light-absorbing carbonaceous aerosols. *Atmos. Chem. Phys.* **2006**, *6*, 3131−3148.
(6) Lukács, H.; Gelencser, A.; Hammer, S.; Puxbaum, H.; Pio, C.; Legrand, M.; Kasper- Giebl, A.; Handler, M.; Limbeck, A.; Simpson, D.; Preunkert, S. Seasonal trends and possible sources of brown carbon based on 2-year aerosol measurements at six sites in Europe. *J. Geophys. Res.* **2007**, *112*, D23S18.
(7) Alexander, D. T. L.; Crozier, P. A.; Anderson, J. R. Brown carbon spheres in East Asian outflow and their optical properties. *Science* **2008**, *321*, 833−836.
(8) Hecobian, A.; Zhang, X.; Zheng, M.; Frank, N. H.; Edgerton, E. S.; Weber, R. J. Water-soluble organic aerosol material and the light absorption characteristics of aqueous extracts measured over the Southeastern United States. *Atmos. Chem. Phys.* **2010**, *10*, 5965−5977.
(9) Lack, D. A.; Cappa, C. D. Impact of brown and clear carbon on light absorption enhancement, single scatter albedo and absorption wavelength dependence of black carbon. *Atmos. Chem. Phys.* **2010**, *10*, 4207−4220.
(10) Park, R. J.; Kim, M. J.; Jeong, J. I.; Yooun, D.; Kim, S. A contribution of brown carbon aerosol to the aerosol light absorption and its radiative forcing in East Asia. *Atmos. Environ.* **2010**, *44*, 1414−1421.
(11) Bahadur, R.; Praveen, P. S.; Xu, Y.; Ramanathan, V. Solar absorption by elemental and brown carbon determined from spectral observations. *Proc. Natl. Acad. Sci. U. S. A.* **2012**, *109*, 17366−17371.
(12) IPCC. *Fifth Assessment Report: Climate Change 2013*; Cambridge University Press: New York, 2013.
(13) Liu, J.; Scheuer, E.; Dibb, J.; Diskin, G. S.; Ziemba, L. D.; Thornhill, K. L.; Anderson, B. E.; Wisthaler, A.; Mikoviny, T.; Devi, J. J.; et al. Brown carbon aerosol in the North American continental troposphere: Sources, abundance, and radiative forcing. *Atmos. Chem. Phys.* **2015**, *15*, 7841−7858.
(14) Washenfelder, R. A.; Attwood, A. R.; Brock, C. A.; Guo, H.; Xu, L.; Weber, R. J.; Ng, N. L.; Allen, H. M.; Ayres, B. R.; Baumann, K.; et al. Biomass burning dominates brown carbon absorption in the rural southeastern United States. *Geophys. Res. Lett.* **2015**, *42*, 653−664.
(15) Laskin, A.; Laskin, J.; Nizkorodov, S. A. Chemistry of atmospheric brown carbon. *Chem. Rev.* **2015**, *115*, 4335−4382.
(16) Costabile, F.; Gilardoni, S.; Barnaba, F.; Di Ianni, A.; Di Liberto, L.; Dionisi, D.; Manigrasso, M.; Paglione, M.; Poluzzi, V.; Rinaldi, M.; Facchini, M. C.; Gobbi, G. P. Characteristics of brown carbon in the urban Po Valley atmosphere. *Atmos. Chem. Phys.* **2017**, *17*, 313−326.
(17) Hansen, J.; Sato, M.; Ruedy, R. J. *Geophys. Res.-Atmos* **1997**, *102*, 6831−6864.
(18) Chakrabarty, R. K.; Moosmuller, H.; Chen, L. W. A.; Lewis, K.; Arnott, W. P.; Mazzoleni, C.; Dubey, M. K.; Wold, C. E.; Hao, W. M.; Kreidenweis, S. M. Brown carbon in tar balls from smoldering biomass combustion. *Atmos. Chem. Phys.* **2010**, *10*, 6363−6370.
(19) Kirchstetter, T. W.; Thatcher, T. L. Contribution of organic carbon to wood smoke particulate matter absorption of solar radiation. *Atmos. Chem. Phys.* **2012**, *12*, 6067−6072.
(20) Lack, D. A.; Langridge, J. M.; Bahreini, R.; Cappa, C. D.; Middlebrook, A. M.; Schwarz, J. P. Brown carbon and internal mixing in biomass burning particles. *Proc. Natl. Acad. Sci. U. S. A.* **2012**, *109*, 14802−14807.
(21) Chakrabarty, R. K.; Pervez, S.; Chow, J. C.; Watson, J. G.; Dewangan, S.; Robles, J.; Tian, G. Funeral pyres in South Asia: brown carbon aerosol emissions and climate impacts. *Environ. Sci. Technol. Lett.* **2014**, *1*, 44−48.
(22) Chakrabarty, R. K.; Gyawali, M.; Yatavelli, R. L. N.; Pandey, A.; Watts, A. C.; Knue, J.; Chen, L.-W. A.; Pattison, R. R.; Tsibart, A.; Samburova, V.; Moosmüller, H. Brown carbon aerosols from burning of boreal peatlands: microphysical properties, emission factors, and implications for direct radiative forcing. *Atmos. Chem. Phys.* **2016**, *16*, 3033−3040.
(23) Bond, T. C.; Covert, D. S.; Kramlich, J. C.; Larson, T. V.; Charlson, R. J. Primary particle emissions from residential coal burning: Optical properties and size distributions. *J. Geophys. Res.* **2002**, *107* (D21), 8347.
(24) Yang, M.; Howell, S. G.; Zhuang, J.; Huebert, B. J. Attribution of aerosol light absorption to black carbon, brown carbon, and dust in China−interpretations of atmospheric measurements during EAST-AIRE. *Atmos. Chem. Phys.* **2009**, *9*, 2035−2050.
(25) Sun, J. Z.; Zhi, G. R.; Hitzenberger, R.; Chen, Y. J.; Tian, C. G.; Zhang, Y. Y.; Feng, Y. L.; Cheng, M.; Zhang, Y. Z.; Cai, J.; Chen, F.; Qiu, Y. Q.; Jiang, Z. M.; Li, J.; Zhang, G.; Mo, Y. Z. Emission factors and light absorption properties of brown carbon from household coal combustion in China. *Atmos. Chem. Phys.* **2017**, *17*, 4769−4780.
(26) Lambe, A. T.; Cappa, C. D.; Massoli, P.; Onasch, T. B.; Forestieri, S. D.; Martin, A. T.; Cummings, M. J.; Croasdale, D. R.; Brune, W. H.; Worsnop, D. R.; Davidovits, P. Relationship between oxidation Level and optical properties of secondary organic aerosol. *Environ. Sci. Technol.* **2013**, *47*, 6349−6357.
(27) Lee, H. J.; Aiona, P. K.; Laskin, A.; Laskin, J.; Nizkorodov, S. A. Effect of solar radiation on the optical properties and molecular composition of laboratory proxies of atmospheric brown carbon. *Environ. Sci. Technol.* **2014**, *48*, 10217−10226.
(28) Zhong, M.; Jang, M. Dynamic light absorption of biomassburning organic carbon photochemically aged under natural sunlight. *Atmos. Chem. Phys.* **2014**, *14*, 1517−1525.
(29) Updyke, K. M.; Nguyen, T. B.; Nizkorodov, S. A. Formation of brown carbon via reactions of ammonia with secondary organic aerosols from biogenic and anthropogenic precursors. *Atmos. Environ.* **2012**, *63*, 22−31.
(30) Lack, D. A.; Langridge, J. M. On the attribution of black and brown carbon light absorption using the Angstrom exponent. *Atmos. Chem. Phys.* **2013**, *13*, 10535−10543.
(31) Laskin, J.; Laskin, A.; Nizkorodov, S. A.; Roach, P.; Eckert, P.; Gilles, M. K.; Wang, B. B.; Lee, H. J.; Hu, Q. C. Molecular selectivity of brown carbon chromophores. *Environ. Sci. Technol.* **2014**, *48*, 12047−12055.
(32) Arola, A.; Schuster, G.; Myhre, G.; Kazadzis, S.; Dey, S.; Tripathi, S. N. Inferring absorbing organic carbon content from AERONET data. *Atmos. Chem. Phys.* **2011**, *11*, 215−225.
(33) Feng, Y.; Ramanathan, V.; Kotamarthi, V. R. Brown carbon: A significant atmospheric absorber of solar radiation? *Atmos. Chem. Phys.* **2013**, *13*, 8607−8621.
(34) Du, Z. Y.; He, K. B.; Cheng, Y.; Duan, F. K.; Ma, Y. L.; Liu, J. M.; Zhang, X. L.; Zheng, M.; Weber, R. J. A yearlong study of water-soluble organic carbon in Beijing II: light absorption properties. *Atmos. Environ.* **2014**, *89*, 235−241.
(35) Yan, C.; Zheng, M.; Sullivan, A. P.; Bosch, C.; Desyaterik, Y.; Andersson, A.; Li, X.; Guo, X.; Zhou, T.; Gustafsson, Ö.; Collett, J. L., Jr Chemical characteristics and light absorbing property of water-soluble organic carbon in Beijing: Biomass burning contributions. *Atmos. Environ.* **2015**, *121*, 4−12.
(36) Cheng, Y.; He, K. B.; Du, Z. Y.; Engling, G.; Liu, J. M.; Ma, Y. L.; Zheng, M.; Weber, R. J. The characteristics of brown carbon aerosol during winter in Beijing. *Atmos. Environ.* **2016**, *127*, 355−364.
(37) Zhang, T.; Cao, J. J.; Chow, J. C.; Shen, Z. X.; Ho, K. F.; HO, H. S. S.; Liu, S. X.; Han, Y. M.; Watson, J. G.; Wang, G. H.; Huang, R. J. Characterization and seasonal variations of levoglucosan in fine particulate matter in Xi'an. *J. Air Waste Manage. Assoc.* **2014**, *64*, 1317−1327.
(38) Chen, Y.; Bond, T. C. Light absorption by organic carbon from wood combustion. *Atmos. Chem. Phys.* **2010**, *10*, 1773−1787.
(39) Cao, J. J.; Wu, F.; Chow, J. C.; Lee, S. C.; Li, Y.; Chen, S. W.; An, Z. S.; Fung, K. K.; Watson, J. G.; Zhu, C. S.; Liu, S. X. Characterization and source apportionment of atmospheric organic and elemental carbon during fall and winter of 2003 in Xi'an, China. *Atmos. Chem. Phys.* **2005**, *5*, 3127−3137.
(40) Chow, J. C.; Watson, J. G.; Robles, J.; Wang, X. L.; Chen, L. W. A.; Trimble, D. L.; Kohl, S. D.; Tropp, R. J.; Fung, K. K. Quality assurance and quality control for thermal/optical analysis of aerosol samples for organic and elemental carbon. *Anal. Bioanal. Chem.* **2011**, *401*, 3141−3152.
(41) Ho, K. F.; Ho, S. S. H.; Huang, R. J.; Liu, S. X.; Cao, J. J.; Zhang, T.; Chuang, H. C.; Chan, C. S.; Hu, D.; Tian, L. Characteristics of water-

DOI: 10.1021/acs.est.8b02386
Environ. Sci. Technol. 2018, 52, 6825−6833

soluble organic nitrogen in fine particulate matter in the continental area of China. *Atmos. Environ.* **2015**, *106*, 252−261.
(42) Wang, J. Z.; Xu, H. M.; Guinot, B.; Li, L. J.; Ho, S. S. H.; Liu, S. X.; Li, X. P.; Cao, J. J. Concentrations, sources and health effects of parent, oxygenated- and nitrated- polycyclic aromatic hydrocarbons (PAHs) in middle-school air in Xi'an, China. *Atmos. Res.* **2017**, *192*, 1−10.
(43) Ram, K.; Sarin, M. M. Absorption coefficient and site-specific mass absorption efficiency of elemental carbon in aerosols over urban, rural, and high-altitude sites in India. *Environ. Sci. Technol.* **2009**, *43*, 8233−8239.
(44) Kirchstetter, T. W.; Thatcher, T. L. Contribution of organic carbon to wood smoke particulate matter absorption of solar radiation. *Atmos. Chem. Phys.* **2012**, *12*, 6067−6072.
(45) Kirillova, E. N.; Andersson, A.; Tiwari, S.; Srivastava, A. K.; Bisht, S. D.; Gustafsson, Ö. Water-soluble organic carbon aerosols during a full New Delhi winter: Isotope-based source apportionment and optical properties. *J. Geophys. Res. Atmos.* **2014**, *119*, 3476−3485.
(46) Liu, J.; Bergin, M.; Guo, H.; King, L.; Kotra, N.; Edgerton, E.; Weber, R. J. Size-resolved measurements of brown carbon in water and methanol extracts and estimates of their contribution to ambient fine particle light absorption. *Atmos. Chem. Phys.* **2013**, *13*, 12389−12404.
(47) Sun, H.; Biedermann, L.; Bond, T. C. Color of brown carbon: A model for ultraviolet and visible light absorption by organic carbon aerosol. *Geophys. Res. Lett.* **2007**, *34*, L17813.
(48) Levinson, R.; Akbari, H.; Berdahl, P. Measuring solar reflectance−Part I: defining a metric that accurately predicts solar heat gain. *Sol. Energy* **2010**, *84*, 1717−1744.
(49) Kirillova, E. N.; Andersson, A.; Han, J.; Lee, M.; Gustafsson, Ö. Sources and light absorption of water-soluble organic carbon aerosols in the outflow from northern China. *Atmos. Chem. Phys.* **2014**, *14*, 1413−1422.
(50) Zhang, X. L.; Lin, Y. H.; Surratt, J. D.; Weber, R. J. Sources, composition and absorption angstrom exponent of light-absorbing organic components in aerosol extracts from the Los Angeles Basin. *Environ. Sci. Technol.* **2013**, *47*, 3685−3693.
(51) Phillips, S. M.; Bellcross, A. D.; Smith, G. D. Light absorption by brown carbon in the southeastern United States is pH-dependent. *Environ. Sci. Technol.* **2017**, *51*, 6782−6790.
(52) Fountoukis, C.; Nenes, A. ISORROPIA II: a computationally efficient thermodynamic equilibrium model for K^+−Ca^{2+}−Mg^{2+}−NH_4^+−Na^+−SO_4^{2-}−NO_3^-−Cl^-−H_2O aerosols. *Atmos. Chem. Phys.* **2007**, *7*, 4639−4659.
(53) Wang, G. H.; Zhang, R. Y.; Gomez, M. E.; et al. Persistent sulfate formation from London Fog to Chinese haze. *Proc. Natl. Acad. Sci. U. S. A.* **2016**, *113*, 13630−13635.
(54) Elser, M.; Huang, R.-J.; Wolf, R.; Slowik, J. G.; Wang, Q.; Canonaco, F.; Li, G.; Bozzetti, C.; Daellenbach, K. R.; Huang, Y.; Zhang, R.; Li, Z.; Cao, J.; Baltensperger, U.; El-Haddad, I.; Prévôt, A. S. H. New insights into $PM_{2.5}$ chemical composition and sources in two major cities in China during extreme haze events using aerosol mass spectrometry. *Atmos. Chem. Phys.* **2016**, *16*, 3207−3225.
(55) Li, X.; Chen, Y.; Bond, T. C. Light absorption of organic aerosol from pyrolysis of corn stalk. *Atmos. Environ.* **2016**, *144*, 249−256.
(56) Park, S. S.; Yu, J. Chemical and light absorption properties of humic-like substances from biomass burning emissions under controlled combustion experiments. *Atmos. Environ.* **2016**, *136*, 114−122.
(57) Lin, P.; Bluvshtein, N.; Rudich, Y.; Nizkorodov, S.; Laskin, J.; Laskin, A. Molecular chemistry of atmospheric brown carbon inferred from a nationwide biomass burning event. *Environ. Sci. Technol.* **2017**, *51*, 11561−11570.
(58) Zhao, S. Y.; Tie, X. X.; Cao, J. J.; Li, N.; Li, G. H.; Zhang, Q.; Zhu, C. S.; Long, X.; Li, J. D.; Feng, T.; Su, X. L. Seasonal variation and four-year trend of black carbon in the mid-west China: The analysis of the ambient measurement and WRF-Chem modeling. *Atmos. Environ.* **2015**, *123*, 430−439.
(59) Jacobson, M. Z. Isolating nitrated and aromatic aerosols and nitrated aromatic gases as sources of ultraviolet light absorption. *J. Geophys. Res.* **1999**, *104*, 3527−3542.
(60) Samburova, V.; Connolly, J.; Gyawali, M.; Yatavelli, R. L. N.; Watts, A. C.; Chakrabarty, R. K.; Zielinska, B.; Moosmüller, H.; Khlystov, A. Polycyclic aromatic hydrocarbons in biomass-burning emissions and their contribution to light absorption and aerosol toxicity. *Sci. Total Environ.* **2016**, *568*, 391−401.
(61) Lin, P.; Aiona, P. K.; Li, Y.; Shiraiwa, M.; Laskin, J.; Nizkorodov, S. A.; Laskin, A. Molecular characterization of brown carbon in biomass burning aerosol particles. *Environ. Sci. Technol.* **2016**, *50*, 11815−11824.
(62) Mohr, C.; Lopez-Hilfiker, F. D.; Zotter, P.; Prevot, A. S.; Xu, L.; Ng, N. L.; Herndon, S. C.; Williams, L. R.; Franklin, J. P.; Zahniser, M. S.; Worsnop, D. R.; Knighton, W. B.; Aiken, A. C.; Gorkowski, K. J.; Dubey, M. K.; Allan, J. D.; Thornton, J. A. Contribution of nitrated phenols to wood burning brown carbon light absorption in Detling, UK during winter time. *Environ. Sci. Technol.* **2013**, *47*, 6316−6324.
(63) Teich, M.; van Pinxteren, D.; Wang, M.; Kecorius, S.; Wang, Z.; Müller, T.; Mocnik, G.; Herrmann, H. Contributions of nitrated aromatic compounds to the light absorption of water-soluble and particulate brown carbon in different atmospheric environments in Germany and China. *Atmos. Chem. Phys.* **2017**, *17*, 1653−1672.
(64) Desyaterik, Y.; Sun, Y.; Shen, X.; Lee, T.; Wang, X.; Wang, T.; Collett, J. L. Speciation of brown carbon in cloud water impacted by agricultural biomass burning in eastern China. *J. Geophys. Res.- Atmos.* **2013**, *118*, 7389−7399.
(65) Jo, D. S.; Park, R. J.; Lee, S.; Kim, S. W.; Zhang, X. A global simulation of brown carbon: implications for photochemistry and direct radiative effect. *Atmos. Chem. Phys.* **2016**, *16*, 3413−3432.
(66) Hammer, M. S.; Martin, R. V.; van Donkelaar, A.; Buchard, V.; Torres, O.; Ridley, D. A.; Spurr, R. J. D. Interpreting the ultraviolet aerosol index observed with the OMI satellite instrument to understand absorption by organic aerosols: implications for atmospheric oxidation and direct radiative effects. *Atmos. Chem. Phys.* **2016**, *16*, 2507−2523.

DOI: 10.1021/acs.est.8b02386
Environ. Sci. Technol. 2018, 52, 6825−6833

4. Conclusion and Future Work

4.1 Summary of Main Results

This project investigates the chemical nature and sources of atmospheric particulate matter in urban areas in Ireland (Dublin and Galway) and China (Shijiazhuang, Beijing, and Xi'an). The key findings are summarized as follows:

1) Dublin city experiences frequent particulate air pollution events in winter, with episodic PM_1 concentrations reaching 300 μg m^{-3}. Solid fuels, such as peat and wood, though consumed by <13% of the households, contribute up to 70% of the pollution. Similarly, in Galway, on the west coast of Ireland, pollution from solid fuel burning is a major cause of poor air quality in winter. Thus, emissions of solid fuel burning, especially peat burning, should be targeted to improve the air quality across Ireland.
2) The summer time aerosol in Galway is dominated by secondary organic and inorganic aerosol, together accounting for up to 91% of the total NR-PM_1. Secondary aerosol was found to originate from the secondary formation during long-range transport likely from eastern Ireland, the UK and/or France.
3) The sources of PM_1 in urban Shijiazhuang, China during winter were mainly from traffic, biomass burning, cooking, and coal combustion. The low OOA fraction (27%) in OA and the low sulfur oxidation degree (F_{SO4}) of 0.18 indicated the dominance of primary particulate emissions in this top polluted city.
4) Traffic-related emissions were dominant during low pollution periods in wintertime Beijing, contributing ~65% of the total trace elements (Fe, Zn, Pb, Mn, Cd, As, Sr, Co, V, Cu, and Ni) mass. However, coal combustion-related particulate trace elements were found to dominate the health risks during pollution periods.
5) The sources of glycolic acid sulfate, phenyl sulfate, and benzyl sulfate in wintertime Xi'an, China were mainly anthropogenic while hydroxyacetone sulfate had a biogenic origin.
6) Brown carbon (BrC) was mainly associated with biomass burning in winter Xi'an China, the mass concentration of which was ~5 times higher than that in summer. BrC was found to

affect the radiative balance significantly as indicated by its high fractional solar absorption relative to element carbon (42 - 76%).

4.2 Future Work

In light of the results presented in this thesis, several issues related to the chemical nature and sources of PM in urban areas remain unanswered and require further research. There is a need to further characterize the urban aerosols especially during pollution episodes, including reducing the uncertainty of source apportionment, and the quantification of the potential health and climate effects associated with emissions from solid fuel burning and traffic. To achieve these goals, measurements covering these multiple aspects should be carried out routinely by using state-of-the-art techniques including ACSM with source apportionment, multi-wavelength Aethalometer, radiocarbon determination, reactive oxygen species (ROS) measurement, and cloud condensation nuclei (CCN) counter. The combination of ACSM with radiocarbon measurement will reduce the uncertainty of the source apportionment while combining source apportionment with ROS measurement (e.g., using DTT essay) will potentially quantify the health risks associated with specific sources. Finally, CCN counter will provide some insights on cloud formation efficiency of particles from different sources.